UNIWERSYTET MIKOŁAJA KOPERNIKA W TORUNIU

WYDZIAŁ CHEMII

Katedra Chemii Materiałów, Adsorpcji i Katalizy

Zespół Technologii Wodorowych i Magazynowania Energii

mgr Małgorzata Skorupska

Rozprawa doktorska

Otrzymywanie i charakterystyka katalitycznych materiałów węglowych zawierających heteroatomy azotu oraz ocena ich przydatności jako materiału elektrodowego w bateriach typu metal–powietrze oraz w superkondensatorach

Rozprawa doktorska napisana pod kierunkiem:

Dr hab. Anny Ilnickiej, prof. UMK (promotor)

Prof. dr hab. Jerzego P. Łukaszewicza (promotor pomocniczy)

Toruń 2023

Preparation and characterization of catalytic carbon materials containing nitrogen heteroatoms and evaluation of their suitability as electrode material in metal-air batteries and in supercapacitors

NARODOWE CENTRUM NAUKI

Praca powstała w wyniku realizacji projektu badawczego PRELUDIUM-18 o nr 2019/35/N/ST5/02691 finansowanego ze środków Narodowego Centrum Nauki oraz Grantów dla Młodych Naukowców Wydziału Chemii Uniwersytetu Mikołaja Kopernika w Toruniu.

Podziękowania

„Nikomu z nas życie, zdaje się, bardzo łatwo nie idzie, ale cóż robić, trzeba mieć odwagę i głównie wiarę w siebie, w to, że się jest do czegoś zdolnym i że do tego czegoś dojść potrzeba. A czasem wszystko się pokieruje dobrze, wtedy kiedy najmniej się człowiek tego spodziewa."

Maria Skłodowska-Curie
Fragment z książki *„Maria Curie"*

Składam serdeczne podziękowania* Pani dr hab. Annie Ilnickiej, prof. UMK *za zaangażowanie, wsparcie merytoryczne, ogromną cierpliwość i wyrozumiałość, poświęcony czas na liczne dyskusje, a także inspirację do dalszego zagłębiania zagadnień naukowych.

Pragnę podziękować również Panu* prof. dr hab. Jerzemu P. Łukaszewiczowi *za cenne wskazówki, wsparcie merytoryczne, a także możliwość pracy w zespole pod jego kierownictwem, co stało się czystą przyjemnością.

W tym miejscu chciałabym również podziękować rodzinie i przyjaciołom za nieustanną motywację w dążeniu do celu a szczególne podziękowania składam mojemu narzeczonemu, Michałowi Lewandowskiemu, za nieocenioną pomoc w osiągnięciu życiowej równowagi oraz wiarę we mnie i moje możliwości.

Spis treści

1. Wprowadzenie

Wraz z rosnącą liczbą ludności i rozwojem gospodarki, globalne zapotrzebowanie na energię nieustannie wzrasta. Ostatnie lata pokazują, że rozwój technologiczny w zakresie elektrochemicznego magazynowania energii, opiera się głównie na opracowaniu nowych materiałów o specyficznych właściwościach dostosowanych do wymagań procesów elektrochemicznych. W szczególności badania skupiają się na poszukiwaniu nowych, efektywnie działających materiałów elektrodowych, co stanowi dla nas znaczące wyzwanie technologiczne. Zarówno proces magazynowania, jak i konwersji energii stanowią kluczowe wyzwania w dzisiejszym świecie, dążącym do pełnej elektryfikacji. Istnieje wiele różnych systemów i technologii, które pozwalają na magazynowanie energii, jednym z najbardziej powszechnych rodzajów ogniw elektrochemicznych są baterie. Ogniwa wykorzystują reakcje elektrochemiczne zarówno do magazynowania, jak i uwalniania energii. Innymi równie ważnymi urządzeniami do magazynowania energii, jednak o odmiennych cechach użytkowych są superkondensatory. Magazynowanie energii w superkondensatorach typu EDLC (ang. Electrochemical Double – Layer Capacitor) opiera się na gromadzeniu elektrycznego ładunku w warstwie podwójnej oraz wykorzystaniu elektrochemicznych procesów zachodzących na granicy faz pomiędzy elektrodami, a elektrolitem. Kluczowym elementem mechanizmu ładowania/rozładowania jest adsorpcja i desorpcja jonów elektrochemicznie aktywnych substancji na powierzchni elektrod, co umożliwia przechowywanie i uwalnianie ładunku elektrycznego w sposób znacznie szybszy niż w tradycyjnych bateriach [1]. W ostatnich latach wciąż rosnące wymagania są stawiane magazynom energii, gdyż dzięki nim możliwe jest racjonalne wykorzystanie odnawialnych źródeł energii (OZE), takich jak energia wiatrowa czy słoneczna, które generują energię w zależności od pory dnia i warunków atmosferycznych, czyli w sposób niestabilny i nieciągły.

W urządzeniach do magazynowania i konwersji energii takich jak baterie typu metal-powietrze, ogniwa paliwowe oraz elektrolizery, kluczową rolę odgrywa reakcja redukcji tlenu (ang. oxygen reduction reaction, ORR). Reakcja ORR jest procesem katalitycznym, w którym zachodzi redukcja tlenu cząsteczkowego (O_2) z powietrza w obecności katalizatora do pochodnych tlenu na IV stopniu utleniania [2, 3]. Badania teoretyczne i doświadczalne odgrywają istotną rolę w zrozumieniu tych mechanizmów zachodzących na powierzchni katalizatorów. Mechanizmy zachodzące podczas reakcji redukcji tlenu na grafenie domieszkowanym azotem mogą przebiegać wg różnych

mechanizmów zależnych od pH, stężenia elektrolitu oraz rodzaju użytego katalizatora [4-6]. W aktualnie prowadzonych badaniach zrozumienie mechanizmu reakcji ORR stało się kluczowym wyzwaniem. Reakcja redukcji tlenu może przebiegać na drodze dwuetapowej (dwu- i dwuelektronowej) lub jednoetapowej (czteroelektronowej) redukcji. Proces dwuetapowy polega na dwuelektronowej redukcji cząsteczki tlenu do produktu pośredniego, czyli nadtlenku wodoru (H_2O_2) wykorzystując dwa elektrony podczas transferu elektronowego. Następnie produkt pośredni redukowany jest do dwóch cząsteczek wody. Z kolei mechanizm czteroelektronowy polega na bezpośredniej redukcji tlenu cząsteczkowego do dwóch cząsteczek wody lub jonów hydroksylowych za pomocą przeniesienia czterech elektronów.

W środowisku alkalicznym dwuetapowa reakcja redukcji tlenu przebiega następująco:

$$O_2 + H_2O + 2e^- \rightarrow HO_2^- + OH^- \quad (1a)$$

$$HO_2^- + H_2O + 2e^- \rightarrow 3OH^- \quad (1b)$$

W środowisku kwaśnym dwuetapowa reakcja redukcji tlenu przebiega następująco:

$$O_2 + 2H^+ + 2e^- \rightarrow 2H_2O_2 \quad (2a)$$

$$H_2O_2 + 2H^+ + 2e^- \rightarrow 2H_2O \quad (2b)$$

Bezpośrednia reakcja czteroelektronowej redukcji tlenu w środowisku alkalicznym oraz kwasowym przebiega następująco:

$$O_2 + 2H_2O + 4e^- \rightarrow 4OH^- \quad \text{(środowisko alkaliczne)} \quad (3)$$

$$O_2 + 4H^+ + 4e^- \rightarrow 2H_2O \quad \text{(środowisko kwasowe)} \quad (4)$$

W ostatnim czasie wiele uwagi poświęca się domieszkowaniu grafenu heteroatomami. Gdy domieszką jest azot niektóre atomy węgla są zastępowane atomami azotu, a także pojawiają się specyficzne defekty, powodując zniekształcenia strukturalne w grafenie. Z punktu widzenia mechaniki kwantowej, atomy azotu w grafenie mogą działać jako akceptory elektronów, tworząc stany akceptorowe w paśmie przewodnictwa. Prowadzi to do lokalnych zaburzeń aromatyczności charakterystycznej dla czystego grafenu. Zdolność atomów azotu do przyjmowania elektronów powoduje powstawanie dodatnich ładunków cząstkowych na sąsiednich atomach węgla. W konsekwencji, bezpośrednio wpływa to na proces adsorpcji cząsteczek OOH i dalsze rozerwanie wiązań O–O w cząsteczce tlenu. Przeprowadzone obliczenia gęstości spinowej i gęstości ładunku dla określonej struktury grafenu domieszkowanego azotem wykazały, że atomami węgla o znacznej gęstości ładunku dodatniego są atomy bezpośrednio sąsiadujące z

wbudowanym atomem azotu [6]. Natomiast atomy o dużej gęstości spinowej to drugi lub trzeci sąsiadujący atom węgla [7]. W jednoetapowej reakcji redukcji tlenu podczas gdy, atom wodoru przyłącza się do atomu tlenu, tworzy wiązanie między atomami tlenu i wodoru, jednocześnie zrywając wiązanie O–O. Powoduje to powstawanie grup wodorotlenkowych OH, wtedy płaszczyzna grafenu ulega przekształceniu. Następuje dysocjacja cząsteczek OH, zaś w reakcji dwuetapowej tworzy się półprodukt H_2O_2, który redukuje się do wody. W reakcji jednoetapowej biorące udział elektrony ($4e^-$) redukują atomy tlenu bezpośrednio do cząsteczek wody. Na koniec cząsteczki wody odłączają się od powierzchni grafenu. Grafen powraca do swojego pierwotnego kształtu i jest gotowy do kolejnego cyklu redukcji tlenu [7].

Odpowiednio dobrane katalizatory mogą skutecznie zmniejszać zapotrzebowanie energetyczne oraz zwiększyć wydajność samych urządzeń. Rozwój i opracowywanie nowych efektywnie działających, stabilnych oraz trwałych katalizatorów do zastosowań elektrochemicznych stanowi istotne wyzwanie w kontekście najbliższej przyszłości. Obecnie komercyjnie stosowanymi materiałami elektrodowymi w bateriach typu metal-powietrze oraz ogniwach paliwowych są metale szlachetne (platyna) lub tlenki metali szlachetnych (tlenek irydu, tlenek rutenu) wykorzystywane jako materiał katodowy. Poszukiwanie alternatywnych katalizatorów niezawierających metali szlachetnych stało się głównym wyzwaniem aktualnie prowadzonych badań. Ze względu na wysoką cenę oraz ograniczone zasoby tych pierwiastków, materiały elektrodowe obecnie badane w laboratoriach zawierają metale przejściowe takie jak mangan [8, 9], żelazo [10, 11] czy kobalt [12], które mogą wykazywać porównywalną aktywność katalityczną do platyny. Materiały zawierające metale przejściowe mogą działać na zasadzie nośnika elektronów. Inną równie ważną grupę katalizatorów stanowią materiały węglowe domieszkowane heteroatomami niemetalicznymi. Przykładem tego typu katalizatorów są struktury grafenu domieszkowanego azotem [13-15], tlenku grafenu (GO) [16, 17], czy nanorurki węglowe (CNT) domieszkowane azotem [18-21], a także materiały węglowe domieszkowane siarką [22]. Praca **[D1]** włączona do dysertacji stanowi aktualny przegląd literaturowy metod otrzymywania materiałów węglowych na bazie grafenu, nanorurek węglowych, porowatych materiałów węglowych pochodzenia naturalnego, czy też nanowłókien węglowych. Dzięki temu przeglądowi możliwe było opracowanie schematów syntez w taki sposób, aby otrzymać materiały węglowe/grafenowe do określonych zastosowań elektrochemicznych wg koncepcji wykraczających poza istniejący stan wiedzy i techniki. Głównym założeniem było to, że

tego typu katalizatory powinny działać jako efektywne katalizatory ORR, ponieważ centra aktywne, które miały być wbudowane w strukturę węglową, miały ułatwiać czeroelektronową redukcję tlenu.

Kolejną grupę katalizatorów stanowią polimery przewodzące, które mogą skutecznie przyspieszyć transfer elektronów i wpłynąć pozytywnie na redukcję tlenu. Przykładem polimerów tego typu są polipirol [23, 24], polianilina [24-26] oraz poli(3,4-etyleno-1,4 dioksytiofen) (PEDOT) [27, 28]. Połączenie struktur węglowych domieszkowanych jednocześnie różnymi heteroatomami N, B [29], N, P [30], B, N, P [31] oraz zawierających tlenki metali przejściowych [32] może sprzyjać polepszeniu aktywności katalitycznej, a także trwałości katalizatorów. Wszystkie materiały wykazujące porównywalne właściwości katalityczne do platyny mogą stać się alternatywą jako materiały elektrodowe do zastosowania w reakcji ORR. Nieustannie jednak prowadzone są intensywne badania na temat poprawy wydajności, trwałości, a także pełnego zrozumienia mechanizmu reakcji ORR w celu optymalizacji i opracowania nowych, zrównoważonych rozwiązań energetycznych.

Przełomowe osiągnięcia w obszarze badań poświęconym reakcji redukcji tlenu mają istotne znaczenie dla rozwoju nowych technologicznych rozwiązań powiązanych z energią, a także w przyszłości mogą przyczynić się do wyeliminowania konwencjonalnych źródeł energii opartych na paliwach kopalnych. Zaproponowane nowe rozwiązania otrzymywania efektywnych katalizatorów mogą przyczynić się także się do poprawy efektywności i wydajności katalitycznej poprzez lepsze zrozumienie mechanizmów zachodzących reakcji. Wówczas będzie możliwe przeniesienie badań ze skali laboratoryjnej na skalę produkcyjną.

Zgodnie z ideą magazynowania nadmiarowej energii, superkondensatory należące do kategorii kondensatorów elektrolitycznych (głównie wykorzystujących elektrolity ciekłe) oferują istotne cechy użytkowe. Superkondensatory można podzielić na kondensatory dwuwarstwowe lub inaczej superkondensatory EDLC, pseudosuperkondensatory PC (ang. Pseudo-Capacitor) oraz superkondensatory hybrydowe HSC (ang. Hybrid Supercapacitor) [33, 34]. Pierwszy typ superkondensatorów EDLC jest najpopularniejszym rodzajem superkondensatorów oraz jest szeroko dostępny komercyjnie. Urządzenia te wykorzystują oddziaływanie elektrostatyczne do gromadzenia energii w warstwie podwójnej na granicy faz między powierzchnią elektrody, a elektrolitem. Pojemność dwuwarstwy zależy od potencjału energii powierzchniowej zmagazynowanej elektrostatycznie na granicy faz. W

superkondensatorach EDLC nie zachodzi wymiana elektronów w elektrodowej reakcji redox a energia magazynowana jest w warstwie podwójnej. Istotnym parametrem do uzyskania wyjątkowo wysokiej pojemności jest rozwinięte pole powierzchni właściwej elektrod oraz grubość warstwy Helmhotza, czyli warstwy podwójnej. O wysokiej trwałości świadczy ilość cykli ładowania/rozładowania, która dla superkondensatorów EDLC może wynosić od kilku tysięcy cykli do nawet kilkunastu tysięcy cykli.

Drugą grupą superkondensatorów są tak zwane pseudosuperkondensatory, ten rodzaj urządzeń jest stosowany rzadziej niż superkondensatory EDLC. Zasada działania tych superkondensatorów bardziej przypomina zasadę działania akumulatorów niż kondensatorów. Polega to na zjawisku pseudopojemności, która jest procesem, podczas którego materiały elektrod pośredniczą w przenoszeniu elektronów i zachodzą powierzchniowe reakcje redox. Zjawisko to powstaje na powierzchniach elektrod a przepływ prądu następuje w wyniku przeniesienia elektronu i zajścia reakcji redox. Podczas ładowania i rozładowania zachodzą reakcje utleniania oraz redukcji i zachodzi transfer energii między elektrolitem a elektrodą. Energia nie jest magazynowana w warstwie dielektrycznej, ale powstaje poprzez energię wiązań odpowiednich molekuł. Za sprawą reakcji redox superkondensatory pseudopojemnościowe charakteryzują się większą gęstością energii. Wadą tych urządzeń jest mała stabilność, zależna od mechanizmu działania, który powoduje, że podczas cykli ładowania/rozładowania, elektrody ulegają szybszej degradacji chemicznej i mechanicznej w stosunku do superkondensatorów EDLC, w rezultacie charakteryzując się krótszą żywotnością cyklu.

Trzecim typem superkondensatorów to wymienione wcześniej superkondensatory hybrydowe, które powstały stosunkowo niedawno i prezentują bardziej zaawansowany mechanizm działania łączący działanie superkondensatorów EDLC oraz pseudosuperkondensatorów. Główną zaletą jest ich większa objętościowa oraz grawimetryczna gęstość energii, a także możliwość dostarczenia prądu o dużym natężeniu. Na elektrodzie ujemnej, która zwykle wykonana jest z wysokopojemnościowego materiału elektrodowego na bazie tlenków metali, węgli domieszkowanych metalami bądź polimeru przewodzącego, zachodzą reakcje redoks. Na elektrodzie dodatniej, zwykle wykonanej z węgla aktywnego, zachodzi magazynowanie energii elektrostatycznej w podwójnej warstwie, dzięki czemu superkondensatory hybrydowe są w stanie dostarczyć duże gęstości prądowe [35]. Obecnie ten typ superkondensatorów jest otrzymywany i badany w warunkach laboratoryjnych, dlatego też dalsze badania, a także rozwój w dziedzinie magazynowania energii są niezbędne.

Kluczowe wyzwanie stanowi poprawa parametrów strukturalnych elektrod, a także ich właściwości elektrochemicznych.

Typowy superkondensator EDLC składa się z elektrod o dużej porowatości i polu powierzchni właściwej, na których jest magazynowana energia. Zazwyczaj materiały węglowe są stosowane jako elektrody do urządzeń magazynowania energii, jako elektrody w superkondensatorach oraz w bateriach typu litowo-jonowego [36]. Aktywacja materiałów węglowych jest powszechną metodą do zwiększenia pola powierzchni właściwej. Działania te mogą obejmować fizyczną aktywację (powietrze, para wodna, CO_2 itp.) oraz chemiczną (H_2O_2, H_3PO_4, HNO_3, KOH, K_2CO_3, $ZnCl_2$) [37-39]. Aktywacja materiałów węglowych może przyczynić się nie tylko do wzrostu pola powierzchni właściwej, ale także można równolegle i skutecznie wprowadzić heteroatomy do struktury węgla [40]. Zastosowanie kwasu azotowego może skutkować wprowadzeniem do struktury heteroatomów głównie tlenu, ale również i azotu [41]. Wykorzystanie H_3PO_4 jako aktywatora materiałów węglowych wpływa korzystnie na zwiększenie pola powierzchni BET do około 1000–1500 $m^2 g^{-1}$ dla próbek otrzymywanych nawet przy niskich temperaturach 400–600°C, a także przy zastosowaniu niższych stosunków materiału węglowego do aktywatora, wynoszących 1:1–3 [42]. Wykorzystanie kwasu ortofosforowego (V) w roli aktywatora ułatwia sieciowanie poprzez kondensację i tworzenie się wiązań fosforowych takich jak estry fosforowe czy polifosforanowe, które chronią porowatą strukturę przed nadmiernym spaleniem, zapobiegając zapadnięciu się struktury [43]. Duże pole powierzchni właściwej z rozbudowanym systemem porów, powoduje wzrost adsorpcji jonów, tym samym zwiększając pojemność właściwą elektrod. Innym, szeroko stosowanym, aktywatorem do zwiększenia pola powierzchni materiałów węglowych jest wodorotlenek potasu, KOH. Może on powodować wzrost pola powierzchni właściwej węgli aktywnych nawet do 3000 m^2g^{-1}, metoda ta jest znana od roku 1984 [44]. Wpływ na mikroporowatą strukturę ma nie tylko stosunek reagentów KOH do materiału węglowego, ale także temperatura i czas aktywacji [45].

Materiały wykorzystywane aktualnie w superkondensatorach to nanomateriały węglowe [46, 47], tlenki metali [48], polimery przewodzące [49] oraz ich nanokompozyty, a także nowatorskie materiały takie jak struktury metaloorganiczne [50], struktury MXene [51] czy azotki metali [52]. Superkondensatory oprócz elektrod zawierają elektrolit pełniący rolę „magazynu" jonów oraz umożliwia on swobodny przepływ jonów. Elektrolity wykorzystywane w superkondensatorach mogą

być oparte na elektrolitach wodnych, roztworach soli organicznych, a niekiedy spotyka się również superkondensatory wykorzystujące elektrolity stałe [53]. Zaletą superkondensatorów jest ich wysoka moc, co przekłada się na dostarczanie energii w bardzo krótkim czasie, dlatego sprawdzają się jako urządzenia wymagające intensywnego poboru mocy, np. w układach magazynowania/odzyskiwania energii w trakcie hamowania samochodów elektrycznych [54]. Superkondensatory wytrzymują wielokrotne cykle ładowania i rozładowywania, rzędu kilku tysięcy razy bez znacznej utraty ich pojemności [35, 55]. Pomimo wszystkich przytoczonych zalet istnieje jeszcze wiele wyzwań w celu opracowywania efektywnie działającego superkondensatora, jednym z nich jest niska gęstość energii (ang. Energy density – E_d) w porównaniu do tradycyjnych baterii [56]. W literaturze pojawiają się doniesienia na temat opracowywania nowych materiałów elektrodowych o większej pojemności właściwej (C_s), dzięki którym możliwe jest zwiększenie gęstości energii superkondensatora. Mimo postępu w ostatnich latach, wciąż głównym wyzwaniem jest wytwarzanie innowacyjnych superkondensatorów, które będą miały zwiększoną gęstość energii, pojemność właściwą, a także zwiększone okno potencjału, czy zoptymalizowaną strukturę elektrod. Pomimo, że wytwarzanie poszczególnych składowych superkondensatorów nie jest stosunkowo skomplikowane, to uzyskanie korelacji między odpowiednią porowatą strukturą materiału elektrodowego, a rozmiarem jonów elektrolitu stanowi istotne wyzwanie. Elektrolity, a dokładnie ich zakres potencjału oraz zakres temperatury, w którym mogą pracować superkondensatory, odgrywają kluczową rolę w określeniu gęstości mocy. Kolejnymi ważnymi kryteriami wyboru elektrolitu są wysokie stężenia jonów, praca w szerokim oknie potencjału, a także doskonała stabilność elektrochemiczna połączona z niską rezystancją szeregową, mniejszą lotnością toksycznością i niskim kosztem [57]. Dotychczas najczęściej stosowanymi wodnymi elektrolitami były: KOH [58], Na_2SO_4 [59], H_2SO_4 [60] oraz elektrolity aprotonowe [35], takie jak sole litu heksafluorofosforan litu ($LiPF_6$), tetrafluoroboran litu ($LiBF_4$), tetrafluoroboran litu ($LiBF_4$) czy nadchloran litu ($LiClO_4$), a także ciecze jonowe [61]. W celu poprawy wydajności superkondensatora, należy skupić badania na poznaniu mechanizmu magazynowania energii odbywającemu się na granicy faz elektrolit/elektroda. Wciąż aktualnym wyzwaniem jest zaprojektowanie elektrod w taki sposób, aby tworzyły porowate mikrostruktury, które będą mogły aktywnie uczestniczyć w wymianie jonowej, a także kontrolować interakcje międzyfazowe by zoptymalizować oddziaływania między

różnymi fazami (np. elektrody, elektrolitu, separatora) w celu uzyskania struktury o wysokiej wydajności elektrochemicznej.

Opracowywane innowacyjnych katalizatorów i adsorbentów do magazynowania i konwersji energii ma istotne znaczenie w przyspieszeniu transformacji energetycznej, a także w osiągnięciu bardziej czystego i zrównoważonego środowiska, poprzez:

- Zwiększenie efektywności i wydajności – innowacyjne katalizatory, projektowane powinny być w taki sposób, aby służyły bardziej wydajniej i efektywniej reakcji redukcji tlenu. Poprawa właściwości w reakcji ORR sprawia, że zastosowane elektrody w ogniwach paliwowych lub bateriach typu metal-powietrze będą dostarczać większą ilość energii przy niskim zużyciu reagentów.
- Obniżenie kosztów produkcji – katalizatory, które będą oparte na tanich materiałach elektrodowych i będą optymalnie zaprojektowane, skutecznie obniżą koszty produkcji, ponadto mogą spowodować wdrożenie w przyszłości ich produkcji w skali przemysłowej.
- Otrzymywanie innowacyjnych katalizatorów przyczynia się do trwałości i stabilności urządzeń, co wpływa na dłuższą żywotność ogniw paliwowych czy baterii typu metal-powietrze, w których są stosowane.
- Wspomaganie odnawialnych źródeł energii – skutecznie działające katalizatory w reakcji ORR, mogą poprawić właściwości elektrolizerów w produkcji czystego wodoru.
- Redukcja emisji gazów cieplarnianych – może stać się korzyścią podczas wytwarzania bardziej wydajnych katalizatorów do reakcji ORR w elektrycznych lub hybrydowych pojazdach. Ponadto, może skutecznie obniżyć emisję gazów cieplarnianych dzięki zwiększeniu wydajności silników elektrycznych, a także dzięki wydłużeniu czasu jazdy na jednym pełnym ładowaniu.
- Poprawa wydajności reakcji redukcji tlenu przyczynić się może do zwiększenia atrakcyjności technologii elektromobilności. Zwiększenie zasięgów pojazdów elektrycznych, może skutecznie zwiększyć popyt na rynku i przyspieszyć procesy przejścia na bardziej ekologiczny i zrównoważony system transportu.

Wobec powyższego, opracowanie, a w dalszej perspektywie wprowadzenie na rynek nowych materiałów katalitycznych dla reakcji ORR np. w bateriach typu metal-powietrze, a także materiałów elektrodowych w superkondensatorach ma ogromne znaczenie globalne, może przynieść wiele korzyści, a także pozytywnie wpłynąć na rozwój dziedzin i technologii związanych z magazynowaniem i konwersją energii.

2. Hipotezy badawcze i cel rozprawy

Rozwój prac nad projektowaniem i otrzymywaniem nowych, wydajnych katalizatorów ORR może prowadzić do poprawy ich aktywności katalitycznej oraz stabilności. Badania skupiają się na poszukiwaniu alternatywnych katalizatorów, które będą mogły skutecznie zastąpić platynę np. w reakcji ORR. Przystępując do realizacji badań, postawiłam kluczową hipotezę, że nadanie materiałom węglowym unikalnej struktury porowatej i modyfikacja ich powierzchni poprzez zmianę składu chemicznego będzie miało korzystny wpływ na przebieg reakcji ORR. Odpowiednia struktura katalizatora i obecność heteroatomów mogą mieć istotne znaczenie dla aktywności katalitycznej w reakcji ORR, a w szczególności spodziewałam się, iż zdefektowana struktura ma istotny wpływ na tę reakcję w środowisku alkalicznym. Zakładałam, że odpowiednie heterostruktury powierzchniowe będą wpływać na zwiększoną adsorpcję tlenu, transport elektronów i redukcję cząsteczek tlenu w środowisku alkalicznym. Zazwyczaj do wytwarzania materiałów elektrodowych wykorzystywane są materiały nanostrukturalne, takie jak nanorurki węglowe, grafen o nanometrycznych rozmiarach płatków, kropki kwantowe lub nanokompozyty. Nanostrukturyzowana powierzchnia zapewnia większe pole powierzchni właściwej, a co za tym idzie, zwiększoną liczbę miejsc aktywnych. Liczne w takim przypadku defekty powierzchniowe mogą przyczyniać się do powstania unikatowej struktury elektronicznej i sprzyjać zwiększeniu przewodności elektrycznej. Zakładałam, że zoptymalizowana metoda syntezy pozwoli na uzyskanie materiału elektrodowego o korzystnej morfologii oraz optymalnej porowatości pozwalającej na nieustanny kontakt elektrolitu z centrami katalitycznymi, odpowiednią dyfuzję jonów czy szybki transfer elektronów/jonów, a także odpowiedni stopień dyspersji miejsc aktywnych. Wymienione wyżej parametry mają istotny wpływ na poprawę właściwości katalitycznych czy przewodzących a w konsekwencji przyczyniają się do poprawy efektywności urządzeń, w których są wykorzystywane.

Kluczową hipotezą jest założenie, że zastosowanie domieszek w postaci heteroatomów w strukturze katalizatora, może pozytywnie wpłynąć na jego aktywność m.in. w reakcji ORR. Założyłam, że wprowadzenie odpowiednich grup funkcyjnych doprowadzi do zmian struktury elektronowej matrycy węglowej mającej wpływ na właściwości chemiczne i katalityczne. Heteroatomy azotu stworzą centra aktywne, które korzystnie wpłyną na adsorpcję i redukcję cząsteczek tlenu. Zakładałam, że zgłębianie wiedzy na temat mechanizmu reakcji elektrochemicznych w powiązaniu z otrzymywaniem materiału elektrodowego, może dostarczyć bardzo istotnych informacji

na temat zoptymalizowanej strategii syntezy katalizatorów, a także przyczynić się do opracowania odpowiedniego składu i struktury materiałów katalitycznych. Weryfikacja tego założenia to praca **[D1],** która stanowi aktualny przegląd literaturowy dotyczący metod otrzymywania materiałów węglowych domieszkowanych heteroatomami azotu na bazie grafenu, nanorurek węglowych, porowatych materiałów węglowych pochodzenia naturalnego, czy też nanowłókien węglowych do zastosowań w reakcji redukcji tlenu.

Wszystkie postawione hipotezy badawcze służą rozwinięciu wiedzy na temat otrzymywania nowych i innowacyjnych katalizatorów elektrodowych, a także poprawie ich właściwości oraz efektywności i wydajności w reakcji redukcji tlenu. Przeprowadzone przeze mnie przegląd literaturowy oraz szczegółowe badania fizykochemiczne i elektrochemiczne mogą przyczynić się do lepszego zrozumienia mechanizmu procesu redukcji tlenu.

Powyższa kluczowa hipoteza stała się podstawą do sformułowana głównego celu niniejszej rozprawy doktorskiej, którym jest opracowanie metod otrzymywania materiałów katalitycznych, domieszkowanych heteroatomami azotu oraz posiadających zróżnicowane właściwości strukturalne i powierzchniowe. Istotną nowością jest konstrukcja i testowanie otrzymanych katalizatorów w prototypowych układach superkondensatorów i badanie reakcji redukcji tlenu w roztworach alkalicznych.

W celu realizacji nadrzędnego celu badawczego sformułowano następujące cele szczegółowe:

I. Modyfikacja struktury grafenowej/grafitowej może wpłynąć na sterowanie porowatością oraz zmianę morfologii materiałów, poprzez zastosowanie odpowiednich metod:

a. zastosowanie promieniowania mikrofalowego przyczyniającego się do utworzenia eksfoliowanej struktury grafitowej **[D2]**;
b. wykorzystanie templatów twardych ($CaCO_3$ **[D3]** i Na_2CO_3 **[D4]**) w celu rozwinięcia struktury materiałów węglowych;
c. wykorzystanie kwasu ortofosforowego (V) do aktywacji materiałów grafenowych oraz rozwoju porowatości **[D5]**.

II. Wzbogacenie struktury grafenowej heteroatomami wykorzystując naturalne oraz organiczne nośniki azotu:

a. zastosowanie naturalnych nośników (zielone algi morskie **[D2]**; *Chlorella vurgalis*, żelatyna, chitozan **[D4]**);
b. zastosowanie organicznego materiału chemicznego azodikarbonamidu (ADC) **[D3]**.

III. Elektrochemiczna weryfikacja otrzymanych materiałów do zastosowania jako elektrody w:
a. bateriach typu metal-powietrze, dla których kluczowa jest reakcja redukcji tlenu **[D2]**, **[D3]**, **[D4]**.
b. superkondensatorach, w celu sprawdzenia pojemności elektrochemicznej **[D5]**.

3. Część eksperymentalna

3.1. Wyniki badań i dyskusja

3.1.1. Materiały katalityczne na bazie grafitu ekspandowanego – badanie wpływu różnych rozpuszczalników i promieniowania mikrofalowego na właściwości katalityczne w reakcji redukcji tlenu

Do tej pory technika oparta na zastosowaniu promieniowania mikrofalowego była wykorzystywana w celu uzyskania niezdefektowanej monowarstwy grafenu [62] lub zredukowanego tlenku grafenu [63]. Brak doniesień literaturowych o jednoetapowym otrzymywaniu eksfoliowanych struktur grafenowych przy jednoczesnym domieszkowaniu heteroatomami azotu przyczynił się do podjęcia prac badawczych zmierzających do otrzymania tą metodą nowych materiałów. Postawiono zatem dwie hipotezy badawcze. Jedna z nich dotyczy zastosowania promieniowania mikrofalowego jako skutecznego procesu przyczyniającego się do utworzenia eksfoliowanej struktury grafitowej. Druga z kolei odnosi się do wzbogacenia otrzymanej struktury grafenowej heteroatomami wykorzystując naturalne, zielone algi morskie (*Chlorella vulgaris*), których obecność przyczynia się do poprawy aktywności katalitycznej w reakcji redukcji tlenu. W celu poparcia tych tez, zastosowano szereg fizyko-chemicznych oraz elektrochemicznych technik badawczych.

Zaproponowana synteza opierała się na jednoetapowym procesie wykorzystującym promieniowanie mikrofalowe. Proces prowadzono w dwóch różnych rozpuszczalnikach alkoholu etylowym (EtOH) lub dimetyloformamidzie (DMF). Jako materiały wyjściowe zastosowano ekspandowany handlowo dostępny grafit (EG, Sinograf, Toruń, Polska) oraz zielone algi morskie (*Chlorella vulgaris)*, będące źródłem węgla oraz jednocześnie azotu. Poglądowy schemat przeprowadzonej syntezy przedstawiono na rysunku 1, natomiast szczegółowy opis otrzymywania materiałów elektrodowych tą metodą zamieszczony jest w opublikowanej pracy wchodzący w skład dysertacji **[D2]**.

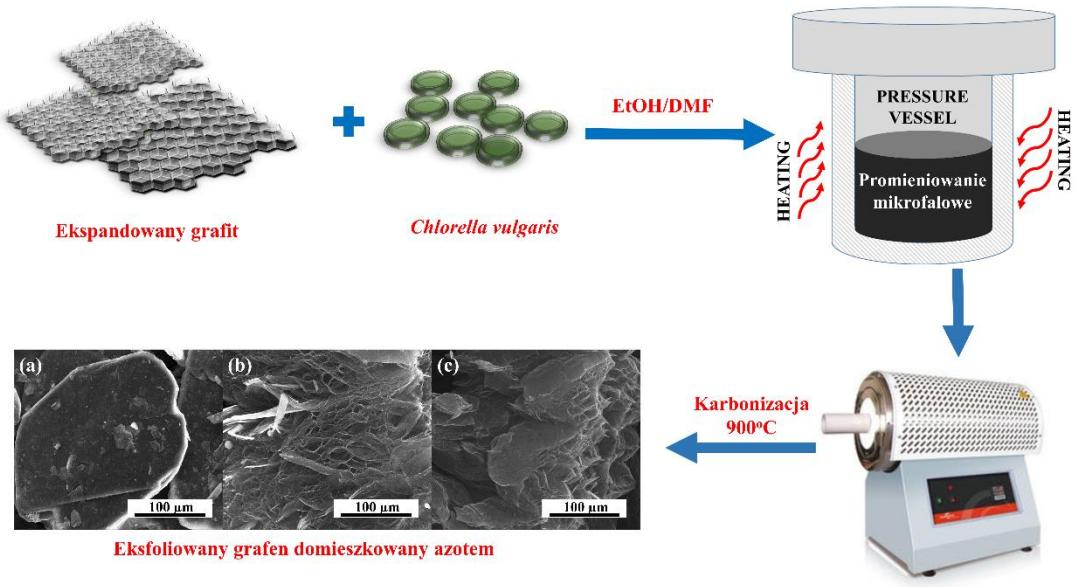

Rys. 1. Schemat syntezy otrzymywania struktur grafenowych za pomocą metody mikrofalowej.

Podstawowym założeniem opracowanej metody modyfikacji i eksfoliacji struktur grafitowych jest wykorzystanie promieniowania mikrofalowego, następnie karbonizacja w wysokich temperaturach. Zaproponowaną metodę wykorzystano w celu przekształcenia naturalnych zielonych alg morskich (*Chlorelli vulgaris*) w struktury węglowe zawierające dodatkowo azotowe grupy funkcyjne. Zielone algi morskie są prekursorem amorficznej, zawierającej atomy azotu, materii węglowej przylegającej do płatków grafenu. Wybrano ten naturalny nośnik azotu ze względu na użyteczne cechy, takie jak łatwość mieszania z płatkami grafenu w EtOH lub DMF oraz wysoką zawartość azotu w jego strukturze. W otrzymanych materiałach faza węglowa pochodząca z alg morskich występuje w postaci zawierających azot mostków między płatkami grafenu, które będą miały kluczowe znaczenie dla ich potencjalnych zastosowań.

Obrazy uzyskane za pomocą skaningowego mikroskopu elektronowego (SEM) pozwoliły na określenie wpływu procesu mikrofalowego oraz rodzaju rozpuszczalnika na strukturę otrzymanych materiałów grafenowych. Na rysunku 2 przedstawiono strukturę materiałów otrzymanych w roztworze EtOH dla próbek 0A-10 i 1A-10 oraz w roztworze DMF dla próbek 0B-10 i 1B-10. Struktura materiału otrzymanego bez stosowania procesu karbonizacji jest zbliżona do czystego grafitu, gdzie warstwy grafenowe nakładają się wzajemnie. Struktura materiałów po procesie karbonizacji zawiera eksfoliowane płatki

grafenowe, co potwierdzają obrazy otrzymane za pomocą skaningowego mikroskopu elektronowego.

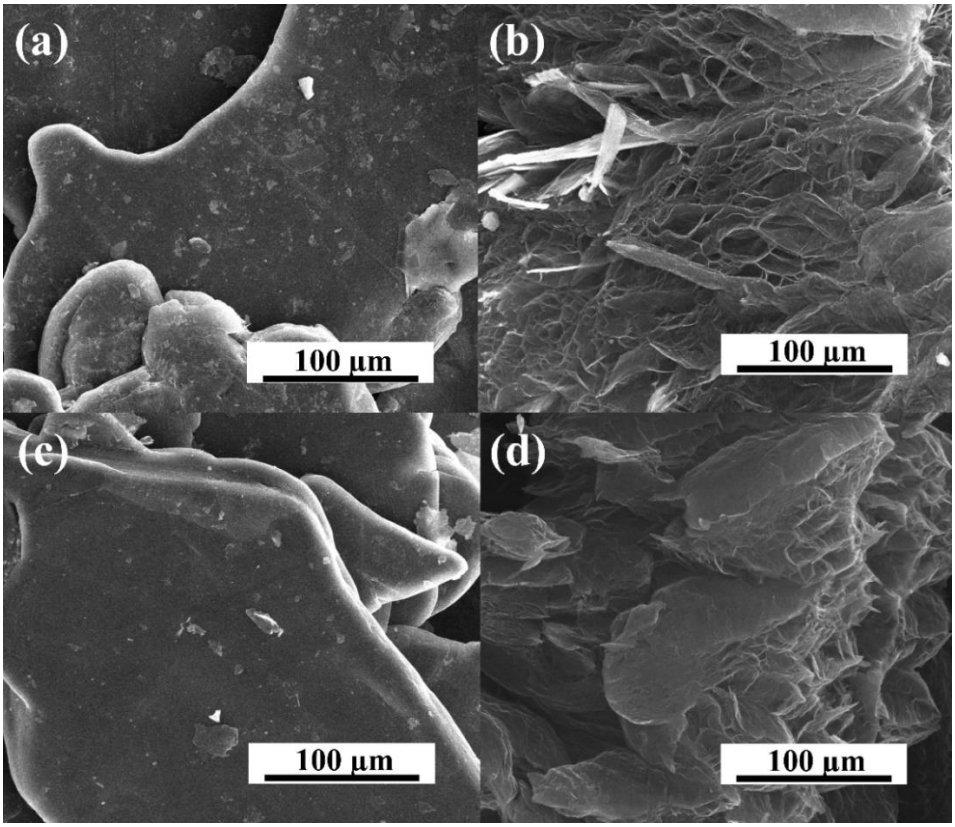

Rys. 2. Obrazy SEM dla próbek: (a) 0A-10, (b) 1A-10, (c) 0B-10, (d) 1B-10.

Przeprowadzono również analizę z wykorzystaniem mikroskopii sił atomowych (AFM), która pozwoliła na określenie grubości i rozmiarów arkuszy grafenowych. W pracy dołączonej do dysertacji [**D2**] przedstawiono profile wysokości dla próbek 1A-30 oraz 1B-30 otrzymanych po 30 minutach przebywania w reaktorze mikrofalowym. Wyniki analizy AFM wskazują, że grubość arkuszy grafenu dla serii 1A-T mieści się w zakresie 3.6–6.8 nm, natomiast dla serii 1B-T mieści się w zakresie 5.6–16.5 nm. Warto zaznaczyć, że wyniki analizy są zgodne z wynikami badań spektroskopii Ramana, które pozwoliły na sformułowanie stwierdzenia, że prowadzenie procesu w reaktorze mikrofalowym wpłynęło na otrzymanie grafenu wielowarstwowego, niezależnie od rodzaju użytego rozpuszczalnika. Analiza morfologii i struktury próbek wskazuje, iż zastosowanie reaktora mikrofalowego pozwala na kontrolę grubości oraz właściwości strukturalnych materiałów poprzez zastosowanie odpowiednich rozpuszczalników i dobranie odpowiedniego czasu prowadzonego procesu.

Zbadano również wpływ rodzaju użytego rozpuszczalnika (EtOH i DMF) oraz czasu przebywania w reaktorze mikrofalowym na zawartość procentową atomów węgla, wodoru i azotu. Stwierdzono, że zarówno rodzaj rozpuszczalnika, jak i czas przebywania w reaktorze mają wpływ na skład pierwiastkowy otrzymanych materiałów. Kluczowa dla badań analiza zawartości azotu, dla próbek 0A-T oraz 0B-T potwierdziła, iż próbki przygotowane bez dodatku nośnika azotu miały znacznie niższą zawartość procentową tego pierwiastka niż próbki z dodatkiem *Chlorelli vulgaris*. Zatem, azot został skutecznie wprowadzony do struktur z udziałem eksfoliowanego grafenu przy użyciu naturalnego nośnika azotu. Dla próbki 1A-10, która została traktowana przez 10 minut promieniami mikrofalowymi, zawartość procentowa azotu wynosiła 2.44% wag., jest to najwyższa zawartość azotu dla serii wykorzystującej EtOH jako medium dyspergujące. Wraz z wydłużającym się czasem reakcji dla serii wykorzystującej EtOH odnotowano, znaczny spadek zawartości azotu w otrzymanych próbkach. Po 90 minutach traktowania łącznie materiału węglowego oraz nośnika azotu promieniowaniem mikrofalowym zawartość azotu wynosiła 0.65% wag. (próbka 1A-90), co wskazuje, że wydłużenie czasu działania promieniowania mikrofalowego powoduje spadek zawartości azotu w otrzymanych materiałach.

Dla serii 1B-T, w której jako rozpuszczalnika użyto DMF, zauważono wzrost zawartości azotu w próbkach wraz ze wzrostem czasu przebywania w reaktorze mikrofalowym. Najwyższą zawartość azotu, wynoszącą 0.89% wag., odnotowano dla próbki 1B-90 traktowanej promieniowaniem mikrofalowym przez okres 90 minut. Pomimo wzrostu procentowej zawartości azotu, wartości te nadal były niższe niż dla próbki z serii 1A-10 traktowanej przez 10 minut promieniowaniem mikrofalowym. Otrzymane wyniki wskazują, iż przy niewielkim nakładzie energii i krótkim czasie prowadzenia reakcji oraz odpowiednio dobranym rozpuszczalniku, można osiągnąć wyższe zawartości procentowe atomów azotu, które będą miały kluczowe znaczenie dla późniejszych zastosowań.

Analiza XPS potwierdziła obecność azotu w badanych materiałach, wskazując na dominację dwóch charakterystycznych typów wiązań azotu: azotu pirolowego zidentyfikowanego przy wartości energii wiązania 399.1 eV i azotu czwartorzędowego przy wartości energii wiązania 400.8 eV. Ogólna zawartość atomów azotu dla wszystkich próbek z serii 1A-T mieściła się w zakresie 0.6 do 2.7% at., co wskazuje, iż domieszkowanie azotem struktur na bazie grafenu za pomocą zielonych alg morskich jest skuteczną i efektywną metodą wprowadzenia azotowych grup funkcyjnych.

Elektrochemiczna weryfikacja

Charakter aplikacyjny otrzymanych materiałów potwierdzono, przeprowadzając testy elektrochemiczne. Materiały poddano testom elektrochemicznym w trójelektrodowym układzie pomiarowym, składającym się z elektrody odniesienia Ag/AgCl w 3 M KCl, przeciwelektrody – blaszki platynowej, natomiast jako elektrodę roboczą wykorzystano otrzymane katalizatory naniesione na elektrodę z węgla szklistego (ang. glassy carbon, GC). Dla porównania przeprowadzono również badania elektrochemiczne dla komercyjnego katalizatora firmy Sigma Aldrich, węgla z 20% wag. zawartością platyny (Pt/C). Przygotowany tusz dyspergowano w łaźni ultradźwiękowej przez 30 min, następnie naniesiono na elektrodę GC o średnicy 3 mm. Masa katalizatora naniesionego na powierzchnię elektrody GC wynosiła około 0.4 mg cm^{-2}. Przed przystąpieniem do badań elektrochemicznych roztwór elektrolitu nasycano O_2 następnie N_2 przez okres 20 minut. Aktywność próbek w reakcji redukcji tlenu oceniano w roztworze 0.1 mol L^{-1} KOH w temperaturze pokojowej, wykorzystując woltamperometrię cykliczną (CV). Pomiary wykonano przy szybkości skanowania 10 mV s^{-1}. Wykorzystano również woltamperometrię liniową (LSV) dla której pomiary wykonano przy szybkości skanowania 5 mV s^{-1} i prędkości obrotów w zakresie 800–2800 obr./min. Liczbę elektronów (n) bezpośrednio uczestniczących w reakcji ORR obliczono za pomocą równania (1) i (2) Koutecky'ego-Levicha (K-L):

$$J^{-1} = J_L^{-1} + J_K^{-1} = (B\omega^{1/2})^{-1} + J_K^{-1} \qquad (1)$$

$$B = 0.62nFC_0(D_0)^{2/3}\nu^{-1/6} \qquad (2)$$

Na rysunku 3a przedstawiono krzywe woltamperometrii cyklicznej (CV) dla próbek z serii 1A-T w roztworze alkalicznym. Dla próbek otrzymanych w EtOH zaobserwowano wyraźne piki katodowe, które wskazują na istniejącą aktywność katalityczną w reakcji redukcji tlenu. Dla próbek 1A-10, 1A-30, 1A-60 i 1A-90, piki katodowe występowały przy różnych potencjałach, tj. odpowiednio 0.75 V, 0.74 V, 0.81 V i 0.76 V vs RHE, co potwierdza, że materiały z serii 1A-T posiadają dobre właściwości elektrokatalityczne i mogą być obiecującymi katalizatorami dla reakcji redukcji tlenu. Natomiast w przypadku próbek z serii 1B-T, otrzymanych w DMF, zaobserwowano mniejszą aktywność katalityczną w porównaniu z próbkami z serii 1A-T.

Wszystkie otrzymane wyniki elektrochemiczne dla próbek z serii 1B-T zamieszczone są w pracy **[D2]** dołączonej do dysertacji.

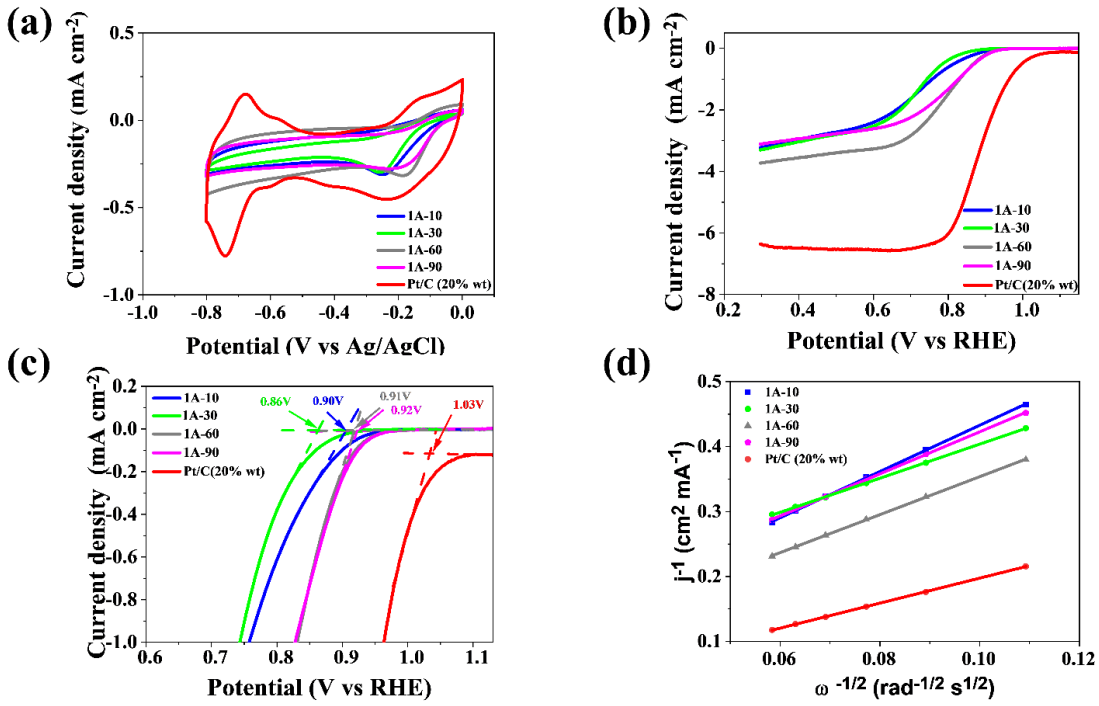

Rys. 3. Wyniki dla serii 1A-T porównane z katalizatorem Pt/C: (a) krzywe CV zmierzone z prędkością skanowania 100 mV s^{-1} w elektrolicie nasyconym O_2, (b) krzywe LSV zmierzone z prędkością skanowania 5 V s^{-1}, z prędkością obrotów 1600 obr./min, (c) potencjał początkowy, (d) krzywe K-L dla próbek przy 0.45 V.

Krzywe CV dla próbek z serii 1B-T wykazywały mniejszą gęstość prądu oraz niewyraźny pik katodowy. To sugeruje, że materiały z serii 1B-T posiadają mniejszą aktywność katalityczną w badanej reakcji, co może być związane z wpływem rodzaju rozpuszczalnika (DMF) na proces otrzymywania tych materiałów.

Krzywe woltamperometrii liniowej LSV zostały zmierzone dla próbek z dwóch serii (1A-T i 1B-T) oraz dla komercyjnego materiału elektrodowego Pt/C. Na rysunku 3b przedstawiono krzywe LSV dla próbek z serii 1A-T przy prędkości obrotowej 1600 rpm. Próbka 1A-60 wykazała najwyższą gęstość prądu granicznego spośród próbek z serii 1A-T. Wyniki wskazują, że próbka 1A-60, mimo niskiej zawartości azotu (0.65% wag.), posiada dobre właściwości katalityczne w reakcji ORR. Wartość potencjału początkowego (rys. 3c) dla tej próbki wynosi 0.91 V, świadczy to o zajściu redukcji tlenu na katalizatorze. Krzywe LSV dla próbek z serii 1B-T, ze względu na niską gęstość graniczną próbki, w których wykorzystano DMF wykazują typową dwuelektronową

ścieżkę redukcji tlenu podobnie jak materiały węglowe. Wyliczona liczba przenoszonych elektronów podczas reakcji redukcji tlenu pozwoliła na określenie mechanizmu.

Wykazano, że próbki 1A-30 oraz 1A-60 charakteryzowały się zbliżonym mechanizmem, gdzie wyznaczona liczba elektronów (n) wynosi odpowiednio 3.46 oraz 3.10, podczas, gdy pozostałe materiały otrzymane w serii 1B-T wykazują dwuelektronową ścieżkę redukcji tlenu (Tabela 1). Przedstawione wyniki pozwalają na stwierdzenie, że otrzymane materiały posiadają bardzo obiecujące właściwości katalityczne. Ponadto elektrokatalizatory domieszkowane heteroatomami azotu, w szczególności, odpowiednimi azotowymi grupami funkcyjnymi w strukturze grafenu, są odpowiedzialne za katalizowanie reakcji ORR.

Tabela 1. Liczba przeniesionych elektronów w reakcji ORR w 0.1 mol L^{-1} KOH dla próbek z serii 1A-T oraz 1B-T w porównaniu do komercyjnego katalizatora Pt/C.

Katalizator	**Liczba przenoszonych elektronów w reakcji ORR (n)**
Pt/C	4.00
1A-10	2.55
1A-30	3.46
1A-60	3.10
1A-90	2.90
1B-10	2.55
1B-30	2.42
1B-60	2.49
1B-90	2.57

Podsumowanie

W odpowiedzi na postawione hipotezy, iż możliwa jest modyfikacja struktury grafenowej za pomocą promieniowania mikrofalowego, odnotowano tworzenie się 3D struktur zbudowanych z eksfoliowanych płatków grafenowych z jednoczesnym wzbogaceniem w atomy azotu, wykorzystując naturalne, zielone algi morskie (*Chlorella*

vurgalis). Otrzymane struktury są w większości efektywnie działającymi katalizatorami w reakcji ORR. W szczególności ustalono, że:

- zoptymalizowana metoda syntezy materiałów katalitycznych do zastosowania w reakcji redukcji tlenu, wykorzystująca metodę mikrofalową, jest skuteczną techniką do modyfikacji struktury ekspandowanego grafitu. W badaniach przeprowadzonych na ekspandowanym graficie, który poddano promieniowaniu mikrofalowemu przez okres 30 minut w rozpuszczalniku EtOH, odnotowano najlepsze właściwości elektrochemiczne.
- proces syntezy opierający się na zastosowaniu zielonych alg morskich (*Chlorella vulgaris*), jako nośnika azotu jest skutecznym podejściem. Analiza XPS wykazała, że zawartość procentowa azotu w próbce 1A-10 wyniosła 1.7% at., w strukturze materiału zidentyfikowano pirolowe grupy funkcyjne oraz azot czwartorzędowy, co miało istotny wpływ na jego działanie katalityczne.
- przeprowadzone badania pozwoliły na wytypowanie najlepiej działających w reakcji redukcji tlenu materiałów. Otrzymane materiały wykorzystujące w metodzie syntezy EtOH, charakteryzują się czteroelektronową ścieżką redukcji, co w konsekwencji sugeruje, że są one wysoce wydajne i selektywne w tej reakcji w środowisku zasadowym.

3.1.2. Materiały katalityczne na bazie grafenu – badanie wpływu $CaCO_3$ oraz ADC na modyfikację struktury oraz właściwości katalityczne w reakcji redukcji tlenu

Zgodnie z hipotezą badawczą, iż wykorzystanie templatów twardych np. $CaCO_3$ skutecznie przyczyni się do rozwinięcia struktury porowatej materiałów węglowych z jednoczesnym zachowaniem możliwość wzbogacania heteroatomami np. wykorzystując azodikarbonamid (ADC) w charakterze nośnika azotu, zaproponowano rozwiązanie, pozwalające na wykorzystanie otrzymanych materiałów jako katalizatorów reakcji ORR. Zgodnie z powyższą hipotezą, nadrzędnym celem prowadzonych badań było zwiększenie porowatości oraz odległości pomiędzy arkuszami grafenowymi. Zaproponowana metoda polegała na mechanicznym zmieszaniu bądź zawieszeniu wszystkich substratów (grafenu, $CaCO_3$ oraz ADC w odpowiednich stosunku reagentów) w wodnej mieszaninie karagenu. Dodatkowo, wykorzystano proces liofilizacji w celu usunięcia wody z próbek. Otrzymaną masę poddano procesowi karbonizacji w temperaturach 700°C, 800°C oraz 900°C. Schemat syntezy przedstawiono na rysunku 4, natomiast szczegółowy opis syntezy znajduje się w artykule naukowym **[D3]** dołączonym do dysertacji.

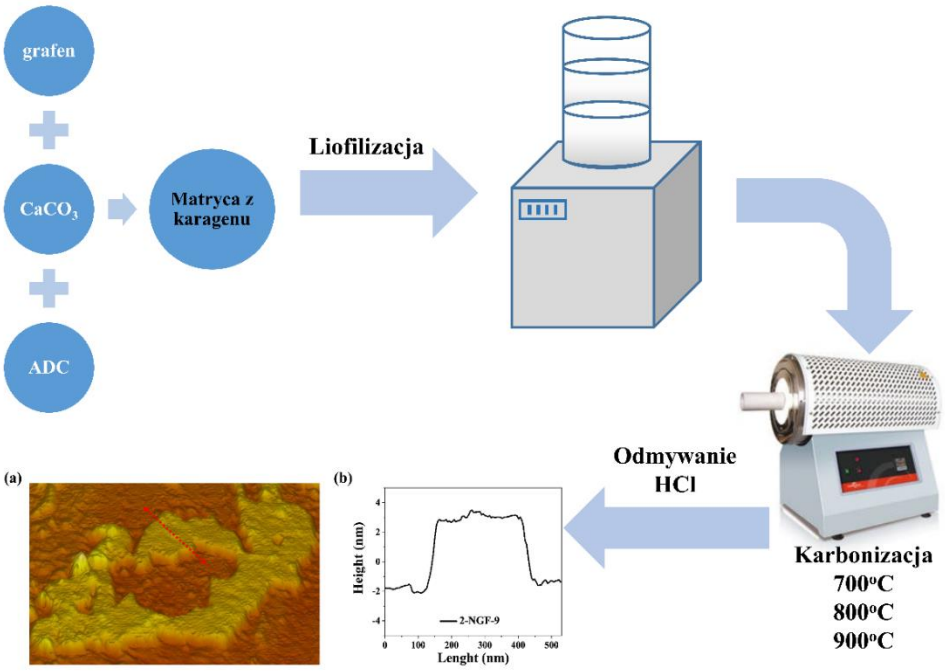

Rys. 4. Schemat syntezy otrzymywania grafenu modyfikowanego za pomocą twardego templatu $CaCO_3$ oraz ADC.

Otrzymane materiały oznaczono 1-NGF-T i 2-NGF-T, gdzie: 1 i 2 wskazują na stosunek masowy odczynników $CaCO_3$:ADC wynoszący odpowiednio 2:1 i 1:2; NGF oznacza piankę grafenową domieszkowaną azotem; T jest zastosowaną temperaturą karbonizacji 700°C, 800°C i 900°C, którą oznaczono odpowiednio jako 7, 8 i 9.

W celu zbadania wpływu zastosowanych modyfikacji na strukturę otrzymanych materiałów wykorzystano transmisyjny mikroskop elektronowy o wysokiej rozdzielczości (HRTEM). Struktura widoczna na obrazach HRTEM (rys. 5) świadczy o tendencji do nakładania się warstw grafenowych pomimo zastosowania templatu ($CaCO_3$).

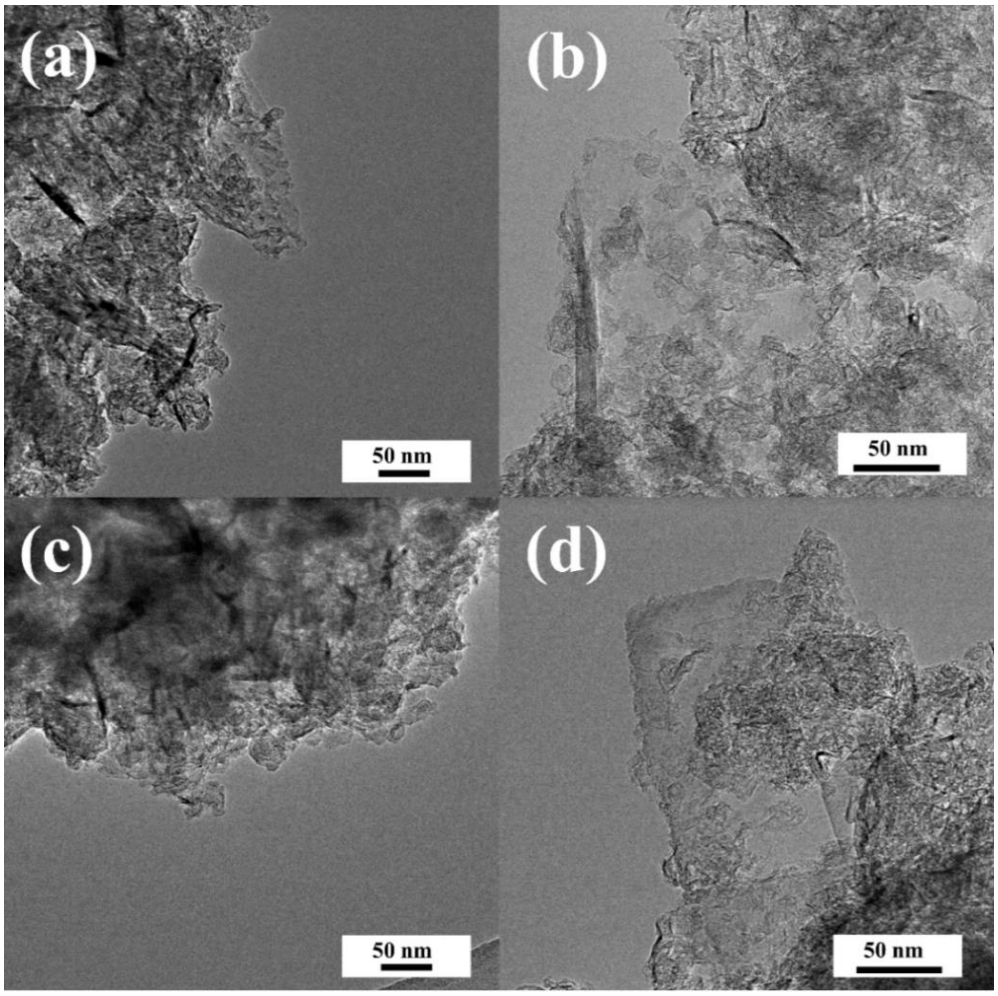

Rys. 5. Obrazy HRTEM dla próbek: (a) 1-NGF-8, (b) 2-NGF-8, (c) 1-NGF-9, (d) 2-NGF-9.

Ponadto zastosowany proces liofilizacji miał na celu zachowanie stanu separacji płatków grafenowych i utworzonej z nich struktury 3D. Jednak wiązania podtrzymujące strukturę 3D okazały się na tyle nietrwałe, że podczas przemywania próbek kwasem chlorowodorowym (usuwanie templatu węglanowego) ma miejsce zapadanie się

struktury 3D, co widoczne jest na rys. 5a i 5c dla próbek 1-NGF-8 i 1-NGF-9 (stosowano wyższe ilości $CaCO_3$). Struktura 3D oparta na elementach składających się z mniejszej ilości zlepionych arkuszy grafenowych, występuje dla próbek 2-NGF-8 i 2-NGF-9 z mniejszą zawartością węglanu wapnia (rys. 5b, 5d). Porowatość i wielkość pola powierzchni właściwej określono na podstawie wyników otrzymanych metodą niskotemperaturowej sorpcji azotu. Potwierdzono, że zastosowanie templatu węglanu wapnia nie wpłynęło znacząco na zwiększenie pola powierzchni właściwej S_{BET} (Tabela 2).

Wyniki analizy elementarnej (zawartość węgla, azotu i wodoru) dla serii 1-NGF-T, 2-NGF-T oraz wyjściowego materiału (GNPs) umieszczono w Tabeli 2. Dla serii 2-NGF-T wzrost temperatury karbonizacji prowadzi do wzrostu zawartości węgla w otrzymanych materiałach węglowych.

Tabela 2. Zawartość pierwiastków C, H i N określona za pomocą analizy elementarnej oraz pole powierzchni właściwej S_{BET} dla próbek z serii 1-NGF-T, 2-NGF-T oraz GNPs.

Próbka	**Zawartość procentowa pierwiastków (% wag.)**			**S_{BET} ($m^2\ g^{-1}$)**
	C	**H**	**N**	
GNPs	87.32	0.90	0.72	750
1-NGF-7	86.25	1.77	1.83	635
1-NGF-8	83.71	0.94	2.35	620
1-NGF-9	92.94	0.72	1.02	657
2-NGF-7	82.31	1.86	3.01	640
2-NGF-8	87.60	0.95	3.18	533
2-NGF-9	93.09	0.67	0.95	562

Dla serii 1-NGF-T i 2-NGF-T największą zawartość azotu odnotowano dla próbek karbonizowanych w temperaturze 800°C. Wykazano, że dla próbki 1-NGF-8 zawartość procentowa azotu wynosiła 2.35% wag. z kolei dla próbki 2-NGF-8 wynosiła 3.18% wag. Dlatego też można stwierdzić, że na zawartość procentową azotu ma wpływ nie tylko rodzaj zastosowanego nośnika azotu (ADC), ale również temperatura karbonizacji. Wraz z rosnącą temperaturą karbonizacji rośnie zawartość azotu, niemniej jednak próbki karbonizowane w 900°C wykazuję przeciwną tendencję i wykazują najniższą zawartość procentową azotu.

Pomiary XPS wykonano w celu określenia jakościowej i ilościowej zawartości grup funkcyjnych obecnych na powierzchni otrzymanych struktur grafenowych. Skład pierwiastkowy poszczególnych grup funkcyjnych przedstawiono w Tabeli 3. Szczegółowa analiza widm N1s pozwoliła na zidentyfikowanie grup azotowych obecnych w analizowanych materiałach. Czynnikiem determinującym aktywność katalityczną w reakcji ORR nie jest całkowita zawartość azotu, lecz zawartość poszczególnych azotowych grup funkcyjnych wbudowanych w strukturę grafenową. Na podstawie dekonwolucji widma N1s zidentyfikowano cztery pasma, charakteryzujące się energiami wiązań przy wartościach 398.5 eV, 400.2 eV i 402.3 eV oraz 404.5 eV odpowiadające azotowi pirydynowemu (N-6), azotowi pirolowemu (N-5), azotowi czwartorzędowemu (N-Q) oraz pirydynowemu N-tlenkowi (N-X).

Tabela 3. Skład pierwiastkowy pianek grafenowych domieszkowanych azotem określony za pomocą analizy XPS dla próbek z serii 1-NGF-T oraz 2-NGF-T.

Próbka	**C (at. %)**	**O (at. %)**	**N (at. %)**	**Azotowa grupa funkcyjna (% at.)**				**(N-5) i (N-6) (% w stosunku do całkowitego N)**
				N-5	**N-6**	**N-Q**	**N-X**	
1-NGF-7	94.1	3.9	2.1	1.3	0.2	0.3	0.3	71%
1-NGF-8	93.5	4.1	2.2	1.5	0.4	0.2	0.1	86%
1-NGF-9	95.0	3.7	1.0	0.8	0.1	0.0	0.1	90%
2-NGF-7	93.4	3.9	2.7	1.5	0.7	0.3	0.2	81%
2-NGF-8	94.6	3.1	1.9	1.2	0.5	0.1	0.1	89%
2-NGF-9	94.7	4.2	0.7	0.5	0.2	0.0	0.0	100%

Powstanie odpowiednich grup funkcyjnych azotu było możliwe dzięki zastosowaniu w zaproponowanej metodzie azodikarbonamidu, który jest organicznym związkiem chemicznym posiadającym grupy aminowe oraz podwójne wiązanie azotu N=N, które uległy przekształceniu w wysokich temperaturach prowadzonych procesów karbonizacji. W niniejszych badaniach wykazano, że temperatura karbonizacji ma istotny wpływ na zawartość azotu.

Elektrochemiczna weryfikacja

W celu potwierdzenia hipotezy badawczej dotyczącej aplikacyjności otrzymanych materiałów, zbadano aktywność katalityczną w reakcji ORR wykonując testy

elektrochemiczne w trójelektrodowym układzie zgodnie z procedurą przygotowania katalizatorów opisaną w pracy **[D3]**. Wszystkie otrzymane materiały wykazywały zwiększoną aktywność katalityczną w reakcji ORR, co można zaobserwować na woltamperogramach CV oraz krzywych LSV (rys. 6) dla próbek z serii 1-NGF-T. Pozostałe wyniki dla serii 2-NGF-T są zamieszczone w pracy [**D3**]. Sprawdzono wpływ temperatury karbonizacji na modyfikację struktury i właściwości elektrochemiczne otrzymanych nowych materiałów. Analiza wyników dla serii 1-NGF-T wskazuje, że próbka karbonizowana w temperaturze 900°C (1-NGF-9), najlepiej katalizuje reakcję ORR w środowisku zasadowym. Pik katodowy wyraźnie widoczny na rysunku 6a przesunięty jest w stronę dodatnich wartości i wynosi 0.83 V vs RHE. Potencjał początkowy (rys. 6b, 6d) dla próbki 1-NGF-9 wynosi 0.89 V vs RHE, wartość ta świadczy o szybkości zajścia reakcji redukcji tlenu. Kształt krzywej LSV dla próbki 1-NGF-9 jest bardzo zbliżony do kształtu komercyjnego katalizatora Pt/C i wykazuje duży prąd ograniczający dyfuzję wynoszący 5.30 mA cm^{-2}. Pozostałe materiały z serii 1-NGF-T charakteryzowały się niższą aktywnością katalityczną w porównaniu z próbką 1-NGF-9, która wykazywała czteroelektronową reakcję redukcji tlenu. Najwyższa aktywność katalityczna dla próbki 1-NGF-9 jest wynikiem wpływu rozbudowanej struktury porowatej skorelowanej z odpowiednim rodzajem azotowych grup funkcyjnych. Próbka o najwyższej aktywności katalitycznej posiada największą zawartość mezoporów, co wpływa korzystnie na łatwość wzbogacenia struktury w heteroatomy azotu, dostępność dla elektrolitu oraz ułatwia przenoszenie elektronów w środowisku zasadowym. Ponadto karbonizowanie próbek w temperaturze 900°C wpłynęło korzystnie na wyższy procentowy udział grup N-5 i N-6 w stosunku do ogólnej zawartości azotu. Liczbę przenoszonych elektronów dla serii 1-NGF-T oraz 2-NGF-T w reakcji ORR zbadane podczas weryfikacji elektrochemicznej przedstawiono w Tabeli 4. Liczba przeniesionych elektronów dla próbek 1-NGF-7 i 1-NGF-8 wynosiła odpowiednio 3.04 i 3.43. Pirydynowe i pirolowe grupy funkcyjne, zlokalizowane na krawędziach arkuszy grafenonwych, reagujące z grupami hydroksylowymi pochodzącymi z alkalicznych form elektrolitu tworzą jednocześnie centra aktywne, co w konsekwencji korzystnie wpływa na właściwości elektrochemiczne analizowanych materiałów. Seria 2-NGF-T wykazała również zwiększoną aktywność katalityczną w reakcji ORR, co potwierdza obecność pików katodowych na krzywych CV. Materiał karbonizowany w temperaturze 900°C wykazał bardzo wysoką gęstość prądu widoczną na krzywych LSV w porównaniu do próbek otrzymanych w temperaturze 700°C lub 800°C.

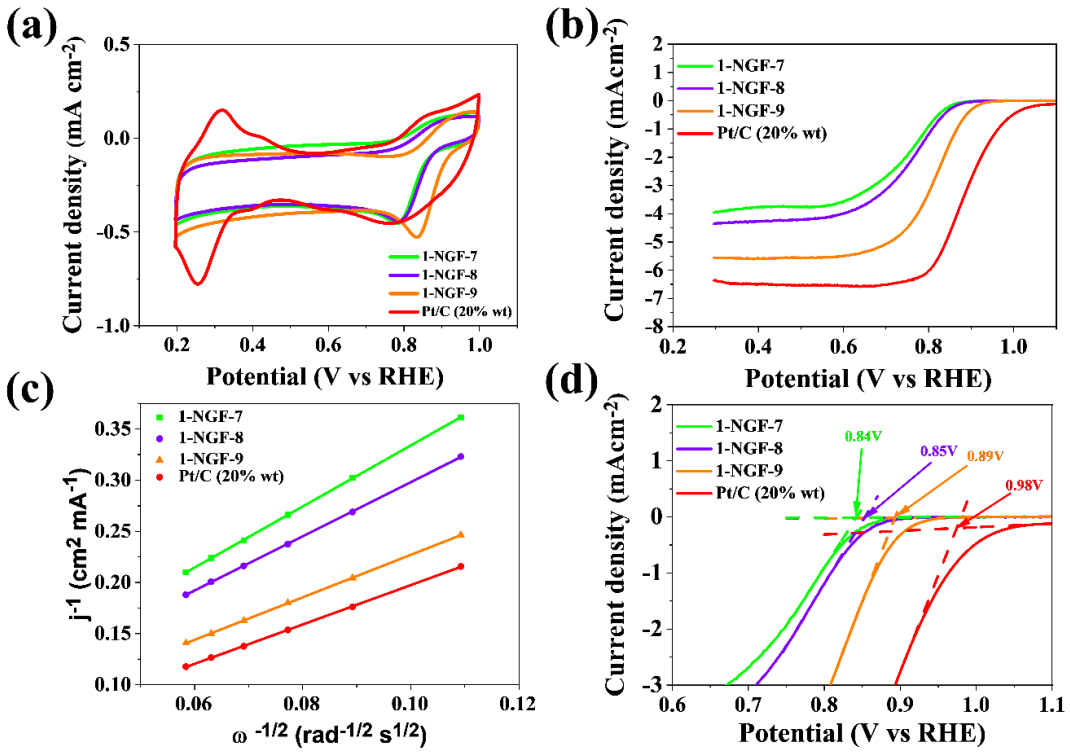

Rys. 6. Wyniki wydajności elektrochemicznej dla próbek z serii 1-NGF-T i Pt/C mierzone w nasyconym O_2 0.1 mol L^{-1} KOH: (a) krzywe CV otrzymane z szybkością skanowania 10 mV s^{-1}, (b) krzywe LSV otrzymane z szybkością skanowania 5 mV s^{-1} i prędkością obrotową 1600 obr./min, (c) krzywe K–L przy 0.5 V vs RHE, (d) potencjał początkowy.

Tabela 4. Liczba przeniesionych elektronów w reakcji ORR w 0.1 mol L^{-1} KOH dla próbek z serii 1-NGF-T oraz 2-NGF-T oraz komercyjnego katalizatora Pt/C.

Katalizator	Liczba przenoszonych elektronów w reakcji ORR (n)
Pt/C	4.00
1-NGF-7	3.04
1-NGF-8	3.43
1-NGF-9	4.00
2-NGF-7	3.32
2-NGF-8	3.35
2-NGF-9	3.82

Podobne wartości potencjału początkowego i prądu ograniczającego dyfuzję wskazują na niewielkie zróżnicowanie materiału, jednak wykazują aktywność katalityczną w stosunku do GNPs. Liczby elektronów przeniesionych dla próbek 2-NGF-7, 2-NGF-8 i 2-NGF-9

wynosiły odpowiednio 3.32, 3.35 i 3.82, co zbliża procesy elektrodowe do czteroelektronowej redukcji tlenu.

Wysoki wzrost aktywności katalitycznej otrzymanych materiałów w porównaniu do wyjściowych płatków grafenowych (GNPs) wynika z obecności aktywnych elektrochemicznie grup funkcyjnych zawierajacych azot. Tego typu grupy azotowe silnie wpływają na mechanizm reakcji redukcji tlenu. Aktywność katalityczną próbek 1-NGF-9 i 2-NGF-9 można przypisać obecności azotu pirydynowego, który determinuje aktywność elektrokatalityczną. W połączeniu z sąsiednim atomem węgla znacznie zwiększa efektywnośc reakcji ORR. Jako, że węgiel jest bardziej elektroujemnym pierwiastkem niż azot, może to prowadzić do oddania pary elektronowej do sąsiadujących atomów prowadząc do utworzenia się centrów aktywnych z dodatnimi ładunkami. Ponadto, pirolowe grupy azotowe są odpowiedzialne za wydajność ORR w środowisku alkalicznym. Dlatego też połączony efekt tych dwóch grup (azotu pirydynowego i azotu pirolowego) w próbkach 1-NGF-9 i 2-NGF-9, o najwyższej łącznej zawartości grup N-6 i N-5 wynoszacej 90% i 100% w całkowitej zawartości azotu, jest związany z największą liczbą przeniesionych elektronów. Wszystkie materiały otrzymane proponowaną metodą wykazały znaczącą aktywność katalityczną w reakcji ORR. Z badań wynika, że przebieg reakcji ORR wg mechanizmu czteroelektronowego przede wszystkim zależy od obecności odpowiednich grup azotowych, a w mniejszym stopniu od całkowitej procentowej zawartości azotu. Obecność pirolowych i pirydynowych grup funkcyjnych wpływa na szybką kinetykę reakcji na krawędziach grafenu wielowarstwowego. Otrzymane wyniki potwierdzają tezę, że aktywność katalityczna nie jest wprost proporcjonalna do całkowitej zawartości azotu, a otrzymane materiały są obiecującymi potencjalnymi elektrokatalizatorami dla baterii cynkowo-powietrznej.

Podsumowanie

W odpowiedzi na postawioną hipotezę badawczą, wykorzystanie templatów twardych $CaCO_3$ skutecznie przyczyni się do rozwinięcia struktury materiałów węglowych oraz wzbogacenie struktury grafenowej heteroatomami wykorzystując organiczny materiał chemiczny azodikarbonamid (ADC), pozwoli na wykorzystanie otrzymanych materiałów jako materiały katalityczne dla reakcji ORR, ustalono, że:

– wykorzystanie węglanu wapnia prowadzi do jego częściowego rozkładu pod wpływem wysokich temperatur karbonizacji (900°C), powodując powstanie struktury

porowatej o określonej wielkości porów. Ostatecznie nie wpłynęło to znacząco na zwiększenie pola powierzchni właściwej S_{BET} otrzymanych materiałów (zestawienie wyników w pracy **[D3]**).

- ADC zastosowany jako modyfikator i nośnik azotu przyczynił się do skutecznego wprowadzenia atomów azotu w zakresie od 0.7% do 2.7% zawartości atomowej. Zaobserwowano powstawanie grup azotowych typu pirydynowego (N-6), pirolowego (N-5), czwartorzędowego (N-Q) oraz pirydynowego N–tlenku (N-X). Odpowiedni rozmiar porów i obecność azotowych grup funkcyjnych pozwoliły na dobór właściwości otrzymywanych materiałów w taki sposób, aby wykazywały potencjalne zastosowanie elektrokatalityczne.
- przeprowadzone modyfikacje korzystnie wpłynęły na polepszenie aktywności katalitycznej w reakcji ORR w porównaniu do czystego grafenu. Otrzymane wyniki elektrochemiczne potwierdziły, że modyfikacja struktury grafenowej poprzez wprowadzenie azotowych grup funkcyjnych znacząco poprawiła jego zdolności katalityczne w reakcji ORR. Za pomocą testów elektrochemicznych potwierdzono aktywność otrzymanych materiałów w reakcji redukcji tlenu, co świadczy o możliwości potencjalnego wykorzystania nowych materiałów elektrodowych w urządzeniach do magazynowania i konwersji energii.

3.1.3. Materiały katalityczne na bazie grafenu – badanie wpływu naturalnych nośników azotu, żelatyny i chitozanu na modyfikację struktury oraz właściwości katalityczne w reakcji redukcji tlenu

W celu zweryfikowania hipotezy badawczej, iż wykorzystanie templatu twardego (Na_2CO_3) powoduje rozwinięcie struktury materiałów węglowych z zachowaniem możliwości wzbogacenia struktury grafenowej atomami azotu przez wykorzystanie naturalnych nośników azotu (żelatyny i chitozanu), przeprowadzono badania opisane w pracy **[D4]**. Działania te jednocześnie przyczynią się do poprawy właściwości katalitycznych w stosunku do reakcji ORR. Dla weryfikacji tej hipotezy zaproponowano metodę syntezy materiałów grafenowych przedstawioną na rysunku 7.

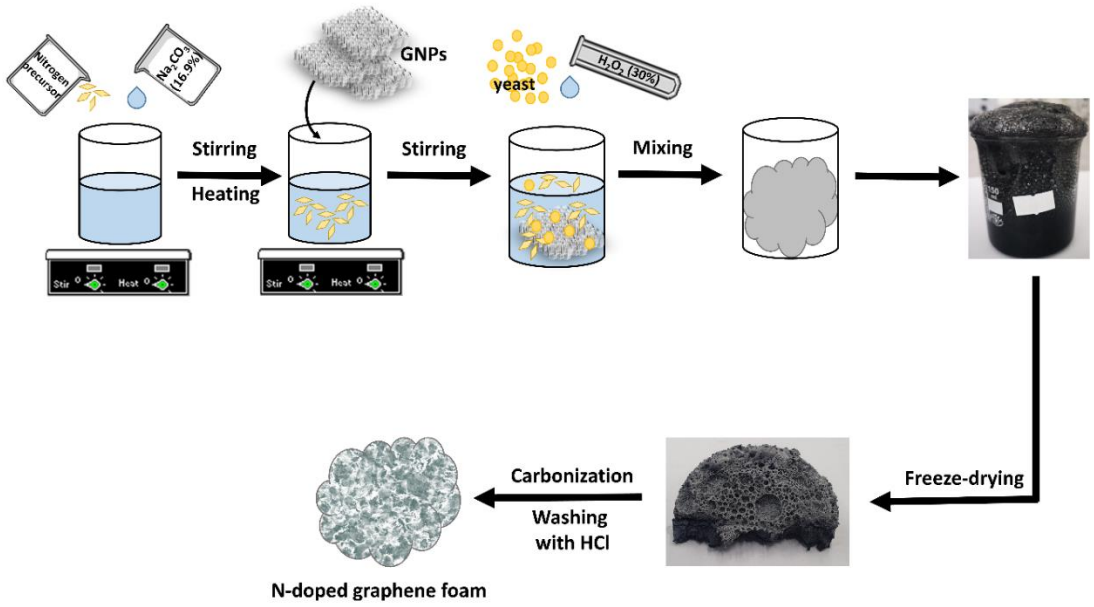

Rys. 7. Schemat syntezy pianek grafenowych prowadzonych z użyciem naturalnych polimerów żelatyny i chitozanu.

Komercyjne nanopłatki grafenowe (GNPs) zostały użyte jako źródło węgla, a żelatyna lub chitozan jako źródło azotu i medium do tworzenia hydrożelu. W pierwszej serii (1F) żelatynę i Na_2CO_3 (16.9% w/v) rozpuszczono w wodzie destylowanej, podgrzano do temperatury 90°C, następnie mieszano do momentu rozpuszczenia żelatyny, po czym dodano GNPs. Stosunek żelatyny do GNPs wynosił 2.5:1. Następnie do mieszaniny dodano drożdże i mieszano, w kolejnym kroku dodano perhydrol (30%). Drożdże i

perhydrol zostały użyte w celu utworzenia spienionej struktury. Drożdże działały jako katalizator rozkładu perhydrolu na wodę i tlen, przyspieszając w ten sposób proces rozkładu i utrzymując cząsteczki tlenu w matrycy żelatyny lub chitozanu. W drugiej serii (2F) chitozan został przygotowany w taki sam sposób jak w serii 1F, z tym wyjątkiem, że do żelowania chitozanu dodano roztwór składający się z mieszaniny H_2O/HCl. W obu seriach 1F i 2F próbki były poddane procesowi liofilizacji w celu usunięcia wody i utrzymaniu struktury trójwymiarowej. Materiał grafenowy po procesie liofilizacji przypominał pianę grafenową z widocznymi makroporami. Po procesie liofilizacji próbki poddano procesowi karbonizacji prowadzonemu w atmosferze N_2 w temperaturze 600°C, 700°C, 800°C lub 900°C. Do otrzymanych próbek dodano kwas chlorowodorowy w celu usunięcia wszystkich nieprzereagowanych substratów, następnie odmyto wodą destylowaną do uzyskania neutralnego pH, następnie suszono w suszarce elektrycznej aż do całkowitego odparowania wody. Materiały grafenowe domieszkowane azotem otrzymane z użyciem żelatyny oznaczono jako 1F_T, gdzie T oznacza temperaturę prowadzonego procesu karbonizacji wynoszącą 600°C, 700°C, 800°C lub 900°C. Druga seria materiałów grafenowych domieszkowanych azotem otrzymanych z wykorzystaniem chitozanu została oznaczona jako 2F_T.

Dla próbek 1F_800 i 2F_800 (rys. 8) widoczne są stosy składające się z kilku nakładających się na siebie warstw grafenowych, odległość między poszczególnymi warstwami grafenu wynosi 0.35 nm, co odpowiada wartości odległości opisywanej w literaturze dla aglomeratów grafenowych.

Pole powierzchni właściwej BET dla otrzymanych materiałów porównano z S_{BET} dla wyjściowego materiału GNPs (Tabela 5). W serii 1F_T próbka karbonizowana w temperaturze 800°C ma najwyższe pole powierzchni właściwej, wynoszące 861 $m^2 g^{-1}$. Powierzchnia właściwa pozostałych próbek 1F_600, 1F_700 i 1F_900 wynosiła odpowiednio 453 $m^2 g^{-1}$, 768 $m^2 g^{-1}$ i 795 $m^2 g^{-1}$. Dla serii 2F_T wraz ze wzrostem temperatury karbonizacji obserwowany jest wzrost pola powierzchni właściwej. Materiał 2F_600 otrzymany w temperaturze 600°C wykazuje najniższe pole powierzchni właściwej wynoszące 287 $m^2 g^{-1}$, zaś próbka 2F_900 karbonizowana w temperaturze 900°C ma najwyższe pole powierzchni właściwej równe 941 $m^2 g^{-1}$. Wartość otrzymanego pola powierzchni dla próbki 2F_900 jest wyższa, niż dla GNPs, o 191 $m^2 g^{-1}$.

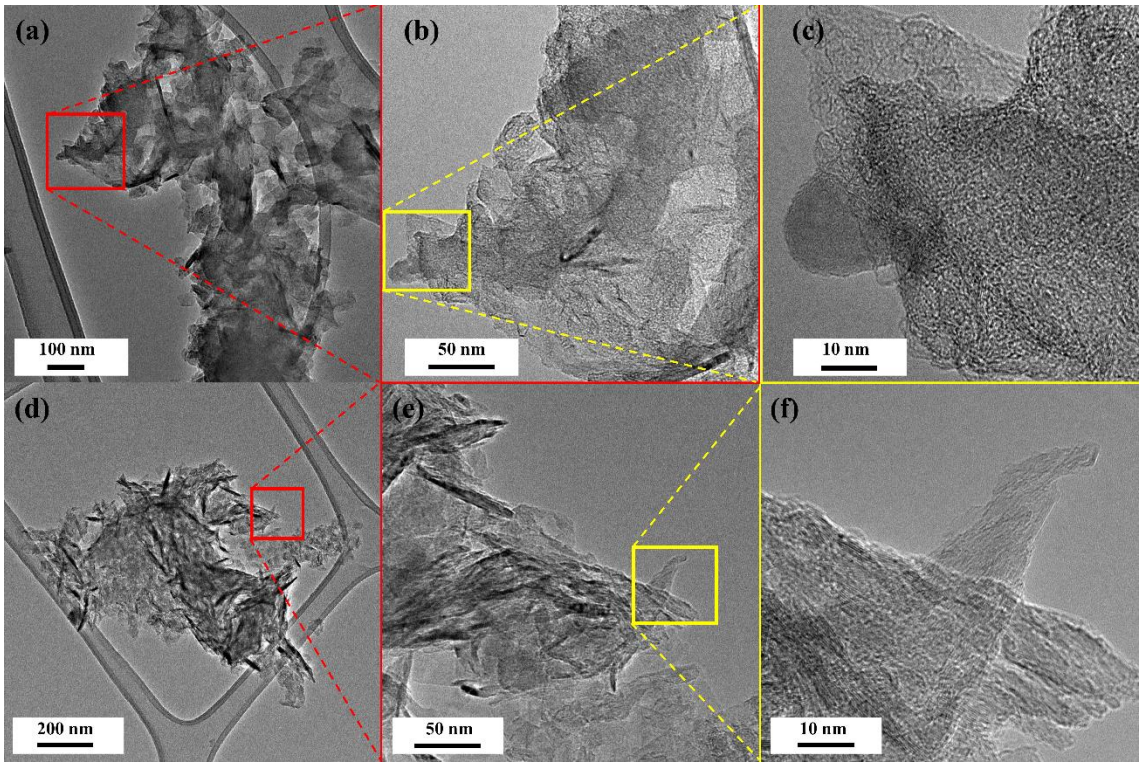

Rys. 8. Obrazy HRTEM dla próbek: (a–c) 1F-800 i (d–f) 2F-800, otrzymane przy różnych powiększeniach.

W celu zweryfikowania zakładanego celu, którego wynikiem miało być domieszkowanie azotem materiałów węglowych za pomocą żelatyny i chitozanu wykorzystano analizę elementarną, której wyniki zamieszczono w Tabeli 5.

Tabela 5. Skład pierwiastkowy atomów węgla, wodoru i azotu oraz pole powierzchni właściwej BET dla próbek z serii 1F_T i 2F_T oraz GNPs.

Próbka	**Zawartość procentowa pierwiastków (% wag.)**			**S_{BET}** **($m^2\ g^{-1}$)**
	C	**H**	**N**	
GNPs	87.32	0.90	0.72	750
1F_600	79.61	1.84	6.39	453
1F_700	83.54	1.63	3.93	768
1F_800	88.75	1.33	2.86	861
1F_900	96.07	0.97	2.39	795
2F_600	76.91	2.32	5.72	287
2F_700	78.74	1.41	5.16	648
2F_800	81.88	1.97	3.39	769
2F_900	93.65	0.93	2.43	941

W serii 1F_T procentowa zawartość azotu spada z 6.39% wag. do 2.39% wag. wraz ze wzrostem temperatury karbonizacji odpowiednio z 600°C do 900°C. Dla drugiej serii materiałów grafenowych 2F_T domieszkowanych azotem za pomocą chitozanu obserwowana jest analogiczna tendencja spadku zawartości azotu wraz ze wzrostem temperatury z 5.72% wag. do 2.43% wag. Obserwowana zmiana zawartości azotu jest wynikiem rozkładu nietrwałych grup azotowych, która następuje w wyższych temperaturach, co w konsekwencji skutkuje spadkiem całkowitej zawartości azotu w otrzymanych materiałach.

Analizę XPS przeprowadzono dla próbki 1F_800 (rys. 9a), a otrzymane wyniki pozwoliły na określenie rodzaju obecnych na powierzchni grup funkcyjnych. Szczegółowa analiza wysokorozdzielczych widm XPS C1s (rys. 9b) oraz O1s (rys. 9c) została przedstawiona w pracy [**D4**].

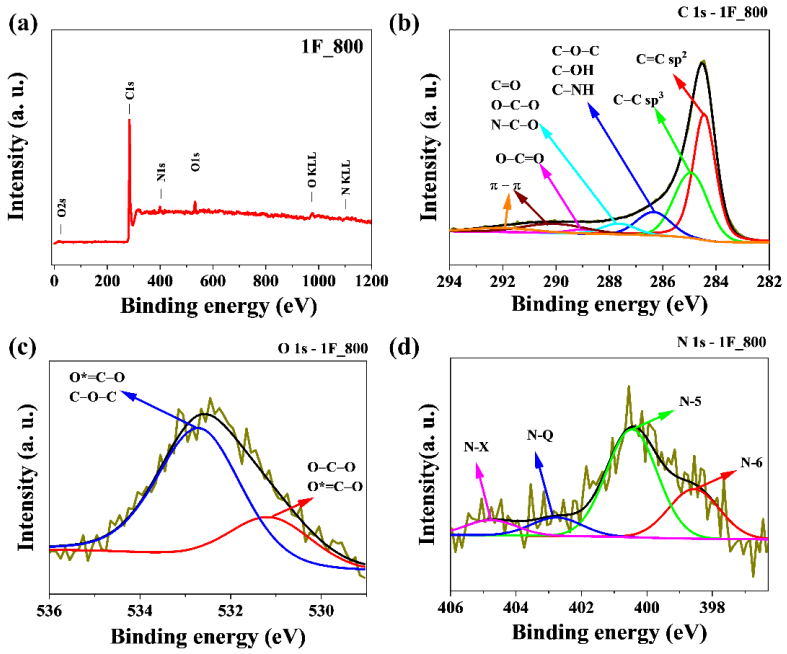

Rys. 9. (a) Widmo poglądowe XPS oraz widma wysokiej rozdzielczości: (b) C1s, (c) O1s, (d) N1s dla próbki 1F_800.

Dekonwolucja widma N1s (rys. 9d) pozwoliła na identyfikację czterech pasm odpowiadających energii wiązania 398.5 eV, 400.2 eV, 402.3 eV i 404.5 eV, które można przypisać obecności azotu pirydynowego (N-6), pirolowego (N-5), czwartorzędowego (N-Q) oraz pirydynowego N-tlenku (N-X). W przypadku próbki 2F_800 pasmo zlokalizowane przy wartości energii wiązania 404.5 eV nie jest widoczne, co oznacza, że tego typu wiązania N-X nie występują w tej próbce. Szczegółowa analiza zawartości

odpowiednich pierwiastków zidentyfikowanych dla otrzymanych materiałów została przedstawiona w Tabeli 6. Najwyższa łączna procentowa zawartość grup N-5 oraz N-6 przeliczona w stosunku do całkowitej zawartości azotu wynosi 92.11% dla próbki 2F_800 otrzymanej z wykorzystaniem chitozanu.

Tabela 6. Skład pierwiastkowy materiałów grafenowych domieszkowanych azotem określony za pomocą analizy XPS dla próbek 1F_800 oraz 2F_800.

Próbka	**C (at. %)**	**O (at. %)**	**N (at. %)**	**Azotowa grupa funkcyjna (at. %)**				**(N-5) i (N-6) (% w stosunku do całkowitej zawartości azotu)**
				N-5	**N-6**	**N-Q**	**N-X**	
1F_800	93.9	3.5	2.8	1.6	0.7	0.3	0.2	82.14
2F_800	89.9	6.3	3.8	2.3	1.2	0.3	0.0	92.11

Elektrochemiczna weryfikacja

Potencjalne zastosowanie otrzymanych materiałów grafenowych z wykorzystaniem naturalnych nośników azotu żelatyny i chitozanu zostało zweryfikowane z wykorzystaniem testów elektrochemicznych. Potwierdzona została hipoteza, że zastosowanie naturalnych nośników azotu sprzyja poprawie aktywności katalitycznej w reakcji ORR. Otrzymane materiały zostały przetestowane w celu określenia mechanizmu reakcji redukcji tlenu prowadzonej w roztworze alkalicznym. Krzywe woltamperometryczne (rys. 10a) otrzymane dla serii 1F_T posiadają charakterystyczne piki katodowe, co wskazuje na aktywność katalityczną otrzymanych materiałów. W przypadku próbek w serii 2F_T wyniki testów elektrochemicznyych zestawiono w pracy dołączonej do dysertacji [**D4**]. Pik katodowy dla próbek z serii 1F_T znajdował się w zakresie potencjałów od 0.77 do 0.80 V względem odwracalnej elektrody wodorowej (RHE). W serii 1F_T gęstość prądu na woltamperogramach CV dla próbki 1F_800 jest największa, w odnieieniu do pozostałych próbek z tej serii. W przypadku serii 2F_T widoczne jest przesunięcie piku katodowego w kierunku dodatnich wartości potencjału. Szczytowy zakres, w którym zachodzi redukcja tlenu dla próbek z serii 2F_T wynosi od 0.75 do 0.81 V vs RHE. W serii 2F próbka 2F_900 wykazuje kwadratowy kształt krzywych CV, a gęstość prądu jest największa dla tej próbki.

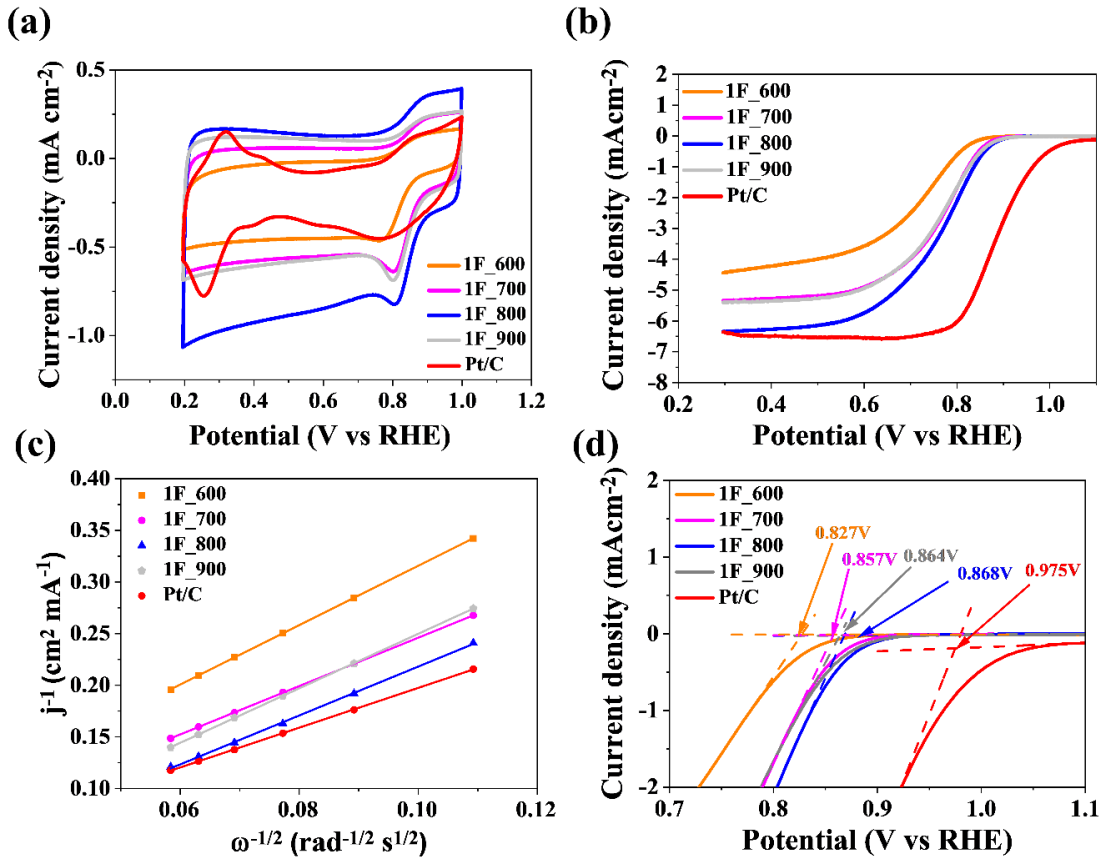

Rys. 10. Wyniki wydajności elektrochemicznej dla próbek z serii 1F_T i Pt/C w 0.1 mol L^{-1} KOH nasyconym O_2 (a) krzywe CV mierzone z szybkością skanowania 10 mV s^{-1}, (b) krzywe LSV mierzone z szybkością skanowania 5 mV s^{-1} i prędkością obrotową 1600 obr./min, (c) krzywe K–L przy 0.5 V vs RHE, (d) potencjał początkowy dla próbek z serii 1F_T.

Analizując woltamperogramy LSV (rys. 10b) przy szybkości skanowania 5 mV s^{-1} i szybkości przemiatania 1600 rpm, można wyselekcjonować najbardziej efektywne katalizatory reakcji ORR. Podobny kształt i zbliżoną wartość prądu granicznego do komercyjnego materiału Pt/C wykazuje próbka 1F_800. Dla drugiej serii 2F_T kwadratowy kształt z najwyższą gęstością prądu wykazują próbki karbonizowane w 800°C i 900°C (2F_800 i 2F_900). Biorąc pod uwagę wszystkie otrzymane materiały, dla próbek w serii 2F_T reakcja redukcji tlenu zachodzi szybciej i jest bardziej wydajna, co może być związane z występowaniem odpowiednich grup azotowych. Łączna zawartość procentowa grup N-5 i N-6 w stosunku do całkowitej zawartości azotu dla próbki 2F_800 jest bardzo wysoka i wynosi 92.11%. Dla serii 1F_T otrzymanej z wykorzystaniem żelatyny, wartości potencjału początkowego mieszczą się w zakresie od 0.83 do

0.87 V vs RHE. Najwyższą wartość potencjału początkowego, równą 0.87 V vs RHE ma próbka 1F_800. Wartości potencjału początkowego dla drugiej serii otrzymanej z udziałem chitozanu (2F_T) mieszczą się w zakresie od 0.81 do 0.90 V vs RHE, a najwyższą wartość odnotowano dla próbki 2F_900, która wynosi 0.9 V vs RHE. Na podstawie analizy krzywych LSV zmierzonych przy różnych prędkościach w zakresie od 800 do 2800 obr./min oraz wykorzystując równania i krzywe K-L, określono liczbę elektronów zaangażowanych w reakcję ORR i przedstawino w Tabeli 7. Obecność czwartorzędowych grup azotowych oraz przewaga grup pirydynowych wpłynęła na aktywność katalityczną otrzymanych materiałów w reakcji redukcji tlenu w roztworze alkalicznym. Należy podkreślić, że uzyskano materiały elektrodowe o bardzo wysokich wartościach i potwierdzających czteroelektronową redukcję tlenu w reakcji ORR.

Tabela 7. Liczba przeniesionych elektronów w reakcji ORR w 0.1 mol L^{-1} KOH dla próbek z serii 1F_T oraz 2F_T oraz Pt/C.

Katalizator	**Liczba przeniesionych elektronów w reakcji ORR (n)**
Pt/C	4.00
1F_600	3.16
1F_700	3.88
1F_800	3.84
1F_900	3.44
2F_600	3.19
2F_700	3.45
2F_800	3.99
2F_900	3.43

Podsumowanie

W odpowiedzi na postawioną hipotezę badawczą, iż zastosowanie modyfikacji struktury grafenowej poprzez wykorzystanie templatu twardego (Na_2CO_3) powoduje rozwinięcie struktury materiałów węglowych, w połączeniu ze wzbogaceniem struktury grafenowej atomami azotu (naturalne nośniki żelatyna i chitozan), przyczynia się do poprawy właściwości katalitycznych otrzymanych materiałów węglowych. Możliwe jest

ich zastosowanie jako materiałów elektrodowych dla reakcji ORR. W szczególności ustalono, że:

- w zaproponowanej metodzie modyfikacji grafenu istotną rolę odgrywało dodatkowe wykorzystanie drożdży oraz H_2O_2, które ostatecznie wpłynęło na utworzenie piankowych struktur grafenowych;
- wprowadzono skutecznie atomy azotu za pomocą naturalnych nośników (żelatyny i chitozanu) na poziomie 2.8 – 3.8% at. Biorąc pod uwagę również aspekt ekonomiczny, materiały węglowe bez metali ciężkich w strukturze, skutecznie eliminują konieczność wprowadzenia dodatkowych etapów utylizacji;
- wyniki testów elektrochemicznych wskazują na czteroelektronowy mechanizm redukcji cząsteczki tlenu (w roztworze alkalicznym). Wprowadzone azotowe grupy funkcyjne znacząco wpływają na właściwości elektrochemiczne zbliżając działanie otrzymanych elektrokatalizatorów do elektrod na bazie platyny.

3.1.4. Materiały elektrodowe na bazie sacharozy – badanie wpływu aktywatora H_3PO_4 oraz chitozanu na modyfikację struktury oraz właściwości elektrodowe w superkondensatorach symetrycznych

Praca [**D5**] jest elementem weryfikacji omawianych już wyżej hipotez badawczych. W pracy tej założono, że zwiększenie porowatości materiału elektrodowego i ukierunkowanie jego zdolności do magazynowania jonów, możliwe jest dzięki zastosowaniu kwasu H_3PO_4 oraz chitozanu jako nośnika azotu. W założeniach zaplanowana metoda będzie miała korzystny wpływ na takie właściwości jak przewodnictwo elektryczne oraz pojemność, szczególnie istotne dla zastosowania w superkondensatorach. Kwas ortofosforowy (V) znany jest jako tzw. aktywator sprzyjający rozwojowi struktury porowatej w materiałach węglowych ze znacznym udziałem mezoporów, które ułatwiają dyfuzję elektrolitu. Ogólny przebieg syntezy wraz z nazwami próbek przedstawiono na rysunku 11, syntezę porowatych materiałów węglowych przeprowadzono dla dwóch serii. W pierwszej serii do sacharozy dodano nanopłatki grafenu i dobrze wymieszano. W drugiej serii do sacharozy dodawano chitozan, uprzednio rozpuszczony w 1% roztworze CH_3COOH, a następnie wymieszano. Stosunek masowy reagentów sacharozy do chitozanu oraz sacharozy do grafenu wynosił 3:1 oraz 5:3, w następnym etapie dodano 3 lub 4.5 cm^3 H_3PO_4. Otrzymane materiały poddano procesowi karbonizacji prowadzonemu w temperaturze 900°C w atmosferze N_2.

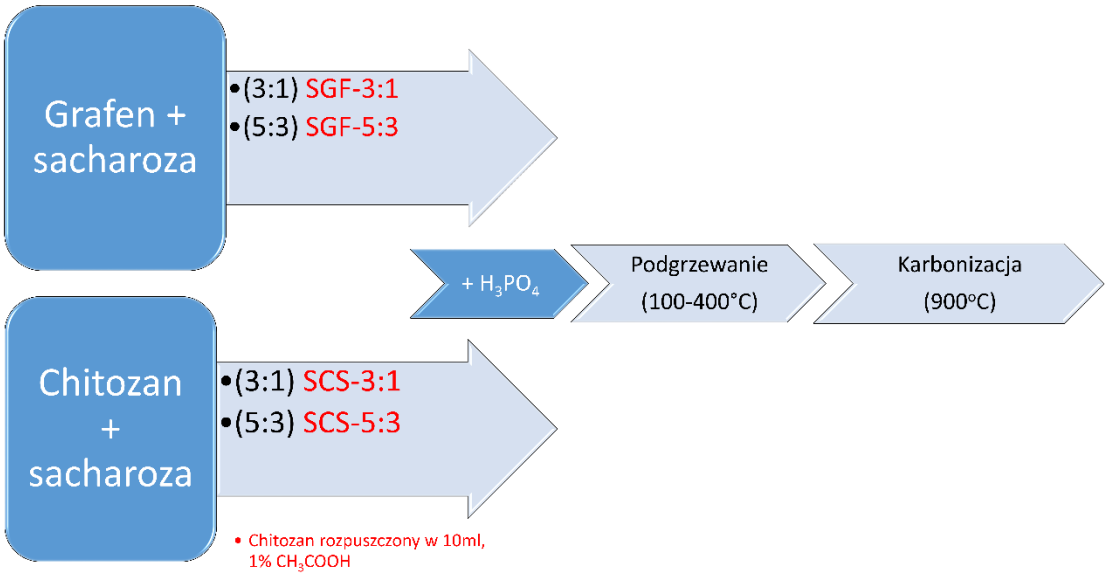

Rys. 11. Schemat syntezy struktur grafenowych otrzymanych z wykorzystaniem sacharozy, chitozanu oraz grafenu.

Nazwy próbek odpowiadały symbolom dla poszczególnych substratów użytych podczas syntezy: mieszaninę sacharozy (S) i chitozanu (CS) łącznie w nazwie oznaczono SCS, mieszaninę sacharozy (S) i grafenu (GF) łącznie w nazwie oznaczono SGF. Stosunek masowy (R) użytych odczynników, S:CS i S:GF, wynosił 3:1 lub 5:3. Wobec powyższego otrzymane próbki oznaczono SCS-R (SCS-3:1, SCS-5:3) i SGF-R (SGF-3:1, SGF-5:3).

Na rysunku 12 przedstawiono obrazy SEM dla próbek otrzymanych z sacharozy z dwoma różnymi modyfikacjami, chitozanem (SCS-R) i grafenem (SGF-R). Obrazy dla próbek z serii SGF-R (rys. 12a, 12c) i próbek z serii SCS-R (rys. 12b, 12d) wskazują na różnice w morfologii. Próbki zawierające w strukturze komercyjny grafen mają nierówną, chropowatą strukturę, natomiast próbki otrzymane z udziałem chitozanu mają gładką strukturę. Dla próbek posiadających bardziej gładką powierzchnię odnotowano nieznacznie niższe pola powierzchni właściwej tj. porównując odpowiednio próbki SGF-3:1 (1111 $m^2\ g^{-1}$) i SGF-5:3 (771 $m^2\ g^{-1}$) z próbkami SCS-3:1 (1313 $m^2\ g^{-1}$) i SCS-5:3 (841 $m^2\ g^{-1}$). Pole powierzchni właściwej (S_{BET}) próbek otrzymanych przy stosunku wagowym reagentów 5:3 jest niższe niż dla próbek otrzymanych dla stosunku reagentów 3:1 (Tabela 8). Wobec powyższego stwierdzono, że odpowiedni stosunek reagentów (3:1) oraz odpowiednia zawartości aktywatora (3 cm^3) wpływają korzystnie na wzrost S_{BET} otrzymanych materiałów węglowych.

Tabela 8. Skład pierwiastkowy węgla, wodoru i azotu oraz pole powierzchni właściwej S_{BET} dla próbek z serii SGF-R i SCS-R.

Próbka	**Zawartość procentowa (% wag.)**			**S_{BET} ($m^2\ g^{-1}$)**
	C	**H**	**N**	
GR	87.32	0.90	0.72	750
SGF-3:1	90.18	0.71	0.60	1111
SCS-3:1	67.79	1.54	1.97	1313
SGF-5:3	79.72	1.13	0.30	771
SCS-5:3	62.49	1.97	2.13	841

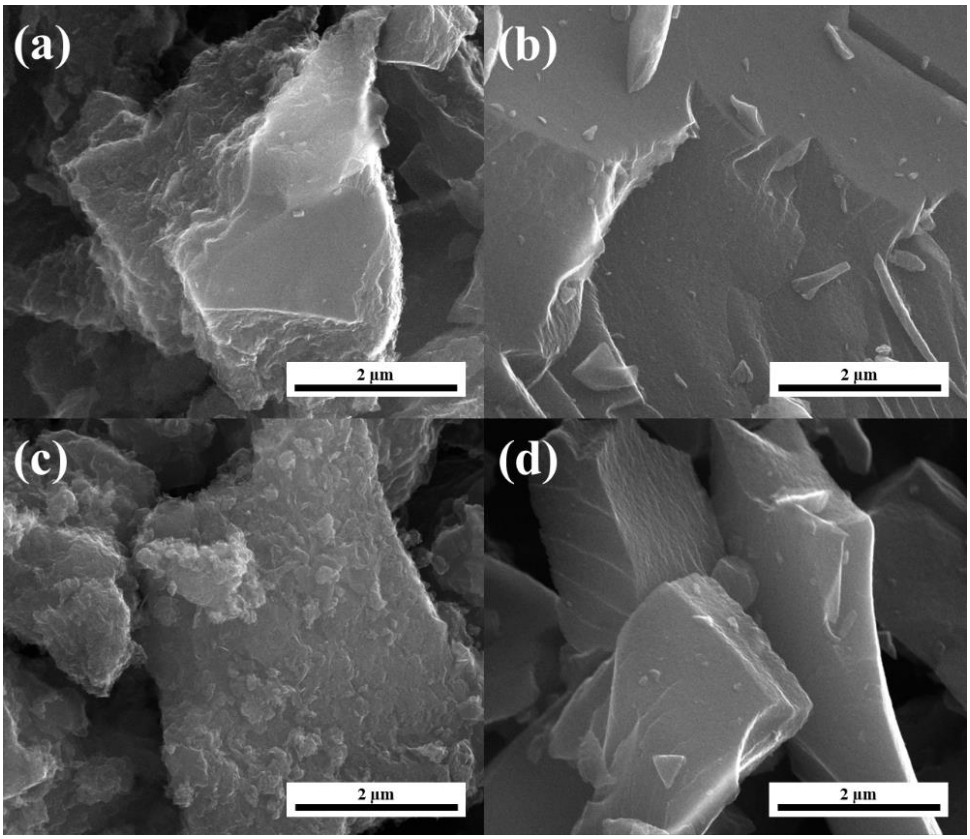

Rys. 12. Obrazy SEM dla próbek: (a) SGF-3:1, (b) SCS-3:1, (c) SGF-5:3 oraz (d) SCS-5:3.

Zastosowanie chitozanu przyczyniło się do otrzymania struktury węglowej domieszkowanej atomami azotu, co potwierdzają wyniki analizy elementarnej. Zawartość procentowa azotu dla próbek otrzymanych z wykorzystaniem chitozanu wynosi 1.97% wag. dla próbki SCS-3:1 i 2.13% wag. dla próbki SCS-5:3, podczas gdy zawartość azotu dla próbek otrzymanych z grafenem znacznie spadła i wynosi zaledwie 0.6% wag. dla próbki SGF-3:1 i 0.3% wag. dla próbki SGF-5:3. Przyczyną niskiej zawartości azotu dla próbek zawierających grafen jest brak wykorzystania podczas syntezy chitozanu. W celu ustalenia dokładnego składu pierwiastkowego oraz stanów chemicznych atomów obecnych na powierzchni materiałów węglowych wykorzystano technikę XPS. Analizie poddano próbki SGF-3:1 oraz SCS-3:1, a widma XPS przedstawiono na rysunku 13 dla próbki SCS-3:1, otrzymane wyniki potwierdziły obecność azotowych grup funkcyjnych. Próbka SGF-3:1 zawierała 0.9% at. azotu, podczas gdy próbka SCS-3:1 wykazuje wyższą zawartość wynoszącą 2.1% at. Zatem, potwierdzono, że domieszkowanie prekursora fazy węglowej (sacharozy) chitozanem (lub innym nośnikiem azotu) jest skutecznym sposobem regulacji zawartości azotu w

otrzymywanych materiałach węglowych. Widmo N1s dla próbki domieszkowanej azotem tj. SCS-3:1, zawiera jedno pasmo przy wartości energii wiązania 400.7 eV pochodzące od azotu czwartorzędowego (N-Q). Ponadto w otrzymanych próbkach zidentyfikowano obecność niewielkiej ilości fosforu. Widmo P2p (rys. 13d) potwierdza obecność fosforu w grupach P–C i P–O, co odpowiada pasmom przy wartościach energii wiązania 133.5 eV i 134.3 eV. Otrzymane wyniki potwierdzają, iż wykorzystanie kwasu ortofosforowego (V) jako aktywatora, powoduje efekt uboczny w postaci tworzenia wiązań fosforowych w formie grup estrowych czy polifosforanowych.

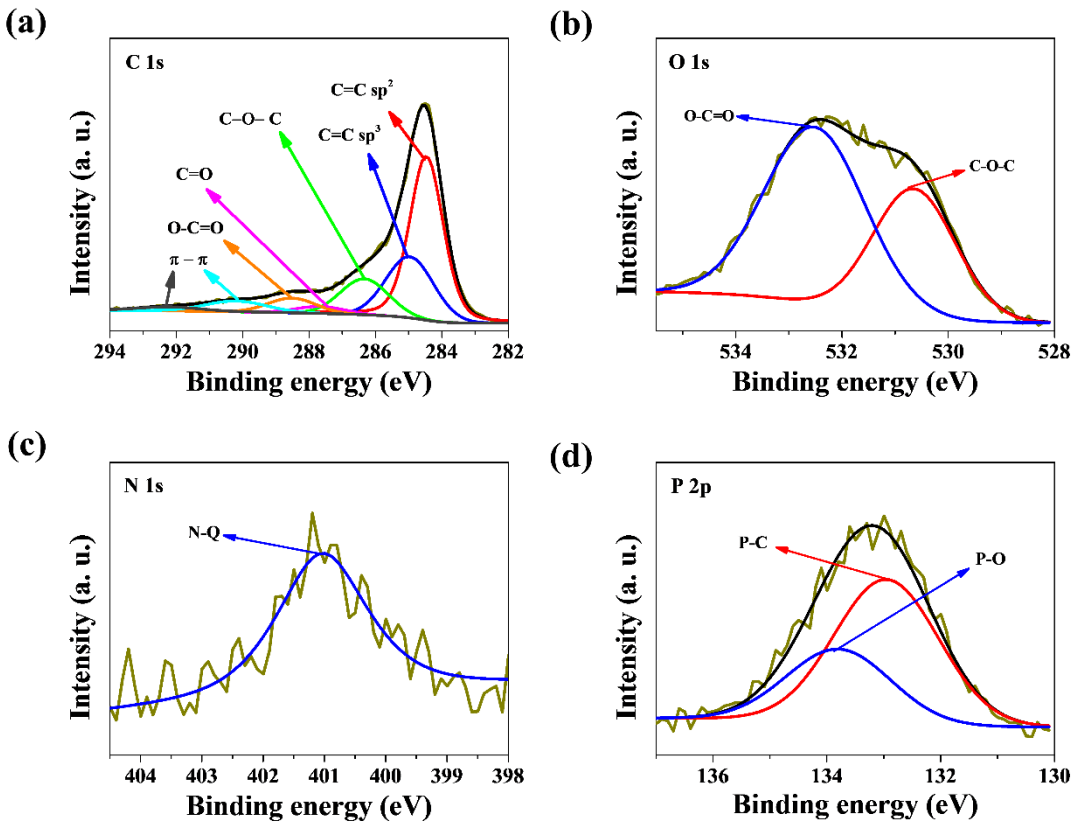

Rys. 13. Widma XPS o wysokiej rozdzielczości: (a) C1s; (b) O1s, (c) N1s i (d) P2p dla próbki SCS-3:1.

Elektrochemiczna weryfikacja

Zbudowano laboratoryjny model symetrycznego superkondensatora do badania otrzymywanych materiałów węglowych, którego schemat przedstawiono na rysunku 14.

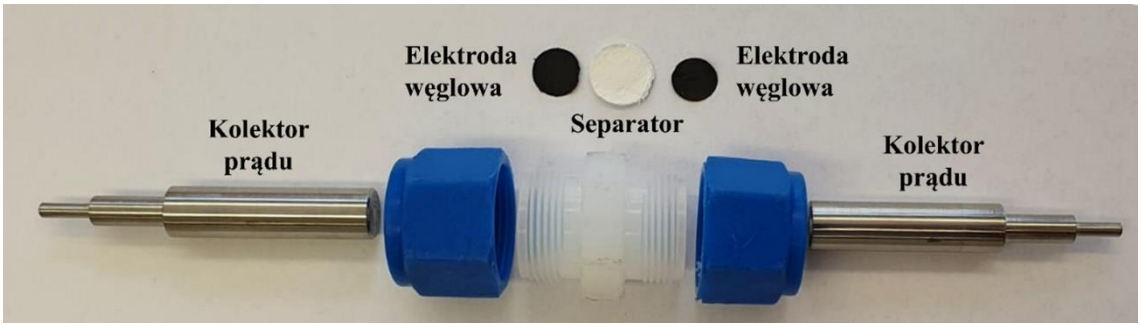

Rys. 14. Układ do badań dla superkondensatora dwuelektrodowego.

Właściwości elektrochemiczne próbek węglowych określono na podstawie przeprowadzonych badań elektrochemicznych. W tym celu przeprowadzono szczegółową charakteryzację otrzymanych materiałów za pomocą woltamperometrii cyklicznej (CV), cykli galwanostatycznego ładowania i rozładowania (GCD) oraz spektroskopii impedancyjnej (EIS) dla układu dwuelektrodowego. Szczegółowy opis przygotowania elektrod do pomiarów elektrochemicznych zamieszczony jest w pracy **[D5]**. Badania elektrochemiczne przeprowadzono w wodnym roztworze elektrolitu 6 mol L^{-1} KOH. Ładowanie/rozładowanie przeprowadzono przy różnych gęstościach prądu z zakresu od 0.1 do 1 mA g^{-1}. Impedancję elektrochemiczną mierzono w zakresie częstotliwości od 10^{-1} do 10^{5} Hz, amplituda wynosiła 10 mV. Pojemność właściwa C_s (F g^{-1}) (Równanie 1), gęstość energii E (Wh kg^{-1}) (Równanie 2) i gęstość mocy P (W kg^{-1}) (Równanie 3) zostały obliczone na podstawie następujących równań:

$$Cs = I \times \Delta t/(m \times \Delta V) \quad (1)$$

$$E = (C \times \Delta V2)/(8*3.6) \quad (2)$$

$$P = (E \times 3600)/\Delta t \quad (3)$$

gdzie: *I* to prąd ładowania i rozładowania (A), *Δt* to czas rozładowania (s), *ΔV* to zmiana potencjału w czasie rozładowania (V), *m* to średnia całkowita masa materiałów aktywnych w obu elektrodach.

Prostokątny kształt krzywej CV widoczny na rysunku 15 sugeruje szybką reorganizację podwójnej warstwy elektrycznej przy przełączanych potencjałach i świadczy o szybkim transporcie jonów, zapewniany przez idealny mechanizm magazynowania ładunku dla elektrostatycznych superkondensatorów dwuwarstwowych, EDLC.

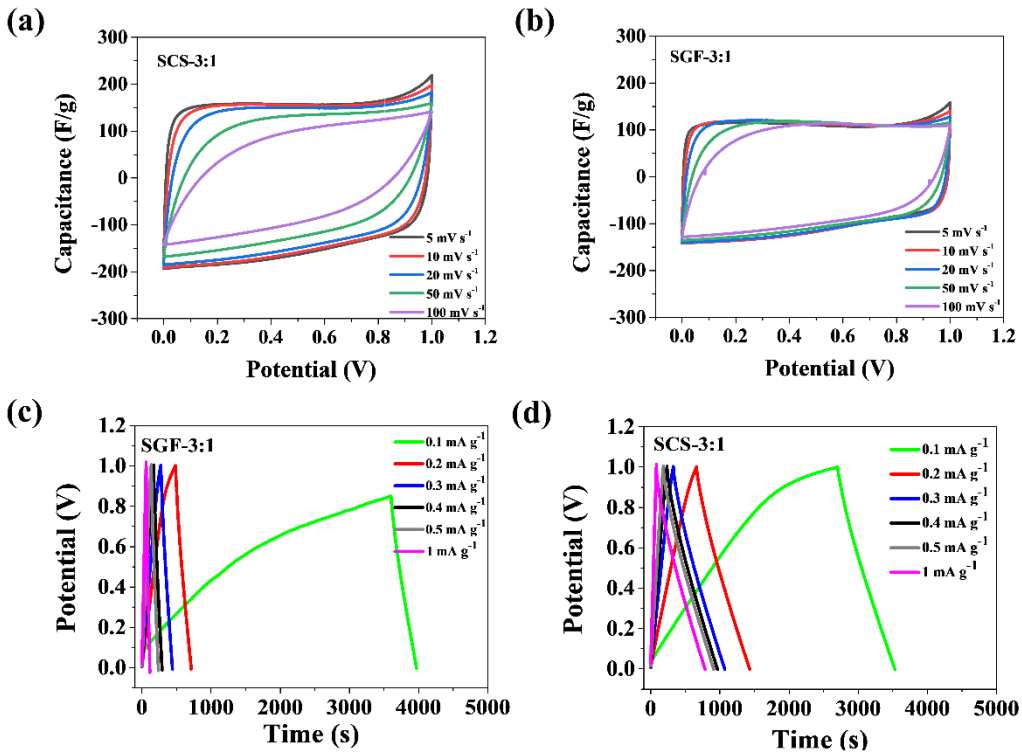

Rys. 15. Testy wydajności elektrochemicznej przeprowadzone dla próbek SCS-3:1 i SGF-3:1: (a, b) krzywe CV zmierzone przy różnych szybkościach skanowania w zakresie od 5 do 100 mV s^{-1}; (c, d) krzywe galwanostatyczne ładowania/rozładowania (GCD) zmierzone przy różnym obciążeniu prądowym z zakresu od 0.1 mA g^{-1} do 1 mA g^{-1}.

Prostokątny kształt krzywych zaobserwowano zarówno dla elektrody SCS-3:1, jak i SGF-3:1, co sugeruje idealne zachowanie pojemnościowe (rys. 15a, 15b). Dla próbki SCS-3:1 kształt krzywych CV otrzymanych przy różnych szybkościach skanowania mierzonych w układzie dwuelektrodowym jest prostokątny. Kluczową rolę w określaniu pojemności właściwej odgrywa powierzchnia właściwa i porowatość otrzymanych materiałów w szczególności wielkość porów powinna być większa niż jony elektrolitu. Próbki o najwyższym polu powierzchni posiadają najwyższą objętość mikroporów, równocześnie próbki te powinny charakteryzować się największą pojemnością właściwą i najniższą rezystancją, co zostało potwierdzone na podstawie otrzymanych wyników.

Pojemność właściwą (Cs) obliczono przy użyciu krzywych rozładowania galwanostatycznego (rys. 15c, 15d). Patrząc na krzywe ładowania i rozładowania próbek SCS-3:1 i SGF-3:1, elektroda SCS-3:1 wykazuje największą pojemność właściwą. Przy gęstości prądu 1 A g^{-1}, pojemność właściwa wynosiła 143 F g^{-1} dla elektrody SCS-3:1, zaś przy gęstości prądu 2 A g^{-1}, pojemność właściwa wynosiła 107 F g^{-1} dla próbki

SGF-3:1 (rys. 16a, 16b). Zastosowany stosunek reagentów w próbce SCS-3:1 korzystnie wpłynął na poprawę pojemności właściwej, poprzez interakcję otrzymanego materiału z anionami w elektrolicie alkalicznym. Porowata struktura otrzymanych materiałów zapewnia wystarczającą przestrzeń dla elektrolitu i umożliwia transport jonów, a tym samym poprawia wydajność superkondensatorów.

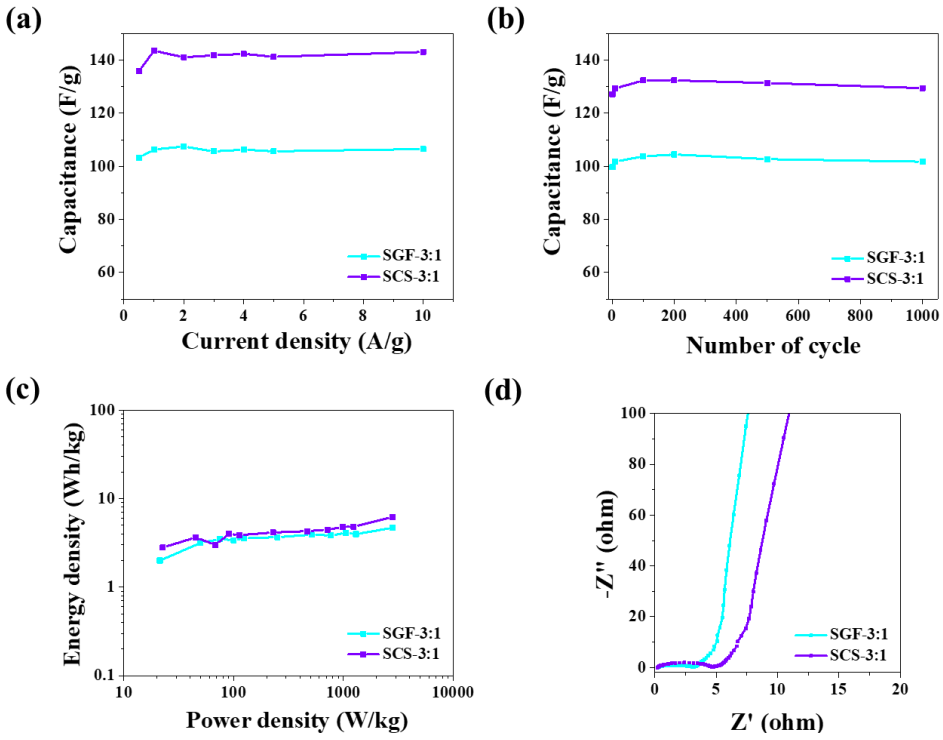

Rys. 16. Testy wydajności elektrochemicznej prowadzone dla próbek SCS-3:1 i SGF-3:1: (a) pojemność właściwa w funkcji gęstości prądu, (b) pojemność właściwa w funkcji liczby cykli, (c) pojemność właściwa w funkcji gęstości mocy, (d) krzywe Nyquista.

Pojemność właściwa podczas długotrwałych cykli ładowania/rozładowania elektrody SGF-3:1 wzrasta od wartości początkowej do 104 F g^{-1} w wyniku samoczynnej aktywacji. Po 200 cyklach rozładowania obserwuje się powolny spadek wartości pojemności właściwej, niemniej jednak po 1000 cyklach pojemność właściwa pozostaje na poziomie 97% (102%) retencji. Elektroda SCS-3:1 wykazuje pojemność właściwą, która wraz ze zwiększającą się ilością cykli powoli wzrasta do 132 F g^{-1} po 100 cyklach, po czym następuje spadek wartości pojemności właściwej, również do 97% (101%) retencji po 1000 cyklach (rys. 16b). Na podstawie powyższych danych wskazano, że mikroporowate elektrody węglowe na bazie sacharozy stosowane w superkondensatorach mają dobrą stabilność i retencję pojemności. Na rysunku 16c przedstawiono wykres

zależności między gęstościami energii, a gęstościami mocy, obliczone na podstawie pomiarów ładowania i rozładowania. Materiały otrzymane proponowaną metodą wykazują przy gęstości mocy 2.8 kW kg^{-1} dla próbek SGF-3:1 oraz SCS-3:1, gęstość energii wynoszącą odpowiednio 4.7 Wh kg^{-1} i 6.2 Wh kg^{-1}.

Podsumowanie

W odpowiedzi na postawioną hipotezę badawczą, iż modyfikacja struktury poprzez zwiększenie porowatości i aktywacja z zastosowaniem kwasu H_3PO_4 oraz chitozanu jako nośnika azotowych grup funkcyjnych wpływa pozytywnie na właściwości przewodzące i pojemnościowe do wykorzystania otrzymanych materiałów jako elektrod w superkondensatorach, ustalono, że:

- kwas H_3PO_4, jako aktywator skutecznie modyfikuje porowatą strukturę materiałów węglowych. Najwyższe pole powierzchni właściwej odnotowano dla próbek SGF-3:1 oraz SCS-3:1, dla których S_{BET} wynosi odpowiednio 1111 $m^2 g^{-1}$ oraz 1313 $m^2 g^{-1}$. Wszystkie otrzymane materiały posiadają porowatą strukturę, a zastosowanie chitozanu wpłynęło korzystnie na polepszenie właściwości elektrodowych.
- zaproponowane modyfikacje poprzez zastosowanie chitozanu jako nośnika azotu, pozwoliły na osiągnięcie wysokiej zawartości azotu równej 2.1% at. dla próbki SCS-3:1, ponadto wykazano obecność azotu czwartorzędowego (N-Q).
- poprzez testy elektrochemiczne określono parametry pojemności właściwej, które były zadowalające dla tego typu materiałów. Dla elektrody otrzymanej z wykorzystaniem chitozanu SCS-3:1, pojemność właściwa wynosiła 143 F g^{-1}, przy gęstości prądu 1 A g^{-1} zaś dla próbki otrzymanej z wykorzystaniem grafenu SGF-3:1, pojemność właściwa wynosiła 107 F g^{-1}, przy gęstości prądu równej 2 A g^{-1}.
- wyniki przeprowadzonych testów elektrochemicznych pozwoliły na wytypowanie najkorzystniejszego stosunku reagentów sacharozy do chitozanu lub grafenu, który wynosił 3:1, ostatecznie ma on wpływ na właściwości pojemnościowe, całkowitą zawartość azotu oraz na trwałość i wydajność w cyklach ładowania i rozładowania dla badanych superkondensatorów. Stwierdzono wysoką stabilność po 1000 cykli ładowania/rozładowania dla materiałów otrzymanych ze stosunkiem reagentów 3:1, co pozwala na stwierdzenie, iż otrzymane materiały elektrodowe będą mogły w przyszłości zastąpić komercyjne materiały elektrodowe na bazie metali ciężkich.

4. Podsumowanie i wnioski

Wyniki badań przeprowadzonych w ramach niniejszej rozprawy doktorskiej pozwoliły na przygotowanie podsumowania oraz wysunięcie następujących wniosków:

1. Modyfikacja struktury przyczyniająca się do rozwinięcia porowatości możliwa jest dzięki wykorzystaniu odpowiednio dobranych modyfikatorów (żelatyna, chitozan), templatów ($CaCO_3$, Na_2CO_3), a także aktywatora (H_3PO_4). Stosując odpowiednie parametry syntezy, odpowiedni czas utrzymania w reaktorze mikrofalowym, odpowiedni dobór rozpuszczalników czy zastosowanie wysokiej temperatury karbonizacji (600–900°C) możliwe jest korzystne przekształcenie struktury i dostosowanie odpowiedniej ilości warstw grafenowych, rozmiaru porów oraz zwiększenie pola powierzchni właściwej.
2. Wzbogacenie struktury węglowej poprzez zastosowanie odpowiednich nośników azotu (zielone algi morskie, żelatyna, chitozan, azodikarbonamid) przyczynia się do wprowadzenia do struktur węglowych azotowych grup funkcyjnych zawierających: azot pirydynowy (N-6), azot pirolowy (N-5), azot czwartorzędowy (N-Q) oraz azot pirydynowy N-tlenku (N-X). Połączenie właściwego doboru nośnika azotu oraz rozwinięcia parametrów strukturalnych materiału węglowego sprzyja tworzeniu azotowych grup funkcyjnych, których obecność wpływa korzystnie na aktywność katalityczną w reakcji ORR oraz zdolność do tworzenia warstwy podwójnej o znacznej pojemności elektrycznej.
3. Elektrochemiczna weryfikacja otrzymanych materiałów węglowych stosowanych jako elektrody w reakcji ORR i superkondensatorach potwierdziła możliwości aplikacyjne badanych materiałów. Zastosowanie odpowiednich metod syntezy oraz surowców powoduje, że otrzymane węglowe katalizatory w reakcji ORR wykazują zdolność do czteroelektronowej reakcji redukcji tlenu, pomimo braku platyny w ich składzie. Podobnie, można wytworzyć węglowe materiały elektrodowe przydatne do budowy superkondensatorów (EDLC), których walory aplikacyjne wynikają z parametrów strukturalnych (pole powierzchni właściwej, struktura porowata) jak i obecności azotowych grup funkcyjnych.

5. Publikacje naukowe wchodzące w skład rozprawy doktorskiej

[D1] M. Skorupska, A. Ilnicka, J. P. Łukaszewicz, *Successful Manufacturing Protocols of N-Rich Carbon Electrodes Ensuring High ORR Activity: A Review*, Processes, 2022, 10(4), 643; https://doi.org/10.3390/pr10040643 (IF=3.5, MEiN=70)

Poniższy artykuł naukowy stanowi przegląd literaturowy dotyczący materiałów domieszkowanych azotem do zastosowań jako materiały katalityczne w reakcji redukcji tlenu. W pracy krótko wyjaśniono mechanizm redukcji tlenu w środowisku zasadowym i kwaśnym. Przedstawiono zestawienie technik syntezy materiałów węglowych m.in. materiałów na bazie grafenu, nanorurek węglowych, porowatych materiałów węglowych naturalnego pochodzenia, a także nanowłókien grafenowych. Wiele doniesień literaturowych skupia swoją uwagę na metodach chemicznego osadzania z fazy gazowej (ang. chemical vapor deposition, CVD), która jest jedną ze skutecznych metod otrzymywania czystego grafenu, niemniej jednak uwzględniając aspekt ekonomiczny metoda ta nie jest wystarczająco wydajna do produkcji na skalę przemysłową. Ponadto w zaprezentowanym artykule przedstawiano również metody, które mają potencjał do komercjalizacji i produkcji na dużą skalę. Potencjał taki wykazuje m.in. połączenie dwóch metod hydrotermalnej oraz pirolizy, które za sprawą niewielkich modyfikacji, zmian źródła węgla i azotu, a także odpowiednio dobranych temperatur procesu mogą przyczynić się do otrzymywania materiałów o właściwościach porównywalnych z komercyjnymi katalizatorami na bazie metali ciężkich. W przedstawionym przeglądzie literaturowym opisano również hipotezy dotyczące bezpośredniego wpływu na aktywność katalityczną azotowych grup funkcyjnych (N-5, N-6, N-Q). Jednakże należy pamiętać, że wszystkie te grupy mają wpływ na właściwości katalityczne w reakcji ORR lecz z różnym skutkiem. Grupy pirydynowe odpowiadają za wzrost potencjału początkowego podczas gdy azot czwartorzędowy wpływa na graniczną gęstość prądu, dlatego też poprzez zmianę ich zawartości, możliwa jest kontrola aktywności katalitycznej. Ponadto, właściwości strukturalne i morfologia próbki, odgrywają pośrednią rolę w zmianie właściwości katalitycznych, które mogą ułatwić bądź utrudnić dostęp do miejsc aktywnych. Podsumowując, wykazano, że wysoka wydajność elektrokatalizatorów na bazie węgla zależy od odpowiedniej korelacji pomiędzy przewodnictwem elektronów, powierzchnią właściwą, a zawartością azotowych grup funkcyjnych.

processes

MDPI

Review

Successful Manufacturing Protocols of N-Rich Carbon Electrodes Ensuring High ORR Activity: A Review

Malgorzata Skorupska [1], Anna Ilnicka [1,*] and Jerzy P. Lukaszewicz [1,2]

[1] Faculty of Chemistry, Nicolaus Copernicus University in Torun, Gagarina 7, 87-100 Torun, Poland; m.skorupska@doktorant.umk.pl (M.S.); jerzy_lukaszewicz@o2.pl (J.P.L.)
[2] Centre for Modern Interdisciplinary Technologies, Nicolaus Copernicus University in Torun, Wilenska 4, 87-100 Torun, Poland
* Correspondence: ailnicka@umk.pl; Tel.: +48-609273793

Abstract: The exploration and development of different carbon nanomaterials happening over the past years have established carbon electrodes as an important electrocatalyst for oxygen reduction reaction. Metal-free catalysts are especially promising potential alternatives for replacing Pt-based catalysts. This article describes recent advances and challenges in the three main synthesis manners (i.e., pyrolysis, hydrothermal method, and chemical vapor deposition) as effective methods for the production of metal-free carbon-based catalysts. To improve the catalytic activity, heteroatom doping the structure of graphene, carbon nanotubes, porous carbons, and carbon nanofibers is important and makes them a prospective candidate for commercial applications. Special attention is paid to providing an overview on the recent major works about nitrogen-doped carbon electrodes with various concentrations and chemical environments of the heteroatom active sites. A detailed discussion and summary of catalytic properties in aqueous electrolytes is given for graphene and porous carbon-based catalysts in particular, including recent studies performed in the authors' research group. Finally, we discuss pathways and development opportunities approaching the practical use of mainly graphene-based catalysts for metal–air batteries and fuel cells.

Keywords: heteroatom doping; carbon-based nanostructure; doped graphene; oxygen reduction reaction; air electrode; metal-free electrocatalysts

Citation: Skorupska, M.; Ilnicka, A.; Lukaszewicz, J.P. Successful Manufacturing Protocols of N-Rich Carbon Electrodes Ensuring High ORR Activity: A Review. *Processes* **2022**, *10*, 643. https://doi.org/10.3390/pr10040643

Academic Editor: Angela Scala

Received: 28 February 2022
Accepted: 17 March 2022
Published: 25 March 2022

1. Introduction

In recent years, the technological revolution has been based predominantly on new materials with specific properties that could become alternatives to uneconomic and environmentally unfriendly materials. The search for new electrode materials can be ascribed to this trend; it is one of the key issues that need to be resolved regarding the construction of effective novel devices for energy storage and/or generation. The elimination of noble metals from electrodes is commonly seen as an essential technological problem to be solved in the upcoming years.

The oxygen reduction reaction (ORR) plays a vital role in those energy storage devices, such as fuel cells and metal–air batteries, whose high energy density makes them promising solutions [1–5]. Diverse forms of carbon materials, primarily graphene, carbon nanotubes (CNTs), amorphous carbon, and carbon nanofibers, are summarized in this paper and have been studied intensively regarding their effectiveness as electrocatalysts for ORR [6]. Carbon structures are doped with heteroatoms (e.g., boron, nitrogen, sulfur, or phosphorus) [7–10] to enhance the materials' catalytic activity. Despite extensive knowledge of the excellent activity of heteroatom-doped carbon materials in the oxygen reduction reaction, their mechanism and the function they play in ORR are still under investigation. Theoretical studies and experimental works on nitrogen-doped graphene structures consistently demonstrate promising catalytic properties that could lead such

modified materials to successfully replace platinum-based carbon catalysts. The frequently discussed substitution of carbon atoms at the edge of the graphene sheet by nitrogen gives an incomplete picture of the doping mechanism and function. Recently, experimental results have brought new insights into this topic. In the case of graphene, it has been shown that doping with nitrogen atoms causes the formation of nitrogen functional groups, not only at the edges of graphene sheets, but also built into the structure, forming pyrrolic nitrogen (N-5), pyridinic nitrogen (N-6), and graphitic nitrogen (N-Q) [11]. Thus, many problems remain to be solved [12] in the area of carbon material applicability to ORR. Due to the low catalytic activity of carbon materials in acidic solutions, further design and fabrication of new materials to be used in energy storage devices is required.

Insertion of nitrogen atoms onto the surface of graphene materials can also lead to the formation of defects, for instance, at the edges of carbon tubes and graphene planes. Another set of effects may occur upon carbonization at high temperatures, which in general increases the level of graphitization and defect dissolution. These two counter-structural effects may in parallel contribute to the change of velocity and the quantity of ORR active sites, resulting in either improvement or decay of catalytic activity in ORR. It has been proven that defects of different sorts often have significant effects on the mechanism of ORR in an alkaline medium, while an analogous effect in an acidic medium is observed less intensively [13]. It has been suggested that a higher heteroatom content level results in an increased amount of defects in the structure and contributes to improved catalytic activity [14]. Nevertheless, it is a fact that a nitrogen atom in the graphene structure couples its electron pairs together with a carbon of sp^2 hybridization in the π system. The N-6 groups located in the hexahedral carbon ring are incapable of donating an electron to the delocalized π aromatic system. Conversely, N-Q groups built into the carbon atom site in the graphene plane are capable of donating an electron to the delocalized π structure [15]. Such doping is crucial for ORR improvement, since the π electrons in the hexagonal carbon rings hardly participate in the processes comprising the whole oxygen reduction reaction. Therefore, the added electrons coming from the nitrogen atom result in a higher energy density, increasing the energy level in the highest level of the carbon molecular orbital. Following the same mechanism, heteroatom dopants that exhibit an electron deficit, such as the boron atom, seek additional electrons and thus couple their orbitals in the carbon π system. Still, the problem of the most active sites is unclear. The four-electron reduction of oxygen is attributed to N-pyridine functional groups by some, while others attribute this ability to N-Q groups or the presence of both groups in the structure [16–18]. However, what researchers agree on is the hypothesis that the nitrogen atom affects the carbon structure, thus inducing the ability to adsorb oxygen molecules from the air by breaking the double bond in the O_2 molecule [19]. While H_2O molecules are produced during oxygen reduction, it is most beneficial when the electrode is hydrophobic. This avoids flooding of the electrode, which would result in blocking newly diffused oxygen molecules. The introduction of nitrogen into the structure nullifies the hydrophobic properties due to, among other things, the fact that the pretreatment of carbonaceous materials takes place with, for example, nitric acid (HNO_3), which effectively contributes to the deterioration of the catalytic activity in ORR [20,21]. During the synthesis of doped carbon structures, coassembly of oxygen groups and heteroatom groups can occur, thereby producing a defective structure and reducing the hydrophobic properties of the final material. In addition, if the electrode is devoid of these properties, the electrolyte in which the test is being conducted itself can be impaired, reducing the wettability of the electrode material. As a result, electrodes have a short lifetime.

Electrocatalytic activity is affected not only by the amount of nitrogen functional groups, but also by the type (pyridinic, graphitic, or pyrrolic nitrogen) of groups present in the structure. Nevertheless, a correlation between the percentage nitrogen content and the final catalytic activity of the materials obtained is evident. As the level of nitrogen percentage increases, the catalytic activity in ORR also increases. However, it is argued that pyridinic nitrogen and graphitic nitrogen lead to an increased catalytic activity in

the oxygen reduction reaction that bypasses the pyrrolic-nitrogen functional group. Even at the very introduction of nitrogen into the carbon structure of sp^2, it may be found that nitrogen changes the electronic properties of the carbon atoms due to the higher electronegativity of the introduced element. This change in structure, not only electron but also geometric, increases the adsorption of oxygen molecules and makes it easier to break the bond between two oxygen atoms in an O_2 molecule. As it may turn out, it is not entirely clear which nitrogen functional groups have a direct effect on catalytic activity. There are many factors that can hinder the interpretation and cause confusing hypotheses; for example, a defective structure and graphitization of carbon materials can also favorably affect the electrochemical properties in ORR [16]. The exact role of the action of N-6 and N-Q groups was attributed by Dai et al. [22], suggesting that the higher is the amount of N-6 groups, the greater it affects the increase in the initial potential, while N-Q groups affect the limiting current density in the oxygen reduction reaction. Therefore, an increased amount of these functional groups will favorably influence the final catalytic properties and the value of electrons transferred. This point is also not clear. In the pyridine nitrogen groups, which are built into the six-membered ring at the edges of the carbon structure, alkaline media can catalyze in the disproportionation of peroxide ions produced during the oxygen reduction reaction [23]. N-6 groups, due to their position, are able to donate one electron-p to the p-system in the carbon structure layers. In contrast, N-Q bonded to three neighboring atoms has the ability, due to its similar configuration with carbon, to donate electrons to the n-system [19], as shown in Figure 1.

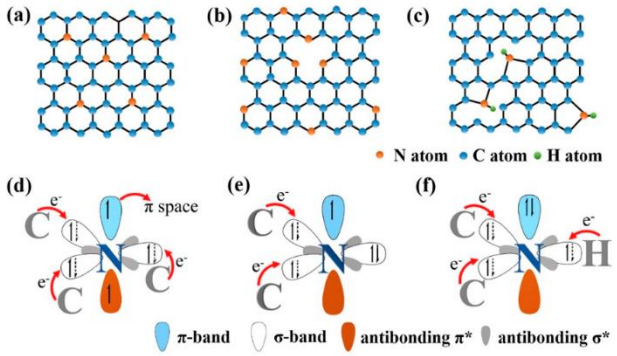

Figure 1. (**a**–**c**) Types of bonding between nitrogen and carbon configurations existing in the carbon materials: N-Q, N-6, and N-5. (**d**–**f**) A scheme of the doped atom electronic structure. Indication: * antibonding molecular orbital. Adapted from [19], with permission from *Carbon*, 2017.

The oxygen reduction reaction is a key reaction occurring at the cathode of certain energy storage devices (metal–air batteries and fuel cells), and as such is a crucial limiting factor that influences their performance [24]. It is therefore of critical importance to develop electrode materials that are highly stable and effective in ORR in both acidic and basic environments. Alkaline media is usually used, as acidic electrolytes can corrode the anodes in metal–air batteries, though this is also not without disadvantages [25]. In metal–air batteries, the charging and discharging processes are similar to those in fuel cells, and the metal ions are contained in the electrolyte. The oxygen reduction reaction occurring at the cathode can most generally be represented by several steps that occur in aqueous electrolytes: (a) oxygen molecules from the air adsorb and diffuse on the surface of the electrocatalyst; (b) electrons coming from the anode electrode are transported to the adsorbed oxygen molecules; (c) under the influence of electrons, a weakening of the bond occurs and thus the O=O bond is cleaved; (d) finally, OH^- ions that had been formed in the electrolyte are removed [25–27]. ORR can follow a more efficient one-step

pathway and exhibit a four-electron reduction of oxygen to OH^- ions (in alkaline medium, Equation (1)) or to H_2O (in acidic medium, Equation (2)), or a less efficient two-electron oxygen reduction pathway.

$$O_2 + 2H_2O + 4e^- \rightarrow 4OH^- \text{ (alkaline medium)} \quad (1)$$

$$O_2 + 4H^+ + 4e^- \rightarrow 2H_2O \text{ (acidic medium)} \quad (2)$$

For the two-electron oxygen reduction reaction, there is a two-step process with the formation of H_2O_2 intermediates, their reduction (Equations (3) and (5)), and chemical disproportionation, which increases the reaction time and requires more energy; it is necessary to minimalize this type of pathway because H_2O_2 can be aggressive while decomposing into free radicals. In both environments, the same intermediate product is present, which needs to be reduced to OH^- (Equation (4)) or to H_2O (Equation (6)), and this does not necessarily occur in one active site. In an alkaline medium, the two-electron oxygen reduction process proceeds as follows:

$$O_2 + H_2O + 2e^- \rightarrow HO_2^- + OH^- \quad (3)$$

$$HO_2^- + H_2O + 2e^- \rightarrow 3OH^- \quad (4)$$

In an acidic medium, the two-electron oxygen reduction reaction proceeds as follows:

$$O_2 + 2H^+ + 2e^- \rightarrow H_2O_2 \quad (5)$$

$$H_2O_2 + 2H^+ + 2e^- \rightarrow 2H_2O \quad (6)$$

The oxygen evolution reaction is the reverse of the oxygen reduction reaction that occurs in energy storage systems and devices. For the efficient operation of such devices, it is important that the electrode materials exhibit high stability and activity in both reactions. Slow kinetics in ORR and OER significantly reduce the performance of such devices. This problem is therefore widely researched and developed to produce catalysts that are stable in specific environments and also exhibit enhanced oxygen reduction and evolution activity for efficient reactions [28]. Researchers are looking for bifunctional catalysts that have the advantageous properties of both oxygen reduction and oxygen evolution simultaneously.

In this paper, we mainly focus on the recent achievements and critical issues affecting the field of metal-free carbon-based electrocatalysts for the oxygen reduction reaction and strategies of enhancing catalytic activity. We paid attention to nitrogen or codoped carbon nanostructures and the correlation between ORR activity and surface properties of the carbon nanomaterials. Finally, we offer personal perspectives and identify the main challenges that need to be addressed.

2. Metal-Free Cathode Electrocatalysts for Oxygen Reduction Reaction

2.1. Graphene-Based Electrocatalysts

The attention of scientists has recently been drawn to the rapid development of technology and thus the continuous demand for energy carriers, in particular electronic devices, electric vehicles, portable energy storage devices including lithium-ion batteries, fuel cells, and metal–air. Despite the existing vast knowledge and numerous publications reporting on the progress of research and development of the materials from which these devices are built, there are still various problems preventing the commercialization of many electrode materials [29,30]. The growing awareness of environmental protection demands the use of catalysts that are environmentally friendly as well as cheap and easy to recycle. In recent years, Zn–air-type batteries have gained particular interest. The Zn–air batteries that are to replace classical lead–acid and lithium-ion batteries demonstrate low production cost, high energy density, and specific capacity at low weight [31]. Researchers are continuously developing original solutions for electrode materials with high energy density, high current capacity, and safety in production and use. In order to meet these

needs, it is important to develop new methods of obtaining these materials that will successfully replace those commercially available. The current state of knowledge confirms the uniqueness of graphene and graphene-based materials. As it is known, graphene is a material with a two-dimensional (2D) structure [32]; its thickness is the size of a single atom, so it has great potential in nanotechnology. The first synthesis was based on a simple method of peeling off layers of graphite using adhesive tape to obtain a single sheet of evenly spaced carbon atoms in the shape of a honeycomb [33]. Materials based on graphene exhibit very favorable traits; even a small amount of graphene results in high mechanical and thermal stability due to its unique mechanical properties (thermal conductivity is in the range of 3000–5000 WmK^{-1}, while tensile strength is 42 Nm^{-1}) [34]. A small graphene addition affects the properties of the final product; therefore, graphene is used as a composite material or electrode material to improve its catalytic properties. The activity of pristine graphene is not high compared with commercial platinum-based electrode materials [35]. Researchers are trying to find optimal conditions for the simplest possible one-step method of obtaining heteroatom-doped graphene materials. They try to improve the electrochemical properties by modifying the structure, not only by introducing heteroatoms into the graphene structure, but by using transition metal oxides and/or transition metal molecules or polymers [36,37]. A noteworthy solution for improving the catalytic activity is the use of graphene derivatives, such as heteroatom-doped graphene quantum dots showing improved activity of electrode materials not only in ORR but also in the oxygen evolution reaction (OER) and hydrogen evolution reaction (HER) as compared with commercial electrode materials (e.g., Pt/C) [38,39]. Heteroatom-doped quantum dots are generally used to achieve a synergistic effect, which results in an increase in catalytic activity due to numerous active sites, such as defects, quasiparticles, or interfaces. The observed superb ORR performance was attributed to the charge transfer between graphene quantum dots (GQDs) and graphene nanoribbon components in tight contact, along with the numerous surface/edge defects. The heterogeneous electron transfer rate can be accelerated by increasing the density of electronic states, relating to the amount of edge defects [40]. The introduction of heteroatoms into the carbon structure causes defects in the structure that supports active sites as well as electrolyte penetration, which allows oxygen better access to the structure [41]. The structure of quantum dots resembles single- or few-layer graphene due to the precursor used in production, which is usually graphene, graphene oxide (GO), or compounds with benzene structures [42]. Heteroatom-doped graphene quantum dots can be used in combination with not only carbon material, such as graphene or carbon nanotubes, but also graphene nanowires to increase the catalytic activity of potential electrode materials [43].

This chapter specifically focuses on heteroatom-doped graphene materials and the effect types of syntheses have on the doping of carbon ORR tures, which have a significant impact on the catalytic properties in oxygen reduction reaction.

2.1.1. Synthesis of Nitrogen-Doped Graphene-Based Materials via Pyrolysis Method

An up-to-date literature review proves that graphene materials, graphene-based materials, and those with graphene-like structures are all attractive materials in terms of their properties and wide applicability. The current state of knowledge assumes that there are several ways of enriching carbon materials with nitrogen or other heteroatoms; nevertheless, nitrogen has the most positive effect on catalytic properties due to its similar atomic size and similar electronegativity [44]. There are many raw materials rich in nitrogen or other heteroatoms that, upon thermal treatment, are converted into specific functional groups or volatile compounds that enhance catalytic activity. In order for specific atoms to efficiently embed themselves into graphene structures during the carbonization process, they need a favorable correlation with carbon before thermal treatment [45]. In our recent scientific reports, we have been able to develop efficient nitrogen-doped graphene-based electrode materials [46,47]. In one of the proposed synthesis methods, we used inexpensive and environmentally friendly reagents [46], employing electroexfoliation in 1 M Na_2SO_4 to

obtain graphene sheets. Nitrogen doping of the obtained graphene structures was carried out by pyrolysis in an inert gas flow, but first, the exfoliated graphene was mixed with a nitrogen precursor, green algae (*Chlorella vulgaris*). The nitrogen content of the obtained nitrogen-doped graphene was equal to 1.8–2.2% at. However, despite this low level, the catalytic activity in the oxygen reduction reaction was comparable to the commercial Pt/C catalysis with 20% wt. of Pt. The number of transferred electrons (n) in ORR was equal to 3.78 for the sample carbonized at 800 °C. These materials were applied in practice in a Zn–air battery. In these research studies, it has been shown that even a low nitrogen content of less than 2% at. can already have a beneficial effect on the stability of the catalyst during charging–discharging of a battery. The materials obtained do not require the use of advanced recycling and are environmentally friendly as they do not contain heavy metals. In another paper by Skorupska et al. [47], metal-free graphene foams were produced using a microwave reactor and two different solvents, ethyl alcohol (EtOH) and dimethylformamide (DMF). Expanded graphite was used for the synthesis, while green algae (*Chlorella vulgaris*) were used as a natural nitrogen precursor, which incorporated N-Q and N-5 functional groups under high temperature. The calculated electron transfer number for the oxygen reduction reaction was 3.46, while for the starting material itself, without the nitrogen precursor, the value of n was 2. The methods developed so far have become an alternative way to produce completely metal-free catalysts, which have similar catalytic properties, with comparable potential for use as an electrode in metal–air batteries or fuel cells. As reported in our scientific papers, as well as written about by Qin et al. [48], ORR activity is influenced by the total content of N-6 and N-Q groups. Among other compounds, ammonium acetate [49], urea [44,50], melamine [44,51], cyanamide [44] or dicyandiamide [52,53], inorganic salts [44] such as ammonium chloride (NH_4Cl), ammonium nitrate (NH_4NO_3), ammonia gas [54], and polymers such as polypyrrole [55], polyaniline [56–58], triblock copolymers of poly (ethylene oxide)–poly(propylene oxide)–poly (ethylene oxide) [59], poly (sodium 4-styrenesulfonate), and poly (4-styrenesulfonic acid–comaleic acid) [60] are used as carriers of nitrogen functional groups converted under high-temperature processes. Quite unusual nitrogen precursors were used by Zhang et al. [61]. They designed a doped carbon material with a graphene structure using three different precursors of nitrogen, 1,3-diaminobenzene, 2,6-diaminopyridine, and 5-aminouracil (Figure 2a), to test the most beneficial nitrogen group configuration. Different configurations of these precursors produce the appropriate combination of nitrogen functional groups in the obtained materials. In this case, the most beneficial for the oxygen reduction reaction were pyridinic-N and graphitic-N functional groups with 5-aminouracil and 2,6-diaminopyridine used as precursors. These materials exhibit the highest limiting current density in linear sweep voltammetry (LSV), and the onset potential is more positive than other nitrogen groups' configurations (Figure 2b). The most advantageous configuration for N-doped graphene ($N/C\text{-}N_P + N_G$) of the four-electron oxygen reduction reaction is a combination of N-6 and N-Q groups along with N-Q predominating. However, there is no clear statement as to which acts as the most advantageous in this group. Lu et al. [62] showed that the total nitrogen content is not as important in catalytic activity as the corresponding nitrogen groups, here N-6. The use of GO and urea compounds during pyrolysis in a temperature range of 200 to 900 °C occurs at a level between 12.41% at. and 3.36% at. of nitrogen, respectively. Even small amounts of nitrogenous N-6 or N-Q functional groups, other heteroatoms, and transition metals have a beneficial influence on the catalytic properties in the oxygen reduction reaction. Increasing the nitrogen content can be achieved by using a lower carbonization temperature; however, the carbon content becomes relatively low at such temperatures [63,64].

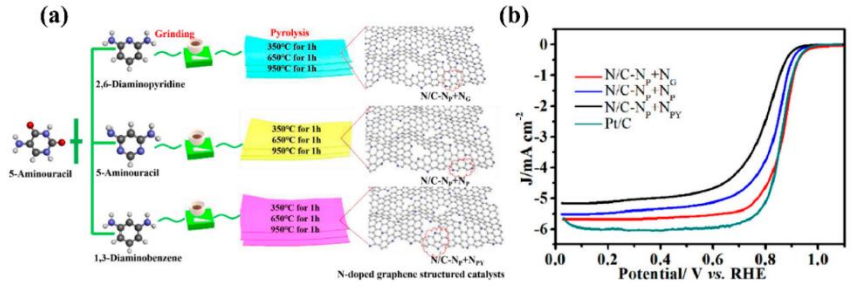

Figure 2. (**a**) Scheme of the synthesis process of precursor–modulated N–doped carbon materials; (**b**) linear scanning voltammetry curves for obtained materials. Adapted from [61], with permission from *Electrochimica Acta*, 2021.

Conversely, increasing the pyrolysis temperature increases the materials' graphitization degree from about 75% to about 85%, causing their electrical conductivity to increase [64,65]. This is the case not only for graphene materials, but generally for carbon materials of various origins. Additionally, Kabir et al. confirmed, by using the density functional theory (DFT) theoretical methods, that temperature has a significant influence on the formation of nitrogen functional groups [66,67]. They additionally put forward the hypothesis that 850 °C is the optimal temperature for the formation of an adequate amount of pyrrolic-N and pyridinic-N functional groups, with a ratio of 0.45, which increases current density in alkaline and acidic media, along with a proper correlation of the starting material and nitrogen precursor [68]. Nevertheless, an obstacle that can be encountered in the preparation of nitrogen-doped graphene materials is their structure. The pore system based on micro- and, mainly, mesopores increases oxygen access to active sites in the structure from air. As follows, surface area is important in the oxygen reduction reaction. However, in the pyrolysis process, a graphene structure has low crystallinity and tends to collapse and exhibit a low specific surface area. Therefore, the use of additional templates (silica or carbonate minerals (Na_2CO_3, $CaCO_3$)) causes an increase in the specific surface area [69,70]. Generally, the use of activators, such as KOH and NH_3 gas, is dangerous to the installation and increases the risk of damage, which in turn may cause an increase in security measures, which have a direct impact on the final production costs [63]. Table 1 summarizes the ORR activity of nitrogen-doped graphene synthesized via the pyrolysis method.

Table 1. Summary of nitrogen-doped graphene obtained via the pyrolysis method as an electrocatalyst for ORR.

Type of Sample	Precursor of Graphene	Precursor of Heteroatom(s)	S_{BET} [1] (m^2 g^{-1})	Electrolyte	Heteroatom Content	Electron Transfer Number	Ref.
N-graphene	GO [2]	PDA [3]	62.6	0.1 M KOH	n.d. [4]	3.98	[8]
N-graphene	GO	BMIM BF_4 [5]	n.d.	0.1 M KOH	4.9–7.2% at.	3.19	[11]
N-graphene	GO	Melamine	1599	0.1 M KOH	2.8% at.	2.9	[36]
N-graphene	GO	PDA	185	0.1 M KOH	3.20% at.	3.98	[37]
N-graphene	Graphite	*Chlorella vulgaris*	n.d.	0.1 M KOH	1.6–2.2% at.	3.17–3.78	[46]
N-graphene	Expanded graphite	*Chlorella vulgaris*	n.d.	0.1 M KOH	0.10–2.44% at.	2.55–3.46	[47]
N-graphene	PG [6]	NH_4 (AC)	364.5	0.1 M KOH	n.d.	3.4–4	[49]
N-graphene	GO	urea	n.d.	0.1 M KOH	7.86% at.	3.6–4	[50]
N-graphene	GO	Dicyandiamide	670	0.1 M KOH/ 0.1 M $HClO_4$	5.07% at.	>3.9	[52]
N-graphene	GO	NH_3	816	0.1 M KOH	2.4–4.6% at.	~2.75–3.25	[54]
N-graphene	GO	Urea	3.15.43	0.1 M KOH	3.46–6.65% at.	3.92	[62]
N-graphene	GO	Urea	n.d.	0.1 M KOH	8.59–20.59% at.	2.3–2	[64]

Table 1. *Cont.*

Type of Sample	Precursor of Graphene	Precursor of Heteroatom(s)	S_{BET} [1] (m^2 g^{-1})	Electrolyte	Heteroatom Content	Electron Transfer Number	Ref.
N-graphene	Graphene nanoplatelets	ADC [7]	533–657	0.1 M KOH	0.7–2.7% at.	3.04–4	[70]
N,S-graphene	GO	PDA/ 2-mercaptoethanol	273.0	0.1 M KOH	N-4.1% at. S-6.1% at.	3.52	[8]
N,S-graphene	GO	Cysteine	n.d.	0.1 M KOH	N-1.02% at. S-1.32% at.	3.47–3.72	[45]
B,N,P-graphene	GO	Boric acid/cyanamide/ phenylphosphine	443.0	0.1 M KOH/ 0.1 M $HClO_4$	N-6.45% at. B-9.98% at. P-0.6% at.	3.5	[69]

[1] S_{BET}—the specific surface area determined by the Brunauer–Emmett–Teller equation; [2] GO—graphene oxide; [3] PDA—polydopamine; [4] n.d.—not determined; [5] BMIM BF_4—1-butyl-3-methylimidazolium tetrafluoroborate; [6] PG—porous graphene; [7] ADC—azodicarbonamide.

2.1.2. Synthesis of Nitrogen-Doped Graphene-Based Materials via Hydro(Solvo)Thermal Method

Another very promising method of obtaining heteroatom-doped materials is the hydrothermal method. It is usually used in combination with pyrolysis to obtain reduced graphene oxide as a matrix for the introduction of other atoms, which would favorably influence the structure and electrochemical properties. The hydrothermal method involves introducing graphene materials such as GO or a carbon precursor, dopant atoms, and/or templates plus additives into a pressure vessel, usually made of Teflon, and then prolonged heating at about 100 to 210 °C for at least several hours, thereby creating a vacuum in the reaction vessel. A schematic of the hydro(solvo)thermal process is presented in Figure 3.

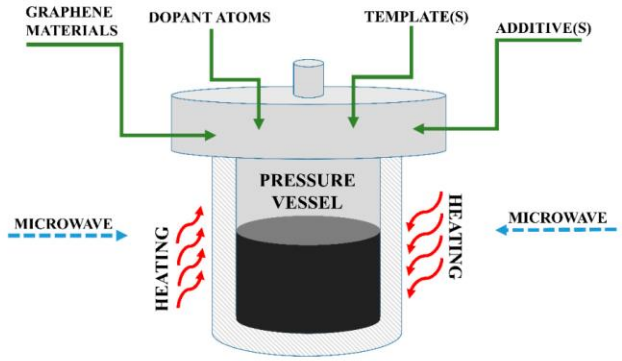

Figure 3. Schematic of stainless-steel autoclave and Teflon pressure vessel used for hydro(solvo)thermal synthesis.

In 2015, Zhou et al. [52] used synthesized graphene oxide to introduce nitrogen atoms into its structure using dicyandiamide. A hard template, silica with a particle size of about 7 nm, and $FeCl_2 \times 4\ H_2O$ were used as the separator and the reaction catalyst, respectively. They obtained graphene foam using hydrothermal treatment and stable material through pyrolysis at 900 °C in nitrogen flow for 1 h. The material was pyrolyzed twice. They demonstrated in this paper that the use of nitrogen doping and a transition metal at the same time effectively enhances the activity of the active sites, being advantageous in the oxygen reduction reaction in both alkaline and acidic media. They attribute high ORR activity to the mesoporous structure, which affects the rate of electrolithium flow, and the nitrogen functional groups (N-6 and N-Q), which are involved in the ORR reaction mechanism. Typically, researchers use a two-step synthesis of heteroatom-doped electrocatalysts: reduce

graphene oxide via a hydrothermal method using toxic reagents (e.g., hydrazine [71]), and then incorporate the heteroatoms permanently into the structure via pyrolysis [72] or apply an annealing to stabilize and introduce heteroatoms into the structure [73]. Figure 4a–f presents a scheme of the synthesis process, as well as a cross section of the structure determined by scanning electron microscopy (SEM), transmission electron microscopy (TEM), and atomic force microscopy (AFM) methods.

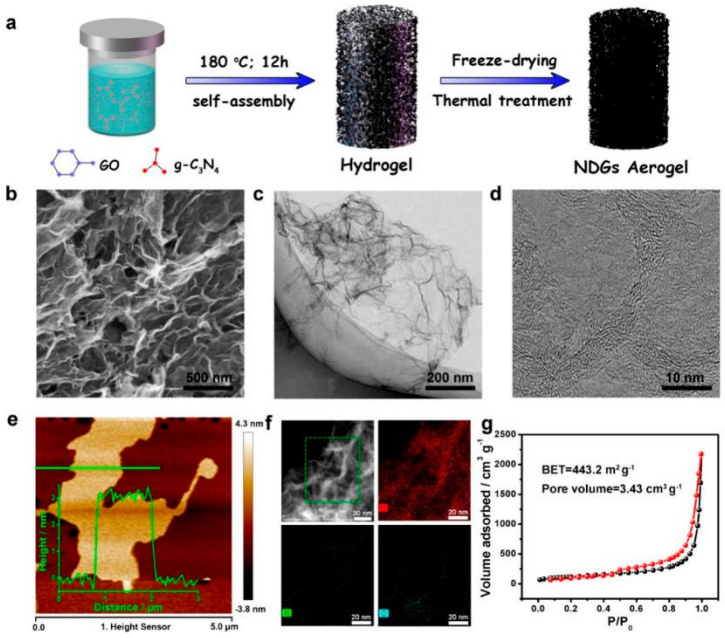

Figure 4. (**a**) Scheme of sample synthesis. (**b**) SEM, (**c**) TEM, (**d**) HRTEM, (**e**) AFM image, (**f**) elemental mapping images, and (**g**) N_2 adsorption–desorption isotherms of a representative sample. Adapted from [72], with permission from *ACS Energy Letters*, 2018.

An adsorption–desorption isotherm proving porosity is presented in Figure 4g. This approach increases the cost of production, disposal, and time taken to fabricate electrode materials. In their research work, Miao et al. [74] performed a two-step synthesis of nitrogen-doped graphene. They showed that the specific surface area calculated by the Brunauer–Emmett–Teller (BET) is not a factor for enhanced activity in ORR. The effect of doping the graphene structure with heteroatoms is a decrease in the surface area. This is due to the incorporation of other atoms in the pores and at the edges of the graphene layer, thus causing a stronger defect in the structure, which in turn may have a positive effect on ORR. Nevertheless, the higher the ratio of mesopores in the structure, the easier the transport of oxygen and electrolyte in ORR [75].

Nonmetallic elements other than nitrogen (e.g., sulfur [76], phosphorus [77,78], boron [79–81], and fluorine [79]) have also been introduced to obtain effective electrocatalysts. The role sulfur plays in the oxygen reduction reaction can be attributed to the generation of positive charge by causing a change in the electron structure of carbon atoms. The produced sulfur-doped graphene materials show high electrocatalytic activity and stability in acidic and basic environments, making them environmentally friendly. Compared with nitrogen, phosphorus has a greater ability to create defects in graphene structures, and

in a different way, than nitrogen, due to its larger atomic size. Boron, on the other hand, has a similar electron configuration ($1s^2$ $2s^2$ $2p^1$) with a difference of one valence atom relative to carbon ($1s^2$ $2s^2$ $2p^2$). The B-doped graphene structure does not observe significant changes in the graphene lattice (C–C bonds) due to the slightly longer B–C bond [82]. The most favorable choice of atoms involved in codoping is one of an element with higher electronegativity and the other with a lower electronegativity than carbon (2.55) [83]. It is possible to increase the performance of ORR by introducing doping; nevertheless, it does not beat the performance of a platinum-based catalyst. Double and triple doping of graphene with heteroatoms, such as N-S [75,84], N-B [80,83], N-P [85], B-P/BNP [86], or N-S-P [87], is more advantageous, creating a synergistic effect. This effect increases the catalytic activity of doped graphene materials to more than that of materials doped with a single type of atom. There are also reports of triple doping with heteroatoms in different configurations. Much information is provided by the work of Lin et al. [86] on doping graphene using boron and phosphorus, followed by activation through NH_3, which also increases the active sites in the graphene material. The carbon precursor in this work was GO, while the B and P precursors were boron phosphate (BPO_4). All components were subjected to a hydrothermal method. In this work, the transfer electrons for mono-, double-, and triple-doping carbon materials were compared, and it was noted that the synergistic effect between different heteroatoms, in this case B–N–P, can lead to enhanced catalytic properties in ORR. For a catalyst to exhibit a four-electron oxygen reduction reaction, it has to satisfy the premise that the more positive the cathodic potential of the ORR peak and onset potential, the higher the kinetic limiting current, which may affect the final interpretation of the ORR mechanism pathway. Zhao in 2018 [88] investigated the influence of doping order with phosphorus atoms first and nitrogen atoms second on the final content and type of nitrogen functional groups (schematic of synthesis, Figure 5a). They proved experimentally and theoretically that this approach can significantly improve the catalytic activity of N-doped carbon materials. The bonding of carbon with phosphorus can occur outside the structure (externally) or be incorporated into the carbon structure (internally) (Figure 5b). Due to C–P bonding in the external system, it is possible to decrease the energy needed for the formation of C–N bond (graphite N), causing the content of N-Q functional groups to increase. The situation is quite interesting, since the mechanism of graphite-N formation at P-doped sites is theoretically presented. During nitrogen adsorption, the bond between carbon and phosphorus elongates and weakens so that graphite P can be replaced by graphite-N functional groups. Aside from codoping with heteroatoms only, codoping with nitrogen and transition metal oxides or molecules is also popular. Wu et al. [89] obtained three-dimensional (3D) structured graphene derived from nitrogen-doped graphene oxide by introducing polypyrrole and iron acetate as an iron (II, IIII) oxide (Fe_3O_4) precursor into the reaction vessel. The resulting catalyst had a higher current density in an alkaline medium, and its electron transfer exhibited a four-electron oxygen reduction pathway. Heteroatom-doped catalysts are also used as support materials for platinum or ruthenium metals, increasing their catalytic activity in oxygen reduction reactions in different environments [90]. As it is well known, the hydrothermal method is characterized by long synthesis times in order to efficiently dope with heteroatoms/transition metals or obtain the desired structural effect. Consequently, Kim et al. [91] made a successful attempt to speed up the hydrothermal synthesis by using microwaves, which effectively and quickly heat up the reaction vessel quickly [92]. Table 2 summarizes the ORR activity of nitrogen-doped graphene synthesized via the hydrothermal method.

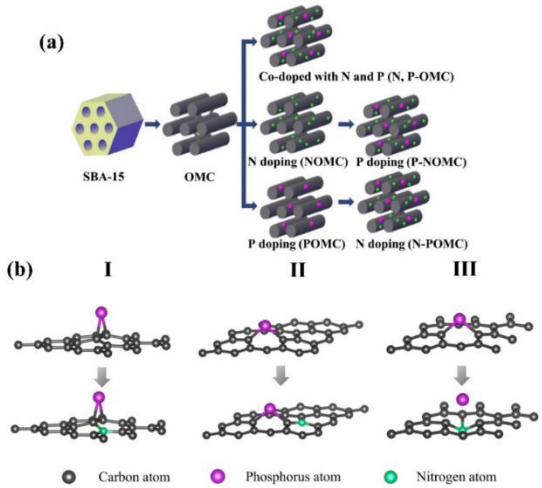

Figure 5. (**a**) Scheme of the synthesis of the N,P dual-doped OMCs; (**b**) scheme of the orientation effect of the first doped P and then doped N: (I) outside, (II) inside, (III) self-sacrifice type. Adapted from [88], with permission from the *International Journal of Hydrogen Energy*, 2018.

Table 2. Summary of nitrogen-doped graphene synthesized via the hydrothermal method as electrocatalyst for ORR.

Type of Sample	Precursor of Graphene	Precursor of Heteroatom(s)	S_{BET} (m^2 g^{-1})	Electrolyte	Heteroatom Content	Electron Transfer Number	Ref.
N-graphene	GO	Dicyandiamide	16.4–443.2	0.1 M KOH/ 0.5 M H_2SO_4	1.48–11.04% at.	~4	[72]
N-graphene	CCl_4 [1]	Pyrrole	363.7–413.6	0.1 M KOH	2.8–2.9% at.	3.88–3.81	[73]
N-graphene	GO	Urea	177.6–280.4	0.1 M KOH	3.98–6.56% at.	3.27–3.89	[74]
N-graphene	GO	Urea	489–592	0.1 M KOH	7.6–7.8% wt.	2.62–3.11	[75]
N-graphene	GO	Urea	69	0.1 M KOH	n.d. [2]	3.61	[79]
N-graphene	GO	NH_3 (gas)	n.d.	0.1 M KOH	2.8% at.	2.63	[83]
N,B-graphene	GO	NH_3/boric acid	n.d.	0.1 M KOH	N-16.57% at. B-14.37% at.	3.97	[83]
N,B-graphene	GO	$(NH_4)_2B_4O_7 \times 4H_2O$	n.d.	0.1 M KOH	N-4.25–4.43% at. B-3.03–3.55% at.	3.05–3.84	[91]
N,F-graphene	GO	Urea/TFA [3]	103	0.1 M NaOH	n.d.	3.41	[79]
N,S-graphene	GO	Urea/thiourea	374–441	0.1 M KOH	N-1.5–1.9% wt. S-1.9–2.1% wt.	3–4.05	[75]
N,S-graphene	GO	Thiourea	354.8	0.1 M KOH	N-3.13% at. S-1.31% at.	>3	[87]
N,S-graphene	GO	NH_4SCN	220	0.1 M KOH	N-4–19.7% wt. S-4.1–28.7% wt.	3.9	[84]
N,B,P-graphene	GO	NH_3/BPO_4	93–372	0.1 M KOH	N-1.98–4.50% at. B-3.73–6.53% at. P-3.07–3.80% at.	3.13–3.71	[86]
N,P,S-graphene	GO	Thiourea/TPP [4]	250.2–301.3	0.1 M KOH	N-2.88–4.34% at. S-0.89–1.24% at. P-0.96–1.31% at.	>3.4	[87]

[1] CCl_4—tetrachloromethane; [2] n.d.—not determined; [3] TFA—trifluoroacetic acid; [4] TPP—triphenylphosphine.

2.1.3. Synthesis of Nitrogen-Doped Graphene-Based Materials via Chemical Vapor Deposition Method

World literature reports that the chemical vapor deposition (CVD) method [93,94] is the one proposed so far for obtaining graphene-based electrocatalyst materials, despite

being based on uneconomical raw materials, requiring special conditions and precautions during synthesis, and using complicated apparatus. The CVD method works well in obtaining pure graphene, but is impractical on an industrial scale. Nevertheless, this method is used, which is beneficial for the content of functional groups that play a key role in the oxygen reduction reaction. The process takes place in a reaction chamber into which gaseous substrates, or heteroatom precursors, are introduced for doping in such a way that appropriate chemical reactions take place on a substrate heated to high temperatures (>800 °C). The schematic process of graphene synthesis is presented in Figure 6. Graphene is produced through different methods using high temperatures (e.g., thermal heating, plasma-enhanced CVD (PECVD) [95], or laser ablation in the presence of a catalyst (Cu, Ni)), where the carbon source and heteroatom precursors remain in close contact with hydrogen, which controls the properties of graphene. Methane (CH_4) [96,97] and ethane (C_2H_6) [93] are typically used as gaseous carbon precursors for graphene synthesis [96]. Other carbon sources can be gaseous, as well as solid or liquid [98]. Hydrocarbons decomposing to atomic sizes adsorb on the catalyst, forming specific graphene structures. One of the most popular ways to grow graphene structures of large volume and high quality is by characteristic growth on a copper sheet or foil using gaseous methane as a carbon precursor. However, this strategy for obtaining graphene is time-consuming and requires a decomposition barrier of methane (<1000 °C), the applied copper foil is not stable, and its catalytic capacity decreases as the volume of the graphene structure increases. All these factors affect energy consumption, which increases the cost of producing high-quality graphene. The homogeneity and quality of graphene, as well as the rate of the nanomaterial's formation, are negatively affected by any change in growth conditions, including the substrate/catalyst type used, synthesis temperature, pressure, carbon precursor, hydrogen or heteroatoms, and the velocity of the gas stream [99]. Doping is an effective way of properly tailoring the properties of graphene to the application of the nanomaterial in various energy storage devices. Heteroatom precursors, on the other hand, are used either simultaneously during the CVD process or in subsequent steps of heteroatom-doped graphene synthesis [100]. Nitrogen doping is usually performed using gaseous nitrogen with the simultaneous flow of carbon precursors. Commonly used carbon precursors in the CVD method includes NH_3 gas [96,97,101]. Metal-doped graphene materials possess favorable properties for the oxygen reduction reaction because of their extended structure for improved ion transportation during the redox reaction. Wu et al. [102] used the CVD method with two selected precursors, NH_3 gas and thiourea, to obtain nitrogen- and sulfur-doped graphene. As the synergetic effect improves the catalytic activity, researchers also undertake doping using analogous materials with other heteroatoms (S, B, P) and/or transition metals, all due to the growing desire to replace currently used commercial electrode materials [103]. On the other hand, Qiu et al. [94] investigated the effect of codoping with nitrogen and nickel, as well as single doping, on catalytic activity and ORR pathway determination for the potential application as metal–air batteries. They reported that Ni atoms anchored on the graphene surface and the doped nitrogen improved catalytic properties for OER and ORR reactions in an alkaline electrolyte.

The preparation of porous material using the CVD method involves chemically etching the metal substrate on which graphene structure growth occurred. While even long-lasting etching does not allow for the complete removal of metals, it can still positively influence the electrochemical properties of the obtained materials [104]. When the CVD method is used to obtain graphene, the product is a material of high quality and homogeneity, which can be beneficial for the next step of doping with graphitic C_3N_4 [14]. A combination of hard templating and the CVD method is also possible. Want et al. [105] used MgO as a template on which the graphene structure was deposited in a classical CVD method, producing a material with a specific surface area of 1440 $m^2\ g^{-1}$ and a pore volume of 2.18 $cm^3\ g^{-1}$. The result was a biofunctional catalyst for the reaction of reduction and evolution of oxygen. Shi et al. [106], using the same idea of templating by MgO, methane, and pyridine, proposed a method to obtain graphene with nitrogen dopants anchored

either in the structure or on its surface. They showed that a more advantageous concept of producing efficient electrocatalysts in ORR is to dope the graphene coating on 3D templates. This way, the final material has the morphology of the template and, after its removal, is able to expose active sites on the surface, favoring energy storage [107,108]. The final nitrogen content on the doped graphene surface was 1.81% at., and the high specific surface area was equal to 1531 $m^2\ g^{-1}$, which together with the low defect density determined by Raman spectroscopy establishes an effective influence on the final electron transfer value in the oxygen reduction reaction, equaling 3.34. The one-step CVD synthesis method results in a uniform distribution of doped atoms in the structure with a small amount on the surface. The ORR process occurs due to the active sites having direct contact with the substrate. This means that some heteroatoms in the structure do not participate in the electron transfer process and do not contribute much to the catalytic activity of the catalyst. As established earlier, a material's atomic nitrogen content decreases as temperature increases. The CVD method makes it possible to tune the functional groups in such a way as to have them exhibit the most favorable properties for particular applications. With CVD, it is primarily possible to incorporate nitrogen in the form of N-6 and N-Q nitrogen groups. When the temperature is increased and the process is prolonged, CVD causes the amount of N-6 functional groups to decrease [109]. Previous reports indicate a limitation in the application of CVD-obtained graphene materials in acidic electrolytes due to difficulties in modifying the structure [97]. It follows that the synthesis and application of doped graphene in ORR using an acid electrolyte requires more analysis and alternative modifications to form effective electrode materials. Table 3 summarizes the ORR activity of nitrogen-doped graphene synthesized via the CVD method.

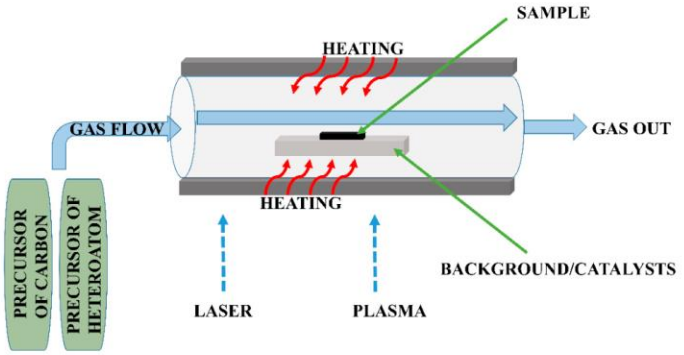

Figure 6. Schematics of synthesis chemical vapor deposition method.

Table 3. Summary of nitrogen-doped graphene synthesized via the CVD method as an electrocatalyst for ORR.

Type of Sample	Source of Carbon	Precursor of Heteroatom(s)	S_{BET} ($m^2\ g^{-1}$)	Electrolyte	Heteroatom Content	Electron Transfer Number	Ref.
N-graphene	CH_4	gC_3N_4/NH_3	830	0.1 M KOH	0.7–6.5% at.	3.86–3.88	[14]
N-graphene	CH_4	N_2 (gas)	311.7–400.2	0.1 M KOH/ 0.1 M $HClO_4$	3.8–6.7% at.	>3.9	[95]
N-graphene	CH_4	NH_3 (gas)	n.d. [1]	0.1 M $HClO_4$	n.d.	n.d.	[97]
N-graphene	CH_4	NH_3 (gas)	n.d.	0.1 M KOH	n.d.	3.6–4	[101]
N-graphene	CH_4	NH_3 (gas)	1440	0.1 M KOH	3.41% at.	>3	[105]
N-graphene	CH_4	Pyridine	1531–1732	0.1 M KOH	1.18–1.81% at.	3.34	[106]

Table 3. *Cont.*

Type of Sample	Source of Carbon	Precursor of Heteroatom(s)	S_{BET} (m^2 g^{-1})	Electrolyte	Heteroatom Content	Electron Transfer Number	Ref.
N-graphene	Pyridine	Pyridine	1000	0.1 M KOH	2.26–4.95% at.	1.1–3.9	[109]
N,S-graphene	C_2H_5OH	Thiourea	43.8–119.5	0.1 M KOH	N-4.50% at. S-0.77% at.	3.6–3.8	[102]
N,S-graphene	Pyrimidine/ thiophene	Pyrimidine/ thiophene	640	0.1 M NaOH	N-2–9.6% at. S-0.7–3.2% at.	3.2–4.1	[103]

[1] n.d.—not determined.

2.2. Carbon Nanotube-Based Electrocatalysts

As previously mentioned, despite considerable progress in nanomaterial engineering and the functionalization of materials for practical electrode applications, there is still an intense search for a cost-effective, high-performance, metal-free, and environmentally friendly method of producing materials. Many researchers focus their projects on metal-free carbon nanotubes, which have been shown to have favorable oxygen reduction properties and could become a viable alternative to commercial noble metal-based electrocatalysts. Carbon nanotubes are one of the remarkable nanomaterials that have a wide scope of potential applications in many fields, all due to their outstanding chemical stability and well-established surface functionalization techniques [110–112]. Gong et al. [113] demonstrated that nitrogen-doped carbon nanotubes possess unique properties towards an efficient oxygen reduction reaction. On that basis, an intensive search for alternative catalysts based on heteroatom-doped carbon is visible in the literature [114,115]. Many methods are known for the preparation of carbon nanotubes differing in the number of layers; this number affects the electrical and chemical properties of CNTs. As is known, among CNTs one can find single-walled carbon nanotubes (SWCNTs) consisting of one graphene layer with hexagonal packing with a diameter in the range of 0.4–2 nm and a large surface area, or multiwalled carbon nanotubes (MWCNTs) consisting of two or several layers building a cylinder wall with a diameter in the range of 1–3 nm and better conductive properties than the SWCNTs [116]. The most common methods for obtaining carbon materials in the form of cylindrical coiled graphite sheets include electric arc discharge, chemical vapor deposition, and laser ablation [110,111,117]. Carbon nanotubes have the noteworthy property of retaining atoms of other elements in a cylindrical structure. This makes CNTs attractive carbon electrode materials for fuel cells, energy storage devices, batteries, or supercapacitors. Other applications of CNTs include biosensors and devices for photocatalytic water splitting [118]. Carbon nanotubes also have applications as catalyst carriers in polymer energy fuel cells (PEFCs). Like metal-free electrocatalysts, catalysts containing transition metal oxides or base metals are also being intensively investigated [119]. During the pyrolysis of dicyandiamide, small amounts of added metal chlorides are responsible for the generation of active sites favoring the oxygen reduction reaction [120–122]. However, the main materials effective in the oxygen reduction reaction are heteroatom-doped and contain single atoms of nitrogen, sulfur, boron, phosphorus, or transition metal oxides, or are combined in double- or triple-doped carbon nanostructures. Nitrogen doping is the most widely studied. The preparation of doped carbon nanotubes can be carried out directly during their preparation, by treating previously synthesized carbon materials with heteroatom precursors [19,20]. The one-step synthesis is based on the generation of nanomaterials by pyrolysis while simultaneously embedding heteroatom precursors, while the second procedure involves a two-step synthesis, producing or obtaining previously created CNT carbon material, and then deposition/addition of heteroatoms using heteroatom precursors. One well-known strategy for obtaining efficient electrocatalysts in ORR is to combine different graphene materials exhibiting attractive end-material properties. An example is the combination of doped graphene quantum dots in carbon nanotubes (Figure 7), which is advantageous because of the apparent enhanced catalytic activity. The resulting hybrids of quantum dots and carbon nanotubes exhibit catalytic

properties owing to the heteroatom-doped dots and high conductivity owing to carbon nanotubes [123]. Carbon materials doped with transition metals also exhibit better catalytic properties in the reduction reaction or oxygen evolution reaction than expensive Pt-, Pd-, or Ir-based materials [124–127].

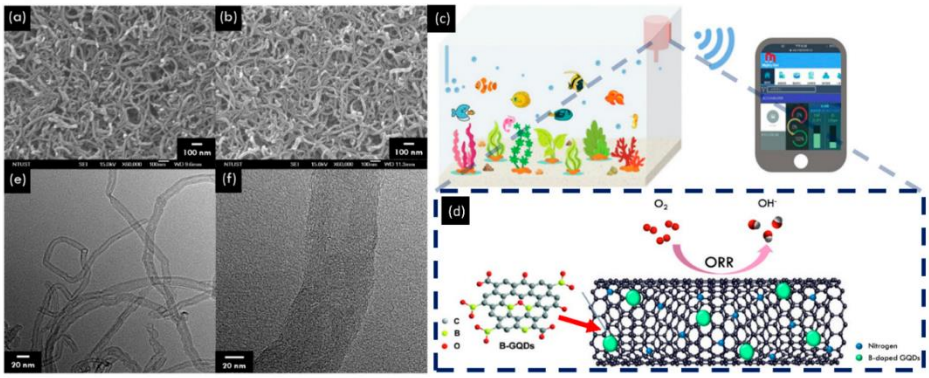

Figure 7. FE–SEM images of (**a**) CNTs, (**b**) NCNTs, (**c**) scheme of the practical application of determining dissolved oxygen, (**d**) scheme of BGQD/NCNT sample, TEM images of obtained samples in (**e**) low magnification and (**f**) high magnification. Adapted from [123], with permission from *Carbon*, 2022.

2.2.1. Synthesis of Nitrogen-Doped Carbon Nanotube-Based Materials via Pyrolysis Method

A factor contributing to the great interest in electrode materials and alternative energy source generation is the desire to reduce the cost of producing environmentally friendly, widely available carbon-based materials. To find a solution to this problem, researchers have tested various materials; the obtained electrode materials, alternative to those commercially available and typically environmentally unfriendly, are supposed to lower production costs, reduce emissions, and, above all, work effectively and have their practical application.

Nitrogen doping of carbon nanotubes is well known and has been widely studied through theoretical research, largely due to the ideal model of determining the effects of nitrogen atoms and nitrogen functional groups have in ORR [128]. Studies have also been carried out on doping with boron, sulfur, phosphorus, or silica. The researchers, after theoretical studies, came to the conclusion that nitrogen remains the atom showing superior enhanced catalytic properties in ORR. Nevertheless, Wang et al. [129] suggested a catalyst with the best achievable activity in ORR from the thermodynamic point of view that can be obtained by collating many heteroatoms in the structure, causing a synergistic effect, modifying the curvature of carbon nanotubes, and introducing characteristic defects at the ends of CNTs [130]. Gong et al. [113] were the first to demonstrate that pyrolysis-generated N-doped carbon nanotubes in the vertical position, in the presence of gaseous ammonia, exhibit enhanced catalytic activity and long-term stability in an alkaline medium, thus achieving similar performance to commercial electrodes based on platinum. The most proven method of obtaining doped carbon materials is their carbonization in the presence of a precursor for the given heteroatoms, which are directly transformed into typically volatile substances by entering into a direct reaction building into the carbon structure. The results shown by An et al. [131] demonstrate that the N-6 functional group derived from polypyrrole (nitrogen precursor) in the CNT core-shell structure plays a major role during electron transfer in the oxygen reduction reaction. The research group of Sa et al. [115] presented a synergistic effect between the CNTs' core structure and the heteroatom-doped sheath layer. The researchers demonstrated that the amount and appropriate type of

heteroatom in the sheath layer can be controlled through the correct selection of ionic liquids. This approach of creating CNT core structures that can facilitate electron transport to active sites and a cover layer doped with various heteroatoms to further enhance catalytic activity greatly contributes to improving activity in the oxygen reduction reaction. Many researchers are focused on the selection of appropriate synthesis parameters. Materials with core CNT core-shell structures can have better catalytic properties compared with double or triple heteroatom-doped carbon nanotube structures and become attractive materials for high-performance energy storage devices [115,132].

As combining the properties of two materials, in this case, carbon nanotubes and graphene, may be a good idea to improve the catalytic properties, Jiang et al. [133] investigated (a) the effect of carbonization temperature, (b) the ratio of CNTs and the precursor porous carbon structure, and (c) the effect of the ratio of carbon precursor to melamine (nitrogen precursor) on the catalytic performance of obtained materials in ORR in alkaline medium. The results show that the surface area, together with porosity, affect the catalytic activity, perhaps due to providing a large number of less active sites with better mass transfer at the same time. This is due to the amount of the nitrogen N-Q and N-6 functional groups, which affects catalytic activity in ORR. From a careful analysis, we can also find that the sample carbonized at 900 °C had more available active sites than other materials, carbonized at 800 or 1000 °C. By investigating the effect of the ratio of carbon nanotubes to glucose (as a precursor of the porous carbon sheath), the mass ratios subjected to hydrothermal treatment were examined. The lowest ratio came to 1:20, the average to 1:40, and the highest ratio to 1:80. Increasing the porous carbon precursor amount affects the final thickness of the nanoporous sheath layer. This ultimately translates into catalytic activity. A thin layer, and thus a smaller surface area, does not provide enough active sites. On the other hand, the highest ratio, 1:80, makes the shielding layer of carbon nanotubes so thick that electron transport in the oxygen reduction reaction is hindered by the low electron conductivity of the glucose-derived carbon material relative to the CNTs core. The best catalytic properties were exhibited by an average mass ratio of the reactants, 1:40. In the same work, the researchers also investigated the low, medium, and high (1:5, 1:10, 1:20) melamine content in the carbonized samples for catalytic activity in the oxygen reduction reaction. The catalyst-based electrode activity with 1:10 and 1:20 ratios showed increased initial and half-wave electrode potential. The enhanced catalytic activity was influenced by the higher amount of nitrogen precursor used; the core constructed from CNTs and a nitrogen-doped carbon nanoporous structure exhibited enhanced catalytic properties. The nanotubes formed a three-dimensional structure that was responsible for improved electron transfer, while the doped shell acted as active sites in the oxygen reduction reaction. Vikkisk et al. [23] obtained nitrogen-doped multiwalled carbon nanotubes using cyanamide or dicyandiamid. Studied catalysts showed increased selectivity towards the overall four-electron O_2 reduction pathway in alkaline media.

The use of CNTs in their hybrids or composites with graphene prevents agglomeration of graphene layers. The main problem that researchers face with graphene is that it reagglomerates very easily, which results in decreased catalytic activity, reduced specific surface area, and lower availability of active sites for the electrolyte and oxygen. To prevent this process, in many papers researchers used carbon nanotubes to counteract the reagglomeration, resulting in better accessibility for the reactants, ultimately contributing to an efficient oxygen reduction reaction. One example is a paper by Rasto et al. [15], where the authors pyrolyzed hybrids consisting of graphene oxide and multiwalled carbon nanotubes. In these studies, urea and dicyandiamide were used as nitrogen precursors, and doping was achieved by pyrolyzing the mixture of GO and MWCNTs in the presence of these nitrogen-containing compounds. Xue et al. [134] synthesized a composite of nitrogen-doped graphene nanoribbons on CNTs in an NH_3 atmosphere. The obtained materials present satisfactory high activity and stability of proton exchange membrane fuel cells. Table 4 summarizes the ORR activity of nitrogen-doped carbon nanotubes synthesized via the pyrolysis method.

Table 4. Summary of nitrogen-doped carbon nanotubes synthesized via the pyrolysis as an electrocatalyst for ORR.

Type of Sample	Type of Carbon	Precursor of Heteroatom(s)	S_{BET} (m^2 g^{-1})	Electrolyte	Heteroatom Content	Electron Transfer Number	Ref.
N-CNT	CNT	urea/DCDA [1]	n.d.	0.1 M KOH	4–6% at.	>3.5	[15]
N-CNT	CNT	melamine	104.7	0.1 M KOH	0.193% at.	2.77–2.80	[51]
N-CNT	CNT	NH_3/aniline	n.d.	0.1 M KOH	n.d.	2.5–4	[20]
N-CNT	FePc [2]	$NH_{3\,(gas)}$	n.d.	0.1 M KOH	3.6–5.6% at.	1.8–3.9	[113]
N-CNT	CNT	urea	230–284	0.1 M KOH	0.5–1.7% at.	2.9–3.55	[114]
N-CNT	CNT	urea/NH_3	n.d.	0.1 M KOH	n.d.	>3.7	[115]
N-CNT	CNT/GO	PEI [3]/DCDA	n.d.	1 M $HClO_4$	1.5–3.1% at.	3.58–3.94	[120]
N-CNT	C_2H_4	pyrrole	149.46–192.47	0.1 M KOH	5.69–6.90% at.	3.03–3.94	[131]
N-CNT	CNT	melamine	101–479	0.1 M KOH	3.54–15.76% at.	~4	[133]
N-CNT	CNT	CM [4]/DCDA	n.d.	0.1 M KOH	2.3–3.7% at.	4	[23]
N-CNT	CNT	$NH_{3\,(gas)}$	n.d.	0.1 M KOH/ 0.5 M H_2SO_4	3.09% at.	3.88–3.96/ 3.19–3.96	[134]
N,B-graphene	CNT/ BGQDs	$NH_{3\,(gas)}$/ Boric acid	n.d.	0.1 M KOH/0.01 M PBS/0.1 M $HClO_4$	N-0.5% wt. B-4.86% at.	3.2–3.5	[123]
N,S,F-graphene	CNT	BMITFSI [5]	293–489	0.1 M KOH	N-4.67.5% at. S-0.6%–1.1% at. F-0.7%–1.2% at.	3.4–4	[115]

[1] DCDA—dicyandiamide; [2] FePc—iron(II) phthalocyanine; [3] PEI—polyethylenimine; [4] CM—cyanamide; [5] BMITFSI—1-butyl-3-methylimidazolium bis(trifluoromethylsulfonyl)imide.

2.2.2. Synthesis of Nitrogen-Doped Carbon Nanotube-Based Materials via Hydrothermal Method

The modification and design of carbon nanotubes is carried out to effectively incorporate into the structure and produce highly conductive materials [135]. Patil et al. [136] combined the hydrothermal method with pyrolysis at 750 °C. They fabricated electrode materials for reduction reactions and oxygen evolution using carbon nanotubes, but also boron nitride (BN), it being a precursor of both nitrogen and boron. The research was based on the optimization of a suitable composition using different BN weight contents. The enhanced catalytic activity is attributed to synergistic effects between nitrogen and boron, but no clear trend is observed between BN weight content and catalytic properties. A comparison was made between the annealed and the hydrothermally treated material, and it was concluded that high temperature plays an important role in enhancing the activity of the ORR reaction. The onset potential of the pyrolyzed catalyst is more positive compared with the material before carbonization. Therefore, the use of pyrolysis can significantly affect the electrocatalytic properties. However, hydrothermal treatment can not only effectively introduce nitrogen heteroatoms, but also cause an improvement in hydrophobic properties, which affect the stability of the final electrodes. Hydrothermal treatment has been proven to improve the conductivity of multiwalled carbon nanotubes and the corresponding formation of oxygen groups (Figure 8). The observed improvement of catalytic properties in OER and HER reactions mainly takes place by increasing the amount of oxygen functional groups whose ability to attract electrons is stronger; these groups include ketones and carboxyl groups. However, they are also the cause of increasing hydrophilicity [137]. This method may also reduce the number of defects, which in turn can contribute to the deterioration of ORR activity. The hydrothermal method is additionally used to purify end products in order to improve the electrocatalytic properties. Nonetheless, it is worth remembering that even trace amounts of impurities from the synthesis can have a beneficial effect on the ORR process. The hydrothermal method can act as an effective and noninvasive way to functionalize MWCNTs with HNO_3. It can effectively oxidize nanotubes, but at the same time remove the amorphous carbon present on their surface, which can be a drawback in the catalytic chemical vapor deposition process [138]. Nitric acid is often used to introduce oxygen groups and thus provide better functionality of carbon nanotubes. The preoxidation method of MWSNTs was used by Huang et al. [139]. Nitrogen

atoms were doped into functionalized carbon nanotubes through a one-step hydrothermal process by introducing oxidized MWCNTs and ethylenediamine as a nitrogen precursor. Additional support and synergistic effect were produced by the resulting nitrogen-doped GQDs. The resulting double-atom-doped hybrid exhibited catalytic properties improved over a commercial-platinum-based material by showing a four-electron oxygen reduction reaction. This study sheds new light on low-cost synthesis and modification of metal-free carbon catalysts in the oxygen reduction reaction. Chem et al. [140] presented a one-step hydrothermal process for single and dual doping of sulfur and nitrogen. The advantages of this approach are the maintenance of proper electrical conductivity, preservation of a large surface area along with adequate porosity, and preservation of a multiwalled nanotube structure. The hydrothermal method does not require drastic chemicals and synthesis conditions. Therefore, this way of producing electrode materials has a high potential for heteroatom doping of carbon structures. Another approach to producing sulfur-doped carbon nanotubes is double doping as carried out by the research group of El-Sawy et al. [141]. The first modification consisted of a hydrothermal process of oxidized carbon nanotubes together with thiourea, while the second doping was performed through sonication of the obtained product from the first step together with ethanol and benzyl disulfide, carbonized at 1000 °C at the end. The researchers showed that the hydrothermal method was insufficient to obtain the right conductivity of the carbonaceous materials, though it showed the highest sulfur and oxygen content. At the same time, double doping combined with pyrolysis shows higher activity due to numerous active sites. The approach of double doping using different methods can contribute to the development of metal-free electrocatalysts, creating a new perspective on the modification of carbon materials used in the reduction reaction of oxygen, carbon dioxide, or hydrogen evolution.

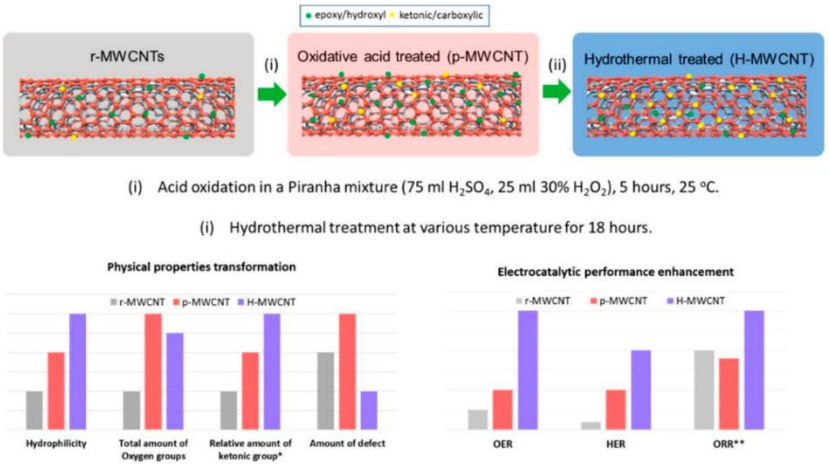

Figure 8. Graph of the effect of the hydrothermal treatment method on the change in physical properties and improvement in electrocatalytic performance (values on the graph for demonstration purposes). Indication: * ketonic group has been demonstrated to catalyze a number of electrochemically important reaction such as OER and HER, ** the ORR performance of r-MWCNT was found to be higher due to the presence of surface bound metal impurities. Adapted from [137], with permission from *ACS Applied Materials & Interfaces*, 2016.

2.2.3. Synthesis of Nitrogen-Doped Carbon Nanotube-Based Materials via Chemical Vapor Deposition Method

The CVD method is a widely studied way to produce carbon nanotubes of very high quality. As a result of the high temperature in the reaction chamber, precursors are broken down into smaller components (final product or as a layer). The precursors can be delivered with the other carbon precursors, or in the furnace, and carried by the carrier gas. Previous studies based on the synthesis of nitrogen-doped carbon nanotubes by CVD using various nitrogen–carbon precursors show less favorable catalytic properties in the oxygen reduction reaction when the medium is acidic rather than alkaline. Alexeyeva et al. [142] synthesized nitrogen-doped carbon nanotubes (with 3% at. of nitrogen) simultaneously using acetonitrile as nitrogen and carbon precursors. The researchers presented a comparison of electrochemical properties of nitrogen-doped carbon nanotubes and pure unmodified ones in the research paper. They conducted electrochemical studies on sulfuric acid and potassium hydroxide as electrolytes. Despite their best efforts, activity in ORR in an acidic medium remained lower than for the catalysts fabricated from carbon nanotubes based on platinum [143]. Wong et al. [144] investigated the effect of different nitrogen precursors on the catalytic properties in acidic medium as well. Iron (II) phthalocyanine was used as a catalyst for one-step doping and growth of carbon nanotubes using the CVD method. Three nitrogen precursors were compared, aniline, diethylamine, and ethylenediamine (EDA). At elevated temperatures, the metal catalyst is decomposed into smaller iron molecules, which form the base for nanotube growth, and the hydrocarbon catalyst, which produces a graphitic structure deposited on the iron base. The iron molecules are removed in the final process with sulfuric acid. The carbon nanotubes produced using EDA exhibited higher electrochemical activity at ORR in an acidic medium relative to the other nitrogen-rich CNTs synthesized with aniline and diethylamine. The electrochemical properties of the best test sample also stemmed from the surface structure, due to corrugation, and the extensive distribution of defects, which can act as active sites or cause better access to the edge functional groups. Other researchers, Gonzalez et al. [145], used melamine as a source of nitrogen and carbon and ferrocene as a catalyst for the growth of N-doped nanotubes to investigate the electrochemical properties in an acidic environment. As expected, the materials produced at 900 °C exhibited higher ORR activity relative to 800 °C synthesis. They concluded through Raman spectroscopy analysis and final electrochemical results that temperature affects the amount of defects generated by introducing more nitrogen heteroatoms. They also investigated the effect of the flow rate of the carrier gas, argon. In this case, they came up with a bold hypothesis that as the flow rate of argon increases, the value of the current density limiting diffusion is higher. However, there are no direct reports that this hypothesis is backed up by many experiments. It is known, however, that the rate at which a carrier gas flows influences physicochemical properties. It appears that a higher carrier gas rate results in a low number of defects, which in turn may contribute to lower activity in the ORR. Therefore, it is important to tune and optimize the synthesis conditions, carrier gas flow, and temperature and select appropriate precursors and catalysts that will benefit nitrogen incorporation into the structures that will be the active sites in ORR in an acidic environment.

The CVD method is also useful for preparing hybrids containing N-CNTs and $LaNiO_3$ [146]. In this synthesis, ammonia and methane were used to obtain the nitrogen-doped nanotubes, and acted as nitrogen and carbon precursors, respectively. Thanks to the La and Ni present in the hybrid, it is possible to support the adsorption of oxygen molecules, as well as facilitate electron transfer. The transition metals do not form direct active sites but support active sites, making them more accessible to provide higher catalytic activity [147,148]. Therefore, the use of other transition metals, such as Co, Zn, and Fe, can increase the catalytic activity, as many researchers suggest that catalytic properties stem from special metal–carbon confluence [147,149]. Not only do transition metals increase catalytic activity; hence in the case of graphene, scientists also try doping carbon nanotubes with other heteroatoms. Yang et al. [150] showed that the number of electrons transferred in the oxygen reduction

reaction increased slightly for boron-doped carbon nanotubes; the number of transferred electrons increased from 2.2 to 2.5 for undoped CNTs and boron-doped CNTs, respectively. In the case of a sample codoped with boron and nitrogen, the transfer also showed a two-electron pathway for oxygen reduction [151]. Although boron doping alone does not show spectacular catalytic activity, the instructive nature of the work is evident, because it provides much information on what to avoid when optimizing synthesis conditions. Table 5 summarizes the ORR activity of nitrogen-doped carbon nanotubes synthesized via CVD and the hydrothermal method.

Table 5. Summary of nitrogen-doped carbon nanotubes synthesized via CVD and the hydrothermal method electrocatalyst for ORR.

Type of Sample	Type of Carbon	Precursor of Heteroatom(s)	S_{BET} (m^2 g^{-1})	Electrolyte	Heteroatom Content	Electron Transfer Number	Ref.
N-CNT	CNT/CQDs	EDA [1]	n.d.	0.1 M KOH	n.d.	3.78–3.85	[139]
N-CNT	CNT	NH_4OH	388	0.1 M KOH	1.32% at.	3.7–3.8	[140]
N-CNT	Acetonitrile	Acetonitrile	n.d.	0.1 M KOH/ 0.5 M H_2SO_4	3% at.	2–3.5/2–4	[142]
N-CNT	FePc	Aniline/DEA [2]/EDA	n.d.	0.5 M H_2SO_4	4.33–6.58% at.	3–3.6	[144]
N-CNT	Pyridine	Pyridine	n.d.	0.5 M H_2SO_4	4.29–5.6% wt. 1.8–2.5% at.	n.d.	[145]
N,B-CNT	CNT	L-aspartic/ orthoboric acid	136.2	0.1 M KOH	N-1.19% at. B-0.51% at.	3.48	[135]
N,B-CNT	CNT	BN [3]	n.d.	0.1 M KOH	n.d.	3.9	[136]
N,S-CNT	CNT	$(NH_4)_2$ S	n.d.	0.1 M KOH	N-2.65% at. S-0.76% at.	n.d.	[140]

[1] EDA—ethylenediamine; [2] DEA—diethylamine; [3] BN—boron nitride.

2.3. Porous Carbon Electrocatalysts Based on Natural Precursors

In the last 10 years, a large number of studies have focused on the synthesis of biomass-derived carbons as attractive electrocatalysts [152]. As mentioned previously, the CVD method is based on the introduction of gaseous carbon precursors or heteroatoms that will be able to deposit on the substrate and form a structure in a bottom-up approach. It is not common to use the CVD method to introduce heteroatoms in a structure based on carbon materials of natural origin. Porous materials of organic origin do not require the conversion of carbon precursors to a gaseous form, and either pyrolysis or hydrothermal methods can produce materials high in nitrogen. Therefore, these two methods are presented in more detail in the following chapters in the context of nanofibers and materials of natural origin.

A particularly promising research subject is the utilization of marine- and freshwater-derived materials as carbon and nitrogen sources, for example, seaweed [153–155], shrimp shells [156,157], fish bone [158], algae [159,160], alginate [161,162], chitin, and chitosan [163–167]. For nitrogen-doped porous carbons obtained from chitin and chitosan, the influence for catalytic properties has porosity and type of functional groups [163]. The effect of additional urea treatment on the textural, chemical, and electrocatalytic properties of the obtained carbons was also presented. The highest number of O_2-reducing electrons, equal to 3.76, was recorded for the sample obtained from chitosan. The total nitrogen content of the samples obtained was in the range of 4.85% to 10.85% wt. Nitrogen was mainly present as N-5 and N-6 groups; however, N-Q and N-X groups were present as well. The share of nitrogen in the form of N-6 and N-5 groups exceeded 80% of the total nitrogen content. For the samples obtained with urea, the total nitrogen content increased to the level of 82.8–84.8% at. Additionally, the significant share of nitrogen functions of N-5 and N-6 and N-Q type increased when increasing the carbonization temperature from 700 to 800 °C. Quílez-Bermejo et al. [58] proved that as the temperature applied during the heat treatment increases, so do increase the catalytic properties in ORR. The authors attribute the enhanced catalytic activity to an increased N-Q number at the edges. The surface area can also be seen to increase with rising carbonization temperature, from which it can be concluded that the specific surface area is one of the factors favoring an increase in catalytic

activity. Increasing the surface area, which comprises a higher density and distribution of microporous structures, may contribute to increasing the effective ORR. However, previous work suggests that there are several factors that need to be achieved and developed in order for ORR to proceed in a four-electron pathway [168]. One strategy is to develop a specific surface area, and thus porosity, which will facilitate the electrolyte and ion diffusion process. The appropriate pore size guarantees permanent electrical contact and ensures long-standing four-electron oxygen reduction [169]. The bimodal distribution of pores favors the kinetics of the ORR and the diffusion of active species [170].

Gelatin is an animal derivative that contains about 16% wt. of nitrogen; therefore, it was used in many studies as a precursor in the synthesis of catalysts [160,171–174]. It is a highly economical reagent because it is a naturally abundant and sustainable resource with high solubility in polar solvents, making it a promising precursor for nitrogen-doped carbons. An example of effective synthesis are carbon samples obtained by a method of templating gelatin with colloidal silica [160]. The hierarchical gelatin-derived porous structure showed a high density of N-containing active sites (ut to 10.08% at.) and a high specific surface area (up to 880 m^2 g^{-1}). These catalysts possess a 3D mesoporous network structure that is highly favorable for rapid ORR species transport. This efficiency is promoted by the simultaneous presence of N-5 and N-Q sites, the amount of the latter being especially important in determining ORR activity. It further depends on the carbonization temperature and greatly benefits from exposed N-Q along the outer and inner carbon sheets with a high surface area. For N-doped gelatin-derived carbons, voltammograms measured in KOH O_2-saturated electrolyte exhibit a well-defined cathodic peak (Figure 9a), and the LSV curves for the produced catalysts show a similar current density to the commercial Pt/C catalyst (presented in Figure 9b). The Koutecky–Levich plots (Figure 9c) for each catalyst were obtained from LSV at various rotational speeds. The highest electron transfer number values (Figure 9d) were equal 3.85 and 3.96; these numbers confirm that catalytic activity was equal to a four-electron ORR pathway of the commercial Pt/C catalyst.

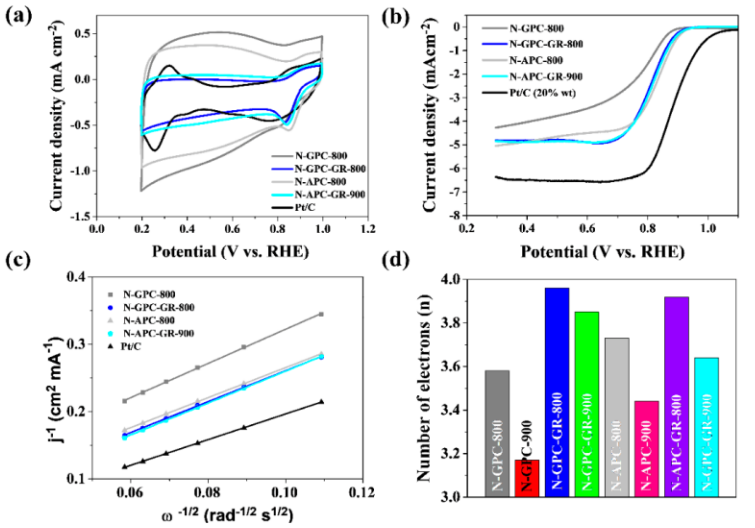

Figure 9. Results of catalyst activity in the oxygen reduction reaction for N–rich–derived carbons and the Pt/C catalyst. (**a**) CV curves of electrocatalysts in an O_2–saturated 0.1 M KOH solution, (**b**) LSV of various electrocatalysts on RDE measured at a scanning speed of 5 mV s^{-1} and a rotation speed of 1600 rpm, (**c**) Koutecky–Levich plot at 0.5 V, (**d**) number of transferred electrons. Adapted from [160], with permission from *Scientific Reports*, 2021.

In the case of nitrogen-free natural precursors such as corn stover [175], ginkgo leaves [176], coconut shell [177], or cellulose [5,178], introducing nitrogen atoms into the structure is required to obtain effective electrocatalysts for ORR. In the case of corn stover, as illustrated in Figure 10, the electrocatalyst was prepared in two major steps of KOH activation and heteroatom doping. First, corn stovers were obtained from an experiment farm and washed with water and ethanol for several times. KOH activation was a crucial element of generating a pore network in carbon this synthesis. However, the activation mechanism has not been well understood due to the large number of variables in both the experimental parameters and the reactivity of different precursors used. Summarily, the reaction starts with solid–solid (carbon and KOH) reactions. In the next step, solid–liquid reactions take place, including the reduction of potassium compounds to form metallic potassium and the oxidation of carbon to carbon oxide and carbonate [179]. For KOH carbon activation, three main activation mechanisms have been widely accepted: (I) etching the carbon framework by the redox reactions between various potassium compounds as chemical activating reagents with carbon, called chemical activation, is responsible for generating the pore network [180–182]; (II) the formation of H_2O and CO_2 in the activation system positively contributes to the further development of the porosity through the gasification of carbon, namely, physical activation; and (III) metallic potassium efficiently intercalates into the carbon lattices of the carbon matrix after its removal by washing, and the expanded carbon lattices cannot return to their previous nonporous structure, creating the high microporosity that is necessary for a large specific surface area [183].

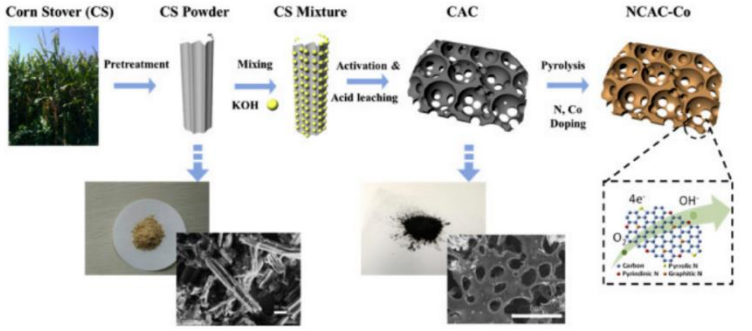

Figure 10. Schematic diagram for synthesis of N and Co, codoping NCAC-Co. Adapted from [175], with permission from *Energy*, 2018.

Depending on the nitrogen reagent used, the modification is carried out in the solid (e.g., in the case of urea), liquid (in the case of amines), or gaseous (in the case of ammonia and nitrogen oxides) [184] phase. Melamine [185], amino acids [186], acrylonitrile [187], and NH_3 gas are mainly reported as nitrogen reagents for the synthesis of nitrogen-doped porous carbon ORR catalysts. In our experience, metal-free carbon foams obtained from amino acids are valuable electrocatalysts for the four-electron oxygen reduction process [186]. A nitrogen content of up to 9.1% wt., a large surface area of up to 1287 $m^2\ g^{-1}$, and a large share of mesopores ensure full exposure of active sites, which is responsible for achieving high catalytic activity in ORR. Moreover, a high carbonization temperature of 800–900 °C ensured high electrical conductivity as a result of a more intensive graphitization process. Table 6 summarizes the ORR activity of nitrogen-doped porous carbons synthesized by pyrolysis of nitrogen-containing or nitrogen-free precursors treated by different methods.

Table 6. Summary of nitrogen-doped porous carbons derived from natural precursors as electrocatalysts for ORR.

Type of Sample	Precursor of C and N	S_{BET} (m^2 g^{-1})	Electrolyte	N Content	Electron Transfer Number	Ref.
N-C [1]	Seaweed	674.63–1217.78	0.1 M KOH	1.8–5.21% at.	3.7	[153]
N-C	Spiral seaweed	199.2–1610.3	0.1 M KOH	4.5–5.1% wt.	4	[154]
N-C	*Sargassum* spp.	3.84–188.87	0.5 M KOH	0.56–0.95% wt.	n.d. [2]	[155]
N-C	Shrimp shell	647.7	0.1 M KOH	7.44% at.	3.8	[156]
N-C	Shrimp shell	13.4–360.2	0.1 M KOH	6.8–11.8% at.	1.36–2.95	[157]
N-C	Fish bone	n.d.	0.1 M KOH	6.02% at.	n.d.	[158]
N,S-C [3]	Algae, MEL [4]	538	0.1 M KOH	2.63% at.	3.97	[159]
N-C	Green algae	366–623	0.1 M KOH	2.16–7.09% wt.	3.44–3.84	[160]
N,Co-C	Alginate	252	0.1 M KOH	2–5.5% at.	>4	[162]
N-C	Alginate	470.9	0.1 M KOH	1% at.	4	[161]
N-C	Chitin, chitosan	625–1801	0.1 M KOH	4.85–10.85% wt.	2.17–3.76	[163]
N-C	Chitosan	907	0.1 M KOH	n.d.	3.9–4	[164]
N-C	Chitosan	78–1317.97	0.1 M KOH	4.7–8.1% wt.	2.2–3.5	[165]
N-C	Chitosan	n.d.	0.1 M KOH	n.d.	3.9–4.1	[166]
N-C	Chitosan	285	0.1 M KOH	3.3–4.5% wt.	n.d.	[167]
N-C	Gelatin	376–839	0.1 M KOH	4.69–5.73% at.	3.41–4.14	[171]
N-C	Gelatin	739.5–933.9	0.1 M KOH	1.19–1.79% at.	3.7–3.85	[172]
N-C	Gelatin	189.8–1215.4	0.1 M KOH	3.6–4.3% at.	3.9–4	[173]
N-C	Gelatin	360–880	0.1 M KOH	3.24–10.08% wt.	3.17–3.85	[160]
N,Fe,Mg-C	Gelatin	370–650	0.1 M KOH	5.8–6.8% wt.	3.9–4.2	[174]
N,Co-C [6]	Corn stover, urea, $CoCl_2$	1877.3	0.1 M KOH	2.56% at.	3.87	[175]
N-C	Ginkgo leaves, NH_3	1436.02	0.1 M KOH	1.59% at.	3.7	[176]
N,P-C [5]	Coconut shells, H_3PO_4, urea	1216	0.1 M KOH	0.5–1.1% at.	4	[177]
N,P-C	Cellulose, MEL, PA [7]	241–612	0.1 M KOH	2.4–4.4% at.	3.58–3.99	[5]
N,P-C	Cellulose, $(NH_4)_3PO_4$	n.d.	PBS [8]	2.17% at.	3.5	[178]

[1] N–C—nitrogen-doped carbon; [2] n.d.—not determined; [3] N,S–C—nitrogen and sulfur-doped carbon; [4] MEL—melamine; [5] N,P–C—nitrogen and phosphorus-doped carbon; [6] N,Co–C—nitrogen and cobalt-doped carbon; [7] PA—phytic acid; [8] PBS—phosphate buffer solution.

2.4. Carbon Nanofiber-Based Electrocatalysts

Carbon nanofibers are very promising carbonaceous materials for electrochemical applications [188]. In the literature, synthesis methods such as pyrolysis [5,189,190] and chemical vapor deposition [191–194] are most widely used in large-scale production. Furthermore, electrospinning [195] is an effective carbon nanofiber synthesis method. Hydrothermal carbonization is an alternative and promising strategy of deriving a carbon nanostructure from biomass. As a carbon and nitrogen source, nitrogen-containing carbohydrates are used primarily, such as chitosan [196–199], glucosamine [200–202], and amino acids [203]. Song et al., during the hydrothermal synthesis of nitrogen-doped carbon nanofiber, used glucosamine hydrochloride and ultrathin tellurium nanowires as templates [204]. Microscopic observations indicated that the diameter of nanofibers declined from 150 to 100 nm after the pyrolysis and CO_2 activation processes (Figure 11a,b). To investigate the elemental distribution in N-CNFs-900–0.5 h, elemental mapping was undertaken using energy-filtered transmission electron microscopy (EFTEM) imaging as the analysis method (Figure 11c). The images revealed that nitrogen atoms were homogeneously distributed in the nanofibers. After heat treatment in an inert atmosphere at 900 °C and further activation with CO_2 at 1000 °C, the highly porous N-doped carbon nanofibers with a BET surface area of up to 1324.25 m^2 g^{-1} with N-5, N-6, and N-Q functional groups on the surface were produced (Figure 11d–f). The material activated with CO_2 for 4 h exhibited the optimal balance of porosity, nitrogen content, and electricity for ORR activity. The

N-CNFs-900–4 h sample displayed 3.74–4.02 transferred electrons in alkaline electrolyte at potentials ranging from −0.30 to −0.90 V.

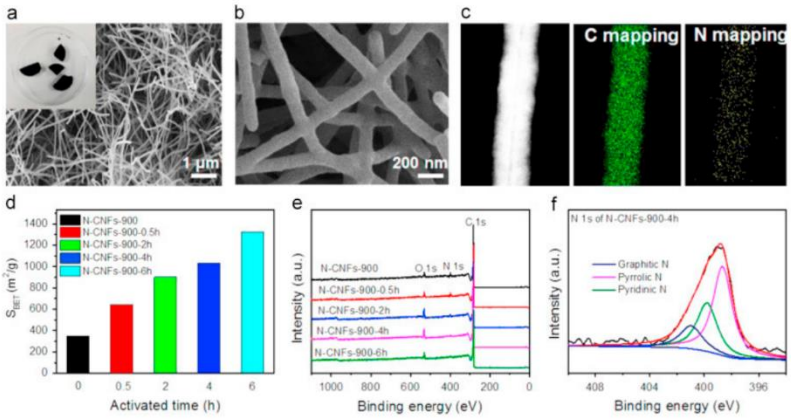

Figure 11. Characterization of the conductive and porous N-CNF aerogels obtained after pyrolysis and CO_2 activation. (**a**,**b**) SEM images at different magnifications; (**c**) EFTEM image and elemental mapping; (**d**) comparison of the BET surface areas; (**e**) XPS survey spectra; (**f**) high-resolution N1s spectra of the N-CNFs-900–4 h. Adapted from [204], with permission from *Nano Energy*, 2016.

2.4.1. Synthesis of Nitrogen-Doped Carbon Nanofiber-Based Materials via Pyrolysis Method

In the case of N-doped carbon nanofibers fabricated through carbonization, two or more precursors acting as carbon and nitrogen sources are required. By extension, the selection of proper precursors is essential to the formation of effective N-doped carbon nanofibers with high catalytic performance. Biomass is often seen as an environmentally friendly and low-cost precursor; during the last few years, bacterial cellulose in particular has attracted dramatic interest due to its production through ecofriendly microbial fermentation procedures [205]. To obtain a 3D N-CNF structure, Li et al. [206] freeze-dried bacterial-cellulose-coated polypyrrole with added $FeCl_3 \times 6\ H_2O$ before pyrolysis in a N_2 atmosphere. As a result, in the final product, higher catalytic activity was observed for N-CNFs, which possessed a higher level of pyridinic N (2.95% at.), than for pyrrolic N (1.41% at.) and graphitic N (2.02% at.). Another way to introduce nitrogen atoms to a CNF structure is their heat treatment in an NH_3 atmosphere [207]. NH_3 was also an activating agent and caused a high BET equal to 916 $m^2\ g^{-1}$. The tested N-CNF catalyst shows superior ORR activity and higher selectivity with an electron transfer number of 3.97 at 0.8 V when compared with four reference carbon materials (Vulcan XC-72R, Ketjenblack EC-300J, CNTs, and reduced graphene oxide aerogels). Excellent electrochemical stability in alkaline media for only a 20 mV negative shift of half-wave potential after 10,000 potential cycles was also determined for N-CNF aerogel [207]. Mulyadi et al. prepared carbon nanocomposites by mixing the solvothermal-treated CNFs-derived N,S-doped carbon nanofibers with complex particles of melamine–phytic acid [5]. In the next step, the suspension was allowed to sediment before lyophilization at room temperature for 4 days to form the carbon nanocomposite. Pyrolysis of the carbon nanocomposite was performed in a nitrogen atmosphere at 400 °C for 2 h, followed by another 2 h at 900 °C. The best electrocatalytic activity achieved for CNFs consisted of four heteroatoms: nitrogen (3.9% at.), sulfur (0.5% at.), phosphorus (1.9% at.), and oxygen (4.9% at.). For a good linear fitting of Koutecky–Levich plots, the desirable four-electron reduction process is predominant.

Massaglia et al. used a electrospinning technique to obtain N-CNFs from the polyacrylonitrile solution, which was then pyrolyzed at 900 °C in an inert atmosphere [189]. N-CNFs are characterized by a high amount of nitrogen groups on four states; however, the highest atomic percentage falls on graphitic N and pyridinic N, with 55.1% at. and 26.7% at., respectively. An optimal content of both N-Q and N-6 ensures a four-electron pathway towards ORR and guarantees samples' good electrical conductivity. Park et al. also used polyacrylonitrile and polystyrene in the electrospinning method [208]. For samples obtained with the pyrolysis temperature increased from 800 to 1100 °C, the onset potentials were shifted towards a more positive direction, and the limiting current density increased consecutively. For the best catalyst of N-CFs-1100 pyrolyzed at 1100 °C, the number of transferred electrons was 3.7–3.8. These results indicate that the composite samples are very promising electrocatalysts for ORR in an alkaline solution, demonstrating a highly competitive performance but at a much lower cost than the benchmarked Pt/C catalysts.

2.4.2. Synthesis of Nitrogen-Doped Carbon Nanofiber-Based Materials via Chemical Vapor Deposition Method

In the one of the pioneering papers describing the use of N-CNF in ORR, Maldonado and Stevenson prepared electrodes through a CVD method, using xylene, ferrocene, and pyridine as precursors to control nitrogen content [209]. ORR catalysts manufactured in this way showed significant activity towards the reduction of H_2O_2 in alkaline media, it being an essential stage in the whole ORR process. Some papers point out an issue related to the use of oxide catalytic supports of low electronic conductivity; that is, purification steps, such as refluxing in concentrated alkaline and acidic solutions, are necessary before employing the N-CNFs in electrocatalytic applications. An example is given in the paper by Yin et al., where post-treatment procedures with a H_2SO_4/HNO_3 mixture alter the surface chemistry and catalytic properties of the N-CNFs [210].

As reported by Bokach et al., catalytic chemical vapor deposition is an effective method for the production of nitrogen-containing carbon nanofibers in a one-step process, at a 650 °C Fe nanoparticle form, supported on expanded graphite using a mixture of CO, NH_3, and H_2 [211]. The pore formers Li_2CO_3, $(NH_4)_2CO_3$, and polystyrene microspheres were used to improve mass transport within the layer. The BET surface area and nitrogen content for the N-CNFs were 225 $m^2\ g^{-1}$ and 3.3% at., respectively. The observed large pores act as a passage for oxygen and water transport in the thick N-CNF/Fe cathodes, and thus lead to better performance. Conversely, Muthuswamy et al. [212] showed that KOH treatment resulted in similar ORR activity to pristine N-CNFs, despite growth of the surface area (BET) from 270 to 1151 $m^2\ g^{-1}$. After KOH treatment, nitrogen content drastically decreased from 4.7% at. to 0.5% at. Additionally, after activation, iron content decreased from 0.24% at. to 0.02% at.; however, the activity was much like pristine N-CNFs. The authors suggest that, besides iron or nitrogen atoms, there are active sites originating from the distinct carbon environment formed during the N-CNF synthesis. To remove iron particles from the catalyst, Buan et al. treated N-CNFs with concentrated nitric acid [192]. After HNO_3 treatment, nitrogen content was also reduced by 50% in the surface; however, ORR performance in acidic electrolyte was not affected. The authors deduced that the present porphyrin-like Fe–N_4 sites are active sites for oxygen adsorption and reduction on N-CNFs in acidic electrolyte. In a previous paper by Buan et al. [213], the influence of Fe and Ni on ORR activity was described. The oxygen reductions for N-CNF/Ni and N-CNF/Fe were two- and four-electron pathways in both acidic and alkaline electrolyte. The analyzed results may serve as an explanation of why N-doped carbon nanostructures modified by Ni show lower ORR activity when compared with those doped with Fe. However, for ORR the contribution from metallic iron, iron carbide, iron nitride, and CNFs grown from Fe can be ruled out. Table 7 summarizes the ORR activity of effective electrocatalysts based on nitrogen-doped carbon nanofibers.

Table 7. Summary of nitrogen-doped carbon nanofibers as electrocatalysts for ORR.

Type of Sample	Precursor of CNF	Precursor of Heteroatom	S_{BET} (m^2 g^{-1})	Electrolyte	N Content	Electron Transfer Number	Ref.
N-CNF	$C_6H_{13}NO_5xHCl$	$C_6H_{13}NO_5xHCl$	643–1324	0.1 M KOH	1.64–4.67% at.	3.74–4.02	[204]
N-CNF	Bacterial cellulose	C_4H_5N	215–253	0.1 M KOH/ 0.1 M $HClO_4$	4.90–8.33% at.	3.7	[206]
N-CNF	Bacterial cellulose	NH_3	916	0.1 M KOH	5.8% at.	3.96	[207]
N-CNF	PAN [1]	PAN	n.d. [2]	0.1 M KOH	2% at.	3.9	[189]
N-CNF	PAN, PS [3]	PAN	905–1271	0.1 M KOH	n.d.	3.7–3.8	[208]
N-CNF	Xylene	pyridine	130	0.5 M H_2SO_4/0.1 M KOH	4% at.	3.97	[209]
N-CNF/Fe	Graphite	NH_3	225	0.5 M H_2SO_4	3.3% at.	n.d.	[211]
N-CNF/Ni or Fe	Graphite	NH_3	35–226	0.5 M H_2SO_4/0.5 M KOH	1.5–3.9% at.	2–4	[213]
N-CNF	Graphite	NH_3	152–210	0.5 M H_2SO_4	2.4–5.1% at.	n.d.	[192]
N-CNF	Graphite	NH_3	270–1151	0.5 M H_2SO_4	0.24–4.7% at.	n.d.	[212]
N,P,S-CNF	Cellulose nanofibrils	$C_3H_6N_6$, $C_6H_{18}O_{24}P_6$	565–1217	0.5 M H_2SO_4/0.1 M KOH	2.4–4.3% wt.	3.58–3.99	[5]

[1] PAN—polyacrylonitrile; [2] n.d.—not determined; [3] PS—polystyrene.

3. Conclusions and Perspectives

In this review, we focused on nitrogen-doped, carbon-based electrodes as metal-free catalysts toward ORR. First, the mechanism of oxygen reduction in alkaline and acidic media was briefly explained. In the experimental studies, doped graphene showed the capability to catalyze oxygen reduction via a four-electron transfer pathway in alkaline electrolyte. Nevertheless, replacing a commercial Pt/C catalyst in an acidic electrolyte with doped graphene is still impossible and a challenge for research.

In experiments, a good understanding of ORR activity is possible using doped graphene quantum dots, especially with sizes closer to models used in theoretical research. Therefore, future experimental inquiries should focus more on producing graphene quantum dots and on their ORR activity in different electrolytes, as these mechanisms require additional investigation.

The methods presented in this work provide a summary of the main techniques for synthesizing nitrogen-doped carbon materials capable of being commercialized. It is not possible to say directly which synthesis technique is more efficient and promising for obtaining N-doped carbon material. Nevertheless, according to many reports, the CVD method is a good choice for obtaining multilayer carbon materials of high quality. However, one should also keep in mind the economic and ecological aspects in which the pyrolysis method fits perfectly. This method is characterized by an uncomplicated procedure for the preparation of N-doped carbon materials, as well as a significantly higher yield compared with the CVD method. On the other hand, by means of the hydrothermal method, it is possible to obtain a quantity of material that goes beyond the laboratory using safe synthesis conditions. The combination of pyrolysis and hydrothermal methods can be a perspective for obtaining materials doped with heteroatoms. Due to these advantages, methods that have large-scale commercialization potential for industrial application are presented. Small modifications of precursor amount, changes of carbon and nitrogen source, and the choice of proper temperature can contribute to obtaining materials with properties comparable to commercial ones based on heavy metals.

The influence of nitrogen sources on the final catalytic properties of the obtained carbon materials is also a very important aspect of the optimization of synthesis conditions. The selection of an appropriate precursor is a key element to successfully introducing nitrogen in the right type and amount into the carbon structure. The most commonly used nitrogen precursors include urea, melamine, and ammonia, while the most interesting

ones that fit into the concept of green chemistry are natural ones, such as chitosan, green algae, and gelatin, which all contain high amounts of nitrogen. Despite the high nitrogen content of the precursors, the final amount of introduced heteroatom is on the level of several to several tens of percent. When considering the percentage of nitrogen, the type of functional groups introduced must also be taken into account. It is still disputed among scientists attributing the direct effect of pyridine functional groups or quaternary nitrogen on catalytic activity. However, it is important to remember that both of these groups have an effect on catalytic activity. Knowing that pyridine groups are responsible for the increase of the starting potential, while quaternary nitrogen affects the limiting current density in the oxygen reduction reaction, the presence of both groups will effectively improve the final catalytic properties. It is also worth mentioning other structural and morphological properties that may help or hinder access to the active sites. A reasonable nitrogen group content maintains a high population of active sites, where the extra electrons from nitrogen correlate with π electrons in sp^2 carbon materials. Furthermore, the high performance of carbon-based electrocatalysts depends on a good balance between electron conductivity and specific surface area. However, in many papers we are unable to find information about the specific surface area, especially in the case of graphene-based electrodes; knowing that a surface area aids active sites by creating better accessibility to oxygen, an attractive prospect are those carbon foams that have an open pore system, allowing for exposed active sites and the highest possible electrolyte penetration for oxygen to reach all active sites, affecting catalytic activity.

Author Contributions: Conceptualization: A.I., M.S. and J.P.L.; writing—original draft preparation: M.S. and A.I.; writing—review and editing: A.I., M.S. and J.P.L.; supervision: A.I. and J.P.L. All authors have read and agreed to the published version of the manuscript.

Funding: This work was carried out as a result of research project no. 2019/35/N/ST5/02691, financed by the National Science Centre.

Institutional Review Board Statement: Not applicable.

Informed Consent Statement: Not applicable.

Conflicts of Interest: The authors declare no conflict of interest.

References

1. Frattini, D.; Accardo, G.; Ferone, C.; Cioffi, R. Fabrication and characterization of graphite-cement composites for microbial fuel cells applications. *Mater. Res. Bull.* **2017**, *88*, 188–199. [CrossRef]
2. Tan, P.; Chen, B.; Xu, H.; Zhang, H.; Cai, W.; Ni, M.; Liu, M.; Shao, Z. Flexible Zn-and Li-air batteries: Recent advances, challenges, and future perspectives. *Energy Environ. Sci.* **2017**, *10*, 2056–2080. [CrossRef]
3. Li, L.; Fan, W.; Xuan, J.; Leung, M.K.; Zheng, K.; She, Y. Optimal design of current collectors for microfluidic fuel cell with flow-through porous electrodes: Model and experiment. *Appl. Energy* **2017**, *206*, 413–424. [CrossRef]
4. Ren, S.; Duan, X.; Liang, S.; Zhang, M.; Zheng, H. Bifunctional electrocatalysts for Zn-air batteries: Recent developments and future perspectives. *J. Mater. Chem. A* **2020**, *8*, 6144–6182. [CrossRef]
5. Mulyadi, A.; Zhang, Z.; Dutzer, M.; Liu, W.; Deng, Y. Facile approach for synthesis of doped carbon electrocatalyst from cellulose nanofibrils toward high-performance metal-free oxygen reduction and hydrogen evolution. *Nano Energy* **2017**, *32*, 336–346. [CrossRef]
6. ElMekawy, A.; Hegab, H.M.; Losic, D.; Saint, C.P.; Pant, D. Applications of graphene in microbial fuel cells: The gap between promise and reality. *Renew. Sustain. Energy Rev.* **2017**, *72*, 1389–1403. [CrossRef]
7. Duan, J.; Chen, S.; Jaroniec, M.; Qiao, S.Z. Heteroatom-doped graphene-based materials for energy-relevant electrocatalytic processes. *ACS Catal.* **2015**, *5*, 5207–5234. [CrossRef]
8. Qu, K.; Zheng, Y.; Dai, S.; Qiao, S.Z. Graphene oxide-polydopamine derived N,S-codoped carbon nanosheets as superior bifunctional electrocatalysts for oxygen reduction and evolution. *Nano Energy* **2016**, *19*, 373–381. [CrossRef]
9. Jin, J.; Pan, F.; Jiang, L.; Fu, X.; Liang, A.; Wei, Z.; Zhang, J.; Sun, G. Catalyst-free synthesis of crumpled boron and nitrogen co-doped graphite layers with tunable bond structure for oxygen reduction reaction. *ACS Nano* **2014**, *8*, 3313–3321. [CrossRef]
10. Zhang, C.; Mahmood, N.; Yin, H.; Liu, F.; Hou, Y. Synthesis of phosphorus-doped graphene and its multifunctional applications for oxygen reduction reaction and lithium ion batteries. *Adv. Mater.* **2013**, *25*, 4932–4937. [CrossRef]
11. She, Y.; Chen, J.; Zhang, C.; Lu, Z.; Ni, M.; Sit, P.H.-L.; Leung, M.K. Nitrogen-doped graphene derived from ionic liquid as metal-free catalyst for oxygen reduction reaction and its mechanisms. *Appl. Energy* **2018**, *225*, 513–521. [CrossRef]

12. Zhang, C.; Ma, B.; Zhou, Y. Three-dimensional Polypyrrole Derived N-doped Carbon Nanotube Aerogel as a High-performance Metal-free Catalyst for Oxygen Reduction Reaction. *ChemCatChem* **2019**, *11*, 5495–5504. [CrossRef]
13. Bandosz, T.J. Porous Carbons as Oxygen Reduction Electrocatalysts. In *Porous Materials*; Springer: Berlin/Heidelberg, Germany, 2021; pp. 41–77.
14. Wu, J.; Ma, L.; Yadav, R.M.; Yang, Y.; Zhang, X.; Vajtai, R.; Lou, J.; Ajayan, P.M. Nitrogen-doped graphene with pyridinic dominance as a highly active and stable electrocatalyst for oxygen reduction. *ACS Appl. Mater. Interfaces* **2015**, *7*, 14763–14769. [CrossRef]
15. Ratso, S.; Kruusenberg, I.; Vikkisk, M.; Joost, U.; Shulga, E.; Kink, I.; Kallio, T.; Tammeveski, K. Highly active nitrogen-doped few-layer graphene/carbon nanotube composite electrocatalyst for oxygen reduction reaction in alkaline media. *Carbon* **2014**, *73*, 361–370. [CrossRef]
16. Guo, D.; Shibuya, R.; Akiba, C.; Saji, S.; Kondo, T.; Nakamura, J. Active sites of nitrogen-doped carbon materials for oxygen reduction reaction clarified using model catalysts. *Science* **2016**, *351*, 361–365. [CrossRef]
17. Liang, H.-W.; Zhuang, X.; Brüller, S.; Feng, X.; Müllen, K. Hierarchically porous carbons with optimized nitrogen doping as highly active electrocatalysts for oxygen reduction. *Nat. Commun.* **2014**, *5*, 4973. [CrossRef]
18. Ding, W.; Wei, Z.; Chen, S.; Qi, X.; Yang, T.; Hu, J.; Wang, D.; Wan, L.J.; Alvi, S.F.; Li, L. Space-confinement-induced synthesis of pyridinic-and pyrrolic-nitrogen-doped graphene for the catalysis of oxygen reduction. *Angew. Chem.* **2013**, *125*, 11971–11975. [CrossRef]
19. Deng, H.; Li, Q.; Liu, J.; Wang, F. Active sites for oxygen reduction reaction on nitrogen-doped carbon nanotubes derived from polyaniline. *Carbon* **2017**, *112*, 219–229. [CrossRef]
20. Zhao, A.; Masa, J.; Schuhmann, W.; Xia, W. Activation and stabilization of nitrogen-doped carbon nanotubes as electrocatalysts in the oxygen reduction reaction at strongly alkaline conditions. *J. Phys. Chem. C* **2013**, *117*, 24283–24291. [CrossRef]
21. Kruusenberg, I.; Ratso, S.; Vikkisk, M.; Kanninen, P.; Kallio, T.; Kannan, A.M.; Tammeveski, K. Highly active nitrogen-doped nanocarbon electrocatalysts for alkaline direct methanol fuel cell. *J. Power Source* **2015**, *281*, 94–102. [CrossRef]
22. Dai, L.; Xue, Y.; Qu, L.; Choi, H.-J.; Baek, J.-B. Metal-free catalysts for oxygen reduction reaction. *Chem. Rev.* **2015**, *115*, 4823–4892. [CrossRef]
23. Vikkisk, M.; Kruusenberg, I.; Ratso, S.; Joost, U.; Shulga, E.; Kink, I.; Rauwel, P.; Tammeveski, K. Enhanced electrocatalytic activity of nitrogen-doped multi-walled carbon nanotubes towards the oxygen reduction reaction in alkaline media. *RSC Adv.* **2015**, *5*, 59495–59505. [CrossRef]
24. Ma, R.; Ma, Y.; Dong, Y.; Lee, J.-M. Recent advances in heteroatom-doped graphene materials as efficient electrocatalysts towards the oxygen reduction reaction. *Nano Adv.* **2016**, *1*, 50–61. [CrossRef]
25. Wang, Z.-L.; Xu, D.; Xu, J.-J.; Zhang, X.-B. Oxygen electrocatalysts in metal-air batteries: From aqueous to nonaqueous electrolytes. *Chem. Soc. Rev.* **2014**, *43*, 7746–7786. [CrossRef]
26. Ma, R.; Lin, G.; Zhou, Y.; Liu, Q.; Zhang, T.; Shan, G.; Yang, M.; Wang, J. A review of oxygen reduction mechanisms for metal-free carbon-based electrocatalysts. *npj Comput. Mater.* **2019**, *5*, 78. [CrossRef]
27. Cao, R.; Lee, J.S.; Liu, M.; Cho, J. Recent progress in non-precious catalysts for metal-air batteries. *Adv. Energy Mater.* **2012**, *2*, 816–829. [CrossRef]
28. Zhao, J.; Liu, Y.; Quan, X.; Chen, S.; Zhao, H.; Yu, H. Nitrogen and sulfur co-doped graphene/carbon nanotube as metal-free electrocatalyst for oxygen evolution reaction: The enhanced performance by sulfur doping. *Electrochim. Acta* **2016**, *204*, 169–175. [CrossRef]
29. Zhu, C.; Li, H.; Fu, S.; Du, D.; Lin, Y. Highly efficient nonprecious metal catalysts towards oxygen reduction reaction based on three-dimensional porous carbon nanostructures. *Chem. Soc. Rev.* **2016**, *45*, 517–531. [CrossRef]
30. Paul, R.; Du, F.; Dai, L.; Ding, Y.; Wang, Z.L.; Wei, F.; Roy, A. 3D heteroatom-doped carbon nanomaterials as multifunctional metal-free catalysts for integrated energy devices. *Adv. Mater.* **2019**, *31*, 1805598. [CrossRef]
31. Yang, D.; Zhang, L.; Yan, X.; Yao, X. Recent progress in oxygen electrocatalysts for zinc-air batteries. *Small Methods* **2017**, *1*, 1700209. [CrossRef]
32. Cong, H.-P.; Chen, J.-F.; Yu, S.-H. Graphene-based macroscopic assemblies and architectures: An emerging material system. *Chem. Soc. Rev.* **2014**, *43*, 7295–7325. [CrossRef]
33. Novoselov, K.S.; Geim, A.K.; Morozov, S.V.; Jiang, D.-E.; Zhang, Y.; Dubonos, S.V.; Grigorieva, I.V.; Firsov, A.A. Electric field effect in atomically thin carbon films. *Science* **2004**, *306*, 666–669. [CrossRef]
34. Huang, X.; Qi, X.; Boey, F.; Zhang, H. Graphene-based composites. *Chem. Soc. Rev.* **2012**, *41*, 666–686. [CrossRef]
35. Giovanni, M.; Poh, H.L.; Ambrosi, A.; Zhao, G.; Sofer, Z.; Šaněk, F.; Khezri, B.; Webster, R.D.; Pumera, M. Noble metal (Pd, Ru, Rh, Pt, Au, Ag) doped graphene hybrids for electrocatalysis. *Nanoscale* **2012**, *4*, 5002–5008. [CrossRef]
36. Xiao, J.; Bian, X.; Liao, L.; Zhang, S.; Ji, C.; Liu, B. Nitrogen-doped mesoporous graphene as a synergistic electrocatalyst matrix for high-performance oxygen reduction reaction. *ACS Appl. Mater. Interfaces* **2014**, *6*, 17654–17660. [CrossRef]
37. Cong, H.-P.; Wang, P.; Gong, M.; Yu, S.-H. Facile synthesis of mesoporous nitrogen-doped graphene: An efficient methanol-tolerant cathodic catalyst for oxygen reduction reaction. *Nano Energy* **2014**, *3*, 55–63. [CrossRef]
38. Yan, Y.; Gong, J.; Chen, J.; Zeng, Z.; Huang, W.; Pu, K.; Liu, J.; Chen, P. Recent advances on graphene quantum dots: From chemistry and physics to applications. *Adv. Mater.* **2019**, *31*, 1808283. [CrossRef]

39. Fei, H.; Ye, R.; Ye, G.; Gong, Y.; Peng, Z.; Fan, X.; Samuel, E.L.; Ajayan, P.M.; Tour, J.M. Boron-and nitrogen-doped graphene quantum dots/graphene hybrid nanoplatelets as efficient electrocatalysts for oxygen reduction. *ACS Nano* **2014**, *8*, 10837–10843. [CrossRef]
40. Brownson, D.A.; Kampouris, D.K.; Banks, C.E. Graphene electrochemistry: Fundamental concepts through to prominent applications. *Chem. Soc. Rev.* **2012**, *41*, 6944–6976. [CrossRef]
41. Yuan, W.; Zhou, Y.; Li, Y.; Li, C.; Peng, H.; Zhang, J.; Liu, Z.; Dai, L.; Shi, G. The edge-and basal-plane-specific electrochemistry of a single-layer graphene sheet. *Sci. Rep.* **2013**, *3*, 2248. [CrossRef]
42. Tabish, T.; Zhang, S. Graphene Quantum Dots: Syntheses, Properties, and Biological Applications. In *Comprehensive Nanoscience and Nanotechnology*, 2nd ed.; Elsevier: New York, NY, USA, 2016.
43. Jin, H.; Huang, H.; He, Y.; Feng, X.; Wang, S.; Dai, L.; Wang, J. Graphene quantum dots supported by graphene nanoribbons with ultrahigh electrocatalytic performance for oxygen reduction. *J. Am. Chem. Soc.* **2015**, *137*, 7588–7591. [CrossRef] [PubMed]
44. Li, D.; Duan, X.; Sun, H.; Kang, J.; Zhang, H.; Tade, M.O.; Wang, S. Facile synthesis of nitrogen-doped graphene via low-temperature pyrolysis: The effects of precursors and annealing ambience on metal-free catalytic oxidation. *Carbon* **2017**, *115*, 649–658. [CrossRef]
45. Zhang, H.; Niu, Y.; Hu, W. Nitrogen/sulfur-doping of graphene with cysteine as a heteroatom source for oxygen reduction electrocatalysis. *J. Colloid Interface Sci.* **2017**, *505*, 32–37. [CrossRef] [PubMed]
46. Ilnicka, A.; Skorupska, M.; Romanowski, P.; Kamedulski, P.; Lukaszewicz, J.P. Improving the Performance of Zn-Air Batteries with N-Doped Electroexfoliated Graphene. *Materials* **2020**, *13*, 2115. [CrossRef]
47. Skorupska, M.; Ilnicka, A.; Lukaszewicz, J.P. N-doped graphene foam obtained by microwave-assisted exfoliation of graphite. *Sci. Rep.* **2021**, *11*, 2044. [CrossRef] [PubMed]
48. Qin, L.; Ding, R.; Wang, H.; Wu, J.; Wang, C.; Zhang, C.; Xu, Y.; Wang, L.; Lv, B. Facile synthesis of porous nitrogen-doped holey graphene as an efficient metal-free catalyst for the oxygen reduction reaction. *Nano Res.* **2017**, *10*, 305–319. [CrossRef]
49. Hassani, S.S.; Samiee, L.; Ghasemy, E.; Rashidi, A.; Ganjali, M.R.; Tasharrofi, S. Porous nitrogen-doped graphene prepared through pyrolysis of ammonium acetate as an efficient ORR nanocatalyst. *Int. J. Hydrogen Energy* **2018**, *43*, 15941–15951. [CrossRef]
50. Lin, Z.; Waller, G.; Liu, Y.; Liu, M.; Wong, C.P. Facile synthesis of nitrogen-doped graphene via pyrolysis of graphene oxide and urea, and its electrocatalytic activity toward the oxygen-reduction reaction. *Adv. Energy Mater.* **2012**, *2*, 884–888. [CrossRef]
51. Kamedulski, P.; Lukaszewicz, J.P.; Witczak, L.; Szroeder, P.; Ziolkowski, P. The Importance of Structural Factors for the Electrochemical Performance of Graphene/Carbon Nanotube/Melamine Powders towards the Catalytic Activity of Oxygen Reduction Reaction. *Materials* **2021**, *14*, 2448. [CrossRef]
52. Zhou, X.; Bai, Z.; Wu, M.; Qiao, J.; Chen, Z. 3-Dimensional porous N-doped graphene foam as a non-precious catalyst for the oxygen reduction reaction. *J. Mater. Chem. A* **2015**, *3*, 3343–3350. [CrossRef]
53. Gu, D.; Zhou, Y.; Ma, R.; Wang, F.; Liu, Q.; Wang, J. Facile synthesis of N-doped graphene-like carbon nanoflakes as efficient and stable electrocatalysts for the oxygen reduction reaction. *Nano-Micro Lett.* **2018**, *10*, 29. [CrossRef] [PubMed]
54. Yang, S.; Zhi, L.; Tang, K.; Feng, X.; Maier, J.; Müllen, K. Efficient synthesis of heteroatom (N or S)-doped graphene based on ultrathin graphene oxide-porous silica sheets for oxygen reduction reactions. *Adv. Funct. Mater.* **2012**, *22*, 3634–3640. [CrossRef]
55. Cong, K.; Radtke, M.; Stumpf, S.; Schröter, B.; McMillan, D.G.; Rettenmayr, M.; Ignaszak, A. Electrochemical stability of the polymer-derived nitrogen-doped carbon: An elusive goal? *Mater. Renew. Sustain. Energy* **2015**, *4*, 5. [CrossRef]
56. Lai, L.; Potts, J.R.; Zhan, D.; Wang, L.; Poh, C.K.; Tang, C.; Gong, H.; Shen, Z.; Lin, J.; Ruoff, R.S. Exploration of the active center structure of nitrogen-doped graphene-based catalysts for oxygen reduction reaction. *Energy Environ. Sci.* **2012**, *5*, 7936–7942. [CrossRef]
57. Wan, K.; Yu, Z.-P.; Liang, Z.-X. Polyaniline-derived ordered mesoporous carbon as an efficient electrocatalyst for oxygen reduction reaction. *Catalysts* **2015**, *5*, 1034–1045. [CrossRef]
58. Quílez-Bermejo, J.; Morallón, E.; Cazorla-Amorós, D. Oxygen-reduction catalysis of N-doped carbons prepared via heat treatment of polyaniline at over 1100 °C. *Chem. Commun.* **2018**, *54*, 4441–4444. [CrossRef]
59. Cheon, J.Y.; Kim, J.H.; Kim, J.H.; Goddeti, K.C.; Park, J.Y.; Joo, S.H. Intrinsic relationship between enhanced oxygen reduction reaction activity and nanoscale work function of doped carbons. *J. Am. Chem. Soc.* **2014**, *136*, 8875–8878. [CrossRef]
60. Florent, M.; Wallace, R.; Bandosz, T.J. Oxygen electroreduction on nanoporous carbons: Textural features vs nitrogen and boron catalytic centers. *ChemCatChem* **2019**, *11*, 851–860. [CrossRef]
61. Zhang, X.; Zhang, X.; Zhao, S.; Wang, Y.Q.; Lin, X.; Tian, Z.Q.; Shen, P.K. Precursor modulated active sites of nitrogen doped graphene-based carbon catalysts via one-step pyrolysis method for the enhanced oxygen reduction reaction. *Electrochim. Acta* **2021**, *370*, 137712. [CrossRef]
62. Lu, X.; Wang, D.; Ge, L.; Xiao, L.; Zhang, H.; Liu, L.; Zhang, J.; An, M.; Yang, P. Enriched graphitic N in nitrogen-doped graphene as a superior metal-free electrocatalyst for the oxygen reduction reaction. *New J. Chem.* **2018**, *42*, 19665–19670. [CrossRef]
63. Liu, T.; Kou, T.; Bulmahn, D.; Ortuno-Quintana, C.; Liu, G.; Lu, J.Q.; Li, Y. Tuning the electrochemical properties of nitrogen-doped carbon aerogels in a blend of ammonia and nitrogen gases. *ACS Appl. Energy Mater.* **2018**, *1*, 5043–5053. [CrossRef]
64. Xu, X.; Yuan, T.; Zhou, Y.; Li, Y.; Lu, J.; Tian, X.; Wang, D.; Wang, J. Facile synthesis of boron and nitrogen-doped graphene as efficient electrocatalyst for the oxygen reduction reaction in alkaline media. *Int. J. Hydrogen Energy* **2014**, *39*, 16043–16052. [CrossRef]

65. Huang, Z.-H.; Liu, T.-Y.; Song, Y.; Li, Y.; Liu, X.-X. Balancing the electrical double layer capacitance and pseudocapacitance of hetero-atom doped carbon. *Nanoscale* **2017**, *9*, 13119–13127. [CrossRef] [PubMed]
66. Kabir, S.; Artyushkova, K.; Serov, A.; Kiefer, B.; Atanassov, P. Binding energy shifts for nitrogen-containing graphene-based electrocatalysts-experiments and DFT calculations. *Surf. Interface Anal.* **2016**, *48*, 293–300. [CrossRef]
67. Kabir, S.; Artyushkova, K.; Kiefer, B.; Atanassov, P. Computational and experimental evidence for a new TM-N_3/C moiety family in non-PGM electrocatalysts. *Phys. Chem. Chem. Phys.* **2015**, *17*, 17785–17789. [CrossRef]
68. Kabir, S.; Artyushkova, K.; Serov, A.; Atanassov, P. Role of nitrogen moieties in N-doped 3D-graphene nanosheets for oxygen electroreduction in acidic and alkaline media. *ACS Appl. Mater. Interfaces* **2018**, *10*, 11623–11632. [CrossRef]
69. Dong, F.; Cai, Y.; Liu, C.; Liu, J.; Qiao, J. Heteroatom (B, N and P) doped porous graphene foams for efficient oxygen reduction reaction electrocatalysis. *Int. J. Hydrogen Energy* **2018**, *43*, 12661–12670. [CrossRef]
70. Skorupska, M.; Ilnicka, A.; Lukaszewicz, J.P. The effect of nitrogen species on the catalytic properties of N-doped graphene. *Sci. Rep.* **2021**, *11*, 23970. [CrossRef]
71. Wang, Z.; Li, P.; Chen, Y.; He, J.; Zhang, W.; Schmidt, O.G.; Li, Y. Pure thiophene-sulfur doped reduced graphene oxide: Synthesis, structure, and electrical properties. *Nanoscale* **2014**, *6*, 7281–7287. [CrossRef]
72. Wang, Q.; Ji, Y.; Lei, Y.; Wang, Y.; Wang, Y.; Li, Y.; Wang, S. Pyridinic-N-dominated doped defective graphene as a superior oxygen electrocatalyst for ultrahigh-energy-density Zn-air batteries. *ACS Energy Lett.* **2018**, *3*, 1183–1191. [CrossRef]
73. Ma, R.; Ren, X.; Xia, B.Y.; Zhou, Y.; Sun, C.; Liu, Q.; Liu, J.; Wang, J. Novel synthesis of N-doped graphene as an efficient electrocatalyst towards oxygen reduction. *Nano Res.* **2016**, *9*, 808–819. [CrossRef]
74. Miao, H.; Li, S.; Wang, Z.; Sun, S.; Kuang, M.; Liu, Z.; Yuan, J. Enhancing the pyridinic N content of Nitrogen-doped graphene and improving its catalytic activity for oxygen reduction reaction. *Int. J. Hydrogen Energy* **2017**, *42*, 28298–28308. [CrossRef]
75. Fernández-Sáez, N.; Villela-Martinez, D.E.; Carrasco-Marín, F.; Pérez-Cadenas, A.F.; Pastrana-Martínez, L.M. Heteroatom-doped graphene aerogels and carbon-magnetite catalysts for the heterogeneous electro-Fenton degradation of acetaminophen in aqueous solution. *J. Catal.* **2019**, *378*, 68–79. [CrossRef]
76. Zhai, C.; Sun, M.; Zhu, M.; Song, S.; Jiang, S. A new method to synthesize sulfur-doped graphene as effective metal-free electrocatalyst for oxygen reduction reaction. *Appl. Surf. Sci.* **2017**, *407*, 503–508. [CrossRef]
77. Wang, M.; Li, Y.; Fang, J.; Villa, C.J.; Xu, Y.; Hao, S.; Li, J.; Liu, Y.; Wolverton, C.; Chen, X. Superior oxygen reduction reaction on phosphorus-doped carbon dot/graphene aerogel for all-solid-state flexible Al-air batteries. *Adv. Energy Mater.* **2020**, *10*, 1902736. [CrossRef]
78. Li, R.; Wei, Z.; Gou, X.; Xu, W. Phosphorus-doped graphene nanosheets as efficient metal-free oxygen reduction electrocatalysts. *RSC Adv.* **2013**, *3*, 9978–9984. [CrossRef]
79. Musico, Y.L.F.; Kakati, N.; Labata, M.F.M.; Ocon, J.D.; Chuang, P.-Y.A. One-pot hydrothermal synthesis of heteroatom co-doped with fluorine on reduced graphene oxide for enhanced ORR activity and stability in alkaline media. *Mater. Chem. Phys.* **2019**, *236*, 121804. [CrossRef]
80. Tam, T.V.; Kang, S.G.; Kim, M.H.; Lee, S.G.; Hur, S.H.; Chung, J.S.; Choi, W.M. Novel graphene hydrogel/B-doped graphene quantum dots composites as trifunctional electrocatalysts for Zn− air batteries and overall water splitting. *Adv. Energy Mater.* **2019**, *9*, 1900945. [CrossRef]
81. Nankya, R.; Lee, J.; Opar, D.O.; Jung, H. Electrochemical behavior of boron-doped mesoporous graphene depending on its boron configuration. *Appl. Surf. Sci.* **2019**, *489*, 552–559. [CrossRef]
82. Kumar, R.; Sahoo, S.; Joanni, E.; Singh, R.K.; Maegawa, K.; Tan, W.K.; Kawamura, G.; Kar, K.K.; Matsuda, A. Heteroatom doped graphene engineering for energy storage and conversion. *Mater. Today* **2020**, *39*, 47–65. [CrossRef]
83. Zheng, Y.; Jiao, Y.; Ge, L.; Jaroniec, M.; Qiao, S.Z. Two-step boron and nitrogen doping in graphene for enhanced synergistic catalysis. *Angew. Chem.* **2013**, *125*, 3192–3198. [CrossRef]
84. Su, Y.; Zhang, Y.; Zhuang, X.; Li, S.; Wu, D.; Zhang, F.; Feng, X. Low-temperature synthesis of nitrogen/sulfur co-doped three-dimensional graphene frameworks as efficient metal-free electrocatalyst for oxygen reduction reaction. *Carbon* **2013**, *62*, 296–301. [CrossRef]
85. Han, C.; Chen, Z. The mechanism study of oxygen reduction reaction (ORR) on non-equivalent P, N co-doped graphene. *Appl. Surf. Sci.* **2020**, *511*, 145382. [CrossRef]
86. Lin, H.; Chu, L.; Wang, X.; Yao, Z.; Liu, F.; Ai, Y.; Zhuang, X.; Han, S. Boron, nitrogen, and phosphorous ternary doped graphene aerogel with hierarchically porous structures as highly efficient electrocatalysts for oxygen reduction reaction. *New J. Chem.* **2016**, *40*, 6022–6029. [CrossRef]
87. Razmjooei, F.; Singh, K.P.; Song, M.Y.; Yu, J.-S. Enhanced electrocatalytic activity due to additional phosphorous doping in nitrogen and sulfur-doped graphene: A comprehensive study. *Carbon* **2014**, *78*, 257–267. [CrossRef]
88. Zhao, G.; Shi, L.; Xu, J.; Yan, X.; Zhao, T. Role of phosphorus in nitrogen, phosphorus dual-doped ordered mesoporous carbon electrocatalyst for oxygen reduction reaction in alkaline media. *Int. J. Hydrogen Energy* **2018**, *43*, 1470–1478. [CrossRef]
89. Wu, Z.-S.; Yang, S.; Sun, Y.; Parvez, K.; Feng, X.; Müllen, K. 3D nitrogen-doped graphene aerogel-supported Fe_3O_4 nanoparticles as efficient electrocatalysts for the oxygen reduction reaction. *J. Am. Chem. Soc.* **2012**, *134*, 9082–9085. [CrossRef]
90. Bai, J.; Zhu, Q.; Lv, Z.; Dong, H.; Yu, J.; Dong, L. Nitrogen-doped graphene as catalysts and catalyst supports for oxygen reduction in both acidic and alkaline solutions. *Int. J. Hydrogen Energy* **2013**, *38*, 1413–1418. [CrossRef]

91. Kim, I.T.; Song, M.J.; Kim, Y.B.; Shin, M.W. Microwave-hydrothermal synthesis of boron/nitrogen co-doped graphene as an efficient metal-free electrocatalyst for oxygen reduction reaction. *Int. J. Hydrogen Energy* **2016**, *41*, 22026–22033. [CrossRef]
92. Kim, I.T.; Shin, M.W. Synthesis of nitrogen-doped graphene via simple microwave-hydrothermal process. *Mater. Lett.* **2013**, *108*, 33–36. [CrossRef]
93. Sun, X.; Lin, L.; Sun, L.; Zhang, J.; Rui, D.; Li, J.; Wang, M.; Tan, C.; Kang, N.; Wei, D. Low-temperature and rapid growth of large single-crystalline graphene with ethane. *Small* **2018**, *14*, 1702916. [CrossRef] [PubMed]
94. Qiu, H.J.; Du, P.; Hu, K.; Gao, J.; Li, H.; Liu, P.; Ina, T.; Ohara, K.; Ito, Y.; Chen, M. Metal and nonmetal codoped 3D nanoporous graphene for efficient bifunctional electrocatalysis and rechargeable Zn-air batteries. *Adv. Mater.* **2019**, *31*, 1900843. [CrossRef]
95. Wu, Z.; Zhang, Y.; Li, L.; Zhao, Y.; Shen, Y.; Wang, S.; Shao, G. Nitrogen-doped vertical graphene nanosheets by high-flux plasma enhanced chemical vapor deposition as efficient oxygen reduction catalysts for Zn-air batteries. *J. Mater. Chem. A* **2020**, *8*, 23248–23256. [CrossRef]
96. Wei, D.; Liu, Y.; Wang, Y.; Zhang, H.; Huang, L.; Yu, G. Synthesis of N-doped graphene by chemical vapor deposition and its electrical properties. *Nano Lett.* **2009**, *9*, 1752–1758. [CrossRef]
97. Yazici, M.S.; Azder, M.A.; Salihoglu, O. CVD grown graphene as catalyst for acid electrolytes. *Int. J. Hydrogen Energy* **2018**, *43*, 10710–10716. [CrossRef]
98. Yang, J.; Hu, P.; Yu, G. Design of carbon sources: Starting point for chemical vapor deposition of graphene. *2D Mater.* **2019**, *6*, 042003. [CrossRef]
99. Shinde, D.B.; Chaturvedi, P.; Vlassiouk, I.V.; Smirnov, S.N. Unique role of dimeric carbon precursors in graphene growth by chemical vapor deposition. *Carbon Trends* **2021**, *5*, 100093. [CrossRef]
100. Granzier-Nakajima, T.; Fujisawa, K.; Anil, V.; Terrones, M.; Yeh, Y.-T. Controlling nitrogen doping in graphene with atomic precision: Synthesis and characterization. *Nanomaterials* **2019**, *9*, 425. [CrossRef]
101. Qu, L.; Liu, Y.; Baek, J.-B.; Dai, L. Nitrogen-doped graphene as efficient metal-free electrocatalyst for oxygen reduction in fuel cells. *ACS Nano* **2010**, *4*, 1321–1326. [CrossRef]
102. Wu, X.; Xie, Z.; Sun, M.; Lei, T.; Zuo, Z.; Xie, X.; Liang, Y.; Huang, Q. Edge-rich and (N,S)-doped 3D porous graphene as an efficient metal-free electrocatalyst for the oxygen reduction reaction. *RSC Adv.* **2016**, *6*, 90384–90387. [CrossRef]
103. Xu, J.; Dong, G.; Jin, C.; Huang, M.; Guan, L. Sulfur and nitrogen co-doped, few-layered graphene oxide as a highly efficient electrocatalyst for the oxygen-reduction reaction. *ChemSusChem* **2013**, *6*, 493–499. [CrossRef] [PubMed]
104. Zhuang, S.; Nunna, B.B.; Mandal, D.; Lee, E.S. A review of nitrogen-doped graphene catalysts for proton exchange membrane fuel cells-synthesis, characterization, and improvement. *Nano-Struct. Nano-Objects* **2018**, *15*, 140–152. [CrossRef]
105. Wang, H.-F.; Tang, C.; Zhang, Q. Template growth of nitrogen-doped mesoporous graphene on metal oxides and its use as a metal-free bifunctional electrocatalyst for oxygen reduction and evolution reactions. *Catal. Today* **2018**, *301*, 25–31. [CrossRef]
106. Shi, J.-L.; Tang, C.; Huang, J.-Q.; Zhu, W.; Zhang, Q. Effective exposure of nitrogen heteroatoms in 3D porous graphene framework for oxygen reduction reaction and lithium-sulfur batteries. *J. Energy Chem.* **2018**, *27*, 167–175. [CrossRef]
107. Sharma, P.; Minakshi Sundaram, M.; Watcharatharapong, T.; Laird, D.; Euchner, H.; Ahuja, R. Zn Metal Atom Doping on the Surface Plane of One-Dimesional NiMoO4 Nanorods with Improved Redox Chemistry. *ACS Appl. Mater. Interfaces* **2020**, *12*, 44815–44829. [CrossRef]
108. Sharma, P.; Minakshi Sundaram, M.; Watcharatharapong, T.; Jungthawan, S.; Ahuja, R. Tuning the Nanoparticle Interfacial Properties and Stability of the Core-Shell Structure in Zn-Doped $NiMoO_4$@AWO_4. *ACS Appl. Mater. Interfaces* **2021**, *13*, 56116–56130. [CrossRef] [PubMed]
109. Ito, Y.; Qiu, H.J.; Fujita, T.; Tanabe, Y.; Tanigaki, K.; Chen, M. Bicontinuous nanoporous N-doped graphene for the oxygen reduction reaction. *Adv. Mater.* **2014**, *26*, 4145–4150. [CrossRef]
110. Neupane, S.; Li, W. Carbon nanotube arrays: Synthesis, properties, and applications. In *Three-Dimensional Nanoarchitectures*; Springer: Berlin/Heidelberg, Germany, 2011; pp. 261–285.
111. Anzar, N.; Hasan, R.; Tyagi, M.; Yadav, N.; Narang, J. Carbon nanotube-A review on Synthesis, Properties and plethora of applications in the field of biomedical science. *Sens. Int.* **2020**, *1*, 100003. [CrossRef]
112. Wu, Z.; Song, M.; Wang, J.; Liu, X. Recent progress in nitrogen-doped metal-free electrocatalysts for oxygen reduction reaction. *Catalysts* **2018**, *8*, 196. [CrossRef]
113. Gong, K.; Du, F.; Xia, Z.; Durstock, M.; Dai, L. Nitrogen-doped carbon nanotube arrays with high electrocatalytic activity for oxygen reduction. *Science* **2009**, *323*, 760–764. [CrossRef]
114. Huang, B.; Peng, L.; Yang, F.; Liu, Y.; Xie, Z. Improving ORR activity of carbon nanotubes by hydrothermal carbon deposition method. *J. Energy Chem.* **2017**, *26*, 712–718. [CrossRef]
115. Sa, Y.J.; Park, C.; Jeong, H.Y.; Park, S.H.; Lee, Z.; Kim, K.T.; Park, G.G.; Joo, S.H. Carbon nanotubes/heteroatom-doped carbon core-sheath nanostructures as highly active, metal-free oxygen reduction electrocatalysts for alkaline fuel cells. *Angew. Chem.* **2014**, *126*, 4186–4190. [CrossRef]
116. He, H.; Pham-Huy, L.A.; Dramou, P.; Xiao, D.; Zuo, P.; Pham-Huy, C. Carbon nanotubes: Applications in pharmacy and medicine. *BioMed Res. Int.* **2013**, *2013*, 578250. [CrossRef]
117. Poudel, Y.R.; Li, W. Synthesis, properties, and applications of carbon nanotubes filled with foreign materials: A review. *Mater. Today Phys.* **2018**, *7*, 7–34. [CrossRef]

118. Trogadas, P.; Fuller, T.F.; Strasser, P. Carbon as catalyst and support for electrochemical energy conversion. *Carbon* **2014**, *75*, 5–42. [CrossRef]
119. Ratso, S.; Kruusenberg, I.; Sarapuu, A.; Rauwel, P.; Saar, R.; Joost, U.; Aruväli, J.; Kanninen, P.; Kallio, T.; Tammeveski, K. Enhanced oxygen reduction reaction activity of iron-containing nitrogen-doped carbon nanotubes for alkaline direct methanol fuel cell application. *J. Power Source* **2016**, *332*, 129–138. [CrossRef]
120. Choi, C.H.; Chung, M.W.; Kwon, H.C.; Chung, J.H.; Woo, S.I. Nitrogen-doped graphene/carbon nanotube self-assembly for efficient oxygen reduction reaction in acid media. *Appl. Catal. B Environ.* **2014**, *144*, 760–766. [CrossRef]
121. Choi, J.-Y.; Higgins, D.; Chen, Z. Highly durable graphene nanosheet supported iron catalyst for oxygen reduction reaction in PEM fuel cells. *J. Electrochem. Soc.* **2011**, *159*, B86. [CrossRef]
122. Choi, C.H.; Park, S.H.; Woo, S.I. Phosphorus-nitrogen dual doped carbon as an effective catalyst for oxygen reduction reaction in acidic media: Effects of the amount of P-doping on the physical and electrochemical properties of carbon. *J. Mater. Chem.* **2012**, *22*, 12107–12115. [CrossRef]
123. Wang, Y.-X.; Rinawati, M.; Huang, W.-H.; Cheng, Y.-S.; Lin, P.-H.; Chen, K.-J.; Chang, L.-Y.; Ho, K.-C.; Su, W.-N.; Yeh, M.-H. Surface-engineered N-doped carbon nanotubes with B-doped graphene quantum dots: Strategies to develop highly-efficient noble metal-free electrocatalyst for online-monitoring dissolved oxygen biosensor. *Carbon* **2022**, *186*, 406–415. [CrossRef]
124. Lu, X.; Yim, W.-L.; Suryanto, B.H.; Zhao, C. Electrocatalytic oxygen evolution at surface-oxidized multiwall carbon nanotubes. *J. Am. Chem. Soc.* **2015**, *137*, 2901–2907. [CrossRef]
125. Ren, M.; Chang, F.; Miao, R.; He, X.; Yang, L.; Wang, X.; Bai, Z. Strained lattice platinum-palladium alloy nanowires for efficient electrocatalysis. *Inorg. Chem. Front.* **2020**, *7*, 1713–1718. [CrossRef]
126. Chang, F.; Bai, Z.; Li, M.; Ren, M.; Liu, T.; Yang, L.; Zhong, C.-J.; Lu, J. Strain-Modulated Platinum-Palladium Nanowires for Oxygen Reduction Reaction. *Nano Lett.* **2020**, *20*, 2416–2422. [CrossRef] [PubMed]
127. Kong, Z.; Zhang, D.; Lu, Y.; Yang, C.; Du, S.; Li, W.; Tao, L.; Wang, S. Advanced Cathode Electrocatalysts for Fuel Cells: Understanding, Construction, and Application of Carbon-Based and Platinum-Based Nanomaterials. *ACS Mater. Lett.* **2021**, *3*, 1610–1634. [CrossRef]
128. Hu, X.; Wu, Y.; Li, H.; Zhang, Z. Adsorption and activation of O_2 on nitrogen-doped carbon nanotubes. *J. Phys. Chem. C* **2010**, *114*, 9603–9607. [CrossRef]
129. Wang, Y.; Song, W.; Li, M.; Wu, Z. Oxygen reduction reaction mechanisms on heteroatom-doped single-walled carbon nanotube catalysts: Insights from a theoretical study. *J. Electrochem. Soc.* **2019**, *166*, F670. [CrossRef]
130. Zhang, P.; Hou, X.; Mi, J.; He, Y.; Lin, L.; Jiang, Q.; Dong, M. From two-dimension to one-dimension: The curvature effect of silicon-doped graphene and carbon nanotubes for oxygen reduction reaction. *Phys. Chem. Chem. Phys.* **2014**, *16*, 17479–17486. [CrossRef] [PubMed]
131. An, H.; Zhang, R.; Li, Z.; Zhou, L.; Shao, M.; Wei, M. Highly efficient metal-free electrocatalysts toward oxygen reduction derived from carbon nanotubes@ polypyrrole core-shell hybrids. *J. Mater. Chem. A* **2016**, *4*, 18008–18014. [CrossRef]
132. Xie, W.; Li, J.; Song, Y.; Li, S.; Li, J.; Shao, M. Hierarchical carbon Microtube@ Nanotube core-shell structure for high-performance oxygen electrocatalysis and Zn-air battery. *Nano-Micro Lett.* **2020**, *12*, 97. [CrossRef]
133. Jiang, W.-J.; Hu, J.-S.; Zhang, X.; Jiang, Y.; Yu, B.-B.; Wei, Z.-D.; Wan, L.-J. In situ nitrogen-doped nanoporous carbon nanocables as an efficient metal-free catalyst for oxygen reduction reaction. *J. Mater. Chem. A* **2014**, *2*, 10154–10160. [CrossRef]
134. Xue, L.; Li, Y.; Liu, X.; Liu, Q.; Shang, J.; Duan, H.; Dai, L.; Shui, J. Zigzag carbon as efficient and stable oxygen reduction electrocatalyst for proton exchange membrane fuel cells. *Nat. Commun.* **2018**, *9*, 3819. [CrossRef] [PubMed]
135. Pei, Y.; Song, H.; Liu, Y.; Cheng, Y.; Li, W.; Chen, Y.; Fan, Y.; Liu, B.; Lu, S. Boron-nitrogen-doped carbon dots on multi-walled carbon nanotubes for efficient electrocatalysis of oxygen reduction reactions. *J. Colloid Interface Sci.* **2021**, *600*, 865–871. [CrossRef] [PubMed]
136. Patil, I.M.; Lokanathan, M.; Ganesan, B.; Swami, A.; Kakade, B. Carbon nanotube/boron nitride nanocomposite as a significant bifunctional electrocatalyst for oxygen reduction and oxygen evolution reactions. *Chem. Eur. J.* **2017**, *23*, 676–683. [CrossRef]
137. Suryanto, B.H.; Chen, S.; Duan, J.; Zhao, C. Hydrothermally driven transformation of oxygen functional groups at multiwall carbon nanotubes for improved electrocatalytic applications. *ACS Appl. Mater. Interfaces* **2016**, *8*, 35513–35522. [CrossRef] [PubMed]
138. Likodimos, V.; Steriotis, T.A.; Papageorgiou, S.K.; Romanos, G.E.; Marques, R.R.; Rocha, R.P.; Faria, J.L.; Pereira, M.F.; Figueiredo, J.L.; Silva, A.M. Controlled surface functionalization of multiwall carbon nanotubes by HNO_3 hydrothermal oxidation. *Carbon* **2014**, *69*, 311–326. [CrossRef]
139. Huang, Y.; Liao, W. Hierarchical carbon material of N-doped carbon quantum dots in-situ formed on N-doped carbon nanotube for efficient oxygen reduction. *Appl. Surf. Sci.* **2019**, *495*, 143597. [CrossRef]
140. Chen, L.; Cui, X.; Wang, Y.; Wang, M.; Cui, F.; Wei, C.; Huang, W.; Hua, Z.; Zhang, L.; Shi, J. One-Step Hydrothermal Synthesis of Nitrogen-Doped Carbon Nanotubes as an Efficient Electrocatalyst for Oxygen Reduction Reactions. *Chem. Asian J.* **2014**, *9*, 2915–2920. [CrossRef]
141. El-Sawy, A.M.; Mosa, I.M.; Su, D.; Guild, C.J.; Khalid, S.; Joesten, R.; Rusling, J.F.; Suib, S.L. Controlling the active sites of sulfur-doped carbon nanotube-graphene nanolobes for highly efficient oxygen evolution and reduction catalysis. *Adv. Energy Mater.* **2016**, *6*, 1501966. [CrossRef]

142. Alexeyeva, N.; Shulga, E.; Kisand, V.; Kink, I.; Tammeveski, K. Electroreduction of oxygen on nitrogen-doped carbon nanotube modified glassy carbon electrodes in acid and alkaline solutions. *J. Electroanal. Chem.* **2010**, *648*, 169–175. [CrossRef]
143. Alexeyeva, N.; Tammeveski, K.; Lopez-Cudero, A.; Solla-Gullón, J.; Feliu, J. Electroreduction of oxygen on Pt nanoparticle/carbon nanotube nanocomposites in acid and alkaline solutions. *Electrochim. Acta* **2010**, *55*, 794–803. [CrossRef]
144. Wong, W.; Daud, W.; Mohamad, A.; Kadhum, A.; Loh, K.; Majlan, E. Influence of nitrogen doping on carbon nanotubes towards the structure, composition and oxygen reduction reaction. *Int. J. Hydrogen Energy* **2013**, *38*, 9421–9430. [CrossRef]
145. Gonzalez, I.Z.; Valenzuela-Muñiz, A.; Alonso-Nuñez, G.; Farías, M.; Gomez, Y.V. Influence of the synthesis parameters in carbon nanotubes doped with nitrogen for oxygen electroreduction. *ECS J. Solid State Sci. Technol.* **2017**, *6*, M3135. [CrossRef]
146. Alexander, C.T.; Abakumov, A.M.; Forslund, R.P.; Johnston, K.P.; Stevenson, K.J. Role of the carbon support on the oxygen reduction and evolution activities in $LaNiO_3$ composite electrodes in alkaline solution. *ACS Appl. Energy Mater.* **2018**, *1*, 1549–1558. [CrossRef]
147. Yang, G.; Choi, W.; Pu, X.; Yu, C. Scalable synthesis of bi-functional high-performance carbon nanotube sponge catalysts and electrodes with optimum C-N-Fe coordination for oxygen reduction reaction. *Energy Environ. Sci.* **2015**, *8*, 1799–1807. [CrossRef]
148. Yasuda, S.; Furuya, A.; Uchibori, Y.; Kim, J.; Murakoshi, K. Iron-nitrogen-doped vertically aligned carbon nanotube electrocatalyst for the oxygen reduction reaction. *Adv. Funct. Mater.* **2016**, *26*, 738–744. [CrossRef]
149. Mi, J.-L.; Liang, J.-H.; Yang, L.-P.; Wu, B.; Liu, L. Effect of Zn on size control and oxygen reduction reaction activity of Co nanoparticles supported on N-doped carbon nanotubes. *Chem. Mater.* **2019**, *31*, 8864–8874. [CrossRef]
150. Yang, L.; Jiang, S.; Zhao, Y.; Zhu, L.; Chen, S.; Wang, X.; Wu, Q.; Ma, J.; Ma, Y.; Hu, Z. Boron-doped carbon nanotubes as metal-free electrocatalysts for the oxygen reduction reaction. *Angew. Chem. Int. Ed.* **2011**, *50*, 7132–7135. [CrossRef]
151. Zhao, Y.; Yang, L.; Chen, S.; Wang, X.; Ma, Y.; Wu, Q.; Jiang, Y.; Qian, W.; Hu, Z. Can boron and nitrogen co-doping improve oxygen reduction reaction activity of carbon nanotubes? *J. Am. Chem. Soc.* **2013**, *135*, 1201–1204. [CrossRef]
152. Zhang, Z.; Yang, S.; Li, H.; Zan, Y.; Li, X.; Zhu, Y.; Dou, M.; Wang, F. Sustainable carbonaceous materials derived from biomass as metal-free electrocatalysts. *Adv. Mater.* **2019**, *31*, 1805718. [CrossRef]
153. Song, M.Y.; Park, H.Y.; Yang, D.S.; Bhattacharjya, D.; Yu, J.S. Seaweed-derived heteroatom-doped highly porous carbon as an electrocatalyst for the oxygen reduction reaction. *ChemSusChem* **2014**, *7*, 1755–1763. [CrossRef]
154. Liu, F.; Liu, L.; Li, X.; Zeng, J.; Du, L.; Liao, S. Nitrogen self-doped carbon nanoparticles derived from spiral seaweeds for oxygen reduction reaction. *RSC Adv.* **2016**, *6*, 27535–27541. [CrossRef]
155. Escobar, B.; Pérez-Salcedo, K.; Alonso-Lemus, I.; Pacheco, D.; Barbosa, R. N-doped porous carbon from *Sargassum* spp. as metal-free electrocatalysts for oxygen reduction reaction in alkaline media. *Int. J. Hydrogen Energy* **2017**, *42*, 30274–30283. [CrossRef]
156. Zhang, X.; Liu, R.; Zang, Y.; Liu, G.; Wang, G.; Zhang, Y.; Zhang, H.; Zhao, H. Co/CoO nanoparticles immobilized on Co-N-doped carbon as trifunctional electrocatalysts for oxygen reduction, oxygen evolution and hydrogen evolution reactions. *Chem. Commun.* **2016**, *52*, 5946–5949. [CrossRef] [PubMed]
157. Liu, R.; Zhang, H.; Liu, S.; Zhang, X.; Wu, T.; Ge, X.; Zang, Y.; Zhao, H.; Wang, G. Shrimp-shell derived carbon nanodots as carbon and nitrogen sources to fabricate three-dimensional N-doped porous carbon electrocatalysts for the oxygen reduction reaction. *Phys. Chem. Chem. Phys.* **2016**, *18*, 4095–4101. [CrossRef] [PubMed]
158. Wang, H.; Wang, K.; Song, H.; Li, H.; Ji, S.; Wang, Z.; Li, S.; Wang, R. N-doped porous carbon material made from fish-bones and its highly electrocatalytic performance in the oxygen reduction reaction. *RSC Adv.* **2015**, *5*, 48965–48970. [CrossRef]
159. Liu, F.; Peng, H.; You, C.; Fu, Z.; Huang, P.; Song, H.; Liao, S. High-performance doped carbon catalyst derived from nori biomass with melamine promoter. *Electrochim. Acta* **2014**, *138*, 353–359. [CrossRef]
160. Ilnicka, A.; Skorupska, M.; Tyc, M.; Kowalska, K.; Kamedulski, P.; Zielinski, W.; Lukaszewicz, J.P. Green algae and gelatine derived nitrogen rich carbon as an outstanding competitor to Pt loaded carbon catalysts. *Sci. Rep.* **2021**, *11*, 7084. [CrossRef]
161. Xuan, C.; Wu, Z.; Lei, W.; Wang, J.; Guo, J.; Wang, D. Nitrogen-Doped Hierarchical Porous Carbons Derived from Sodium Alginate as Efficient Oxygen Reduction Reaction Electrocatalysts. *ChemCatChem* **2017**, *9*, 809–815. [CrossRef]
162. Shu, J.; Niu, Q.; Wang, N.; Nie, J.; Ma, G. Alginate derived Co/N doped hierarchical porous carbon microspheres for efficient oxygen reduction reaction. *Appl. Surf. Sci.* **2019**, *485*, 520–528. [CrossRef]
163. Ilnicka, A.; Lukaszewicz, J.P.; Shimanoe, K.; Yuasa, M. Urea treatment of nitrogen-doped carbon leads to enhanced performance for the oxygen reduction reaction. *J. Mater. Res.* **2018**, *33*, 1612–1624. [CrossRef]
164. Guo, D.; Wei, H.; Chen, X.; Liu, M.; Ding, F.; Yang, Z.; Yang, Y.; Wang, S.; Yang, K.; Huang, S. 3D hierarchical nitrogen-doped carbon nanoflower derived from chitosan for efficient electrocatalytic oxygen reduction and high performance lithium-sulfur batteries. *J. Mater. Chem. A* **2017**, *5*, 18193–18206. [CrossRef]
165. Rybarczyk, M.K.; Gontarek, E.; Lieder, M.; Titirici, M.-M. Salt melt synthesis of curved nitrogen-doped carbon nanostructures: ORR kinetics boost. *Appl. Surf. Sci.* **2018**, *435*, 543–551. [CrossRef]
166. El-Nagar, G.A.; Hassan, M.A.; Fetyan, A.; Kayarkatte, M.K.; Lauermann, I.; Roth, C. A promising N-doped carbon-metal oxide hybrid electrocatalyst derived from crustacean's shells: Oxygen reduction and oxygen evolution. *Appl. Catal. B Environ.* **2017**, *214*, 137–147. [CrossRef]
167. Rybarczyk, M.K.; Lieder, M.; Jablonska, M. N-doped mesoporous carbon nanosheets obtained by pyrolysis of a chitosan-melamine mixture for the oxygen reduction reaction in alkaline media. *RSC Adv.* **2015**, *5*, 44969–44977. [CrossRef]

168. Wu, K.H.; Wang, D.W.; Su, D.S.; Gentle, I.R. A discussion on the activity origin in metal-free nitrogen-doped carbons for oxygen reduction reaction and their mechanisms. *ChemSusChem* **2015**, *8*, 2772–2788. [CrossRef]
169. Chen, X.; Liang, Y.; Wan, L.; Xie, Z.; Easton, C.D.; Bourgeois, L.; Wang, Z.; Bao, Q.; Zhu, Y.; Tao, S. Construction of porous N-doped graphene layer for efficient oxygen reduction reaction. *Chem. Eng. Sci.* **2019**, *194*, 36–44. [CrossRef]
170. Tan, A.-D.; Wang, Y.-F.; Fu, Z.-Y.; Tsiakaras, P.; Liang, Z.-X. Highly effective oxygen reduction reaction electrocatalysis: Nitrogen-doped hierarchically mesoporous carbon derived from interpenetrated nonporous metal-organic frameworks. *Appl. Catal. B Environ.* **2017**, *218*, 260–266. [CrossRef]
171. Yang, H.; Kou, S.; Li, Z.; Chang, Z.; Wang, M.; Liu, Z.; Lu, G. 3D interconnected nitrogen-self-doped carbon aerogels as efficient oxygen reduction electrocatalysts derived from biomass gelatin. *RSC Adv.* **2019**, *9*, 40301–40308. [CrossRef]
172. Nam, G.; Park, J.; Kim, S.T.; Shin, D.-B.; Park, N.; Kim, Y.; Lee, J.-S.; Cho, J. Metal-Free Ketjenblack Incorporated Nitrogen-Doped Carbon Sheets Derived from Gelatin as Oxygen Reduction Catalysts. *Nano Lett.* **2014**, *14*, 1870–1876. [CrossRef]
173. Wang, Z.-L.; Xu, D.; Zhong, H.-X.; Wang, J.; Meng, F.-L.; Zhang, X.-B. Gelatin-derived sustainable carbon-based functional materials for energy conversion and storage with controllability of structure and component. *Sci. Adv.* **2015**, *1*, e1400035. [CrossRef]
174. Schnepp, Z.; Zhang, Y.; Hollamby, M.J.; Pauw, B.R.; Tanaka, M.; Matsushita, Y.; Sakka, Y. Doped-carbon electrocatalysts with trimodal porosity from a homogeneous polypeptide gel. *J. Mater. Chem. A* **2013**, *1*, 13576–13581. [CrossRef]
175. Liu, Z.; Li, Z.; Ma, J.; Dong, X.; Ku, W.; Wang, M.; Sun, H.; Liang, S.; Lu, G. Nitrogen and cobalt-doped porous biocarbon materials derived from corn stover as efficient electrocatalysts for aluminum-air batteries. *Energy* **2018**, *162*, 453–459. [CrossRef]
176. Pan, F.; Cao, Z.; Zhao, Q.; Liang, H.; Zhang, J. Nitrogen-doped porous carbon nanosheets made from biomass as highly active electrocatalyst for oxygen reduction reaction. *J. Power Source* **2014**, *272*, 8–15. [CrossRef]
177. Borghei, M.; Laocharoen, N.; Kibena-Põldsepp, E.; Johansson, L.-S.; Campbell, J.; Kauppinen, E.; Tammeveski, K.; Rojas, O.J. Porous N,P-doped carbon from coconut shells with high electrocatalytic activity for oxygen reduction: Alternative to Pt-C for alkaline fuel cells. *Appl. Catal. B Environ.* **2017**, *204*, 394–402. [CrossRef]
178. Liu, Q.; Zhou, Y.; Chen, S.; Wang, Z.; Hou, H.; Zhao, F. Cellulose-derived nitrogen and phosphorus dual-doped carbon as high performance oxygen reduction catalyst in microbial fuel cell. *J. Power Source* **2015**, *273*, 1189–1193. [CrossRef]
179. Wang, J.; Kaskel, S. KOH activation of carbon-based materials for energy storage. *J. Mater. Chem.* **2012**, *22*, 23710–23725. [CrossRef]
180. Lozano-Castelló, D.; Calo, J.M.; Cazorla-Amorós, D.; Linares-Solano, A. Carbon activation with KOH as explored by temperature programmed techniques, and the effects of hydrogen. *Carbon* **2007**, *45*, 2529–2536. [CrossRef]
181. Qiao, W.; Yoon, S.-H.; Mochida, I. KOH Activation of Needle Coke to Develop Activated Carbons for High-Performance EDLC. *Energy Fuels* **2006**, *20*, 1680–1684. [CrossRef]
182. Wang, H.; Gao, Q.; Hu, J. High Hydrogen Storage Capacity of Porous Carbons Prepared by Using Activated Carbon. *J. Am. Chem. Soc.* **2009**, *131*, 7016–7022. [CrossRef]
183. Romanos, J.; Beckner, M.; Rash, T.; Firlej, L.; Kuchta, B.; Yu, P.; Suppes, G.; Wexler, C.; Pfeifer, P. Nanospace engineering of KOH activated carbon. *Nanotechnology* **2011**, *23*, 015401. [CrossRef]
184. Nowicki, P.; Pietrzak, R. Węgle aktywne wzbogacone w azot-otrzymywanie, właściwości i potencjalne zastosowania. *Adsorbenty I Katal.* **2012**, *7*, 129–144.
185. Zhang, J.; Qu, L.; Shi, G.; Liu, J.; Chen, J.; Dai, L. N,P-codoped carbon networks as efficient metal-free bifunctional catalysts for oxygen reduction and hydrogen evolution reactions. *Angew. Chem.* **2016**, *128*, 2270–2274. [CrossRef]
186. Ilnicka, A.; Kamedulski, P.; Skorupska, M.; Lukaszewicz, J.P. Metal-free nitrogen-rich carbon foam derived from amino acids for the oxygen reduction reaction. *J. Mater. Sci.* **2019**, *54*, 14859–14871. [CrossRef]
187. Lin, H.; Chen, D.; Lu, C.; Zhang, C.; Qiu, F.; Han, S.; Zhuang, X. Rational synthesis of N/S-doped porous carbons as high efficient electrocatalysts for oxygen reduction reaction and Zn-Air batteries. *Electrochim. Acta* **2018**, *266*, 17–26. [CrossRef]
188. Kaur, P.; Kim, D.-E.; Verma, G.; Park, J.-S.; Sekhon, S.S. Facile and scalable functionalization of carbon nanofibers for oxygen reduction reaction: Role of nitrogen precursor and non-ionic dispersant. *J. Ind. Eng. Chem.* **2021**, *96*, 307–314. [CrossRef]
189. Massaglia, G.; Margaria, V.; Sacco, A.; Castellino, M.; Chiodoni, A.; Pirri, F.C.; Quaglio, M. N-doped carbon nanofibers as catalyst layer at cathode in single chamber Microbial Fuel Cells. *Int. J. Hydrogen Energy* **2019**, *44*, 4442–4449. [CrossRef]
190. Huang, R.; Cao, C.; Liu, J.; Sun, D.; Song, W. N-Doped carbon nanofibers derived from bacterial cellulose as an excellent metal-free catalyst for selective oxidation of arylalkanes. *Chem. Commun.* **2019**, *55*, 1935–1938. [CrossRef]
191. Boskovic, B.O.; Stolojan, V.; Khan, R.U.; Haq, S.; Silva, S.R.P. Large-area synthesis of carbon nanofibres at room temperature. *Nat. Mater.* **2002**, *1*, 165–168. [CrossRef]
192. Buan, M.E.; Cognigni, A.; Walmsley, J.C.; Muthuswamy, N.; Rønning, M. Active sites for the oxygen reduction reaction in nitrogen-doped carbon nanofibers. *Catal. Today* **2020**, *357*, 248–258. [CrossRef]
193. Minea, T.; Point, S.; Granier, A.; Touzeau, M. Room temperature synthesis of carbon nanofibers containing nitrogen by plasma-enhanced chemical vapor deposition. *Appl. Phys. Lett.* **2004**, *85*, 1244–1246. [CrossRef]
194. Hofmann, S.; Ducati, C.; Robertson, J.; Kleinsorge, B. Low-temperature growth of carbon nanotubes by plasma-enhanced chemical vapor deposition. *Appl. Phys. Lett.* **2003**, *83*, 135–137. [CrossRef]
195. Kong, Y.; Li, Y.; Yang, B.; Li, Z.; Yao, Y.; Lu, J.; Lei, L.; Wen, Z.; Shao, M.; Hou, Y. Boron and nitrogen co-doped porous carbon nanofibers as metal-free electrocatalysts for highly efficient ammonia electrosynthesis. *J. Mater. Chem. A* **2019**, *7*, 26272–26278. [CrossRef]

196. Wu, Q.; Gao, M.; Cao, S.; Hu, J.; Huang, L.; Yu, S.; Ragauskas, A.J. Chitosan-based layered carbon materials prepared via ionic-liquid-assisted hydrothermal carbonization and their performance study. *J. Taiwan Inst. Chem. Eng.* **2019**, *101*, 231–243. [CrossRef]
197. Tong, X.; Chen, Z.; Zhuo, H.; Hu, Y.; Jing, S.; Liu, J.; Zhong, L. Tailoring the physicochemical properties of chitosan-derived N-doped carbon by controlling hydrothermal carbonization time for high-performance supercapacitor application. *Carbohydr. Polym.* **2019**, *207*, 764–774. [CrossRef]
198. Zhu, L.; Shen, F.; Smith, R.L., Jr.; Qi, X. High-Performance Supercapacitor Electrode Materials from Chitosan via Hydrothermal Carbonization and Potassium Hydroxide Activation. *Energy Technol.* **2017**, *5*, 452–460. [CrossRef]
199. Simsir, H.; Eltugral, N.; Karagoz, S. Hydrothermal carbonization for the preparation of hydrochars from glucose, cellulose, chitin, chitosan and wood chips via low-temperature and their characterization. *Bioresour. Technol.* **2017**, *246*, 82–87. [CrossRef]
200. Xu, Z.; Chen, J.; Zhang, X.; Song, Q.; Wu, J.; Ding, L.; Zhang, C.; Zhu, H.; Cui, H. Template-free preparation of nitrogen-doped activated carbon with porous architecture for high-performance supercapacitors. *Microporous Mesoporous Mater.* **2019**, *276*, 280–291. [CrossRef]
201. Shi, J.; Yan, N.; Cui, H.; Liu, Y.; Weng, Y.; Li, D.; Ji, X. Nitrogen doped hierarchically porous carbon derived from glucosamine hydrochloride for CO_2 adsorption. *J. CO2 Util.* **2017**, *21*, 444–449. [CrossRef]
202. Qu, H.; Zhang, X.; Zhan, J.; Sun, W.; Si, Z.; Chen, H. Biomass-Based Nitrogen-Doped Hollow Carbon Nanospheres Derived Directly from Glucose and Glucosamine: Structural Evolution and Supercapacitor Properties. *ACS Sustain. Chem. Eng.* **2018**, *6*, 7380–7389. [CrossRef]
203. Pei, S.; Zhang, J.; Gao, M.; Wu, D.; Yang, Y.; Liu, R. A facile hydrothermal approach towards photoluminescent carbon dots from amino acids. *J. Colloid Interface Sci.* **2015**, *439*, 129–133. [CrossRef]
204. Song, L.-T.; Wu, Z.-Y.; Liang, H.-W.; Zhou, F.; Yu, Z.-Y.; Xu, L.; Pan, Z.; Yu, S.-H. Macroscopic-scale synthesis of nitrogen-doped carbon nanofiber aerogels by template-directed hydrothermal carbonization of nitrogen-containing carbohydrates. *Nano Energy* **2016**, *19*, 117–127. [CrossRef]
205. Gorgieva, S.; Trček, J. Bacterial cellulose: Production, modification and perspectives in biomedical applications. *Nanomaterials* **2019**, *9*, 1352. [CrossRef] [PubMed]
206. Li, R.; Shao, X.; Li, S.; Cheng, P.; Hu, Z.; Yuan, D. Metal-free N-doped carbon nanofibers as an efficient catalyst for oxygen reduction reactions in alkaline and acid media. *Nanotechnology* **2016**, *27*, 505402. [CrossRef] [PubMed]
207. Liang, H.-W.; Wu, Z.-Y.; Chen, L.-F.; Li, C.; Yu, S.-H. Bacterial cellulose derived nitrogen-doped carbon nanofiber aerogel: An efficient metal-free oxygen reduction electrocatalyst for zinc-air battery. *Nano Energy* **2015**, *11*, 366–376. [CrossRef]
208. Park, G.S.; Lee, J.-S.; Kim, S.T.; Park, S.; Cho, J. Porous nitrogen doped carbon fiber with churros morphology derived from electrospun bicomponent polymer as highly efficient electrocatalyst for Zn-air batteries. *J. Power Source* **2013**, *243*, 267–273. [CrossRef]
209. Maldonado, S.; Stevenson, K.J. Influence of Nitrogen Doping on Oxygen Reduction Electrocatalysis at Carbon Nanofiber Electrodes. *J. Phys. Chem. B* **2005**, *109*, 4707–4716. [CrossRef]
210. Yin, J.; Qiu, Y.; Yu, J.; Zhou, X.; Wu, W. Enhancement of electrocatalytic activity for oxygen reduction reaction in alkaline and acid media from electrospun nitrogen-doped carbon nanofibers by surface modification. *RSC Adv.* **2013**, *3*, 15655–15663. [CrossRef]
211. Bokach, D.; ten Hoopen, S.; Muthuswamy, N.; Buan, M.E.; Rønning, M. Nitrogen-doped carbon nanofiber catalyst for ORR in PEM fuel cell stack: Performance, durability and market application aspects. *Int. J. Hydrogen Energy* **2016**, *41*, 17616–17630. [CrossRef]
212. Muthuswamy, N.; Buan, M.E.; Walmsley, J.C.; Rønning, M. Evaluation of ORR active sites in nitrogen-doped carbon nanofibers by KOH post treatment. *Catal. Today* **2018**, *301*, 11–16. [CrossRef]
213. Buan, M.E.; Muthuswamy, N.; Walmsley, J.C.; Chen, D.; Rønning, M. Nitrogen-doped carbon nanofibers on expanded graphite as oxygen reduction electrocatalysts. *Carbon* **2016**, *101*, 191–202. [CrossRef]

[**D2] M. Skorupska**, A. Ilnicka, J. P. Łukaszewicz *N-doped graphene foam obtained by microwave-assisted exfoliation of graphite*, Scientific Reports, 2021, 11 (1), 1-11; https://doi.org/10.1038/s41598-021-81769-5 (IF=4.6, MEiN=140)

W pracy przedstawiono wyniki badań przeprowadzonych w celu modyfikacji struktury grafitowej poprzez wykorzystanie promieniowania mikrofalowego oraz wprowadzenie azotowych grup funkcyjnych za pomocą naturalnego nośnika azotu. Wyniki analiz fizyko-chemicznych wykazały, że optymalny czas syntezy w reaktorze mikrofalowym wynosi 30 minut. Testy elektrochemiczne potwierdziły wysoką aktywność katalityczną w reakcji ORR, a wyznaczona liczba przenoszonych elektronów (n) była równa 3.46, co wskazuje, że otrzymany materiał grafenowy wykazuje mechanizm czteroelektronowej ścieżki redukcji tlenu w roztworze alkalicznym. Ponadto stwierdzono, że otrzymane materiały z wykorzystaniem DMF jako medium dyspergującego, nie wykazywały zwiększonej aktywności katalitycznej i przebiegały według dwuelektronowej ścieżki redukcji tlenu, która jest typowa dla materiałów niedomieszkowanych azotem. Na podstawie otrzymanych wyników wyselekcjonowano najlepiej działające medium dyspergujące jakim jest alkohol etylowy, gdyż uzyskano dla tych materiałów najlepsze wyniki elektrochemiczne. Warto podkreślić, że poprawa wydajności elektrochemicznej osiągnięta została z zastosowaniem przyjaznych dla środowiska reagentów oraz bez użycia metali szlachetnych, a także przy zmniejszeniu zużycia energii.

scientific reports

Check for updates

OPEN

N-doped graphene foam obtained by microwave-assisted exfoliation of graphite

Malgorzata Skorupska[1], Anna Ilnicka[1]✉ & Jerzy P. Lukaszewicz[1,2]

The synthesis of metal-free but electrochemically active electrode materials, which could be an important contributor to environmental protection, is the key motivation for this research approach. The progress of graphene material science in recent decades has contributed to the further development of nanotechnology and material engineering. Due to the unique properties of graphene materials, they have found many practical applications: among others, as catalysts in metal-air batteries, supercapacitors, or fuel cells. In order to create an economical and efficient material for energy production and storage applications, researchers focused on the introduction of additional heteroatoms to the graphene structure. As solutions for functionalizing pristine graphene structures are very difficult to implement, this article presents a facile method of preparing nitrogen-doped graphene foam in a microwave reactor. The influence of solvent type and microwave reactor holding time was investigated. To characterize the elemental content and structural properties of the obtained N-doped graphene materials, methods such as elemental analysis, high-resolution transmission electron microscopy, scanning electron microscopy, and Raman spectroscopy were used. Electrochemical activity in ORR of the obtained materials was tested using cyclic voltamperometry (CV) and linear sweep voltamperometry (LSV). The tests proved the materials' high activity towards ORR, with the number of electrons reaching 3.46 for tested non-Pt materials, while the analogous value for the C-Pt (20 wt% loading) reference was 4.

Graphene possesses excellent mechanical and thermal properties[1–3] and a high theoretical specific surface area (2630 $m^2 g^{-1}$)[4]. Therefore, over the past decades, graphene's potential uses have been examined within many fields[5]: fields emission (FE) devices[6], sensors and biosensors[7], optoelectronic devices (transparent electrodes for solar cells), liquid–crystal displays (LCD)[8,9], and electrode materials in batteries and supercapacitors[10,11]. Graphene can exist in the form of zero-dimensional (0D) dots (nanospheres[12], hollow spheres[13]), one-dimensional (1D) fibers (ribbons)[14], two-dimensional (2D) sheets[15], and three-dimensional (3D) foams[16]. 3D graphene foam is a network of connected graphene sheets and, just as 2D graphene, can be widely used to improve the electrical, mechanical, or thermal properties of electrochemical devices. The size, quality, and type of graphene sheet synthesis determines the properties and potential application of the 3D materials[17]. The synthesis of a three-dimensional graphene structure is based on either the assembly of two-dimensional graphene flakes or on a direct synthesis. Many papers describe 3D structure synthesis based on chemical vapor deposition (CVD) of graphene on a nickel foam matrix[18–21]. A relatively new synthesis method is the 3D printing of graphene materials[22–24]. Well-known methods of synthesis produce three-dimensional graphene materials effectively, but they are too expensive and require specialized equipment. The assembly of graphene flakes[25,26] by the hydrothermal method[27] is also popular, although not without disadvantages; self-organization of graphene sheets is the most common problem that researchers want to eliminate[28]. The microwave method[29,30] supports the synthesis of graphene, combining many advantages: it is fast, simple, does not require specialized equipment, and the starting material for foam production can be expanded graphite[31] or sucrose[32].

Graphene foams, due to their excellent porous structure, are a light material that combines the properties of two-dimensional graphene sheets and the three-dimensional system they form when joined together. The large pore volume and subsequent high specific surface area of the material, its thermal stability, high electronic conductivity, and high ion transfer rate all contribute to graphene foams' functionality in energy storage devices[28,33,34]. Hence, to further improve their properties, increase electrode capacity, and power or energy density, many researchers try to dope graphene materials with metal compounds or metal oxides, or to create composites with

[1]Faculty of Chemistry, Nicolaus Copernicus University in Torun, Gagarina 7, 87-100 Torun, Poland. [2]Centre for Modern Interdisciplinary Technologies, Nicolaus Copernicus University in Torun, Wilenska 4, 87-100 Torun, Poland. ✉email: ailnicka@umk.pl

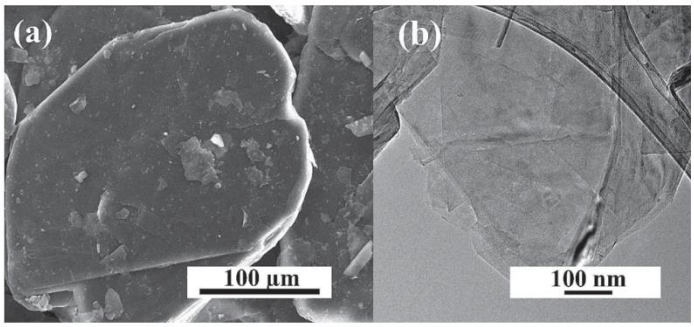

Figure 1. (**a**) SEM and (**b**) HRTEM images of expanded graphite.

other active materials[35–38]. These solutions involve increased production and disposal costs. The fact that these substances are not environmentally friendly leads researchers to try to introduce heteroatoms (mainly nitrogen) into the carbon structure using natural reagents[39,40], thus increasing the range of potential applications of 3D graphene materials.

The synthesis of any metal-free but electrochemically active electrode material is an important contribution to protecting the environment and the key motivation for engaging this research approach. To this end, we present a fast and facile method of producing N-doped graphene foam using a microwave process. In the proposed process, expanded graphite was used as a starting material and green algae *Chlorella vulgaris* as an N-precursor. Different solvents (ethyl alcohol and dimethylformamide) were applied in the microwave reactor study. After the microwave process, the samples were carbonized. The study investigated the influence that the microwave (duration time) and carbonization processes had on graphene structure and nitrogen content.

Results and discussion

Material characterization. The proposed method to obtain N-doped graphene foam using a pressure microwave reactor was confirmed to be effective using instrumental methods. Figure 1 shows the commercial expanded graphite, the substrate for synthesis. The morphology of expanded graphite is flat and graphite sheets overlap in stacks. The scanning electron microscope images allow determining the impact of the microwave process and type of solvent on the structure of the obtained graphene materials. Figure 2 shows the structure of materials obtained in the EtOH solution for samples 0A-10 and 1A-10. For material obtained without the carbonization process, the structure is similar to pristine graphite with the layers not separated (Fig. 2a). The HRTEM images in Fig. 2b indicate that the material consisted of many graphene sheets forming thick stacked layers. Figure 2c,d show SEM and HRTEM images of graphene foams obtained with N-reagent. The carbonization process aided the exfoliation of graphene flakes. The SEM and HRTEM images for samples obtained in DMF are presented in Fig. 3a,b for the 0B-10 sample and Fig. 3c,d for the 1B-10 sample. The morphology of the materials obtained in DMF is very similar to that of materials obtained in EtOH, so further analysis was necessary. In all solvents, the material was exfoliated after carbonization to form graphene foam, creating very light and fluffy structures. The high temperature caused the creation of spaces and a system of very thin graphene walls which incorporated nitrogen atoms. The HRTEM images for all solvents indicate that in both cases very thin parallel layers can be observed. Disordered morphology and clearly overlapping layers are typical for graphene-based materials.

A basic premise of this method of enriching the final material with nitrogen is the use of green algae. After carbonization, it can join graphene flakes (single layer graphene, few layer graphene and multilayer graphene type) into a durable, porous 3D structure resembling a foam or sponge. Aside from providing amorphous carbon matter adhering graphene flakes, green algae is a source of nitrogen. It was selected due to its useful features, such as ease of mixing with graphene flakes in EtOH or DMF and thermal degradation to a non-porous nitrogen-rich matrix. A low carbon matrix yield from the starting green algae mass makes it possible to avoid soaking the graphene flakes and retains the graphene flakes' surface accessibility to chemical reagents, e.g., electrolytes. The green algae-originated carbon phase is assumed to be present in the form N-rich bridges between graphene flakes which enable electron transfer throughout the whole mass of material. The effective exfoliation of materials obtained with a holding time of 10 min in the reactor led to the investigation of the effect that extending holding time had on the structure and elemental composition of graphene foams. The influence on the nitrogen content was examined in two different electrolytes, while the carbonization process was used to change the structure of graphene by creating exfoliated graphene foam with embedded nitrogen functional groups. The elemental analysis was used to determine the composition of the N-doped graphene foams. The influence of the elemental composition for materials in series 0A/B-T and 1A/B-T obtained in different solvents is shown in Table 1. The results for samples obtained in these two series indicate that solvent and holding time in the microwave reactor influence the elemental content of the obtained materials. A high carbon content in the range from 76.06 to 95.52

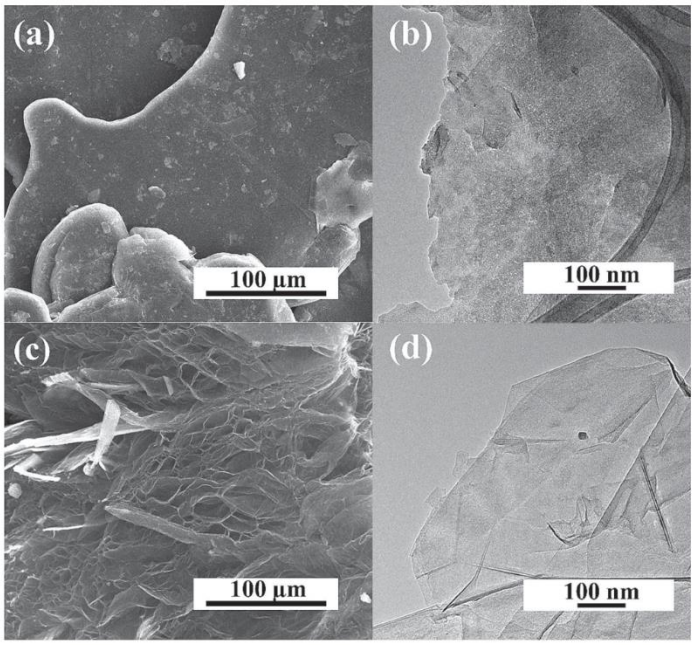

Figure 2. SEM and HRTEM images of graphene foams obtained without and with N-reagent: (**a**,**b**) 0A-10 and (**c**,**d**) 1A-10.

wt% was observed for all samples. The mass content of the samples obtained was typical for graphene-based materials. The nitrogen content in samples prepared without N-reagent was significantly lower than that for samples with *Chlorella vulgaris*. Heteroatoms were successfully introduced into the graphene structure using the natural reagent. For samples synthesized in different solvents with N-reagent, the percentage by mass of nitrogen was high, at 2.44 wt% for the 1A-10 sample. Along with extending the reaction time for the 1A-T series produced in the ethyl alcohol solvent, a significant decrease of the nitrogen content, down to 0.65 wt%, was noted. In the case of the 1B-T series, where DMF was the solvent, an increase in the samples' nitrogen content was observed when holding time was increased. The highest nitrogen content for the 1B-T series was recorded for a sample maintained for 90 min, at 0.89 wt%.

Raman spectroscopy is the method most commonly used to characterize graphene materials[41]. On the Raman spectra for graphene, three characteristic bands can be observed, D, G, and 2D, for which the shift at the 532 nm laser line is 1347 cm^{-1}, 1577 cm^{-1}, and 2698 cm^{-1}[42] respectively. Using Raman spectroscopy analysis, it is possible to estimate the number of graphene sheet layers that have been laid, as well as determine defects in the material obtained. Raman spectra were compiled for the N-doped graphene foams carried out in two selected solvents, EtOH (Fig. 4a) and DMF (Fig. 4b). The holding time in the reactor was 10, 30, 60, or 90 min. Table 2 shows the ratio of intensities of the materials obtained depending on their different reaction times and solvents. The ratio of D and G band intensities indicates the degree of graphitization defect, while I_{2D}/I_G indicates the number of superimposed graphene layers. Comparing the spectra with each other, there is no significant difference in the intensity ratio of 2D to G bands. The ratio is close to 0.5, which indicates that the obtained material possesses several layers. The change in D-band is clearly visible, which may mark the quality of the graphene structure. In the 1A-T series, the I_D/I_G band ratio increases along with the reaction time, indicating quality. The low ratio of D to G-band intensities suggests that graphene material was effectively obtained. These can potentially be used in electrochemical applications as electrodes, as sensors, or biosensors.

In order to determine the thickness and lateral size of graphene sheets which were treated in the microwave reactor, AFM analysis was performed using the 1A-T and 1B-T series of samples, synthesized in two solvents, EtOH (Fig. 5a) and DMF (Fig. 5b). Knowing the thickness of single-layered graphene and the interlayer distance, the measured value corresponds to few graphene layers. The thickness of graphene sheets for series 1A-T and 1B-T is in the range of 3.62–6.78 nm and 5.59–16.45 nm, respectively. This result is consistent with Raman spectroscopy examinations, which also suggests that employing the microwave reactor produces few-layered graphene, regardless of the type of solvent.

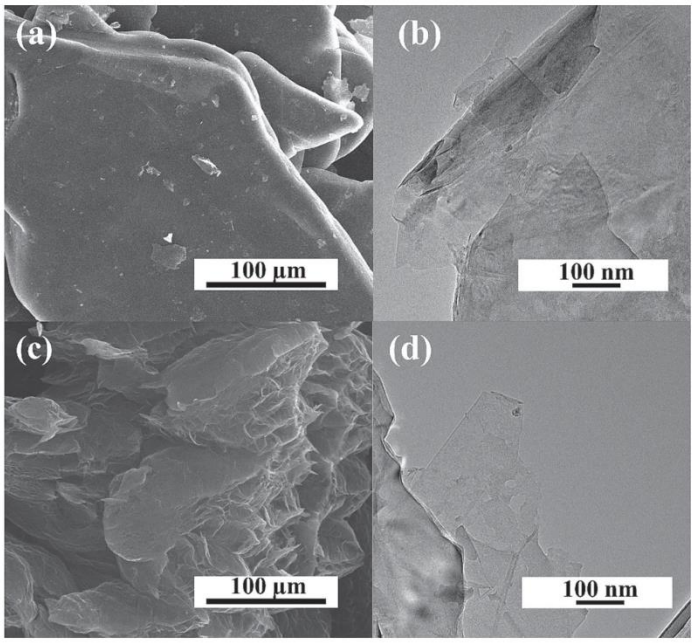

Figure 3. SEM, HRTEM images of graphene foams obtained without and with N-reagent: (**a**,**b**) 0B-10 and (**c**,**d**) 1B-10.

Sample	Content (wt%)		
	C	H	N
EG	73.54	1.50	0.08
0A-10	76.06	1.56	0.14
0B-10	80.70	1.37	0.58
1A-10	88.83	0.58	2.44
1A-30	90.40	0.61	0.97
1A-60	91.09	0.90	0.65
1A-90	91.50	0.83	0.73
1B-10	95.48	0.34	0.10
1B-30	91.27	0.72	0.76
1B-60	89.21	0.92	0.84
1B-90	89.78	0.83	0.89

Table 1. Elemental composition of EG and graphene foams obtained with different solvents and holding times in the microwave reactor.

The surface elemental composition of materials from the 1A-T series was analyzed using X-ray photoelectron spectroscopy. Figure 6a shows a wide survey scan for sample 1A-30 collected from 0 to 1300 eV. XPS spectra of sample 1A-30 for C1s, N1s, and O1s are presented in Fig. 6b–d. The high-resolution spectrum of C1s (Fig. 6b) can be deconvoluted into five peaks centered at 284.6 eV, 285.0 eV, 286.4 eV, 287.7 eV, and 288.6 eV, which can be attributed to bonds of C=C (sp^2), C–C (sp^3), C–O–C, C=O, and O–C=O, respectively. The total content of carbon for all samples, determined by XPS measurement, was in the range from 90.2 to 93.2 at.% (Table 3) and was at the same level as carbon content determined by elemental combustion measurement.

After deconvolution of the high-resolution spectrum of N1s, two characteristic types of bonds were determined for nitrogen in the form of pyrrolic-N and quaternary-N in binding energies of 399.1 eV and 400.8 eV,

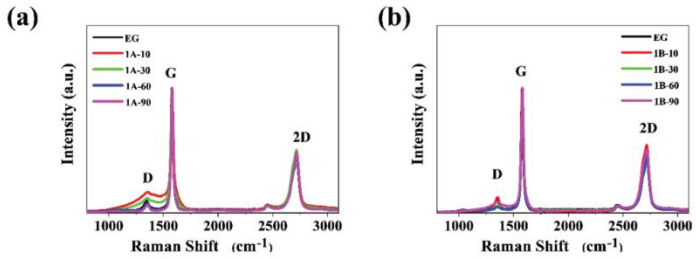

Figure 4. Raman spectra of (**a**) 1A-T and (**b**) 1B-T series compared to pristine EG.

Sample	D-band		G-band		2D-band		I_D/I_G	I_{2D}/I_G
	cm^{-1}	I	cm^{-1}	I	cm^{-1}	I		
EG	1348.0	0.10	1575.5	1	2713.5	0.48	0.10	0.48
1A-10	1353.0	0.17	1580.0	1	2716.0	0.47	0.17	0.47
1A-30	1353.0	0.12	1578.5	1	2716.0	0.50	0.12	0.50
1A-60	1352.5	0.08	1580.0	1	2718.5	0.48	0.08	0.48
1A-90	1353.0	0.07	1580.0	1	2717.5	0.48	0.07	0.48
1B-10	1353.0	0.12	1578.5	1	2716.0	0.55	0.12	0.55
1B-30	1355.5	0.06	1580.0	1	2717.5	0.49	0.06	0.49
1B-60	1353.0	0.05	1580.0	1	2719.0	0.47	0.05	0.47
1B-90	1356.5	0.09	1580.0	1	2715.5	0.50	0.09	0.50

Table 2. Raman band positions and intensities, as well as the intensity ratio of EG and graphene obtained in 1A-T and 1B-T series.

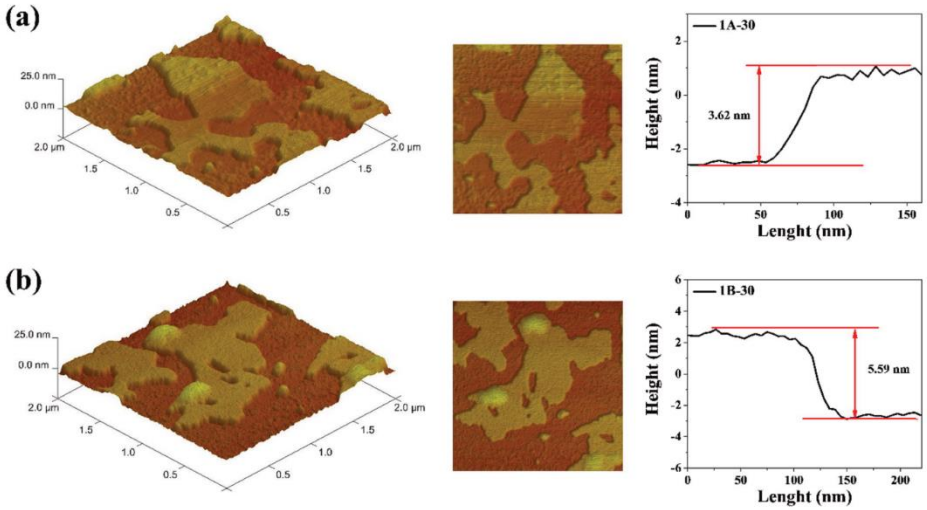

Figure 5. AFM images of (**a**) 1A-30, (**b**) 1B-30 with height profiles of graphene flakes.

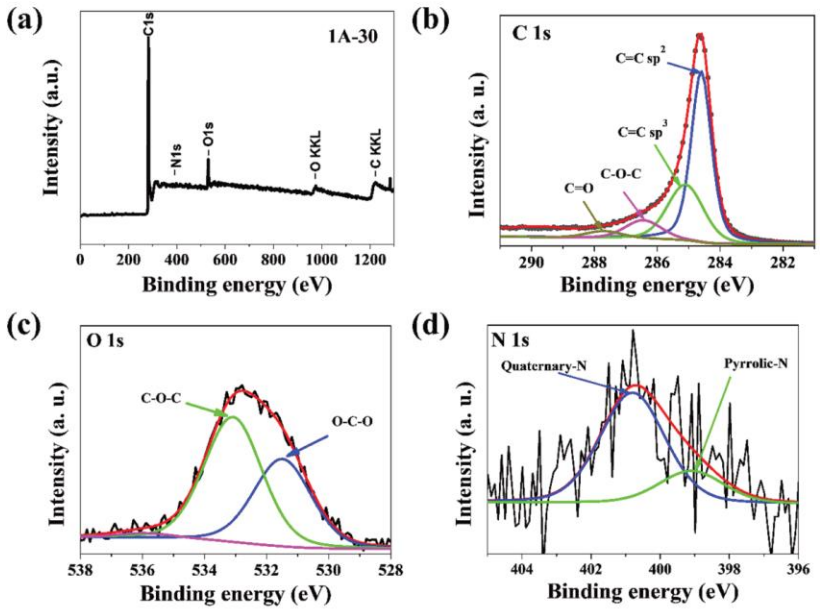

Figure 6. (**a**) XPS survey spectrum and high-resolution XPS spectra of (**b**) C1s, (**c**) O1s, (**d**) N1s for 1A-30 sample.

	Binding energy (eV)									
	284.6	285.0	286.4	287.7	288.6	531.6	533.2	536.0	399.1	400.8
	Elemental content (at.%)									
Sample	C					O			N	
1A-10	35.7	41.3	9.3	3.0	0.9	2.7	4.5	0.2	0.9	0.8
1A-30	57.6	24.0	7.9	2.9	0.0	2.5	3.5	0.1	0.7	0.2
1A-60	66.5	16.0	7.9	2.6	0.0	2.4	3.2	0.1	0.5	0.3
1A-90	59.9	23.5	7.1	2.7	0.0	2.4	2.9	0.3	0.4	0.2

Table 3. Chemical composition analyzed using high-resolution XPS for series 1A-T.

respectively[43]. Modified graphene structures subjected to microwave heating facilitated nitrogen substitution in the graphite plane. The effect of high carbonization temperatures on doped structures was the formation of mainly quaternary-N functional groups, responsible for the materials' effective catalytic activity in the oxygen reduction reaction[44]. Due to access to an electron pair in the graphene structure, the pyrolytic N-group is active in response to the oxygen reduction reaction, which leads to an increase in the catalytic activity of N-doped materials[45]. The overall content of nitrogen atoms for all samples in the 1A-T series was between 0.6 and 2.7 at.%. The XPS results show that nitrogen doping in graphene is successful; there were two characteristic types of nitrogen functional groups that improved catalytic properties in response to ORR results, the highest content belonging to the pyrrolic-N groups. Deconvolution of the high-resolution O1s spectrum fit into three bands at energy values of 531.6 eV, 533.2 eV, and 536.0 eV which correspond to C–O–C, O–C–O, and absorbed H_2O bonds, respectively[46].

Electrochemical performance. In order to check the catalytic activity of the obtained materials in the oxygen reduction reaction, cyclic voltammetry and linear voltammetry measurements were taken. The ORR reaction is distinctive in metal-air batteries and fuel cells, therefore examining the catalytic activity of the produced nitrogen-doped materials was an important aspect of the work. In recent years, heteroatom-doped graphene has become an alternative to platinum-based materials owing to the heteroatoms' improvement of electrochemi-

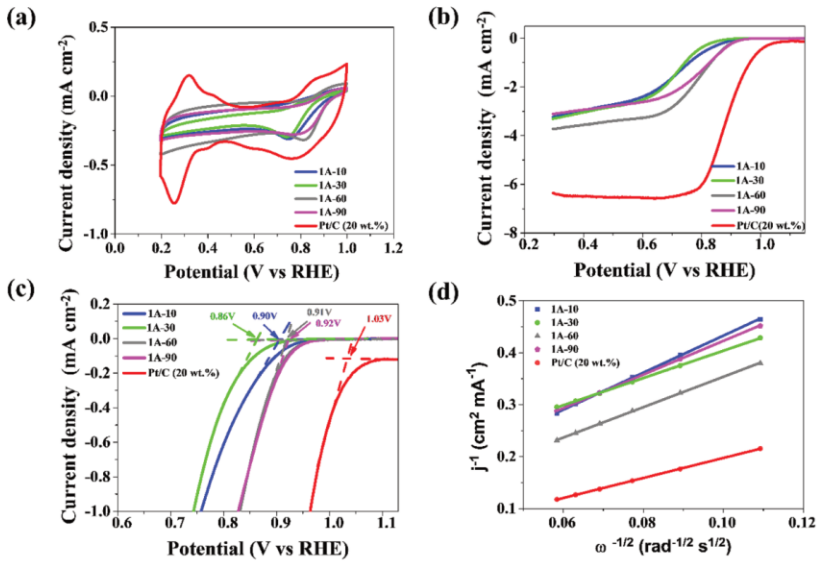

Figure 7. (**a**) CV curves with a scan speed of 100 mV s^{-1} in O_2-saturated electrolyte for the 1A-T series and the Pt/C catalyst; (**b**) LSV curve of the obtained samples and Pt/C catalysts (5 V s^{-1}, 1600 rpm); (**c**) Onset potential of 1A-T and the commercial catalyst; (**d**) Koutecky–Levich plot for the samples at 0.45 V.

cal properties[47,48]. In this case, graphene structures served as a matrix for the introduction of nitrogen, using the natural substrate *Chlorella vurgalis* as the source. As the literature reports, N-precursor is transformed into conductive carbon forms under the influence of high carbonization temperatures, 800–900 °C, which increase electrocatalytic properties[49,50]. The reference material in electrochemical tests was a carbon material based on platinum (20 wt%). All measurements were made in an oxygen-saturated 0.1 M KOH electrolyte for the materials from the 1A-T and 1B-T series, however the plots are presented for the 1A-T series only (Fig. 7). Figure 7a illustrates the CV curves for the samples obtained in the 1A-T series, showing the cathode peaks for samples 1A-10, 1A-30, 1A-60, and 1A-90 at a potential of 0.75 V, 0.74 V, 0.81 V, and 0.76 V relative to the RHE electrode, respectively. This is one proof that the presented method produces materials with good electrocatalytic properties. When examining the catalytic activity in the oxygen reduction reaction, one should keep in mind the measurements of linear voltammetry, which provide the most information regarding the catalytic properties of the obtained materials. Figure 7b shows LSV measurements. The curves were retrieved with oxygen flow at a scanning speed of 5 mV s^{-1}, and rotation speed of 800–2800 rpm. A curve was selected for all samples in the 1A-T series and for the Pt/C reference catalyst (20 wt%) at one rotation speed, 1600 rpm. Sample 1A_60 exhibits the highest current density among the samples obtained, but it is still lower than a commercial material based on platinum. This proves that, despite sample 1A-60 having the lowest nitrogen content at 0.65 wt%, the material shows good catalytic properties in ORR. The value of the onset potential for the 1A-60 sample, shown in Fig. 7c, was 0.91 V, while for the commercial material this value was about 1.03 V. For the other samples, 1A-10, 1A-30, and 1A-90, the value of the onset potential was 0.90, 0.86, and 0.92 V vs RHE, respectively. LSV results are typical for non-metallic graphene-based materials. They contributed to the estimation of the electron transfer number in the oxygen reduction reaction, which primarily describes the path of the ORR reaction. By analyzing the Koutecky–Levich plot (Fig. 7d), it is possible to determine the number of electron transfers. Data gathered from the LSV plot at a value of 0.45 V were used to calculate the number of electrons participating in the reaction. For the commercial material based on platinum, a four-electron reaction was a distinguishing characteristic, while graphene is characterized by a two-electron oxygen reduction reaction[51]. ORR performance parameters for the 1A-T series and commercial platinum-based carbon are presented in Table 4. The values closest to those for the commercial catalyst were those of samples 1A-30 and 1A-60, of 3.46 and 3.10, respectively. A high value of n means that the electron transfer in the oxygen reduction reaction is close to the 4 electron ORR mechanism. The number of transferred electrons for the series of samples obtained with DMF as solvent equals 2.55, 2.42, 2.49, and 2.57 for 1B-10, 1B-30, 1B-60, and 1B-90, respectively. The produced materials show improved properties over pristine graphene, whose typical number of electron transfers in ORR is about 2 electrons[48,52]. The LSV results show that the resulting materials have good catalytic properties. This is proof that the electrocatalysts doped with heteroatomic nitrogen, and mainly nitrogen functional groups in the graphene structure, are responsible for catalyzing the ORR reaction. The products are completely free of any metals and can potentially achieve

Sample	E_{onset} (V vs RHE)	$E_{1/2}$ (V vs RHE)	Diffusion limiting current density (mA cm^{-2})	n (0.45 V)
1A-10	0.90	0.73	2.56	2.55
1A-30	0.86	0.72	2.44	3.46
1A-60	0.91	0.79	3.55	3.10
1A-90	0.92	0.80	3.12	2.80
Pt/C (20 wt%)	1.03	0.88	6.37	4.00

Table 4. ORR performance parameters of series 1A-T and commercial Pt/C catalyst tested in alkaline media.

wide application in the field of electrochemistry. Remarkably, the 1A-60 and 1A-90 exhibited prominent ORR activity with the most positive onset potential (E_{onset}) at 0.91 V and 0.92 V. The half-way potential ($E_{1/2}$) was also highest for 1A-60 and 1A-90 compared to other samples. The prominent ORR activities of 1A-30 and 1A-60 in an alkaline medium may be benefitting from the synergistic effect of the structure and elemental composition. First, the unique few-layer architecture of graphene is conducive to exposing more of the active sites and facilitates the accessibility of oxygen. Second, the nitrogen heteroatoms can induce charge redistribution and facilitate the adsorption of oxygen and the consequent reduction reaction on carbon. The proposed materials' composition is their advantage, because generally structures described for ORR application tend to be decorated with expensive, precious, or environmentally-unfriendly metals or metal oxides, e.g., Pd, Ru[53], perovskie oxides[54], Fe(II)[55], Fe_7C_3[56], or Au[57].

Conclusion

In summary, an effective method of obtaining N-doped graphene in a microwave reactor was developed, one which uses expanded graphite and *Chlorella vurgalis*. Research indicates that the use of a natural N-reagent during synthesis in a microwave reactor in various solvents can contribute to the incorporation of nitrogen atoms into the graphene structure at a level of several percent. It can be concluded that ethyl alcohol and dimethylformamide are good solvents which contribute to the exfoliation of graphene layers and the production of pure graphene material. The high quality of the obtained material, without defects, shows that the method is a promising way of producing heteroatom-doped graphene foams. The optimal time for synthesis in the microwave reactor was 30 min and introduced mainly pyrrolic-N groups descend from N-precursor *Chlorella vurgalis*. The best electrochemical results were obtained for materials using ethanol as a reaction medium. The solvent also influenced the introduction of nitrogen functional groups into the graphene structure. The products showed good catalytic activity owing to the nitrogen functional groups introduced into the graphene structure, which are responsible for the catalytic properties in the oxygen reduction reaction. The tests proved their high activity towards ORR, i.e., the number of electrons n reached 3.46 for tested materials (no Pt added), while the analogous value for the C-Pt (20 wt% loading) reference was only slightly higher and equal 4. For pristine, i.e., non-N-doped graphene, the n value was only 2. It has to be underlined that the progress in electrochemical performance was achieved in an environment-friendly way, not only without the use of noble metals, but also with a reduction in energy consumption. Heteroatom doping of graphene materials is an alternative to more expensive materials based on metals, an alternative that can have promising properties for electrochemical applications and a huge impact on the potential use the composite materials in supercapacitors, metal-air batteries, or fuel cells.

Materials and methods

Preparation of N-doped graphene foam samples. The production of N-doped graphene foams was based on a one-step process using microwave radiation in two dispersed solvents: ethyl alcohol (EtOH), and dimethylformamide (DMF). The starting materials used were expanded commercial graphite (EG, Sinograf, Torun, Poland) and the natural green algae N-precursor, *Chlorella vulgaris*. The compounds were mixed in a solvent with a 1:4 mass ratio of graphene to *Chlorella vulgaris*, then sonicated to obtain a better dispersion. The samples were loaded into a microwave reactor (Microwave 400) and heated under pressure to 180 °C, with the power of about 300–600 W. The microwaving duration was either 10, 30, 60, or 90 min; after this time, the samples were stirred. The obtained mass was then washed with distilled water to remove the solvent and dried at 120 °C overnight. Finally, samples were carbonized at 900 °C with a heating rate of 3 °C min^{-1} and then heated for 4 h under the flow of nitrogen (to provide an inert environment during carbonization). Reference samples were made using the same procedure, but without the addition of an N-precursor nor the carbonization process. For all samples without the addition of *Chlorella vulgaris*, the process in the reactor was maintained for 10 min. The reference samples obtained without carbonization, only the microwave process, are designated as 0A/B-T, where A and B describe the solvent and denote EtOH or DMF, respectively, while T is the time in minutes that the sample was held in the microwave reactor. Samples obtained with the addition of the N-precursor and using carbonization are designated as 1A/B-T, where A and B describe the solvent and mark EtOH or DMF, respectively, and T is the duration of time spent in the microwave.

Characterization methods. The atomic structure of the obtained materials was analyzed using a high-resolution transmission electron microscope (HRTEM FEI Tecnai F20 X-Twin, Brno, Czech Republic) at an accelerating voltage of 200 kV. A scanning electron microscope operating at 30 kV (SEM, 1430 VP, LEO Electron Microscopy Ltd., Oberkochen, Germany) was used to determine the structure of the samples. The elemental

composition of the materials was analyzed by means of a combustion elemental analyzer (Vario MACRO CHN, Elementar Analysensysteme GmbH, Langenselbold, Germany). Raman-microscopic spectroscopy analysis was performed using Renishaw InVia (Renishaw Company, Gloucestershire, the United Kingdom), excitation wavelength 532 nm at an ambient temperature. Nitrogen sorption isotherms were determined through nitrogen physisorption at 77 K in a volumetric apparatus ASAP 2010 (Micromeritics, Norcross, GA, USA). The attachment, bonding configuration, and compositional analysis of the material was carried out by X-ray photoelectron spectroscopy measurements (XPS, PHI5000 VersaProbe II Scanning XPS Microprobe, Chigasaki, Japan). A monochromatic Al-Kα X-ray (1486.6 eV) was used as the operating excitation source. Atomic Force Microscopy (AFM) investigations were conducted using a Scanning Probe Microscope (SPM) apparatus produced by Veeco (Digital Instrument, USA), working under ambient conditions.

Electrochemical measurements. Tests of the obtained materials' electrochemical properties were carried out using the Autolab potentiostat (PGSTAT128N, The Netherlands). The standard measuring setup was made up of three electrodes—an Ag/AgCl electrode in 3 M KCl was the reference, a Pt electrode the counter, while the working electrode was glassy carbon (GC rotating disk electrode with a 5.0 mm diameter) onto which ink, with the catalyst, was applied. The catalyst ink was prepared basing on the dispersion of 2.5 mg of the test sample in a mixture of distilled water and ethanol (ratio 1:4) and Nafion (0.5 wt% Nafion). As a point of comparison, electrochemical studies were also performed on a commercial catalyst from Sigma Aldrich, platinum on graphitized Pt/C carbon (20 wt% Platinum). The prepared ink was pipetted onto glassy carbon in an amount of 15.63 µl and the electrode was dried afterwards. Catalyst content was about 0.4 mg cm^{-2}. Before electrochemical testing, the alkaline solution was saturated with O_2/N_2 for 20 min. The activity of the samples in an oxygen reduction reaction was evaluated by measuring cyclic voltammetry (CV), carried out at a scanning speed of 10 mV s^{-1}, and linear voltammetry (LSV), at a scanning speed of 5 mV s^{-1} and rotation speed of 800–2800 rpm, in a solution of 0.1 M KOH at room temperature. The number of electrons (n) directly participating in ORR was calculated using the Koutecky–Levich equation (K–L):

$$J^{-1} = J_L^{-1} + J_K^{-1} = \left(B\omega^{1/2}\right)^{-1} + J_K^{-1} \quad (1)$$

$$B = 0.62nFC_0(D_0)^{2/3}\nu^{-1/6} \quad (2)$$

where J is defined as the measured density, J_L is the current density limiting diffusion, and J_K is the kinetic current density; ω is the angular velocity of the electrode; n is the number of electron transfers in the reaction; F is the Faraday constant (96,485 C mol^{-1}); C_0 is the concentration of dissolved oxygen (1.2×10^{-6} mol L^{-1} in 0.1 M KOH); D_0 is the diffusion coefficient of dissolved oxygen (1.9×10^{-5} cm^2 s^{-1} in 0.1 M KOH); v is the kinetic viscosity of the electrolyte for 0.1 M KOH, 0.01 cm^2 s^{-1}. The slope of the K-L graph can be obtained using Koutecky–Levich Eqs. (1) and (2), thanks to which it is possible to determine the number of electron transfers in ORR.

Received: 28 August 2020; Accepted: 24 December 2020
Published online: 21 January 2021

References

1. Zhu, Y. *et al.* Graphene and graphene oxide: Synthesis, properties, and applications. *Adv. Mater.* **22**, 3906–3924 (2010).
2. Lee, C., Wei, X., Kysar, J. W. & Hone, J. Measurement of the elastic properties and intrinsic strength of monolayer graphene. *Science* **321**, 385–388 (2008).
3. Balandin, A. A. Thermal properties of graphene and nanostructured carbon materials. *Nat. Mater.* **10**, 569–581 (2011).
4. Bhuyan, M. S. A., Uddin, M. N., Islam, M. M., Bipasha, F. A. & Hossain, S. S. Synthesis of graphene. *Int. Nano Lett.* **6**, 65–83 (2016).
5. Choi, W., Lahiri, I., Seelaboyina, R. & Kang, Y. S. Synthesis of graphene and its applications: A review. *Crit. Rev. Solid State Mater. Sci.* **35**, 52–71 (2010).
6. Kumar, S., Duesberg, G., Pratap, R. & Raghavan, S. Graphene field emission devices. *Appl. Phys. Lett.* **105**, 103107 (2014).
7. Justino, C. I., Gomes, A. R., Freitas, A. C., Duarte, A. C. & Rocha-Santos, T. A. Graphene based sensors and biosensors. *TrAC, Trends Anal. Chem.* **91**, 53–66 (2017).
8. Xu, Y. & Liu, J. Graphene as transparent electrodes: Fabrication and new emerging applications. *Small* **12**, 1400–1419 (2016).
9. Kumar, A., Ganguly, P. & Biradar, A. M. Single layer graphene: an alternative electrode material for ferroelectric liquid crystal based displays. *Liq. Cryst.* **45**, 1620–1625 (2018).
10. Bulbula, S. T., Lu, Y., Dong, Y. & Yang, X.-Y. Hierarchically porous graphene for batteries and supercapacitors. *New J. Chem.* **42**, 5634–5655 (2018).
11. Dai, C. *et al.* Recent progress in graphene-based electrodes for flexible batteries. *InfoMat* (2019).
12. Fan, W. *et al.* Nitrogen-doped graphene hollow nanospheres as novel electrode materials for supercapacitor applications. *J. Power Sources* **243**, 973–981 (2013).
13. Wu, L., Feng, H., Liu, M., Zhang, K. & Li, J. Graphene-based hollow spheres as efficient electrocatalysts for oxygen reduction. *Nanoscale* **5**, 10839–10843 (2013).
14. Sheng, L. *et al.* Ultra-high toughness all graphene fibers derived from synergetic effect of interconnected graphene ribbons and graphene sheets. *Carbon* **120**, 17–22 (2017).
15. Ruiz, L., Xia, W., Meng, Z. & Keten, S. A coarse-grained model for the mechanical behavior of multi-layer graphene. *Carbon* **82**, 103–115 (2015).
16. Huang, Z., Guo, H. & Zhang, C. Assembly of 2D graphene sheets and 3D carbon nanospheres into flexible composite electrodes for high-performance supercapacitors. *Compos. Commun.* **12**, 117–122 (2019).
17. Shen, Z., Ye, H., Zhou, C., Kröger, M. & Li, Y. Size of graphene sheets determines the structural and mechanical properties of 3D graphene foams. *Nanotechnology* **29**, 104001 (2018).
18. Aslam, S. *et al.* Graphene oxide coated graphene foam based chemical sensor. *Mater. Lett.* **235**, 66–70 (2019).
19. Chen, Z., Xu, C., Ma, C., Ren, W. & Cheng, H. M. Lightweight and flexible graphene foam composites for high-performance electromagnetic interference shielding. *Adv. Mater.* **25**, 1296–1300 (2013).

20. He, J., Chen, Y. & Manthiram, A. MOF-derived cobalt sulfide grown on 3D graphene foam as an efficient sulfur host for long-life lithium-sulfur batteries. *IScience* **4**, 36–43 (2018).
21. Sha, J. *et al.* Preparation of three-dimensional graphene foams using powder metallurgy templates. *ACS Nano* **10**, 1411–1416 (2016).
22. Kim, J. H. *et al.* 3D printing of reduced graphene oxide nanowires. *Adv. Mater.* **27**, 157–161 (2015).
23. Sha, J. *et al.* Three-dimensional printed graphene foams. *ACS Nano* **11**, 6860–6867 (2017).
24. Guo, H., Lv, R. & Bai, S. Recent advances on 3D printing graphene-based composites. *Nano Mater. Sci.* **1**, 101–115 (2019).
25. Zou, J. & Kim, F. Diffusion driven layer-by-layer assembly of graphene oxide nanosheets into porous three-dimensional macrostructures. *Nature communications* **5**, 1–9 (2014).
26. Hu, G. *et al.* 3D graphene-foam–reduced-graphene-oxide hybrid nested hierarchical networks for high-performance Li–S batteries. *Adv. Mater.* **28**, 1603–1609 (2016).
27. Karuppanan, K. K. *et al.* 3D-porous electrocatalytic foam based on Pt@ N-doped graphene for high performance and durable polymer electrolyte membrane fuel cells. *Sustain. Energy Fuels* **3**, 996–1011 (2019).
28. Karfa, P., Majhi, K. C. & Madhuri, R. *Self-standing Substrates: Materials and Applications* (eds Inamuddin, Boddula, R. & Asiri, A. M.) 327–351 (Springer International Publishing, 2020).
29. Patra, S., Choudhary, R., Roy, E., Madhuri, R. & Sharma, P. K. Heteroatom-doped graphene 'Idli': A green and foody approach towards development of metal free bifunctional catalyst for rechargeable zinc-air battery. *Nano Energy* **30**, 118–129 (2016).
30. Zhang, T. *et al.* Ultrafast microwave reduction process for high-quality graphene foam with outstanding electromagnetic interference shielding and good adsorption capacity. *FlatChem* **17**, 100117 (2019).
31. Lee, S.-H., Kang, D. & Oh, I.-K. Multilayered graphene-carbon nanotube-iron oxide three-dimensional heterostructure for flexible electromagnetic interference shielding film. *Carbon* **111**, 248–257 (2017).
32. Canencia, F. *et al.* Conducting macroporous carbon foams derived from microwave-generated caramel/silica gel intermediates. *J. Mater. Sci.* **52**, 11269–11281 (2017).
33. Xiong, C. *et al.* The recent progress on three-dimensional porous graphene-based hybrid structure for supercapacitor. *Compos. B Eng.* **165**, 10–46 (2019).
34. Xia, X., Chao, D., Zhang, Y. Q., Shen, Z. X. & Fan, H. J. Three-dimensional graphene and their integrated electrodes. *Nano Today* **9**, 785–807 (2014).
35. Rakhi, R., Chen, W., Cha, D. & Alshareef, H. N. High performance supercapacitors using metal oxide anchored graphene nanosheet electrodes. *J. Mater. Chem.* **21**, 16197–16204 (2011).
36. Manjakkal, L., Núñez, C. G., Dang, W. & Dahiya, R. Flexible self-charging supercapacitor based on graphene-Ag-3D graphene foam electrodes. *Nano Energy* **51**, 604–612 (2018).
37. Garakani, M. A. *et al.* Heterogeneous, mesoporous NiCo 2 O 4–MnO 2/graphene foam for asymmetric supercapacitors with ultrahigh specific energies. *J. Mater. Chem. A* **5**, 3547–3557 (2017).
38. Qian, Y. *et al.* A free-standing Li4Ti5O12/graphene foam composite as anode material for Li-ion hybrid supercapacitor. *Electrochim. Acta* **258**, 1311–1319 (2017).
39. Lin, G. *et al.* Three-dimensional interconnected nitrogen-doped mesoporous carbons as active electrode materials for application in electrocatalytic oxygen reduction and supercapacitors. *J. Colloid Interface Sci.* **527**, 230–240 (2018).
40. Huang, J. *et al.* Extremely elastic and conductive N-doped graphene sponge for monitoring human motions. *Nanoscale* **11**, 1159–1168 (2019).
41. Bokobza, L., Bruneel, J.-L. & Couzi, M. Raman spectra of carbon-based materials (from graphite to carbon black) and of some silicone composites. *J. Carbon Res.* **1**, 77–94 (2015).
42. Malard, L., Pimenta, M., Dresselhaus, G. & Dresselhaus, M. Raman spectroscopy in graphene. *Phys. Rep.* **473**, 51–87 (2009).
43. Wang, T. *et al.* Identifying the active site of N-doped graphene for oxygen reduction by selective chemical modification. *ACS Energy Lett.* **3**, 986–991 (2018).
44. Rahsepar, M., Nobakht, M. R., Kim, H. & Pakshir, M. Facile enhancement of the active catalytic sites of N-doped graphene as a high performance metal-free electrocatalyst for oxygen reduction reaction. *Appl. Surf. Sci.* **447**, 182–190 (2018).
45. Wu, H. *et al.* A graphene-based electrocatalyst co-doped with nitrogen and cobalt for oxygen reduction reaction. *Int. J. Hydrogen Energy* **41**, 20494–20501 (2016).
46. Wei, D. *et al.* Synthesis of N-doped graphene by chemical vapor deposition and its electrical properties. *Nano Lett.* **9**, 1752–1758 (2009).
47. Ouyang, W. *et al.* Exploring the active sites of nitrogen-doped graphene as catalysts for the oxygen reduction reaction. *Int. J. Hydrogen Energy* **39**, 15996–16005 (2014).
48. Tao, H. *et al.* N-Doping of graphene oxide at low temperature for the oxygen reduction reaction. *Chem. Commun.* **53**, 873–876 (2017).
49. Ilnicka, A., Lukaszewicz, J. P., Shimanoe, K. & Yuasa, M. Urea treatment of nitrogen-doped carbon leads to enhanced performance for the oxygen reduction reaction. *J. Mater. Res.* **33**, 1612–1624 (2018).
50. Ilnicka, A., Gauden, P. A., Terzyk, A. P. & Lukaszewicz, J. P. Nano-structured carbon matrixes obtained from chitin and chitosan by a novel method. *J. Nanosci. Nanotechnol.* **16**, 2623–2631 (2016).
51. Yasuda, S., Yu, L., Kim, J. & Murakoshi, K. Selective nitrogen doping in graphene for oxygen reduction reactions. *Chem. Commun.* **49**, 9627–9629 (2013).
52. Lou, F. *et al.* One-step electrochemical synthesis of tunable nitrogen-doped graphene. *J. Mater. Chem. A* **4**, 1233–1243 (2016).
53. Barman, B. K., Sarkar, B. & Nanda, K. K. Pd-coated Ru nanocrystals supported on N-doped graphene as HER and ORR electrocatalysts. *Chem. Commun.* **55**, 13928–13931 (2019).
54. Bu, Y. *et al.* Synergistic interaction of perovskite oxides and N-doped graphene in versatile electrocatalyst. *J. Mater. Chem. A* **7**, 2048–2054 (2019).
55. Komba, N. *et al.* Iron (II) phthalocyanine/N-doped graphene: A highly efficient non-precious metal catalyst for oxygen reduction. *Int. J. Hydrogen Energy* **44**, 18103–18114. https://doi.org/10.1016/j.ijhydene.2019.05.032 (2019).
56. Wen, G.-L. *et al.* Graphene wrapped Fe7C3 nanoparticles supported on N-doped graphene nanosheets for efficient and highly methanol-tolerant oxygen reduction reaction. *J. Colloid Interface Sci.* **556**, 352–359. https://doi.org/10.1016/j.jcis.2019.08.064 (2019).
57. Yan, Y., Yan, S., Yu, Z. & Zou, Z. Low-work-function silver activating N-doped graphene as efficient oxygen reduction catalysts in acidic medium. *ChemCatChem* **11**, 1033–1038. https://doi.org/10.1002/cctc.201801869 (2019).

Acknowledgements

This work was carried out as a result of the research project no 2019/35/N/ST5/02691, financed by the National Science Centre.

Author contributions

M.S.: conceptualization, methodology, formal analysis, investigation, writing—original draft, supervision, project administration, funding acquisition, visualization. A.I.: conceptualization, methodology, formal analysis, writing—original draft, writing—review and editing. J.P.L.: conceptualization, writing—review and editing.

Competing interests

The authors declare no competing interests.

Additional information

Correspondence and requests for materials should be addressed to A.I.

Reprints and permissions information is available at www.nature.com/reprints.

Publisher's note Springer Nature remains neutral with regard to jurisdictional claims in published maps and institutional affiliations.

[D3] M. Skorupska, A. Ilnicka, J. P. Łukaszewicz, *The effect of nitrogen species on the catalytic properties of N-doped graphene*, Scientific Reports, 2021, 11(1), 1-11; https://doi.org/10.1038/s41598-021-03403-8 (IF=4.6, MEiN=140)

Praca przedstawia wyniki badań opartych na zastosowaniu węglanu wapnia jako templatu przyczyniającego się do zwiększenia pola powierzchni właściwej oraz umożliwiającego sterowanie rozmiarem porów w otrzymanych materiałach węglowych. Pomimo mało znaczących zmian w porowatości otrzymanych materiałów, stwierdzono, że zastosowanie $CaCO_3$ miało wpływ na powstanie pustych przestrzeni, co w konsekwencji wpłynęło na polepszenie dostępności dla nośnika azotu i jego zawieszenie w całej masie. Zastosowany azodikarbonamid (ADC) jest skutecznie działającym substratem przyczyniającym się do wprowadzenia w strukturę węglową atomów azotu w formie dwóch określonych grup funkcyjnych N-5 i N-6. Nowatorstwo tej pracy polegało na wykazaniu, że sumaryczna wysoka zawartość azotowych grup funkcyjnych N-5 i N-6 w stosunku do całkowitej zawartości azotu, była istotna dla przebiegu reakcji ORR. Przeprowadzone testy elektrochemiczne potwierdziły aktywność otrzymanych materiałów w reakcji redukcji tlenu, co świadczy o możliwości potencjalnego wykorzystania nowych materiałów elektrodowych w urządzeniach do magazynowania i konwersji energii. Zaproponowana metoda syntezy poprzez wprowadzenie taniego nośnika azotu, a także zastosowanie odpowiednich temperatur karbonizacji przyczyniła się do otrzymania materiałów wykazujących czteroelektronową redukcję tlenu, wynik porównywalny do komercyjnego materiału Pt/C. Główną zaletą zaproponowanej metody jest zastosowanie tanich reagentów i skuteczne wprowadzenie heteroatomów azotu, a co za tym idzie otrzymania materiałów węglowych wykazujących czteroelektronową ścieżkę redukcji tlenu.

scientific reports

Check for updates

OPEN

The effect of nitrogen species on the catalytic properties of N-doped graphene

Malgorzata Skorupska[1], Anna Ilnicka[1]✉ & Jerzy P. Lukaszewicz[1,2]

The production of effective catalysts in the oxygen reduction reaction (ORR) continues to be a great challenge for scientists. A constant increase in demand for energy storage materials is followed by a proportionate increase in the number of reports on electrocatalyst synthesis. The scientific world focuses on environmentally friendly materials synthesized in accordance with the safest possible. In this work, we developed a facile method of obtaining heavy-metal-free electrode materials that are effective in ORR. Graphene-based catalysts were doped using azodicarbonamide (ADC) as the source of nitrogen, then carbonized at high temperatures in the range of 700–900 °C under inert gas flow. The produced materials were tested as catalysts for ORR, which is the most important reaction for Zn–air batteries and fuel cells. All obtained nitrogen-doped graphene foams showed increased catalytic activity in ORR owing to active sites created by nitrogen functional groups on the graphene surface. This paper shows that carbonization temperature has a significant impact on nitrogen content and that a small percentage of nitrogen may have a positive effect on the catalytic activity of the obtained materials. The number of transferred electrons in ORR was found to range from three to the maximal theoretical value, i.e., four.

Materials containing platinum are the best commercial electrocatalysts for the oxygen reduction reaction and serve as a paternal electrode material[1–3]; however, noble-metal-free electrode materials are an attractive alternative from an economical point of view and crucial for protecting the environment. Effective electrocatalysts in fuel cells[4,5], lithium–air batteries[6,7], and zinc–air batteries[8,9] should be active in the oxygen reduction reaction (ORR)[10–12], the key reaction in devices of this sort. Some very promising alternatives to noble-metal electrode materials are carbon materials doped with non-metal heteroatoms, e.g., phosphorus[13–15], boron[14,16] or nitrogen[14,17,18] inserted into the basic carbon structure, of which the most promising catalysts are those containing nitrogen functional groups[19–21], such as pyridine nitrogen (N-6) and pyrrole nitrogen (N-5). At the same time, very high concentrations of heteroatoms and a large amount of defects in the structure can contribute to a decrease in electronic conductivity and disadvantage the oxygen reduction reaction[22]. There are many nitrogen precursors that may be useful for synthesising N-doped carbon catalysts of high activity towards ORR, e.g., melamine[23,24], urea[23,25], adenine[23,26], arginine[23,27], or natural materials, such as green algae or gelatine[28,29]. We have demonstrated in our previous studies that such N-doped materials can be derived from amino acids[30], chitin, and chitosan[31,32], and provide high activity towards ORR. It has been shown that a large specific surface area, as well as a mesoporous structure, had a positive effect on ORR catalytic activity, this being due to good accessibility of catalytically active sites to the electrolyte and to the good charge transport provided by the carbon matrix. It was found that the influence of nitrogen content is not the key factor[18,33].

To our understanding, the key challenge of any work in the field of N-rich carbon electrode materials is finding a non-platinum material with the ability to perform a four-electron reduction of an oxygen molecule. This feature is essential for the entire concept of applying N-rich carbons in fuel cells and reversible batteries (ORR on cathodes) as a replacement of the traditional Pt-loaded electrode materials. Among dozens of cited works, and hundreds or thousands left uncited, the occurrence of a four-electron reaction mechanism can only be attributed to single reports. Thus, the real novelty of our research attempt consists of a successful demonstration of the manufacturing protocol being able to gradually lead to that unique target. Another innovation of this study is the application of non-oxidized graphene rather than the graphene oxide and/or reduced graphene oxide which are used in the dominant synthesis approach in existing studies. The application of pristine graphene instead of oxidized graphene derivatives saves time and manufacturing costs.

[1]Faculty of Chemistry, Nicolaus Copernicus University in Torun, Gagarina 7, 87-100 Toruń, Poland. [2]Centre for Modern Interdisciplinary Technologies, Nicolaus Copernicus University in Torun, Wilenska 4, 87-100 Toruń, Poland. ✉email: ailnicka@umk.pl

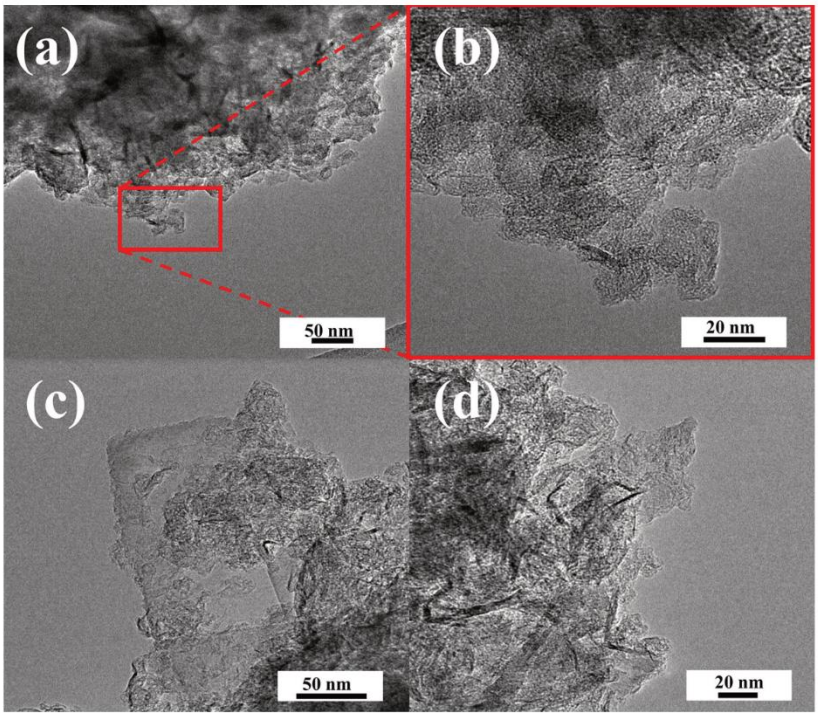

Figure 1. High-resolution transmission electron microscopy images of samples (**a**,**b**) 1-NGF-9, and (**c**,**d**) 2-NGF-9 at different magnifications.

In this paper, we continue the search for more effective non-metal ORR catalysts. It is our assumption that more efficient N-doping is achievable by means of more adequate N-precursors. In the current research, the influence of azodicarbonamide (ADC) and carbonization temperature on nitrogen content and ORR catalytic activity of nitrogen-doped graphene foam was investigated. Additionally, it was hypothesized that the general high nitrogen content is a not the sole steering parameter catalytic activity improvement, but that the type and concentration of pyridine nitrogen and pyrrolic nitrogen also plays a crucial role. Therefore, the content of such N-based functional groups was needs to be determined in context of and effective ORR process.

Results and discussion

Materials characterization. While the structure of all obtained nitrogen-doped graphene foams was characterized using high resolution transmission electron microscopy (HRTEM) images, data for one sample is presented in this paper as fully representative of all obtained results. Figure 1 shows the structure of samples obtained with different weight ratios of reagents (1-NGF-9 and 2-NGF-9) and carbonized at 900 °C.

It is clearly visible that the structure is wrinkled, consisting of many layers superimposed on one another. Other materials show a similar wrinkled, flattened, and irregular structure. Calcium carbonate is assumed to form mesopores 20 nm in size, but the structure collapses when washed with hydrochloric acid, taking the form of graphene nanoplatelets (GNPs).

Samples dispersed in ethanol were transferred to silicon wafers in order to study their surface structure and number of layers through the use of atomic force microscopy (AFM). Graphene sheets exhibit many contrasting regions that can be attributed to the layers of which they consist. When analyzing individual materials, all of them were found to exhibit many overlapping layers, which created a structured graphene material. The results are presented in Fig. 2. Results of Raman spectroscopy confirm that the obtained materials have many overlapping layers which are part of 3D structured graphene.

Elemental analysis was performed in order to investigate the obtained material's nitrogen content and the effect of carbonization temperature on the content of carbon, hydrogen, and nitrogen. This study is important to confirming a previous conclusion stating that the content of nitrogen is not the only factor influencing ORR

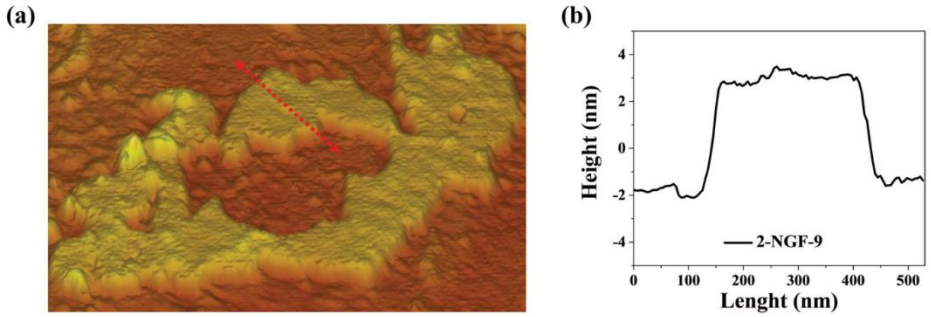

Figure 2. (**a**) AFM analysis highlighting the particular area, (**b**) height profile of marked area of 2-NGF-9.

Sample	Elemental content (wt%)			S_{BET} ($m^2 g^{-1}$)	V_t ($cm^3 g^{-1}$)	V_{mi} ($cm^3 g^{-1}$)	V_{me} ($cm^3 g^{-1}$)	I_D/I_G	I_{2D}/I_G
	C	H	N						
GNPs	87.32	0.90	0.72	750	0.99	0.13	0.86	0.64	0.40
1-NGF-7	86.25	1.77	1.83	635	0.82	0.12	0.70	0.95	0.34
1-NGF-8	83.71	0.94	2.35	620	0.76	0.14	0.62	0.83	0.43
1-NGF-9	92.94	0.72	1.02	657	0.84	0.12	0.72	0.81	0.37
2-NGF-7	82.31	1.86	3.01	640	0.80	0.13	0.67	0.68	0.39
2-NGF-8	87.60	0.95	3.18	533	0.74	0.11	0.63	1.05	0.34
2-NGF-9	93.09	0.67	0.95	562	0.69	0.13	0.56	0.40	0.46

Table 1. Porosity parameters, nitrogen, hydrogen, and carbon content, and ratios of the intensities of G, D, and 2D-bands from the Raman spectra of 1-NGF-T and 2-NGF-T series.

catalytic activity. The individual samples' weight percentages of carbon, nitrogen, and hydrogen are presented in Table 1. The percentage of carbon was in a range of 82 to 93 wt% for all samples. For the 2-NGF-T series, increasing carbonization temperature is directly proportional to increasing carbon content, which indicates an improvement in the materials' degree of graphitization. This trend is only in part maintained in the 1-NGF-T series, where the percentage was 86.25 wt% for a carbonization temperature of 700 °C, then decreased to 83.71 wt% for a carbonization temperature of 800 °C, and then increased to 92.94 wt% for 900 °C.

The percentage of nitrogen is influenced not only by the type of precursor used, but by the carbonization temperature as well. For the series 1-NGF-T and 2-NGF-T, the highest nitrogen content was recorded for a carbonization temperature of 800 °C, in the amount of 2.35 wt% and 3.18 wt%, respectively. For the other samples from the 1-NGF-T series, carbonized at 700 °C and 900 °C, the percentage of nitrogen content was 1.83 wt% and 1.02 wt%, respectively. For samples from the 2-NGF-T series, carbonized at the two extreme temperatures of 700 °C and 900 °C, this content was at the level of 3.01 wt% and 0.95 wt%, respectively.

In order to test the porosity of the samples and determine pore volume, a nitrogen adsorption–desorption analysis was performed. Figure 3a,c summarize the isotherms for all materials obtained and compare them to the GNPs to identify significant differences. According to the IUPAC classification[34], all samples show the character of a type II isotherm, with a slightly pronounced hysteresis loop. The obtained materials did not show significant differences in relation to the GNPs, which suggests that the graphene structure remained stable after the synthesis process. A Brunauer–Emmett–Teller (BET) analysis of the 1-NGF-T series shows that the specific surface areas for the 1-NGF-7, 1-NGF-8, 1-NGF-9 samples was 635 $m^2 g^{-1}$, 620 $m^2 g^{-1}$, and 657 $m^2 g^{-1}$, respectively. The tested materials, 2-NGF-7, 2-NGF 8, 2-NGF-9, showed specific surface areas of 640 $m^2 g^{-1}$, 533 $m^2 g^{-1}$, and 562 $m^2 g^{-1}$, respectively. Thus, a slightly worse decrease in structural parameters (specific surface area and pore volume) was present for N-doped samples compared to the main carbon precursor (non-modified), i.e., graphene nanoplatelets (GNP).

In the second series, where the ADC was used in excess, a decrease in the specific surface area was observed with the increase in carbonization temperature, which could cause the graphene structure to collapse due to gases released in the carbonization process. Pore size distribution was determined based on the two-dimensional-non-localized density function theory (2D-NLDFT) method and is shown in Fig. 3b for the 1-NGF-T series and Fig. 3d for the 2-NGF-T series. For all the materials obtained, there were no significant changes in the pore size relative to the GNPs, showing micro and small mesopores. The lack of significant differences in the porous structure proves the strength of the material. The total pore volume (V_t) for all materials obtained from

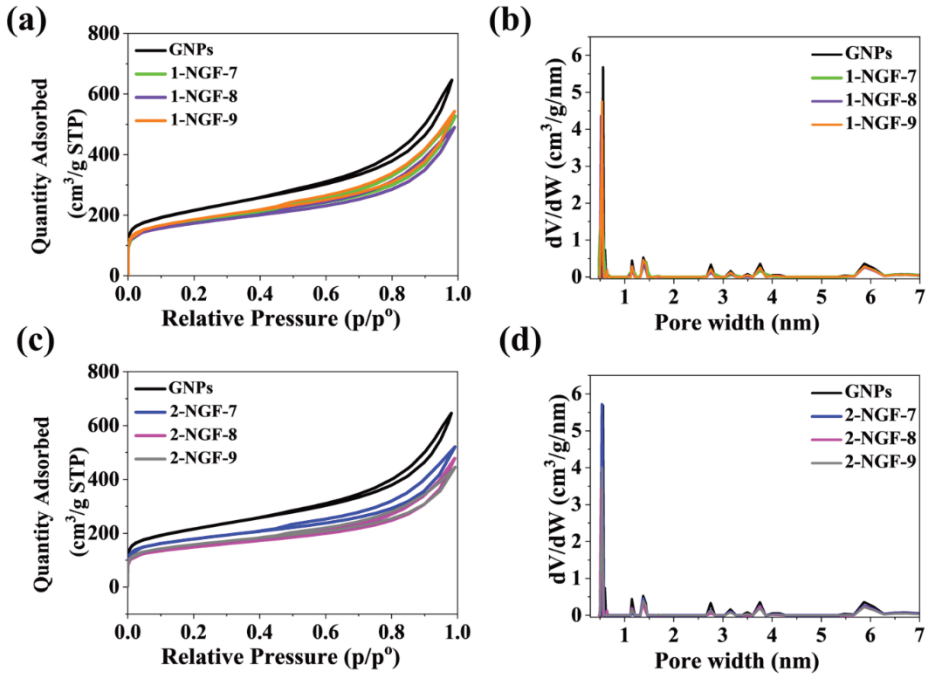

Figure 3. Nitrogen adsorption–desorption isotherms and NLDFT pore size distribution of samples in series (**a**,**b**) 1-NGF-T and (**c**,**d**) 2-NGF-T compared with GNPs.

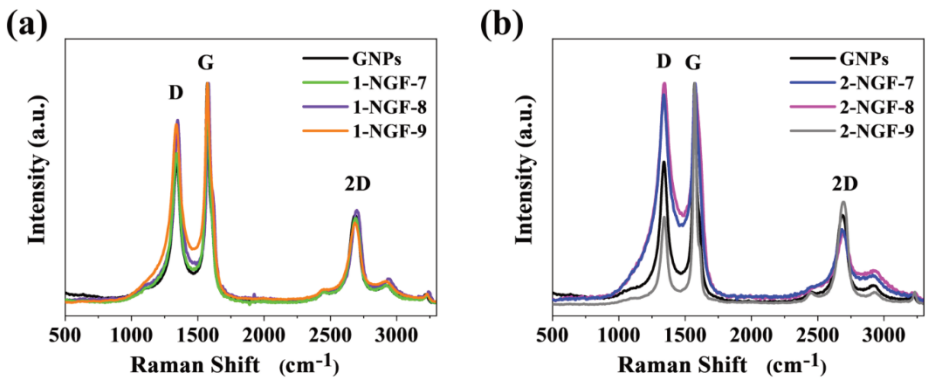

Figure 4. Raman spectra of samples in series (**a**) 1-NGF-T and (**b**) 2-NGF-T, compared with GNPs.

both series did not exceed 1 $cm^3\ g^{-1}$. Other parameters, such as micropore volume and mesopore volume, are presented in Table 1.

The quality of the graphene-based materials obtained and the degree of graphene layers/sheets association can be estimated using Raman spectroscopy (Fig. 4). All materials' spectra contain three visible bands, D, G, and 2D, characteristic for graphene; the paternal Raman shifts for ideal graphene (for the 532 nm laser) are 1350 cm^{-1}

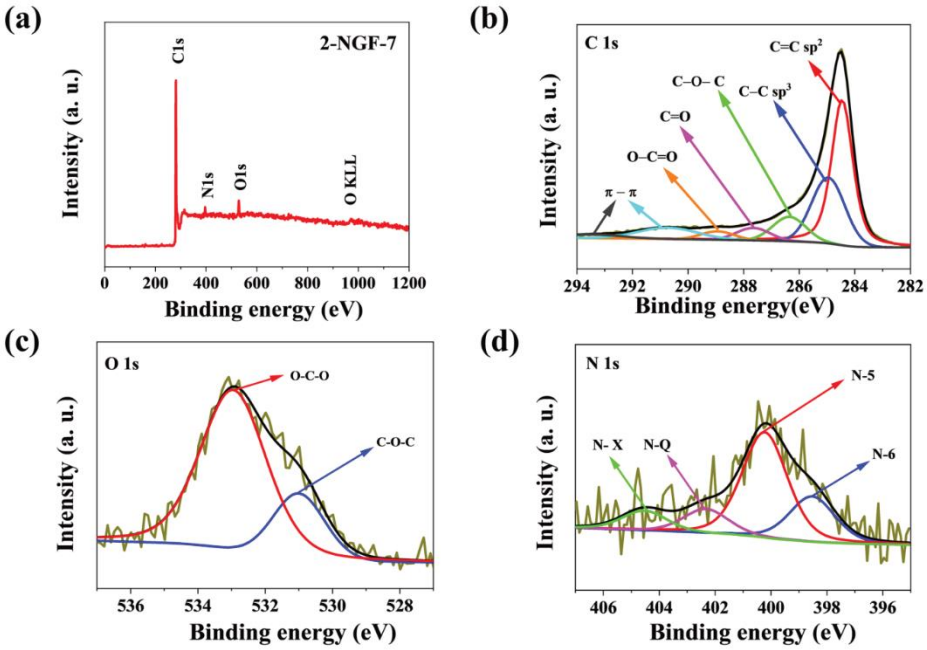

Figure 5. (**a**) The XPS survey spectrum and high resolution XPS spectra of (**b**) C1s, (**c**) O1s, and (**d**) N1s for the 2-NGF-7 sample.

for the D band, 1600 cm^{-1} for the G band, and 2700 cm^{-1} for the 2D band[35]. Raman spectra in Fig. 4a show the 1-NGF-T series compared to GNP's spectrum. As is visible, the spectra overlap and there appear to be no particular changes with reference to the GNPs. The 2-NGF-T series is presented with reference material for GNPs in Fig. 4b. An increase in the D band intensity was observed for samples 2-NGF-7 and 2-NGF-8, which indicates that the introduced heteroatom content caused a defective structure. However, the intensity of the 2D band decreases with the increase of D band intensity. In the case of the 2-NGF-9 sample, the situation is completely different. The intensity of the 2D band increases concurrently with the D band. This indicates a qualitatively better material, with fewer defects and overlapping layers. The higher ratio of the intensity of the 2D and G bands in this sample, 0.46, proves that the material consists of many overlapping layers. Detailed parameters for the intensity and intensity ratios of D to G and 2D to G for all materials, as well as the GNPs, have been normalized and are presented in Table 1. All materials show a high degree of graphitization.

As mentioned previously, the total nitrogen content is not the only factor influencing catalytic activity. The number of nitrogen functional groups on the edges of defective graphene structures is important. XPS measurements were made for a more in-depth analysis, which made it possible to determine the exact content of functional groups on the materials' surfaces (Fig. 5a). We used azodicarbonamide as the nitrogen precursor, responsible for generating appropriate functional groups for ORR. Figure 5b–d show high-resolution XPS spectra for the 2-NGF-7 sample, which were characterized by three main elements: carbon, nitrogen, and oxygen.

All of obtained samples exhibit a similar structural content of carbon and oxygen atoms and the exact elemental composition of the respective nitrogen function groups is presented in Table 2. The C1s spectra for all samples consist of five types of bonds, located at 284.4 eV, 284.9 eV, 286.2 eV, 287.5 eV, 288.6 eV and corresponding to bonds of type C=C (sp^2), C–C (sp^3), C–O–C and/or C–NH, C=O (C-3), O–C–O, respectively[36]. Excitation of the shake-up type confirms the presence of C=C (sp^2) bonds, related to aromatic forms, which appear at binding energies of 290.1 eV and 293.4 eV[36]. Based on the deconvolution of the N1s spectrum, it is possible to identify four peaks, characterized by bond energies at the values of 398.5 eV, 400.2 eV, and 402.3 eV, and 404.5 eV corresponding to the pyridine-nitrogen (N-6), pyrrolic-nitrogen (N-5), and graphitic-nitrogen (N-Q) groups, and N-oxides of pyridinic nitrogen (N-X), respectively[37]. The identified types of nitrogen functional groups should positively affect the catalytic properties of N-doped graphene foams for the oxygen reduction reaction. The content of N-5 and N-6 groups as a percentage of total N are shown in Table 2. Deconvolution of the O1s spectrum shows two types of oxygen bonds, at binding energies of 530.7 eV and 532.8 eV, corresponding to O*=C–O and/or O–C–O and O=C–O* and/or C–O–C, respectively[36,38].

Sample	Total C (at.%)	Total O (at.%)	Total N (at.%)	Nitrogen functional group (at. %)				(N-5) and (N-6) (% relative to total N)
				N-6	N-5	N-Q	N-X	
1-NGF-7	94.1	3.9	2.1	0.2	1.3	0.3	0.3	71
1-NGF-8	93.5	4.1	2.2	0.4	1.5	0.2	0.1	86
1-NGF-9	95.0	3.7	1.0	0.1	0.8	0.0	0.1	90
2-NGF-7	93.4	3.9	2.7	0.7	1.5	0.3	0.2	81
2-NGF-8	94.6	3.1	1.9	0.5	1.2	0.1	0.1	89
2-NGF-9	94.7	4.2	0.7	0.2	0.5	0.0	0.0	100

Table 2. Elemental composition of N-doped graphene foams determined by XPS analysis.

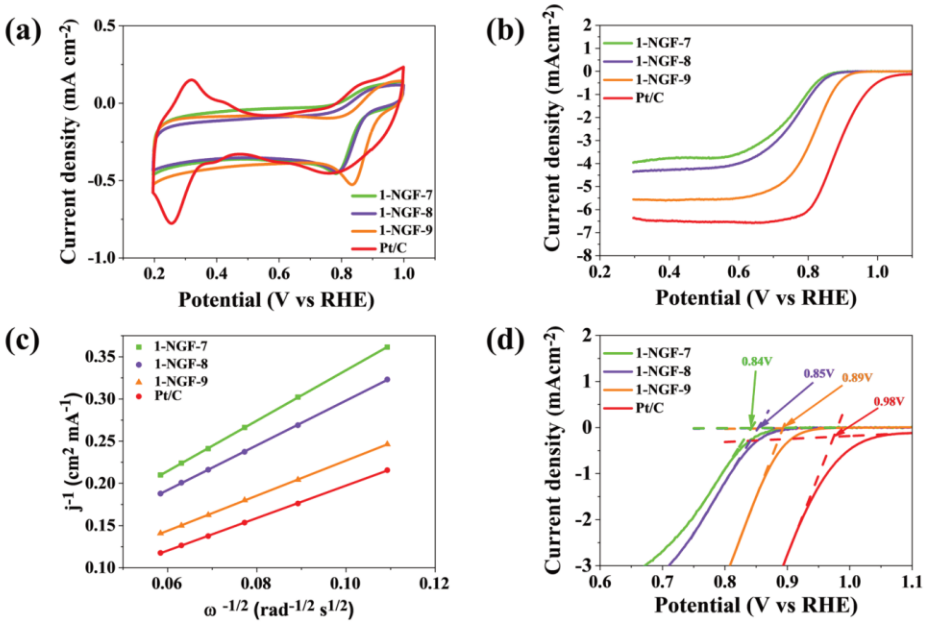

Figure 6. The results of electrochemical performance for 1-NGF-T and Pt/C in saturated-O_2 0.1 mol L^{-1} KOH (**a**) CV plots with a scan rate of 10 mV s^{-1}. (**b**) LSV plots with a scan rate of 5 mV s^{-1} and rotation speed of 1600 rpm, (**c**) Koutecky–Levich plots at 0.5 V vs RHE, (**d**) onset potential for samples in the 1-NGF-T series.

Electrochemical performance. Electrochemical tests were used order to determine the application potential of the obtained nitrogen-doped graphene foams. Materials were tested as electrocatalysts for ORR to assess whether any given one is suitable for use in electrical devices, such as zinc–air batteries or fuel cells. Electrochemical methods, cyclic voltammetry (CV) and linear voltammetry (LSV), were used, then the obtained results were compared with the commercial Pt/C material. The four-electron oxygen reduction reaction is the most desirable path and allows the effective operation of devices based on ORR. Tests were carried out in an oxygen-saturated alkaline electrolyte. The obtained CV and LSV results are shown in Fig. 6 (series 1-NGF-T) and Fig. 7 (2-NGF-T series). The number of electrons transferred in ORR was calculated from the K–L equations and presented as a function of current density (j^{-1}) at a spin speed ω of 0.5 V vs RHE (Fig. 6c). All materials showed increased catalytic activity, as can be observed in the CV voltammograms; detailed data are presented in Table 3. Analysis of the first series, 1-NGF-T, indicates that the sample carbonized at 900 °C (1-NGF-9) was the most effective in ORR. The cathode peak (Fig. 6a) shifted from the more positive values was at 0.83 V vs reversible hydrogen electrode (RHE). Linear voltammetry at 1600 rpm and a scan rate of 0.005 mV s^{-1} (Fig. 6b,d) shows an onset potential of 0.89 V vs RHE. The shape of the LSV curve for 1-NGF-9 is very close to that of the commercial Pt/C catalyst and shows a high diffusion-limiting current of 5.30 mA cm^{-2}. The remaining materials

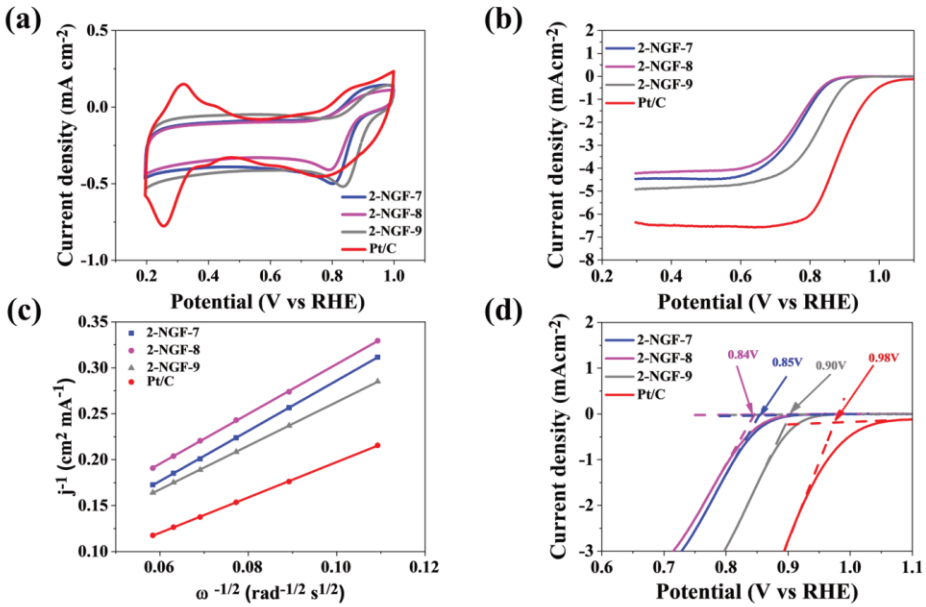

Figure 7. The results of electrochemical performance for 2-NGF-T compared with Pt/C in saturated-O_2 0.1 mol L^{-1} KOH (**a**) CV plots with a scan rate of 10 mV s^{-1}, (**b**) LSV plots with a scan rate 5 mV s^{-1} and rotation speed of 1600 rpm, (**c**) K–L plots at 0.5 V vs RHE, (**d**) onset potential for samples in 2-NGF-T series.

Catalyst	E_p (V vs RHE)	E_{onset} (V vs RHE)	$E_{1/2}$ (V vs RHE)	Diffusion-limiting current (mA cm^{-2})	n (0.5 V)
Pt/C	0.76	0.98	0.88	6.37	4.00
1-NGF-7	0.78	0.84	0.75	3.80	3.04
1-NGF-8	0.79	0.85	0.76	4.16	3.43
1-NGF-9	0.83	0.89	0.82	5.30	4.00
2-NGF-7	0.80	0.85	0.76	4.50	3.32
2-NGF-8	0.79	0.84	0.76	4.06	3.35
2-NGF-9	0.83	0.90	0.82	4.70	3.82

Table 3. ORR performance parameters of obtained N-doped graphene foams compared to commercial Pt/C catalyst, tested in 0.1 mol L^{-1} KOH.

from the 1-NGF-T series had lower catalytic activity compared to sample 1-NGF-9, carbonized at 900 °C, which exhibited a four-electron oxygen reduction reaction. The highest catalytic activity in relation to the remaining materials stems from two factors. One of them is the extensive structure of mesopores (0.72 cm^3 g^{-1}, higher than in all others), which further enhances the availability of the electrolyte and thus facilitates the diffusion of electrons in ORR. The other condition that this sample accomplished is the percentage share of N-5 and N-6 groups in the total nitrogen content, as follows from the XPS analysis, which has a beneficial effect on the oxygen reduction reaction[39].

The number of transferred electrons for samples 1-NGF-7 and 1-NGF-8 was 3.04 and 3.43, respectively (Fig. 8). The pyridine and pyrrole functional groups, despite their low content located at the edges, react with hydroxyl groups derived from alkaline forms of the electrolyte, creating an active site at the same time. The 2-NGF-T series also showed increased catalytic activity in ORR, as indicated by the CV curves in Fig. 7a, where there are clearly visible cathode peaks for materials carbonized at 700 °C, 800 °C, and 900 °C, shifted relative to the positive values and amounting to 0.81, 0.79, and 0.83 V vs RHE, respectively. The material carbonized at 700 °C showed a very high current density in CV measurements compared to other samples in this series. Similar values of the initial potential and the diffusion-limiting current indicate little differentiation of the

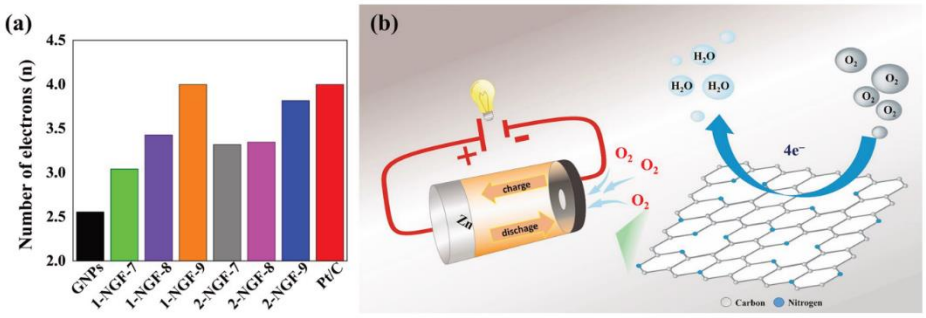

Figure 8. (**a**) The number of transferred electrons in the 1-NGF-T and 2-NGF-T series compared to the commercial catalyst Pt/C and GNPs. (**b**) The schematic diagram of the four-electron oxygen reduction reaction crucial for rechargeable zinc–air battery.

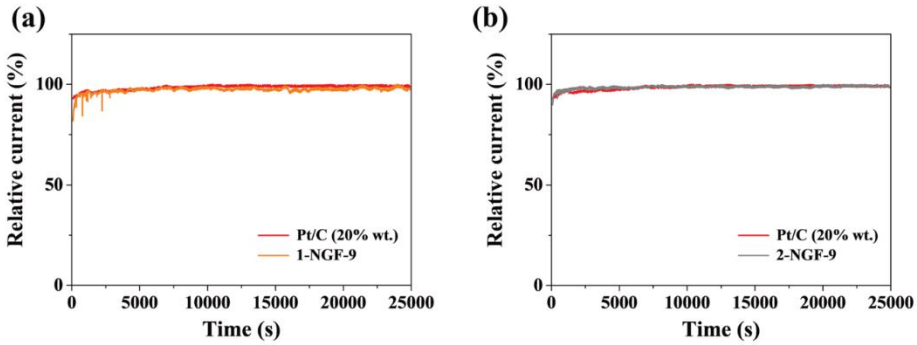

Figure 9. Chronoamperometric responses of (**a**) 1-NGF-9 and (**b**) 2-NGF-9 compared to a Pt/C electrode in O_2-saturated 0.1 M KOH solution at 0.5 V vs RHE.

material, however, they show catalytic activity in relation to the GNPs, with their transferred-electron numbers were 3.32, 3.35, and 3.82 for the 2-NGF-7, 2-NGF-8, and 2-NGF-9 samples, respectively. The high increase in catalytic activity of the obtained materials as compared to the GNPs is due to active functional groups deposited on the edges of the graphene sheets. These kinds of nitrogen groups strongly influence the oxygen reduction reaction[40,41] mechanism. The catalytic activity of 1-NGF-9 and 2-NGF-9 samples can be explained based on the paper by Guo et al., where the authors suggest that pyridinic nitrogen determines electrocatalytic activity[41]. The authors describe that the Lewis base carbon atoms neighboring pyridinic nitrogen, not pyridinic nitrogen itself, are electrocatalytic ORR centers in N-doped carbon materials. Furthermore, pyrrolic nitrogen species are responsible for ORR performance in an alkaline medium[42,43]. Therefore, the combined effect of these two groups (pyridinic nitrogen and pyrrolic nitrogen) in samples 1-NGF-9 and 2-NGF-9, with the highest concentration (N-6 and N-5) of the total nitrogen content (90% and 100%), is related to the highest number of transferred electrons.

Figure 8a summarizes the number of transferred electrons in the oxygen reduction reaction of the obtained materials, the GNPs, and Pt/C. All materials obtained with the proposed method showed catalytic activity. The four-electron oxygen reduction reaction (Fig. 8b) is facilitated by the quality of nitrogen groups, not the percentage of nitrogen, which affects the rapid reaction kinetics at the edges of multilayer graphene. Our results support the notion that the total nitrogen percentage is not directly proportional to catalytic activity[44] and obtained materials are promising electrocatalysts for zinc–air battery.

From an economic point of view, it is important for the production of energy storage devices and metal-air batteries to obtain materials with comparable stability to the commercial platinum-based materials. The stability of materials in the oxygen reduction reaction is one of the most important parameters when evaluating them for potential applications and making attempts to eliminate heavy metals from commercial materials. Chronopotentiometry tests were carried out to estimate the durability of the 1-NGF-9 (Fig. 9a), 2-NGF-9 (Fig. 9b), and

Pt/C electrodes. After a long test of 25,000 s, all samples still remained at a high current stability compared to commercial Pt/C.

Materials and methods

Sample preparation. To prepare nitrogen-doped graphene foams, first carrageenan (1 g) was dissolved in deionized water (30 ml). Then, graphene nanoplatelets (1 g) were mixed with calcium carbonate (1 g) nanoparticles (average particle size 15–40 nm) and dispersed in the carrageenan solution. Lastly, azodicarbonamide (1 g) used as a nitrogen source. Pore-forming material was also added to the obtained solution. This was then mixed for 30 min on a magnetic stirrer, and after this time, the samples were lyophilized for 24 h. The obtained dry mass was carbonized at 700 °C, 800 °C, or 900 °C under the flow of inert gas N_2 at a heating rate of 10 °C min^{-1} and kept at the maximal temperature for 1 h. Since the melting point of ADC is 225 °C, this component was completely removed from the sample during the high-temperature carbonization process. Samples were treated with concentrated HCl (36–38%) for 20 min to remove calcium carbonate and washed with distilled water to the point of neutral pH. The resultant products were denoted as 1-NGF-T and 2-NGF-T, where: 1 and 2 describe the mass ratio of reagents $CaCO_3$:ADC of 2:1 and 1:2, respectively; NGF stands for nitrogen-doped graphene foam; T is the carbonization temperature of 700 °C, 800 °C, and 900 °C, indicated by 7, 8, and 9, respectively.

Physicochemical characterization. A high-resolution transmission electron microscope (HRTEM FEI Tecnai F20 X-Twin, Brno, the Czech Republic) was used to observe the structure of the samples at an accelerating voltage of 200 kV. Raman spectra were obtained using 532 nm laser excitation (microscope InVia Renishaw, Renishaw Company, Gloucestershire, Great Britain). The specific surface area and pore size distribution were ascertained from adsorption and desorption isotherms measured at 77 K by means of an automatic volumetric analyzer (ASAP 2020 Plus, Micromeritics, Norcross, USA). The Brunauer–Emmett–Teller (BET) method was used to determine the specific surface area (S_{BET}). The pore size distribution was calculated using the two-dimensional-non-localized density functional theory method. The single-point total pore volume (V_t) for the obtained materials was measured at the maximum relative pressure of p/p_o. The micropore volume (V_{mi}) was determined using the t-Plot method, while the mespopore volume (V_{me}) was calculated by subtracting V_{mi} from V_t. Information about the elemental composition (carbon, nitrogen and hydrogen) of the nitrogen-doped graphene foams was collected using elemental combustion analysis (Vario MACRO CHN, Elementar Analysensysteme GmbH, Germany). The atoms' chemical state was identified through X-ray photoelectron spectroscopy (XPS) measurements with a VG Scientific ESCALAB-210 (Japan), photoelectron spectrometer with Al Ka radiation (1486.6 eV). Using the Scanning Probe Microscope (SPM) by Veeco (Digital Instrument, USA), the obtained materials were tested in order to determine the values of graphene thickness using atomic force microscopy.

Electrochemical measurements. In order to determine the electrochemical properties of the obtained nitrogen-doped graphene foams, their electrochemical activity was assessed using a rotating disc electrode (RDE) on an Autolab electrochemical analyzer (PGSTAT128N, the Netherlands). In the conventional three-electrode system, the obtained carbon material on a glassy carbon electrode (GCE with a diameter of 3 mm) was used as a working electrode, Ag/AgCl in 3 mol L^{-1} KCl was used as the reference electrode, a platinum wire was used as the counter electrode, and an aqueous solution of 0.1 mol L^{-1} KOH was used as the electrolyte. Platinum-based commercial carbon, Pt/C (20 wt% of Pt), was used as a reference catalyst. The preparation of ink is based on mixing 2.5 mg of the catalyst and its dispersion in 0.55 ml of a mixture of distilled water, ethanol, and Nafion (0.5 wt% of Nafion) for 60 min. The prepared ink was applied to a glassy carbon electrode previously polished by a diamond and alumina polishing pad. Cyclic voltammetry (CV) and linear sweep voltammetry (LSV) measurements were carried out to determine oxygen reduction reaction activity in the obtained nitrogen-doped foams. The CV curves were measured at a scan speed of 10 mV s^{-1}, while the LSV curves were measured at 5 mV s^{-1} and with a rotation speed of 1600 rpm. The 0.1 mol L^{-1} KOH electrolyte solution was saturated with oxygen and nitrogen before CV and LSV measurement. The number of electrons (n) was calculated from the Koutecky–Levich (K–L) equation, based on a full LSV measurement at 0.5 V vs reversible hydrogen electrode (RHE):

$$J^{-1} = {J_L}^{-1} + {J_K}^{-1} = \left(B\omega^{1/2}\right)^{-1} + {J_K}^{-1} \quad (1)$$

$$B = 0.62nFC_0(D_0)^{2/3}\nu^{-1/6} \quad (2)$$

where: J is assigned to the measured current density, J_L is defined as the current density limiting diffusion, and J_K is the kinetic current density; ω is the angular velocity of the electrode; n is the number of direct electrons involved in the reaction; F indicates Faraday's constant (96,485 C mol^{-1}); C_0 denotes the dissolved oxygen concentration and is equal $1.2 * 10^{-6}$ mol L^{-1} in 0.1 mol L^{-1} KOH; D_0 is equal to the diffusion coefficient of dissolved oxygen, $1.9 * 10^{-5}$ cm^2 s^{-1} in 0.1 mol L^{-1} KOH; ν for 0.1 mol L^{-1} KOH is 0.01 cm^2 s^{-1} and is defined as the kinetic viscosity of the electrolyte. A determination of the number n is possible when both equations are used to calculate the slope of the K–L curve.

Conclusions

In conclusion, the obtained nitrogen-doped graphene foams are environmentally friendly, metal-free electrocatalysts with properties comparable to a Pt-based catalyst. The azodicarbonamide used here is an effective precursor of nitrogen atoms, especially N-5 and N-6 groups. The total content of nitrogen functions N-5 and N-6, which in all samples were significant for ORR, was above 82%. The best electrochemical performance was exhibited

by the 1-NGF-9 and 2-NGF-9 samples, carbonized at 900 °C, showing a four-electron oxygen reduction in an alkaline medium despite the lowest nitrogen content. The materials produced here can be successfully used as electrode components in metal–air batteries or fuel cells as some of them are capable of a four-electron reduction of oxygen molecules, with this feature remaining constant in conditions simulating repeatable usage of a zinc–air battery. Further research on surface area development or the introduction of dual heteroatom doping into the graphene structure may expand these materials' range of applications beyond electrode materials for batteries and into supercapacitors or photovoltaic systems.

Received: 19 August 2021; Accepted: 2 December 2021
Published online: 14 December 2021

References

1. Shao, M., Chang, Q., Dodelet, J.-P. & Chenitz, R. Recent advances in electrocatalysts for oxygen reduction reaction. *Chem. Rev.* **116**, 3594–3657 (2016).
2. Yu, X. & Ye, S. Recent advances in activity and durability enhancement of Pt/C catalytic cathode in PEMFC: Part I. Physico-chemical and electronic interaction between Pt and carbon support, and activity enhancement of Pt/C catalyst. *J. Power Sources* **172**, 133–144 (2007).
3. Wu, D., Shen, X., Pan, Y., Yao, L. & Peng, Z. Platinum alloy catalysts for oxygen reduction reaction: Advances, challenges and perspectives. *ChemNanoMat* **6**, 32–41 (2020).
4. Abdelkareem, M. A. *et al.* Transition metal carbides and nitrides as oxygen reduction reaction catalyst or catalyst support in proton exchange membrane fuel cells (PEMFCs). *Int. J. Hydrogen Energy.* **46**, 23529–23547 (2020).
5. Sciarria, T. P. *et al.* Metal-free activated biochar as an oxygen reduction reaction catalyst in single chamber microbial fuel cells. *J. Power Sources* **462**, 228183 (2020).
6. Kang, J.-H. *et al.* Lithium–air batteries: Air-breathing challenges and perspective. *ACS Nano* **14**, 14549–14578 (2020).
7. Chen, K., Yang, D.-Y., Huang, G. & Zhang, X.-B. Lithium–air batteries: Air-electrochemistry and anode stabilization. *Acc. Chem. Res.* **54**, 632–641 (2021).
8. Yi, S. *et al.* Insights into kmno4 etched n-rich carbon nanotubes as advanced electrocatalysts for zn-air batteries. *Appl. Catal. B Environ.* **264**, 118537 (2020).
9. Zheng, X. *et al.* N-, P-, and S-doped graphene-like carbon catalysts derived from onium salts with enhanced oxygen chemisorption for Zn-air battery cathodes. *Appl. Catal. B* **241**, 442–451 (2019).
10. Niu, W. *et al.* Mesoporous N-doped carbons prepared with thermally removable nanoparticle templates: An efficient electrocatalyst for oxygen reduction reaction. *J. Am. Chem. Soc.* **137**, 5555–5562 (2015).
11. Xue, Q. *et al.* 3D nitrogen-doped graphene aerogels as efficient electrocatalyst for the oxygen reduction reaction. *Carbon* **139**, 137–144 (2018).
12. Liao, Y. *et al.* Facile fabrication of N-doped graphene as efficient electrocatalyst for oxygen reduction reaction. *ACS Appl. Mater. Interfaces.* **7**, 19619–19625 (2015).
13. Yang, N., Zheng, X., Li, L., Li, J. & Wei, Z. Influence of phosphorus configuration on electronic structure and oxygen reduction reactions of phosphorus-doped graphene. *J. Phys. Chem. C* **121**, 19321–19328 (2017).
14. Dong, F., Cai, Y., Liu, C., Liu, J. & Qiao, J. Heteroatom (B, N and P) doped porous graphene foams for efficient oxygen reduction reaction electrocatalysis. *Int. J. Hydrogen Energy* **43**, 12661–12670 (2018).
15. Bai, X. *et al.* Theoretical insights on the reaction pathways for oxygen reduction reaction on phosphorus doped graphene. *Carbon* **105**, 214–223 (2016).
16. Cao, H., Cao, J., Wang, F., Zhu, H. & Pu, M. A mesoporous carbon-based catalyst derived from cobalt and boron co-doped melamine formaldehyde gel for oxygen reduction reaction. *Electrochim. Acta* **333**, 135560 (2020).
17. Guo, J. *et al.* Graphitic-N-rich N-doped graphene as a high performance catalyst for oxygen reduction reaction in alkaline solution. *Int. J. Hydrogen Energy* **45**, 32402–32412 (2020).
18. Lemes, G., Sebastián, D., Pastor, E. & Lázaro, M. J. N-doped graphene catalysts with high nitrogen concentration for the oxygen reduction reaction. *J. Power Sources* **438**, 227036 (2019).
19. Dorjgotov, A., Ok, J., Jeon, Y., Yoon, S.-H. & Shul, Y. G. Activity and active sites of nitrogen-doped carbon nanotubes for oxygen reduction reaction. *J. Appl. Electrochem.* **43**, 387–397 (2013).
20. Vazquez-Arenas, J. *et al.* Theoretical and experimental studies of highly active graphene nanosheets to determine catalytic nitrogen sites responsible for the oxygen reduction reaction in alkaline media. *J. Mater. Chem. A* **4**, 976–990 (2016).
21. Du, L. *et al.* Biomass-derived nonprecious metal catalysts for oxygen reduction reaction: The demand-oriented engineering of active sites and structures. *Carbon Energy* **2**, 561–581 (2020).
22. Zhao, H. *et al.* Carbon for the oxygen reduction reaction: A defect mechanism. *J. Mater. Chem. A* **3**, 11736–11739. https://doi.org/10.1039/C5TA02229K (2015).
23. Preuss, K., Siwoniku, A. M., Bucur, C. I. & Titirici, M. M. The influence of heteroatom dopants nitrogen, boron, sulfur, and phosphorus on carbon electrocatalysts for the oxygen reduction reaction. *ChemPlusChem* **84**, 457–464 (2019).
24. Kamedulski, P., Lukaszewicz, J. P., Witczak, L., Szroeder, P. & Ziolkowski, P. The importance of structural factors for the electrochemical performance of graphene/carbon nanotube/melamine powders towards the catalytic activity of oxygen reduction reaction. *Materials* **14**, 2448 (2021).
25. Ramezani, Z. & Dehghani, H. Effect of nitrogen and sulfur co-doping on the performance of electrochemical hydrogen storage of graphene. *Int. J. Hydrogen Energy* **44**, 13613–13622 (2019).
26. Xu, Y. *et al.* Improved oxygen reduction activity of carbon nanotubes and graphene through adenine functionalization. *RSC Adv.* **7**, 26722–26728 (2017).
27. Kim, D.-H. *et al.* The role of arginine as nitrogen doping and carbon source for enhanced oxygen reduction reaction. *Int. J. Hydrogen Energy* **43**, 1479–1488 (2018).
28. Ilnicka, A. *et al.* Green algae and gelatine derived nitrogen rich carbon as an outstanding competitor to Pt loaded carbon catalysts. *Sci. Rep.* **11**, 1–13 (2021).
29. Pongsendana, M., Trisunaryanti, W., Artanti, F. W. & Falah, I. I. Hydrocracking of waste lubricant into gasoline fraction over CoMo catalyst supported on mesoporous carbon from bovine bone gelatin. *Korean J. Chem. Eng.* **34**, 2591–2596 (2017).
30. Ilnicka, A., Kamedulski, P., Skorupska, M. & Lukaszewicz, J. P. Metal-free nitrogen-rich carbon foam derived from amino acids for the oxygen reduction reaction. *J. Mater. Sci.* **54**, 14859–14871 (2019).
31. Okuda, R. *et al.* Chemical activation of nitrogen-doped carbon derived from chitosan with $ZnCl_2$ to produce a high-performance gas diffusion-type oxygen electrode. *Electrochemistry*. **89**, 20-00121 (2020).
32. Ilnicka, A., Lukaszewicz, J. P., Shimanoe, K. & Yuasa, M. Urea treatment of nitrogen-doped carbon leads to enhanced performance for the oxygen reduction reaction. *J. Mater. Res.* **33**, 1612 (2018).

33. Zhan, Y. *et al.* The influence of nitrogen source and doping sequence on the electrocatalytic activity for oxygen reduction reaction of nitrogen doped carbon materials. *Int. J. Hydrogen Energy* **41**, 13493–13503 (2016).
34. Kruk, M. & Jaroniec, M. Gas adsorption characterization of ordered organic–inorganic nanocomposite materials. *Chem. Mater.* **13**, 3169–3183 (2001).
35. Malard, L., Pimenta, M. A., Dresselhaus, G. & Dresselhaus, M. Raman spectroscopy in graphene. *Phys. Rep.* **473**, 51–87 (2009).
36. Rouxhet, P. G. & Genet, M. J. XPS analysis of bio-organic systems. *Surf. Interface Anal.* **43**, 1453–1470 (2011).
37. Li, D. *et al.* Facile synthesis of nitrogen-doped graphene via low-temperature pyrolysis: The effects of precursors and annealing ambience on metal-free catalytic oxidation. *Carbon* **115**, 649–658 (2017).
38. Genet, M. J., Dupont-Gillain, C. C. & Rouxhet, P. G. XPS analysis of biosystems and biomaterials. *Med. Appl. Colloids* 177–307 (2008).
39. Luo, E., Xiao, M., Ge, J., Liu, C. & Xing, W. Selectively doping pyridinic and pyrrolic nitrogen into a 3D porous carbon matrix through template-induced edge engineering: Enhanced catalytic activity towards the oxygen reduction reaction. *J. Mater. Chem. A* **5**, 21709–21714 (2017).
40. Ma, R. *et al.* A review of oxygen reduction mechanisms for metal-free carbon-based electrocatalysts. *npj Comput. Mater.* **5**, 1–15 (2019).
41. Guo, D. *et al.* Active sites of nitrogen-doped carbon materials for oxygen reduction reaction clarified using model catalysts. *Science* **351**, 361–365 (2016).
42. Zheng, J. *et al.* High content of pyridinic-and pyrrolic-nitrogen-modified carbon nanotubes derived from blood biomass for the electrocatalysis of oxygen reduction reaction in alkaline medium. *Electrochim. Acta* **168**, 386–393 (2015).
43. Guo, C.-Z., Chen, C.-G. & Luo, Z.-L. A novel nitrogen-containing electrocatalyst for oxygen reduction reaction from blood protein pyrolysis. *J. Power Sources* **245**, 841–845. https://doi.org/10.1016/j.jpowsour.2013.07.037 (2014).
44. Nagaiah, T. C., Kundu, S., Bron, M., Muhler, M. & Schuhmann, W. Nitrogen-doped carbon nanotubes as a cathode catalyst for the oxygen reduction reaction in alkaline medium. *Electrochem. Commun.* **12**, 338–341 (2010).

Acknowledgements
This work was carried out as a result of the research project no 2019/35/N/ST5/02691, financed by the National Science Centre.

Author contributions
M.S.: conceptualization, methodology, formal analysis, investigation, writing—original draft, supervision, project administration, funding acquisition, visualization. A.I.: methodology, formal analysis, writing—original draft, writing—review and editing. J.P.L.: writing—review and editing.

Competing interests
The authors declare no competing interests.

Additional information
Correspondence and requests for materials should be addressed to A.I.

Reprints and permissions information is available at www.nature.com/reprints.

Publisher's note Springer Nature remains neutral with regard to jurisdictional claims in published maps and institutional affiliations.

[D4] M. Skorupska, A. Ilnicka, J. P. Łukaszewicz, *Modified graphene foam as a high-performance catalyst for oxygen reduction reaction*, RSC Advances, 2023, 13, 25437–25442, https://doi.org/10.1039/D3RA04203K (IF=4.036, MEiN=100)

Niniejsza praca badawcza dotyczyła otrzymania grafenowych elektrod piankowych zsyntetyzowanych z naturalnych polimerów – żelatyny i chitozanu tworząc jednocześnie porowatą, domieszkowaną azotem strukturę. Najlepszymi katalizatorami otrzymanymi tą metodą są materiały karbonizowane w temperaturze 800°C, które wykazują mechanizm czteroelektronowej redukcji tlenu w środowisku alkalicznym. Zastosowane temperatury karbonizacji (600–800°C) nie doprowadziły do rozpadu struktury porów i znacznej eliminacji azotu z matryc węglowych. Wprowadzenie grafenu wpłynęło korzystnie na poprawę przewodności elektrycznej otrzymanych katalizatorów testowanych w reakcji ORR. Ponadto nawet matryce węglowe otrzymane w niższej temperaturze (600°C) charakteryzowały się liczbą przenoszonych elektronów (n) wyższą niż 3 (3.16 i 3.19). Natomiast najwyższą liczbę przenoszonych elektronów wykazywały materiały karbonizowane w 800°C i 900°C wykazując mechanizm czteroelektronowej ścieżki redukcji tlenu porównywalny do komercyjnych materiałów węglowych na bazie platyny.

RSC Advances

PAPER

View Article Online
View Journal | View Issue

Cite this: *RSC Adv.*, 2023, **13**, 25437

Modified graphene foam as a high-performance catalyst for oxygen reduction reaction†

Malgorzata Skorupska, *[a] Anna Ilnicka [a] and Jerzy P. Lukaszewicz[ab]

Received 22nd June 2023
Accepted 21st August 2023

DOI: 10.1039/d3ra04203k

rsc.li/rsc-advances

Gelatine and chitosan were used as natural precursors for nitrogen-doping of the graphene foam structure, creating specific types of active sites. The quantitative and qualitative content of nitrogen groups in the carbon structure was determined, which, under the influence of high temperature, were incorporated and transformed into forms of functional groups favorable for electrochemical application. Electrochemical studies proved that the form of pyridine-N, pyrrole-N, and quaternary-N groups have favorable electrochemical properties in the oxygen reduction reaction comparable to commercial platinum-based electrode materials. Using these materials as electrodes in metal–air batteries or fuel cells may eliminate the use of noble metal-based electrodes.

Introduction

Presently, there is an urgent need to minimize environmental pollution and find sustainable technology for energy production, storage and conversion. All this is due to the growing industry, whose demand for energy is constantly increasing. Over the past few decades, energy storage devices have become the focus of much attention, fuelling rapid progress in the development of electrode materials for devices such as fuel cells and metal–air batteries. Researchers are continually improving current electrocatalysts to make them more environmentally friendly, improve their conductive properties, and efficiency by refining their electrochemical properties. Currently, commercially available electrocatalysts contain noble metals such as platinum, iridium, or ruthenium. Platinum has excellent oxygen reduction reaction (ORR) activity, but the disadvantages are its price and limited sources. From an economic and environmental point of view, noble metal-free electrocatalysts are a noteworthy alternative. The properties that such an electrocatalyst should have are good conductivity, a large specific surface area (SSA), and the absence of noble metals in the structure.[1,2] Graphene and the doping of heteroatoms of the graphene structure with elements such as nitrogen sulphur, boron or phosphorus play a good role in this respect.[3–7] When constructing new electrocatalysts, carbon materials can act directly in the oxygen reduction reaction *via* active sites in the structure, making them an effective energy carrier.[8] Various conductive natural and synthetic polymers are used to enhance the catalytic properties, expand the surface conductive properties or introduce heteroatoms into the structure. The polymeric matrix precursors involved in the synthesis of 3D hybrid materials to date include polymethylmethacrylate, sulfonated polystyrene, and poly(vinylpyrrolidone) beads,[9,10] polyurethane or polydimethylsiloxane,[11] polycaprolactone.[12] Poly(ethylene mine), polyaniline, and polypyrrole have been used as nitrogen precursors.[13,14] Natural polymers include cellulose,[15] starch,[16] wood[17] and also gelatine and chitosan.[18] These polymers are mainly used to improve the properties of carbon materials for biomedical applications. The degree of oxidation of polymers and their stability is very important in energy storage devices.[19] However, in the case of natural polymers, no use has been found for the synthesis of electrode materials for oxygen reduction reactions. The natural polymers are promising alternative to expensive carbon precursors and their use in combination with graphene, can give materials with advanced electrochemical properties.

Despite the observed progress in the synthesis of Pt-free ORR catalysts, some domains still need to be explored. In particular, the application of natural precursors is of interest. If properly selected, natural precursors may ensure the instant transfer of N atoms to carbon matrices upon carbonization of such precursors. If carbonized solely, some natural precursors are transformed into carbon matrices of relatively low electric conductivity unless the carbonization temperature exceeds 800–900 °C. On the other hand, high carbonization temperatures lead to the collapse of pores and diminishing structural parameters such as specific surface area and the total pore volume. In parallel, the N-content also decreases due to the release of volatile species that contain nitrogen at higher temperatures.

[a]*Faculty of Chemistry, Nicolaus Copernicus University in Torun, Gagarina 7, 87-100 Torun, Poland. E-mail: m.skorupska@doktorant.umk.pl*

[b]*Centre for Modern Interdisciplinary Technologies, Nicolaus Copernicus University in Torun, Wilenska 4, 87-100 Torun, Poland*

† Electronic supplementary information (ESI) available: Synthesis and characterization techniques data. Additional electrochemical data. See DOI: https://doi.org/10.1039/d3ra04203k

As mentioned in earlier literature reports, it is true that nitrogen doping increases defects in the structure of graphene, which can be observed by analyzing Raman spectroscopy. The intensity of the D-band indicates a defected structure of the material. As described in an earlier literature review[20] the interaction between nitrogen and the neighboring carbon is significant. The introduction of nitrogen into the sp^2 carbon structure alters the electronic properties of the carbon atoms due to the higher electronegativity of nitrogen. The activity is attributed to the different nitrogen functional groups and, as assumed, with increasing heat treatment temperature, N pyrrole transforms into N pyridine and N quaternary.[21,22] However, indirect factors such as the morphology of the carbon materials must also be taken into account. An appropriate correlation between surface area and oxygen availability and the content of the corresponding functional group can improve the catalytic properties. In the case of the research described in this manuscript, the calculated electron transfer value is indicative of a four-electron pathway which is influenced by a component of all the factors described above. In the present work, we attempt to resolve the problem caused by the mentioned contradictions. Graphene and widely available natural polymers gelatine and chitosan were used low-cost precursors to obtain N-doped graphene foams with porous structure. The effect of the carbonization temperature on the content of nitrogen functional groups and catalytic properties was investigated. The best oxygen reduction properties in the alkaline medium are exhibited in materials carbonized at 800 °C. Several instrumental analyses were performed for broad characterization. Among others, a high-resolution transmission electron microscope was used to determine the structure and morphology of the graphene foams. To the best of our knowledge, it is the first report on the aggregate use of graphene and natural polymers to obtain N-doped graphene foams for practical application in oxygen reduction reaction.

Materials and methods

The N-doped graphene foams were synthesized based on the synthesis stages presented in Scheme S1.† The commercial graphene nanoplatelets (GNPs) were used as the carbon source, and gelatine or chitosan was used as the nitrogen source and the medium for hydrogel formation. In the first series (1F), gelatine and Na_2CO_3 (16.9% w/v) were dissolved in 20 ml of distilled water, heated and stirred continuously to dissolve the reagents completely. The GNPs were added to the clear solution while stirring continuously and then left to stand until the next day. The ratio of gelatine to GNPs was 2.5 : 1. Then 0.5 g of instant yeast was added to the mixture and stirred, followed by 10 ml of perhydrol (30%). Yeast and perhydrol were used in the reaction to form the foamed structure. The yeast acted as a catalyst for the decomposition of perhydrol into water and oxygen, thus accelerating the decomposition process and keeping the oxygen molecules in a dense matrix. In the second series (2F), the chitosan material was prepared the same way as in series 1F except that a solution consisting of 10 ml H_2O/1 ml HCl was added to gel the chitosan. In both series, 1F and 2F samples were freeze-dried to remove water from the foam. After the freeze-drying process, the samples were carbonized in an N_2 atmosphere at 600, 700, 800, or 900 °C with a heating rate of 3 °C min^{-1} and a holding time of 1 hour. The samples obtained after the carbonization process were washed with hydrochloric acid to remove all unreacted substrates and then with distilled water to a neutral pH. They were dried at 110 °C in an electric dryer until completely dry. N-doped graphene foams synthesized with gelatine were denoted as 1F_*T*, where *T* is carbonization temperature 600 °C, 700 °C, 800 °C, 900 °C, respectively. The second series of N-doped graphene foams obtained with chitosan were denoted as 2F_*T*.

The materials were used for the synthesis and the synthesis scheme are described in the ESI.† A description of the techniques used to characterize the materials and electrochemical measurements are also described in the ESI.†

Results and discussion

Materials characterization

The morphology was investigated by high-resolution transmission electron microscopy (HRTEM) analysis. The HRTEM images at various magnifications show the resulting N-doped graphene foams presented in Fig. 1 and S1.†

For samples 1F_800 and 2F_800, a wrinkled structure is observed and also consisted of several overlapping individual graphene layers. The distance between individual graphene layers is within the range of literature data and is 0.35 nm.[23] Such an extended structure and uneven edges, is characteristic of N-doped graphene foams.

The elemental composition of carbon, nitrogen, and hydrogen is summarized in Table 1. For electrochemical application, nitrogen concentration, in particular, will play an important role in the oxygen reduction reaction; therefore, optimizing their concentration is essential.[24] Notably, it is possible to control the limiting current density and effectively use the heteroatoms incorporated into the structure to reduce the overpotential.[25,26] For the 1F_*T* series, the percentage of nitrogen content decreases from 6.39 wt% to 2.39 wt% with an increase in the carbonization temperature from 600 to 900 °C, respectively. The second series of 2F_*T* N-doped graphene foams showed the same trend with a decrease in nitrogen content from 5.72 wt% to 2.43 wt%. This is a typical trend for non-permanent nitrogen groups, which undergo a decomposition process at higher temperatures resulting in a decrease in the total nitrogen content of the materials obtained.[1] In the case

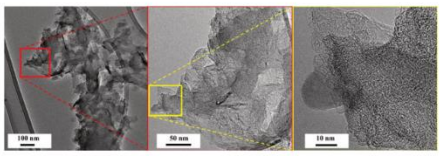

Fig. 1 High-resolution transmission electron microscopy images of 1F_800 sample at different magnifications.

Table 1 Elemental content of C, H and N elements determined by combustion analysis, porosity parameters, and intensity ratios of G, D, and 2D-bands from the Raman spectra of 1F_*T* and 2F_*T* series[a]

Sample	Elemental content (wt%)			S_{BET}	V_t	V_{mi}	V_{me}	I_D/I_G	I_{2D}/I_G
	C	H	N						
GNPs	87.32	0.90	0.72	750	0.99	0.13	0.86	0.64	0.40
1F_600	79.61	1.84	6.39	453	0.44	0.14	0.30	0.99	0.30
1F_700	83.54	1.63	3.93	768	0.64	0.22	0.42	1.01	0.27
1F_800	88.75	1.33	2.86	861	0.77	0.21	0.56	0.81	0.30
1F_900	96.07	0.97	2.39	795	0.77	0.17	0.61	0.90	0.32
2F_600	76.91	2.32	5.72	287	0.34	0.07	0.28	0.90	0.28
2F_700	78.74	1.41	5.16	648	0.51	0.18	0.32	0.99	0.27
2F_800	81.88	1.97	3.39	769	0.56	0.23	0.32	1.03	0.32
2F_900	93.65	0.93	2.43	941	0.64	0.29	0.35	0.94	0.25

[a] S_{BET} – (m^2 g^{-1}), V_t – (cm^3 g^{-1}), V_{mi} – (cm^3 g^{-1}), V_{me} – (cm^3 g^{-1}).

of the carbon content for 1F_*T* and 2F_*T* series, their concentration increase from 79.61 wt% to 96.07 wt% and 76.91 wt% to 93.65 wt% with the increase of carbonization temperature. This relationship is typical for carbonaceous materials as the number of carbon bonds increases with increasing temperature, causing an increase in the degree of graphitization.

The porosity of the obtained N-doped graphene foams was determined by sorption of nitrogen analysis. Fig. S2a and b† present adsorption–desorption isotherms of the materials obtained in 1F_*T* and 2F_*T* series and commercial GNPs. The shape of curves for the obtained samples are characteristic of type-II isotherm with a visible hysteresis loop according to the IUPAC classification.[27] The SSA was calculated by Brunauer–Emmett–Teller (BET) equation and compared with commercial graphene in Table 1. In the 1F_*T* series, the sample carbonised at 800 °C has the highest SSA, 861 m^2 g^{-1}. The specific surface area of samples 1F_600, 1F_700 and 1F_900 is 453 m^2 g^{-1}, 768 m^2 g^{-1} and 795 m^2 g^{-1}, respectively. The decrease in surface area for sample 1F_900 relative to 1F_800 may be due to the collapse of the structure during the intense release of gaseous thermal transformation products. Similar trend was observed for materials obtained from gelatine by Yang *et al.*[28] The 2F_*T* series showed a trend of increasing SSA with increasing carbonization temperature. The obtained material 2F_600 carbonized at 600 °C shows the lowest specific surface area of 287 m^2 g^{-1}. The 2F_900 sample carbonised at 900 °C has a higher SSA than GNPs of about 191 m^2 g^{-1}. The value of the specific surface area of sample 2F_900 was 941 m^2 g^{-1}. The use of two-dimensional-non localised density functional theory (2D-NLDFT) method permitted the determination of the pore size for the N-doped graphene foams. The subtle differences are shown in Fig. S2c and d.† The pore volumes were compared with commercial graphene and are summarised in Table 1. The pore sizes of the materials in detail is described in the ESI.†

The Raman spectra Fig. 2 possess three characteristic bands, D, G, and 2D. The intensity ratio of the D to G bands and 2D to G bands are shown in Table 1. Explanations of the meaning of

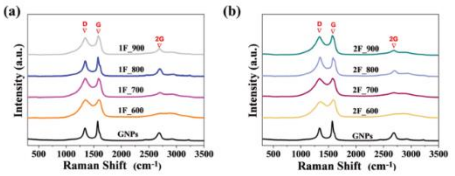

Fig. 2 Raman spectra of samples in series (a) 1F_*T* and (b) 2F_*T* compared to GNPs.

individual peaks and the intensity ratio of D to G bands (I_D/I_G) and 2D to G bands (I_{2D}/I_G) are described in the ESI.†

The type of functional groups in the N-doped graphene foams is very important and influences the catalytic properties. Therefore, X-ray photoelectron spectroscopy (XPS) analysis was used to determine the content of functional groups.

The resulting XPS spectra were taken for 1F_800 and 2F_800 samples. The tests performed made it possible to determine the type of elements present in the XPS survey spectra (Fig. 3a and

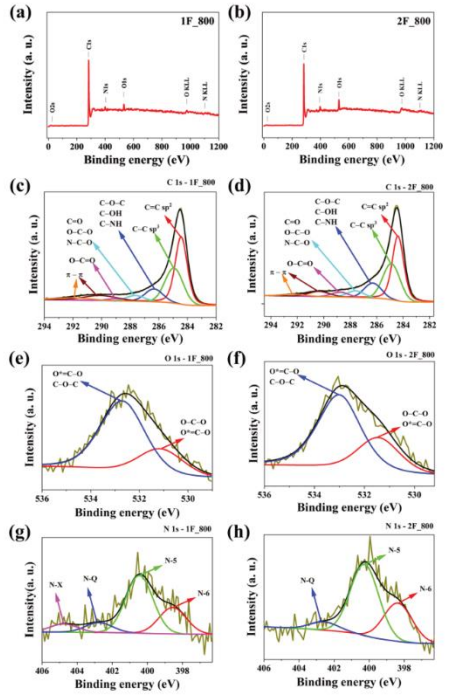

Fig. 3 (a and b) The XPS survey spectra. The high-resolution XPS spectra of (c and d) C 1s, (e and f) O 1s, (g and h) N 1s for 1F_800 and 2F_800 sample.

b). The natural polymers used, gelatine and chitosan, were the sources of carbon and nitrogen atoms. High-resolution spectra were determined for carbon (Fig. 3c and d), oxygen (Fig. 3e and f), and nitrogen (Fig. 3g and h). The individual spectra and corresponding bonds at a given energy value are described in the ESI.† Under the influence of high temperatures, the nitrogen atoms were transformed into the corresponding nitrogen functional groups (Table S1†).

In the literature, researchers described different nitrogen groups responsible for electrochemical activity. In one paper, the authors suggested that pyrrole-N, pyridinic-N and graphitic-N influence activity in the oxygen reduction reaction.[29] In another case, pyridinic-N enhances activity in the oxygen reduction reaction and, in combination with another heteroatom, may also effectively contribute to the use of materials as catalysts for additional application.[30–32]

Electrochemical performance

Catalytic activity is an extremely important parameter when evaluating electrocatalysts determined by cyclic voltammetry (CV) and linear sweep voltammetry (LSV). The potential application of the obtained electrocatalysts was investigated in relation to oxygen reduction reaction, which is a crucial reaction in metal–air batteries or fuel cells. The CV curves (Fig. 4a and S3a†) obtained for both series of materials possess characteristic cathodic peaks, which indicates the catalytic activity of the composites obtained. The cathodic peak for the samples in the 1F_*T* series was in the potential range from 0.77 to 0.80 V *vs.* the reversible hydrogen electrode (RHE). In series 1F, the current density range for sample 1F_800 is the widest, which may indicate high activity over a wide range of current densities. For the 2F_*T* series, a shift of the cathode peak towards positive potential values is evident. The peak range in which oxygen reduction occurs for the samples in the 2F_*T* series is between 0.75 and 0.81 V *vs.* RHE. In series 2F, sample 2F_900 shows the broadest range of current density than the other samples in this series. By analyzing the LSV voltammograms (Fig. 4b and S3b†) and onset potential determined on LSV curves (Fig. 4c and S3c†) at a scan rate of 5 mV s^{-1} and a sweep rate of 1600 rpm, the most effective catalysts in the oxygen reduction reaction can be selected.

Based on the results from the LSV method measured at different speeds in the range from 800 to 2800 rpm, using the equations and the K–L diagram (Fig. 4d and S3d†), the number of electrons involved in the ORR reaction was determined. After calculations determining the number of electrons transferred, it can be concluded that the materials from both series demonstrate a four-electron oxygen reduction pathway (Table 2). Fig. 5 shows the number of electrons involved in the oxygen reduction reaction for samples of 1F_*T* and 2F_*T* series and also for GNPs, and commercial platinum-based catalysts.

Chronopotentiometric tests were carried out to assess the durability of the 1F_800 and 2F_800 electrodes. Stability tests were measured for 5 h at 0.5 V *vs.* RHE. The obtained materials exhibit high durability in the oxygen reduction reaction after 5 h the materials still maintained high current stability, indicating a potential alternative to metal-containing catalytic materials. A graph showing the stability of the best materials is shown in the ESI on Fig. S4.†

Slight differences can be seen in the variation of the carbonization temperature. For the first 1F_*T* series, the number of electrons ranged from 3.16 to 3.88. The highest number close to the four-electron pathway was exhibited by sample 1F_700 at 3.88. Nevertheless, comparing the other parameters, such as current density and diffusion-limiting current, indicates that it is possible to choose the best carbonization temperature for the 1F_*T* series. Therefore, temperatures of 700 °C or 800 °C are required to obtain favorable catalysts synthesized with gelatine. As for the second 2F_*T* series, it is apparent that as the carbonization temperature increases, the electron number also increases, ranging from 3.19 to 3.99. A breakdown of this trend can also be seen for the highest carbonization temperature of 900 °C; for sample 2F_900, the electron number is 3.43. Therefore, the highest electron number involved in the oxygen reduction reaction for

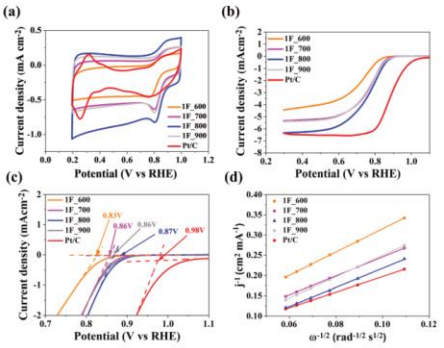

Fig. 4 The results of electrochemical performance for 1F_*T* and Pt/C saturated with O_2 in 0.1 mol L^{-1} KOH (a) CV plots with a scan rate of 10 mV s^{-1}, (b) LSV plots with a scan rate of 5 mV s^{-1} and rotation speed of 1600 rpm, (c) onset potential, (d) Koutecky–Levich plots at 0.5 V *vs.* RHE for samples in the 1F_*T* series.

Table 2 ORR performance parameters of the obtained N-doped graphene foams compared to commercial Pt/C catalyst, tested in 0.1 mol L^{-1} KOH

Catalyst	E_p (V *vs.* RHE)	E_{onset} (V *vs.* RHE)	$E_{1/2}$ (V *vs.* RHE)	Diffusion-limiting current (mA cm^{-2})	n (0.5 V)
Pt/C	0.76	0.98	0.88	6.37	4.00
1F_600	0.77	0.83	0.73	3.93	3.16
1F_700	0.80	0.86	0.77	5.16	3.88
1F_800	0.80	0.87	0.77	6.18	3.84
1F_900	0.80	0.86	0.77	5.25	3.44
2F_600	0.75	0.81	0.72	3.44	3.19
2F_700	0.78	0.86	0.75	4.22	3.45
2F_800	0.80	0.88	0.77	5.93	3.99
2F_900	0.82	0.91	0.79	5.80	3.43

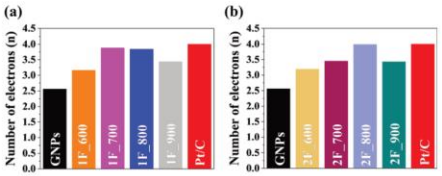

Fig. 5 (a) The number of transferred electrons in the (a) 1F_*T* and (b) 2F_*T* series compared to the commercial catalyst Pt/C and GNPs.

sample 2F_800 is 3.99; this number is equal to the number of electrons transferred for commercial platinum-based carbon.

Conclusions

In summary, the obtained graphene foam electrodes synthesized with natural polymers - gelatine and chitosan are porous and nitrogen-doped. The best graphene-based catalysts are materials carbonized at 800 °C and exhibit a four-electron oxygen reduction pathway in an alkaline medium. The applied carbonization temperatures (up to 800 °C) did not lead to the collapse of the pore structure and the considerable elimination of nitrogen from carbon matrices. The introduction of graphene was seen as an inevitable measure to ensure high electric conductivity of the synthetized ORR catalyst, a key feature for high ORR performance. This plan succeeded, since even carbon matrices obtained at a very low temperature of 600 °C had noticeable values for the number of transferred electrons n (3.16 and 3.19). Moreover, the matrices obtained at the highest carbonization temperature of 900 °C did not suffer from diminished structural parameters and exhibited, for example, a surface area above 795 $m^2\ g^{-1}$, which is even better than the parameter observed for pristine graphene nanoplatelets. In addition, the influence of quaternary nitrogen functional groups and the predominance of pyridinic groups on the catalytic activity of the obtained materials were investigated. In the future, the presented graphene foams will be successfully used as commercial electrodes for energy storage devices such as metal–air batteries and fuel cells.

Conflicts of interest

There are no conflicts to declare.

Acknowledgements

This work was carried out under research project no. 2019/35/N/ST5/02691, financed by the National Science Centre.

References

1 G. Lemes, D. Sebastián, E. Pastor and M. J. Lázaro, *J. Power Sources*, 2019, **438**, 227036.
2 Y. Shao, Z. Jiang, Q. Zhang and J. Guan, *ChemSusChem*, 2019, **12**, 2133–2146.
3 X. Wen, Z. Duan, L. Bai and J. Guan, *J. Power Sources*, 2019, **431**, 265–273.
4 C. Han and Z. Chen, *Appl. Surf. Sci.*, 2020, **511**, 145382.
5 X. Tong, M. Cherif, G. Zhang, X. Zhan, J. Ma, A. Almesrati, F. Vidal, Y. Song, J. P. Claverie and S. Sun, *ACS Appl. Mater. Interfaces*, 2021, **13**, 30512–30523.
6 J. Jin, F. Pan, L. Jiang, X. Fu, A. Liang, Z. Wei, J. Zhang and G. Sun, *ACS Nano*, 2014, **8**, 3313–3321.
7 X. Zheng, J. Wu, X. Cao, J. Abbott, C. Jin, H. Wang, P. Strasser, R. Yang, X. Chen and G. Wu, *Appl. Catal., B*, 2019, **241**, 442–451.
8 Y. Yan, W. I. Shin, H. Chen, S.-M. Lee, S. Manickam, S. Hanson, H. Zhao, E. Lester, T. Wu and C. H. Pang, *Carbon Lett.*, 2021, **31**, 177–199.
9 Z.-L. Wang, D. Xu, H.-G. Wang, Z. Wu and X.-B. Zhang, *ACS Nano*, 2013, **7**, 2422–2430.
10 D. Su, *Chem. Commun.*, 2012, **48**, 7149–7151.
11 S. P. Patole, S. K. Reddy, A. Schiffer, K. Askar, B. G. Prusty and S. Kumar, *ACS Appl. Nano Mater.*, 2019, **2**, 1402–1411.
12 N. B. Tolou, H. Salimijazi, M. Kharaziha, G. Faggio, R. Chierchia and N. Lisi, *Mater. Sci. Eng. C*, 2021, **126**, 112110.
13 Z. Zhao, H. Wang, H. Huang, L. Li and X. Yu, *Colloids Surf., A*, 2021, **626**, 127125.
14 Y. Zhao, J. Liu, Y. Hu, H. Cheng, C. Hu, C. Jiang, L. Jiang, A. Cao and L. Qu, *Adv. Mater.*, 2013, **25**, 591–595.
15 H. Wu, S. Deng, Y. Shao, J. Yang, X. Qi and Y. Wang, *ACS Appl. Mater. Interfaces*, 2019, **11**, 46851–46863.
16 W. Chen, D. Li, L. Tian, W. Xiang, T. Wang, W. Hu, Y. Hu, S. Chen, J. Chen and Z. Dai, *Green Chem.*, 2018, **20**, 4438–4442.
17 K. t. Kaare, E. Yu, A. Volperts, G. Dobele, A. Zhurinsh, A. Dyck, G. Niaura, L. Tamasauskaite-Tamasiunaite, E. Norkus and M. Andrulevicius, *ACS Omega*, 2020, **5**, 23578–23587.
18 A. Olad and H. B. K. Hagh, *Composites, Part B*, 2019, **162**, 692–702.
19 Y. Dai, W. Li, Z. Chen, X. Zhu, J. Liu, R. Zhao, D. S. Wright, A. Noori, M. F. Mousavi and C. Zhang, *J. Mater. Chem. A*, 2019, **7**, 16397–16405.
20 M. Skorupska, A. Ilnicka and J. P. Lukaszewicz, *Processes*, 2022, **10**, 643.
21 Z. Lin, G. H. Waller, Y. Liu, M. Liu and C.-p. Wong, *Carbon*, 2013, **53**, 130–136.
22 B. Bera, A. Chakraborty, T. Kar, P. Leuaa and M. Neergat, *J. Phys. Chem. C*, 2017, **121**, 20850–20856.
23 J. Guo, S. Zhang, M. Zheng, J. Tang, L. Liu, J. Chen and X. Wang, *Int. J. Hydrogen Energy*, 2020, **45**, 32402–32412.
24 E. S. Cardoso, G. V. Fortunato, I. Palm, E. Kibena-Poldsepp, A. S. Greco, J. L. Junior, A. Kikas, M. Merisalu, V. Kisand and V. Sammelselg, *Electrochim. Acta*, 2020, **344**, 136052.
25 Q. Li, S. Zhang, L. Dai and L.-s. Li, *J. Am. Chem. Soc.*, 2012, **134**, 18932–18935.
26 J. Shui, M. Wang, F. Du and L. Dai, *Sci. Adv.*, 2015, **1**, e1400129.
27 M. M. Rahman, M. Muttakin, A. Pal, A. Z. Shafiullah and B. B. Saha, *Energies*, 2019, **12**, 4565.

28 H. Yang, S. Kou, Z. Li, Z. Chang, M. Wang, Z. Liu and G. Lu, *RSC Adv.*, 2019, **9**, 40301–40308.
29 E. J. Biddinger and U. S. Ozkan, *J. Phys. Chem. C*, 2010, **114**, 15306–15314.
30 H. Lei, M. Cui and Y. Huang, *ACS Appl. Mater. Interfaces*, 2022, **14**, 34793–34801.
31 J. Wu, L. Ma, R. M. Yadav, Y. Yang, X. Zhang, R. Vajtai, J. Lou and P. M. Ajayan, *ACS Appl. Mater. Interfaces*, 2015, **7**, 14763–14769.
32 H. Miao, S. Li, Z. Wang, S. Sun, M. Kuang, Z. Liu and J. Yuan, *Int. J. Hydrogen Energy*, 2017, **42**, 28298–28308.

Supporting Information

Modified graphene foam as a high-performance catalyst for oxygen reduction reaction

Malgorzata Skorupska [a,*], Anna Ilnicka [a] and Jerzy P. Lukaszewicz [a,b]

[a] Faculty of Chemistry, Nicolaus Copernicus University in Torun, Gagarina 7, 87-100 Torun, Poland

[b] Centre for Modern Interdisciplinary Technologies, Nicolaus Copernicus University in Torun, Wilenska 4, 87-100 Torun, Poland

[*] Correspondence: m.skorupska@doktorant.umk.pl (M.S.); Tel.: +48 506841438

Materials and methods

Synthesis of N-doped graphene-foams

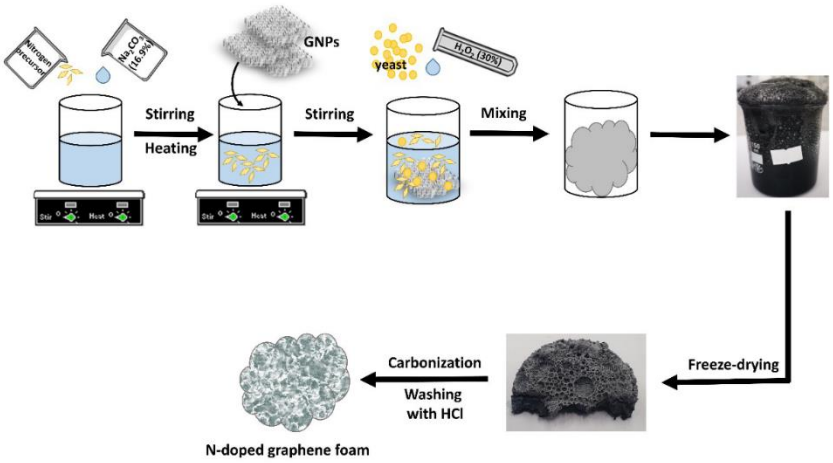

Scheme S1. Synthesis stages of N-doped graphene foams with the photograph of materials before and after freeze-drying.

Physicochemical characterization

Various methods were used for a detailed characterization of the physico-chemical properties of the samples.. A high-resolution transmission electron microscope (HRTEM FEI Tecnai F20 X-Twin, Brno, the Czech Republic) was used to characterize the structure. Raman spectra were obtained using a Raman spectrometer with 532 nm laser excitation (microscope InVia Renishaw, Renishaw Company, Gloucestershire, Great Britain). Low-pressure nitrogen adsorption was measured at 77 K using an automatic volumetric analyser (ASAP 2020 Plus, Micromeritics, Norcross, USA). The SSA was calculated using the Brunauer-Emmett-Teller (BET) equation, the pore distribution was determined by two-dimensional non-localised density functional theory (2D-NLDFT), the micropore volume (V_{mi}) was determined by t-plot

method, the total volume (V_t) was determined at the maximum relative pressure of p/p_0, the mesopore volume (V_{me}) was calculated by subtracting the volume of micropores from total pore volume. The elemental composition was used to determine the weight percentage of nitrogen, carbon, and hydrogen. The elemental analysis was carried out using a combustion analyser (Vario MACRO CHN, Elementar Analysensysteme GmbH, Germany). To determine the type and concentration of functional groups, the X-ray photoelectron spectroscopy (XPS) measurements were carried out with VG Scientific ESCALAB-210 analyzer (Japan); the excitation source was Al Ka ray (1486.6 eV).

Electrochemical measurements

The electrochemical properties were investigated using a rotating disk electrode (RDE) on an Autolab electrochemical analyzer (PGSTAT128N, the Netherlands). The electrochemical system for the oxygen reduction reaction consisted of three electrodes. The reference electrode was Ag/AgCl in 3 mol L^{-1} KCl, the counter-electrode was a platinum plate, and the working electrode was the obtained electrocatalyst applied on a glassy carbon electrode with a diameter of 3 mm and surface area equal 0.07065 cm^2. All electrodes were immersed in 0.1 mol L^{-1} KOH electrolyte. All materials were compared with commercial carbon consisting of platinum 20 wt.% (Pt/C). To apply a suitable amount of material to the glassy carbon electrode (mass loading of 0.4 mg cm^{-2}), an ink preparation of the resulting graphene foams and commercial catalyst (Pt/C) was required. 2.5 mg of carbon material was weighed and dispersed in 0.55 ml of a mixture of distilled H_2O, ethanol and Nafion (0.5 wt.% Nafion). Oxygen reduction reactions were studied by cyclic voltammetry (CV) and linear sweep voltammetry (LSV) measurements. Scan rates were 10 and 5 mV s^{-1} for CV and LSV, respectively. For the appropriate oxygen reduction reaction, 0.1 mol L^{-1} KOH was saturated with oxygen and then nitrogen before each CV and LSV measurement. Stability tests were

measured for 5 h at 0.5 V vs RHE. The number of transferred electrons involved in the oxygen reduction reaction was determined using the Koutecky-Levich (KL) equations at 0.5 V vs RHE.

Koutecky'ego-Levicha (KL) equations:

$$J^{-1} = J_L^{-1} + J_K^{-1} = (B\omega^{1/2})^{-1} + J_K^{-1} \quad (1)$$

$$B = 0.62nFC_0(D_0)^{2/3}\nu^{-1/6} \quad (2)$$

where: J is defined as the measured current density, J_L, and J_K are the limiting diffusion and kinetic current densities, respectively; ω is the angular velocity of the electrode; n is the number of electron transfer involved in the oxygen reduction reaction; F is assigned to Faraday's constant (96485 C mol^{-1}); C_0 is the concentration of oxygen that has been dissolved in the electrolyte ($1.2 * 10^{-6}$ mol L^{-1}); D_0 by definition, is the diffusion coefficient of oxygen introduced into the electrolyte ($1.9 * 10^{-5}$ cm^2 s^{-1}); ν is the kinetic viscosity of electrolyte (0.01 cm^2 s^{-1}); all constants depend on the electrolyte and in this case refer to 0.1 mol L^{-1} of KOH. After the transformation, the value of the slope of the Koutecky-Levich straight line is obtained, and the number of electrons transferred is calculated on this basis.

Results and Discussion

Materials characterization

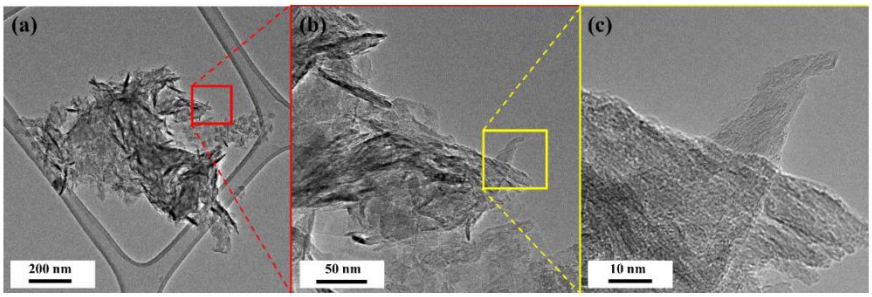

Figure S1. High–resolution transmission electron microscopy images of 2F_800 sample at different magnifications.

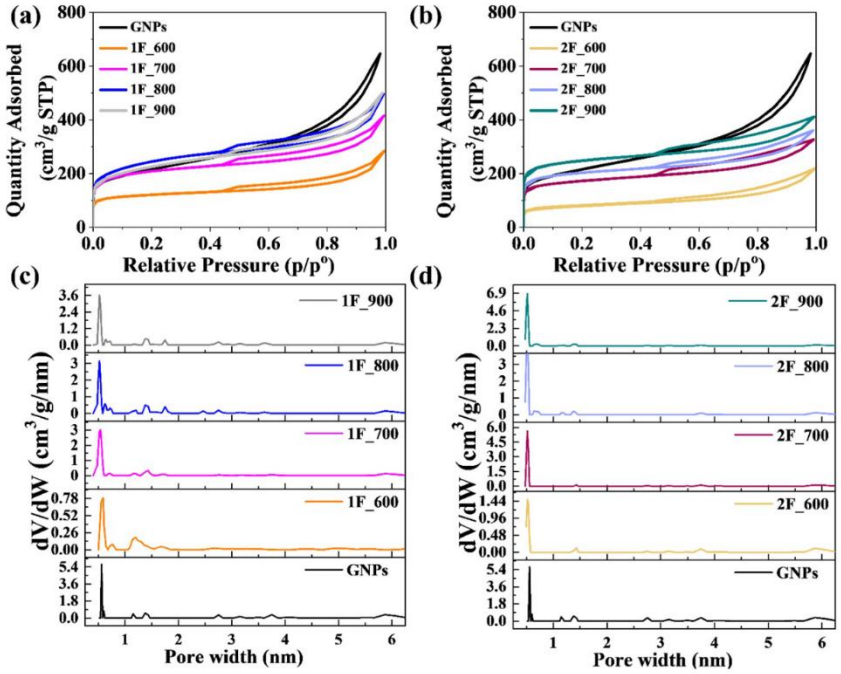

Figure S2. (a, b) Nitrogen adsorption–desorption isotherms and (c, d) pore size distribution of samples in series 1F_T and 2F_T compared with GNPs.

It is noted that the obtained materials do not show significant differences. The pore sizes of the materials obtained in series 1F_T are in the range of micropores (mainly in. 0.51 nm, 0.62 nm, 0.71 nm, 1.37 nm, 1.43 nm, and 1.74 nm) and small mesopores (mainly in 2.36 nm, 2.75 nm, 3.15 nm, 3.61 nm and 5.67 nm). In the case of 2F_T series, the pore size is also in the micropores range (mainly in 0.51 nm, 0.64 nm, 0.71 nm, 1.15 nm, 1.20 nm, 1.37 nm) and small mesopores (mainly in 3.75 nm and 5.87 nm).

The C1s spectrum shows peaks at 284.4 eV, 284.9 eV, 286.2 eV, 287.5eV, 288.6 eV, indicating the presence of C=C (sp^2), C-C (sp^3), C-NH, N-C-O, and O-C=O, respectively (Fig. 3b and Fig. 3f). Deconvolution of the O1s spectrum reveals the presence of O*=C-O and/or O-C-O bonds (530.7eV), and O=C-O* and/or C-O-C type (532.8 eV) (Fig. 3c and Fig. 3g). The N1s spectrum was fitted to four peaks at 398.5 eV, 400.2 eV, 402.3 eV and 404.5 eV, which corresponds to a pyridine-N bond (N-6), a pyrrole-N bond (N-5), quaternary nitrogen (N-Q) and nitrogen oxide –NO_x, (N-X), respectively (Fig. 3d and Fig. 3h). In the case of the 2F_800 sample (Fig. 3h), the band located at the binding energy of 404.5 eV is not visible, which means that this type of N-X bonds are not present in this sample.

Table S1. The total amount of C, O, N elements and detailed concentrations for nitrogen-groups determined by XPS analysis of 1F_800 and 2F_800.

Sample	**Total C (at. %)**	**Total O (at. %)**	**Total N (at. %)**	**Nitrogen functional group (at. %)**				**(N-5) and (N-6) (% relative to total N)**
				N-5	**N-6**	**N-Q**	**N-X**	
1F_800	93.9	3.5	2.8	1.6	0.7	0.3	0.2	82.14
2F_800	89.9	6.3	3.8	2.3	1.2	0.3	0.0	92.11

Figure 2 presents characteristic bands as D band at ~1350 cm^{-1} that is characteristic of the polycrystalline structure of carbon, which is responsible for doping and defects; a G band at a shift of ~1580 cm^{-1}, characteristic of stretching vibrations in a graphitic crystal. The ratio of D to G bands is usually used to represent defects in the carbon structure. The 2D band at a Raman shift of ~2700 cm^{-1} results from a two-photon process and is the overtone of the D peak [2, 3]. Analyzing the Raman spectra shown in Fig. 2 and comparing the parameters in Table 1, it can be seen that the shape of the D and G bands changes with the carbonization temperature. The area under the D-band is increased for samples carbonized at lower temperatures (1F_600 and 2F_600), indicating that carbon with sp^3 hybridization from chitosan or gelatine was subjected to the elimination of oxygen functional groups by oxidative removal [4]. The G-band responsible for defects in the carbon structure strongly depends on the nitrogen content and is also related to the defective structure. As the carbonization temperature increases, the nitrogen content decreases, and the G-band is more pronounced, indicating that the degree of graphitization increases in all materials obtained [5]. Raman spectroscopy was used to determine the quality of N-doped graphene foams, mainly to estimate how many layers of graphene and determine the defect level of the structure. The calculated intensity ratio of the D to G bands (I_D/I_G) indicates that the structure of the multilayer graphene is defective. A high degree of defectiveness is evidenced by an intensity ratio above or close to the value of 1. The samples obtained in both series show a similar intensity ratio, which may indicate that the samples obtained are equally defective. The observed defective structure is closely related to the heteroatoms that are present in the structure. The intensity ratio of I_D/I_G for samples 1F_600 and 2F_600 was 0.99 and 0.90, respectively. The highest I_D/I_G ratio values for samples 1F_700 and 2F_800 were 1.01 and 1.03, respectively. In both series, the most prominent 2D peak occurs for samples carbonized at 800°C (for 1F_800 and 2F_800), which indicates the presence of graphene structures in the

N-doped graphene foams obtained and also suggests the overlapping of multiple layers. The value of the intensity ratio of the 2D to G bands (I_{2D}/I_G ratio) for all samples is below 0.5 (Table 1) indicate that samples contain the multilayer graphene.

Electrochemical performance

A similar shape and comparable limiting current to the commercial platinum-based carbon material is shown by samples 1F_800 from the first series while for the second series 2F_T, the best shape is shown by samples carbonized at 800°C and 900°C (2F_800 and 2F_900). For the second 2F_T series, the oxygen reduction reaction occurs faster and is more efficient for all samples. This may be related to the respective nitrogen functional groups at the edges of the graphene structures, and more specifically, to the correlation of the N-5 and N-6 groups in relation to the total nitrogen content of the samples. The onset potential values (Table 2) determined from the LSV curves in Fig. 4d and Fig. S3d indicate the rapidity of oxygen reduction on the electrocatalyst. For the 1F_T series synthesized with gelatine, the onset potential values are in the range from 0.83 to 0.87 V vs RHE. The highest value is contained in sample 1F_800, which has an onset potential of 0.87 V vs RHE. The onset potential values for the second series synthesized with chitosan, 2F_T, range from 0.81 to 0.90 V vs RHE, and the highest value is recorded for sample 2F_900 of 0.9 V vs RHE.

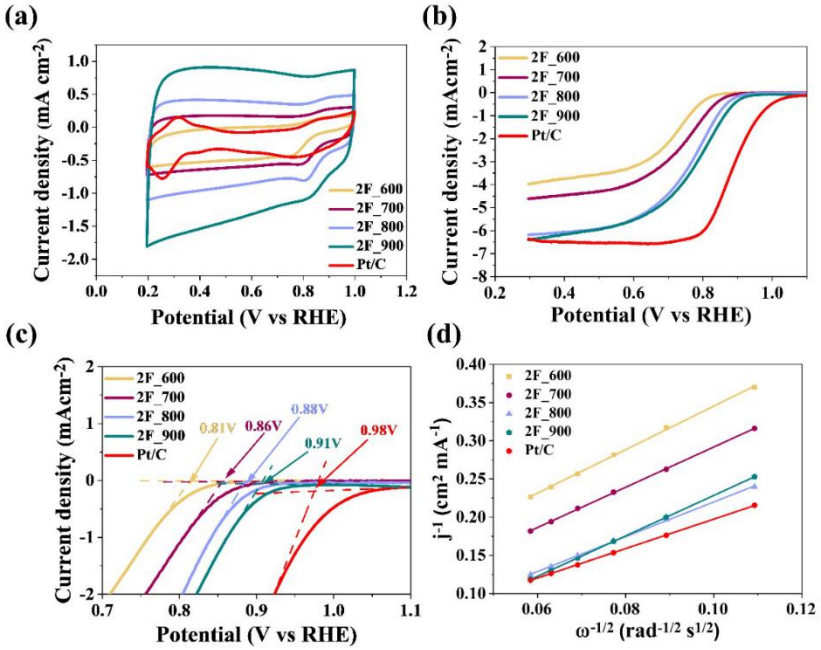

Figure S3. The results of electrochemical performance for 2F_T series and Pt/C in saturated-O_2 0.1 mol L^{-1} KOH (a) CV plots with a scan rate of 10 mV s^{-1}, (b) LSV plots with a scan rate of 5 mV s^{-1} and rotation speed of 1600 rpm, (c) onset potential, (d) Koutecky–Levich plots at 0.5 V vs RHE for samples in the 2F_T series.

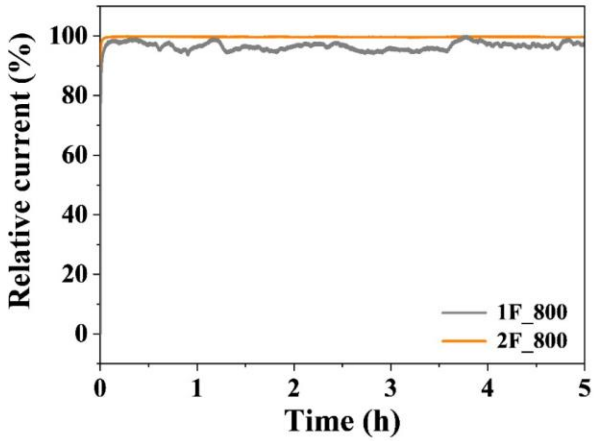

Figure S4. Chronoamperometric curves of 1F_800 and 2F_800 in O_2-saturated 0.1 M KOH solution at 0.5 V vs RHE.

Data availability statement

The datasets generated during and/or analysed during the current study are available in the Open Data Repository - UMK collection https://doi.org/10.18150/9AY0G5.

The datasets used and/or analysed during the current study available from the corresponding author on reasonable request.

References

1. Y. Bian, H. Wang, J. Hu, B. Liu, D. Liu and L. Dai, *Carbon*, 2020, **162**, 66-73.
2. S. A. Chernyak, A. S. Ivanov, D. N. Stolbov, T. B. Egorova, K. I. Maslakov, Z. Shen, V. V. Lunin and S. V. Savilov, *Applied Surface Science*, 2019, **488**, 51-60.
3. A. C. Ferrari and D. M. Basko, *Nature nanotechnology*, 2013, **8**, 235-246.
4. X. Han, M. R. Funk, F. Shen, Y.-C. Chen, Y. Li, C. J. Campbell, J. Dai, X. Yang, J.-W. Kim and Y. Liao, *ACS nano*, 2014, **8**, 8255-8265.
5. G. Mittal, K. Y. Rhee, S. J. Park and D. Hui, *Composites Part B: Engineering*, 2017, **114**, 348-355.

[D5] M. Skorupska, A. Ilnicka, P. Kamedulski, J. P. Łukaszewicz, *The Improvement of Energy Storage Performance by Sucrose-Derived Carbon Foams via Incorporating Nitrogen Atoms*, Nanomaterials, 2021, 11(3), 760; https://doi.org/10.3390/nano11030760 (IF=5.3, MEiN=100)

Uzyskane zaproponowaną metodą materiały, w szczególności modyfikacje ich struktury i wzrost porowatości były możliwe poprzez zastosowanie jednoetapowej procedury syntezy. Synteza ta obejmowała użycie prostych nośników organicznych (sacharozy i chitozanu jako źródeł węgla i azotu) oraz grafenu i H_3PO_4 podczas procesu karbonizacji. Otrzymane próbki wykazują korelację między ilością użytej sacharozy a ich morfologią, zwłaszcza polem powierzchni właściwej i objętością porów. Kiedy stosunek grafenu do sacharozy wynosi 3:1, S_{BET} jest wyższe. Najwyższe S_{BET} odnotowano dla węgla, SCS-3:1, na bazie sacharozy i chitozanu (źródło węgla i azotu) wynoszące 1313 $m^2 g^{-1}$. Wyniki testów elektrochemicznych potwierdzają, że gdy stosunek grafenu i sacharozy wynosi 3:1, otrzymane z tego materiału katody do superkondensatora mają bardziej stabilne działanie w porównaniu do pozostałych próbek. Elektrody dla próbek z serii SGF-R i SCS-R testowane w 6 mol L^{-1} KOH wykazują pojemność właściwą przekraczającą 143 F g^{-1} w temperaturze pokojowej.

Otrzymane materiały będą mogły być w przyszłości z powodzeniem stosowane jako elektrody w bateriach metalowo-powietrznych lub superkondensatorach, ponieważ niektóre z nich są zdolne do czteroelektronowej redukcji cząsteczek tlenu bądź posiadają wysoką pojemność właściwą, przy czym te cechy pozostają stałe w warunkach symulujących powtarzalne użytkowanie baterii cynkowo-powietrznej lub superkondensatorów.

nanomaterials

MDPI

Article

The Improvement of Energy Storage Performance by Sucrose-Derived Carbon Foams via Incorporating Nitrogen Atoms

Malgorzata Skorupska [1], Piotr Kamedulski [1], Jerzy P. Lukaszewicz [1,2] and Anna Ilnicka [1,*]

[1] Faculty of Chemistry, Nicolaus Copernicus University in Torun, Gagarina 7, 87-100 Torun, Poland; m.skorupska@doktorant.umk.pl (M.S.); pkamedulski@umk.pl (P.K.); jerzy_lukaszewicz@o2.pl (J.P.L.)
[2] Centre for Modern Interdisciplinary Technologies, Nicolaus Copernicus University in Torun, Wilenska 4, 87-100 Torun, Poland
* Correspondence: ailnicka@umk.pl; Tel.: +48-609-273-793

Abstract: This paper addresses the problem of improving electrochemical energy storage with electrode materials obtained from common raw ingredients in a facile synthesis. In this study, we present a simple, one-pot route of synthesizing microporous carbon via a very fast reaction of sucrose and graphene (carbon source), chitosan (carbon and nitrogen source), and H_3PO_4. Porous carbons were successfully produced during high temperature carbonization, using nitrogen as a shielding gas. Samples were characterized using X-ray powder diffractometry, elemental analysis, N_2 adsorption-desorption measurements, scanning electron microscopy, and Raman spectroscopy. The developed carbon material possessed a high surface area, up to 1313 $m^2\ g^{-1}$, with no chemical or physical activators used in the process. The structural parameters of the microporous carbons varied depending on the ratio of reagents and mass composition. Samples were prepared both with and without chitosan. The present synthesis route has the advantages of being a single-step approach and only involving low-cost and environmentally friendly sources of carbon. More importantly, microporous carbon was prepared without any activators and potentially offers great application in supercapacitors. Cyclic voltammetry and constant current charge–discharge tests show that sucrose-based porous carbons show excellent electrochemical performance with a specific capacitance of up to 143 F g^{-1} at a current density of 1 A g^{-1} in a 6 M KOH electrolyte.

Keywords: graphene; sucrose; chitosan; carbonization; carbon nanocomposite; microporous structure; surface functional groups

Citation: Skorupska, M.; Kamedulski, P.; Lukaszewicz, J.P.; Ilnicka, A. The Improvement of Energy Storage Performance by Sucrose-Derived Carbon Foams via Incorporating Nitrogen Atoms. *Nanomaterials* **2021**, *11*, 760. https://doi.org/10.3390/nano11030760

Academic Editor: Marcin Wysokowski

Received: 21 February 2021
Accepted: 13 March 2021
Published: 17 March 2021

1. Introduction

Fabrication of electrochemical energy storage devices (batteries and supercapacitors) greatly relies on carbon-based electrodes. Therefore, improving the efficiency of these devices will rely on new findings in the area of carbon electrode material synthesis. Solutions encompassing a wide accessibility of raw materials, acceptable market price, and facile processing are in high demand due to the need of eventual mass production. Natural materials such as biomass and carbohydrates (e.g., glucose, fructose, lactose, and cellulose), which have natural reserves, are being extensively studied as a source of carbon-based materials. Due to its uniform structure, very low price, local availability, and high chemical purity, sucrose is one of the most attractive carbon precursors. There are essentially two main approaches that can be applied to extracting carbon from sucrose, either a hydrothermal [1] or a heat-treatment process [2–5]. To improve the porous structure of sucrose-based carbon, a variety of activation methods have been developed, which use steam [6], $CaCO_3$ [7], $NaHCO_3$ [8], polyurethane as a template [9], CO_2 gas [10], LiOH [11], NaOH [11–13], KOH [11,14,15], H_3PO_4, $ZnCl_2$, $SnCl_2$, or $CaCl_2$ [16]. Another approach to synthesis is to activate sucrose mechanically [17–19]. The micropore volume in a sucrose-based structure

may depend on dehydrating acids (sulphuric, hydrochloric, phosphoric, oxalic, acetic, citric, and tartaric acid) and the cationic component ($Ca(NO_3)_2$, $(NH4)_2SO_4$, $(NH_4)_2CO_3$, NH_4) used during synthesis [20]. Using the carbonization of a triblock copolymer (P123), silica, and sucrose composite, highly ordered mesoporous carbon has been generated [21,22].

Electrode materials based on activated carbon are widely used in supercapacitors [23,24] and Li-ion batteries [25,26]. In our previous research, we found that pyrrolic-N (N-5), pyridinic-N (N-6), and quaternary-N (N-Q) groups, active in catalytic reactions, are present in carbon obtained using chitin, chitosan, green algae, or amino acids as a source [27–29]. Therefore, using one of these precursors during the synthesis of sucrose-based carbon for supercapacitors should augment energy storage performance. Recently, the electrochemical properties of sucrose-derived carbon were improved by doping with N, F, and B, utilizing H_3BO_3 or NH_4F as heteroatom precursors [9]. Huang et al. prepared chemically activated carbon (with KOH) for electric double layer capacitors (EDLC) with a very modest specific capacitance of only ~40 F g^{-1} [30]. For porous carbon materials prepared by Guo et al. via high-temperature pyrolysis, the capacitance equaled 232 F g^{-1} at a current density of 0.1 A g^{-1} [31]. In another study, Subramanian et al. used sucrose pre-treated with ammonia nitrate as the carbon source to prepare a porous carbon with a specific capacitance of 232 F g^{-1} [32]. Silicon nanowires coated with sucrose-derived carbon were prepared for supercapacitor application [33] as well. The disadvantages of the mainstream electrode material production methods are the often multiple-step procedures, environmentally unfriendly reagents, and the presence of metals or metal oxides in the materials' structure.

Recognizing the applicability of sucrose in N-doped carbon electrode materials was the main motivation of the current study. To the best of the authors' knowledge, so far, there have been no reports of a one-pot synthesis of porous carbon foam from materials such as hydrocarbons and graphene, without using an activation agent. In this paper, different carbon and nitrogen contents were prepared in a carbonization process using sucrose and graphene as carbon sources and chitosan as a carbon and nitrogen source; their structural and electrochemical properties were evaluated. By changing the ratio of reagents, well-developed micro or mesoporous structures were obtained. The use of chitosan caused nitrogen groups to be introduced into the porous foam carbon structure.

2. Materials and Methods

2.1. Materials

Graphene nanoplatelets (750 m^2 g^{-1}) and chitosan were purchased from Sigma Aldrich (branch in Poland). Sucrose was purchased from Krajowa Spolka Cukrowa S.A. (Torun, Poland). Other reagents, i.e., H_3PO_4 and CH_3COOH, were purchased from POCH (Gliwice, Poland).

2.2. Preparation of Carbon Foams

Carbon foams were synthesized in one of two ways. In the first path, to 3 or 5 g of sucrose, 1 or 3 g of graphene nanoplatelets was added and mixed well. In the second, to 3 or 5 g of sucrose, 1 or 3 g of chitosan was added, previously dissolved in 10 mL of a 1% CH_3COOH solution, then mixed. In the next step, the mixtures were treated with 3 or 4.5 mL of H_3PO_4 at a 3:1 and 5:3 ratio of reagents, respectively. Samples were then heated on a double electric cooker at temperatures in the range of 100 to 400 °C. After this, materials were carbonized in a N_2 atmosphere at a heating rate of 10 °C min^{-1} until 900 °C was reached. This temperature was maintained for 1h. The process was carried out in a tubular furnace (Thermolyne F21100) (NIST, Gaithersburg, MD, USA). Further in the text, the mixture of sucrose (S) and chitosan (CS) used during synthesis is denoted as SCS. The mixture of sucrose (S) and graphene nanoplatelets (GF) is denoted as SGF. The mass ratio (R) of reagents used, S:CS and S:GF, was either 3:1 or 5:3. The samples in general are indicated as SCS-R (SCS-3:1, SCS-5:3) and SGF-R (SGF-3:1, SGF-5:3).

2.3. Structure Characterization

The morphology of the obtained samples was determined using a scanning electron microscope (SEM 1430 VP, LEO Electron Microscopy Ltd., Oberkochen, Germany) operating at 30 kV. The porous structure of the samples was analyzed via a nitrogen adsorption experiment at 77 K, using an automatic adsorption instrument, ASAP 2020 Plus (Micromeritics, Norcross, GA, USA). Before the analysis, obtained carbons were outgassed in a vacuum at 200 °C for 24 h. The samples' surface areas were calculated using the Brunauer–Emmett–Teller (BET) equation, and the pore size distributions were calculated using the nonlocalized density functional theory (NLDFT) method. The elemental composition of the materials was analyzed by means of a combustion elemental analyzer (Vario CHN, Elementar Analysensysteme GmbH, Langenselbold, Germany). Raman spectra were obtained by a Renishaw InVia Raman analyzer (laser wavelength 532 nm, Renishaw Company, Gloucestershire, UK). X-ray photoelectron spectroscopy (XPS, PHI5000 VersaProbe II Scanning XPS Microprobe, Chigasaki, Japan) measurements were performed using a monochromatic Al Kα X-ray source. Survey spectra were recorded for all samples in the energy range of 0 to 1300 eV with a 0.5 eV step, while high-resolution spectra were recorded with a 0.1 eV step.

2.4. Electrochemical Measurements

The electrochemical performance of carbon samples was studied using cyclic voltammetry (CV) curves, galvanostatic charge–discharge (GCD) cycling, and electrochemical impedance spectroscopy (EIS) plots for a two-electrode system. Electrodes prepared for electrochemical measurements were well-mixed active materials, conductive carbon black (C-140), and polytetrafluoroethylene (PTFE) at a mass ratio of 17:2:1. These, at a diameter of 9.25 mm, were dried in a vacuum oven at 100 °C for 24 h. Electrochemical capacitors were built using two carbon electrodes with comparable mass (4–5 mg). Cyclic voltammetry and galvanostatic charge–discharge data were collected using a potentiostat–galvanostat (PGSTAT128N, Autolab) (Metrohm Autolab B.V., Utrecht, The Netherlands). Electrochemical investigations were performed in 6 M KOH aqueous electrolyte. Cyclic voltammograms were recorded at a scan rate between 5 and 200 mV s^{-1}, in the potential range of 0 to 0.9 V. Charging-discharging was performed at various current densities, from 0.1 to 40 mA g^{-1}. Electrochemical impedance was measured in a frequency range of 10^{-1} to 10^{5} Hz; the amplitude was 10 mV. Two electrodes of similar mass were used in a symmetrical two-electrode supercapacitor. The specific capacitance C_s (F g^{-1}) (Equation (1)), energy density E (Wh kg^{-1}) (Equation (2)), and power density P (W kg^{-1}) (Equation (3)) were calculated based on the following equations:

$$C_s = I \times \Delta t/(m \times \Delta V) \quad (1)$$

$$E = (C \times \Delta V^2)/(8 \times 3.6) \quad (2)$$

$$P = (E \times 3600)/\Delta t \quad (3)$$

where I is the charge and discharge current (A), Δt is the discharge time (s), ΔV is the potential change within the discharge time (V), and m is the total mass of active materials in both electrodes.

3. Results and Discussion

3.1. Characterization of Carbon Materials

New carbon-based materials have been synthesized and characterized according to the specific underlying motivation: recognizing the applicability of sucrose for N-doped carbon electrode materials. Particular attention was paid to the insertion of nitrogen atoms, commonly regarded as the way to improve electric charge storage. Moreover, the authors searched for the most facile synthesis route. Characterization included key features like

surface area and pore structure, microscopic structure and morphology, bulk and surface elemental composition, as well as collection of a complete set of electrochemical profiles.

Figure 1 shows scanning electron micrographs for samples obtained from sucrose with two different modifications—chitosan and graphene. The pores developed under chitosan influence are interdigitated with each other to form a three-dimensional (3D), interconnected frame structure, the morphology of the carbon materials being sensitive to chitosan use. This special structure enables the pores inside the material to communicate with each other and allows the electrolyte to penetrate the electrode material more smoothly, accelerate the transport of electrolyte ions, reduce the "traffic blockage" in the ion transport process, and thus improve capacitance performance [34,35]. The SCS-R samples (Figure 1a,c) and SGF-R samples (Figure 1b,d) exhibit differences in morphology. A smooth surface of carbon can be attributed to a lower specific surface area (S_{BET}) when comparing SGF-3:1 and SGF-5:3 to SCS-3:1 and SCS-5:3 carbon, respectively, as described in Table 1.

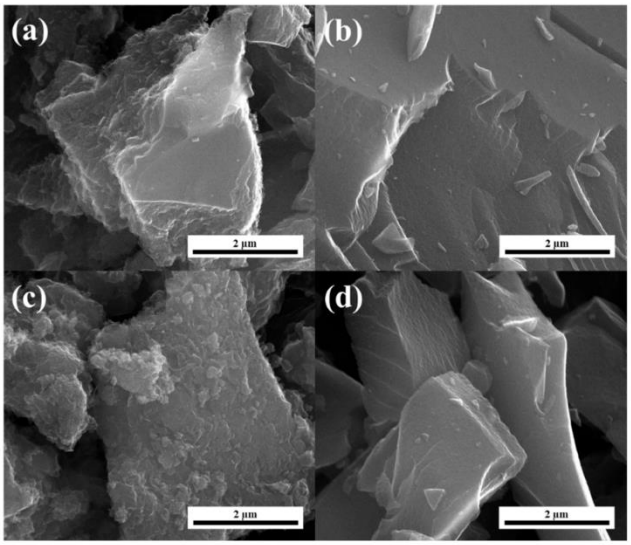

Figure 1. SEM images of the (**a**) mixture of sucrose and graphene nanoplatelets with a 3:1 ratio (SGF-3:1), (**b**) mixture of sucrose and chitosan with a 3:1 ratio (SCS-3:1), (**c**) mixture of sucrose and graphene nanoplatelets with a 5:3 ratio (SGF-5:3), and (**d**) mixture of sucrose and chitosan with a 5:3 ratio (SCS-5:3) sample.

Table 1. Elemental composition and textural parameters of the SGF-R and SCS-R samples.

Sample	Elemental Content (wt%)			S_{BET} [1] (m^2 g^{-1})	V_t [2] (cm^3 g^{-1})	V_{mi} [3] (cm^3 g^{-1})	V_{me} [4] (cm^3 g^{-1})
	C	H	N				
GR	87.32	0.90	0.72	750	1.00	0.13	0.87
SGF-3:1	90.18	0.71	0.60	1111	0.70	0.11	0.59
SCS-3:1	67.79	1.54	1.97	1313	0.60	0.13	0.47
SGF-5:3	79.72	1.13	0.30	771	0.52	0.20	0.32
SCS-5:3	62.49	1.97	2.13	841	0.37	0.30	0.07

[1] S_{BET}—total specific surface area, [2] V_t—volume of total pores; [3] V_{mi}—volume of micropores; [4] V_{me}—volume of mesopores.

The nitrogen adsorption-desorption isotherms of the carbon prepared from sucrose possess the appropriate distinct shape of carbon obtained with graphene or chitosan (Figure 2a,b). The shapes of isotherms belong to type I and IV, according to the International Union of Pure and Applied Chemistry (IUPAC) classification [36]. Using sucrose and graphene or chitosan primarily creates micropores in the structure. As listed in Table 1, the N_2 adsorption experiments indicate that the highest BET surface area is 1111 m^2 g^{-1} for SGF-3:1 and 1313 m^2 g^{-1} for SCS-3:1. Interestingly, the surface areas of samples obtained at a 5:3 weight ratio (lower sucrose content) are lower than those of samples at the 3:1 ratio. The specific surface areas for samples SGF-5:3 and SCS-5:3 are 771 and 841 m^2 g^{-1}, respectively. The total pore volume is given in the range of 0.37 to 0.70 cm^3 g^{-1}. Figure 2c,d provides pore size distribution as obtained using the NLDFT; size distribution appears to be quite narrow. The two different mass ratios of graphene to sucrose (3:1, 5:3) affect pore size. For samples SCS-3:1 and SGF-3:1, micropore size ranges from 0.5 to 1.8 nm. Samples SCS-5:1 and SGF-5:3 show micropores and small mesopores, up to 3.75 nm. The pore size distribution shows that sucrose-derived carbon obtained without any activator would be a suitable electrode material for supercapacitors [37,38].

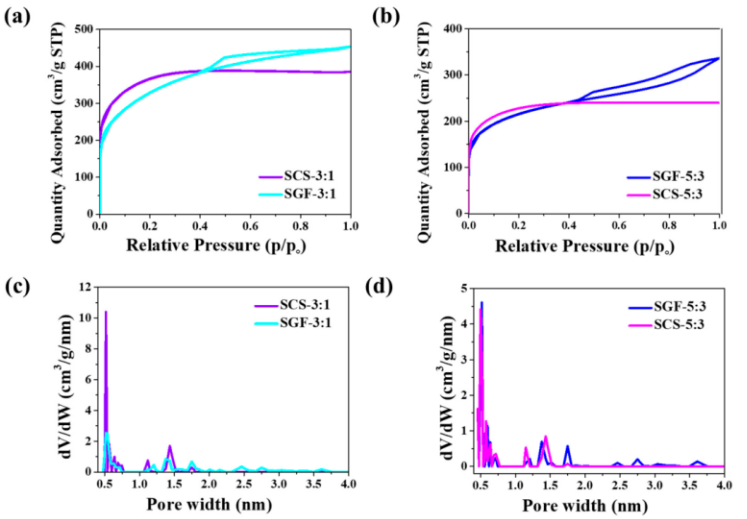

Figure 2. (**a**,**b**) N_2 adsorption–desorption isotherms at 77 K; (**c**,**d**) nonlocalized density functional theory (NLDFT) pore size distribution obtained from adsorption branches of N_2 in the SGF-R and SCS-R samples.

Elemental composition results are given in Table 1. Influence of graphene and chitosan on the carbon and nitrogen content is observable. Use of graphene (GR) caused carbon content to increase to 79.72–90.18 wt.%. For the samples obtained with chitosan, carbon content decreased to 62.49–67.79 wt.%. Generally, higher carbon content is reported for samples synthesized with a higher amount of sucrose. The content of nitrogen for samples obtained with chitosan is 1.97 wt.% for SCS-3:1 and 2.13 wt.% for SCS-5:3, while the nitrogen content for samples obtained with graphene significantly decreased and is only 0.60 wt.% for sample SGF-3:1 and 0.3 wt.% for SGF-5:3. The reason behind the low nitrogen content is a lack of nitrogen precursors.

Raman spectroscopy was used to characterize the graphitization degree of carbon materials [39,40]. Figure 3 shows Raman spectra for the carbon materials synthesized from sucrose and chitosan or graphene. In all cases, Raman spectra exhibit the D-band, G-band,

and 2D-band at a shift of ~1340 cm^{-1}, ~1580 cm^{-1}, and ~2700 cm^{-1}, respectively. The intensity ratio of the D- and G-bands determines the level of graphitization [14,41,42]. The materials here show a disordered location of graphene with the intensity of the D-band and G-band (I_D/I_G) at 1 (Table 2). The lack of significant differences in the I_D/I_G ratio confirms that using sucrose causes defects in the carbon structure.

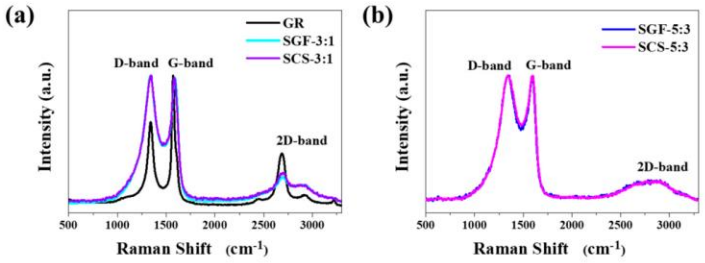

Figure 3. Raman spectra of (**a**) graphene, SGF-3:1 and SCS-3:1, (**b**) SGF-5:3 and SCS-5:3 sample.

Table 2. Fitting results of the Raman spectra for graphene (GR), SGF-R, and SCS-R samples.

Sample	I_D	Raman Shift (cm^{-1})	I_G	Raman Shift (cm^{-1})	I_{2D}	Raman Shift (cm^{-1})	I_D/I_G	I_{2D}/I_G
GR	0.64	1341	1	1570	0.4	2686	0.64	0.4
SGF-3:1	1	1339	0.99	1587	0.23	1699	1.02	0.23
SCS-3:1	1	1341	0.99	1593	0.2	2779	1.01	0.2
SGF-5:3	1	1346	0.98	1583	0.26	2699	1.02	0.26
SCS-5:3	1	1341	1	1598	0.19	2755	1	0.19

However, materials synthesized from ingredients in a 3:1 ratio have a 2D-band which is more pronounced. As the 2D-band decreases, the number of graphene structure defects increases, which is observable for series 5:3. Thus, a transition from a few-layer graphene structure to an amorphous carbon material can be seen [43,44]. A higher number of overlapping graphene layers is observed, and therefore, relative intensities of the 2D-band and G-band (I_{2D}/I_G) are low, around 0.2.

The porous carbon material's surface element composition and chemical states of atoms were analyzed and characterized by XPS. In order to understand the chemical state of carbon, oxygen, and nitrogen atoms, XPS was recorded for samples SGF-3:1 and SCS-3:1; the results are presented in Figure 4.

The C1s spectrum is shown in Figure 4a, where two main characteristic peaks can be fitted: the peak with the strongest intensity at 284.6 eV, which corresponds to the presence of sp^2 C=C bonds, and a characteristic peak at 285.0 eV, which corresponds to sp^3 C-C bonds [45–47]. The C1s spectrum of samples was also deconvoluted and assigned to C-O-C bonds (286.3 eV), C=O or O–C–O bonds (287.7 eV), O–C=O bond (288.6 eV), and π-π (289.6 eV and 292.1 eV) [48]. The spectrum of O1s is shown in Figure 4b, where two main characteristic peaks can be fitted: the most important peak at 532.0 eV, corresponding to the C–O–C group [49], and the peak at 533.3 eV, corresponding to the O−C=O group [50]. The presence of oxygen and the corresponding functional groups can produce pseudo capacitor-induced currents and improve the wettability of the electrode material's surface. This increases the amount of surface charge storage, thus helping to increase the energy density of the supercapacitor. XPS analysis evidenced the presence of nitrogen groups in the SGF-3:1 and SCS-3:1 sucrose-based foams. The results reveal that different samples present a different number of nitrogen heteroatoms. SGF-3:1 shows 0.9% at., while SCS-3:1 shows a higher nitrogen content of 2.1% at. In the case of SGF-3:1, there was no peak observed for nitrogen in the N1s region. Hence, it can be concluded that chitosan is responsible for the N-doping. One type of N-based species was identified in doped SCS-3:1, from the N1s XPS

high-resolution spectrum (Figure 4c), assigned to quaternary-N (N-Q) at 400.7 eV [50–53]. It is important to point out that when N is incorporated into SCS-3:1, the relative contribution of N-species other than quaternary-N is increased compared to SGF-3:1. The N1s spectra imply that N atoms have partially substituted C atoms in the carbon lattice. The XPS spectrum of P2p (Figure 4d) in both samples presents two characteristic bonds of P–C and P–O at binding energies of 133.5 eV and 134.3 eV [54].

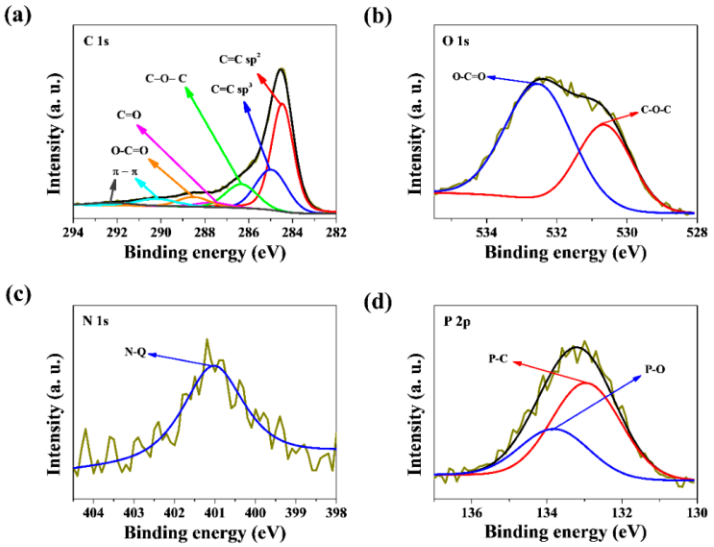

Figure 4. High-resolution XPS spectra: (**a**) C1s; (**b**) O1s, (**c**) N1s, and (**d**) P2p for the SCS-3:1 sample.

3.2. Electrochemical Performance

Experimental results show that the carbon obtained from sucrose with no activator, only graphene and chitosan, possesses properties important for energy storage. The rectangular shape of the CV curve portrays fast re-organization of the electrical double layer at switching potentials and indicates fast ion transport, provided by an ideal EDLC charge storage mechanism [55–57]. A rectangular shape was observed in the curves of both the SCS-3:1 and the SGF-3:1 electrode, implying ideal double-layer capacitance behavior (Figure 5a,b). For sample SCS-3:1, the CV shape in a two-electrode cell is rectangular in all scan rates. The pore size distribution for series 3:1 is strictly microporous without any mesopores, and therefore, BET is higher for this series; these electrodes should possess the highest capacitance and the lowest resistance [58,59]. A key role in determining specific capacitance is played by the specific surface area and microporosity with a pore size larger than the ions of those electrolytes [60].

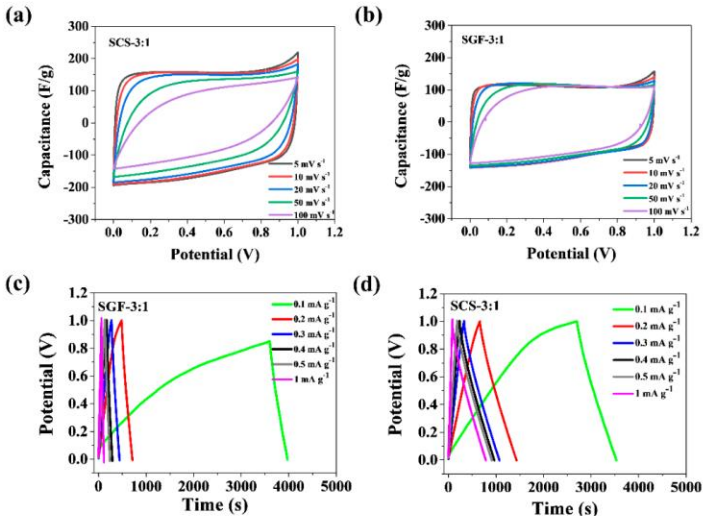

Figure 5. Electrochemical performance tests of the SCS-3:1 and SGF-3:1 samples: (**a**,**b**) cyclic voltammetry (CV) profiles at different scan rates ranging from 5 to 100 mV s^{-1}; (**c**,**d**) galvanostatic charge-discharge curves.

Specific capacitance (C_s) was calculated using galvanostatic discharge curves (Figure 5c,d). Looking at the charge–discharge curves of the SCS-3:1 and SGF-3:1 samples, electrode SCS-3:1 shows the highest capacitance. When the current density equaled 1 A g^{-1}, the specific capacitance was 143 F g^{-1} for electrode SCS-3:1, and when it equaled 2 A g^{-1}, the specific capacitance was 107 F g^{-1} for SGF-3:1 (Figure 6a,b). When compared with other materials [61], those tested show a similar range of supercapacitor operation, in the range of 0 to 0.8 V. Naturally sourced materials' specific capacity also trends similarly to the others, being within the range of 39–246 F^{-1}. The difference between performance and capacity is caused by the presence of different functional groups on the surface, conductivity, wettability in electrolyte, and pore size, from which the diffusion barrier arises [50–52]. The N-Q functional groups identified in sample SCS-3:1 would benefit the enhancement of electrical conductivity, as well as capacitance, by interacting with anions in the alkaline electrolyte [50,62,63]. These microporous materials offer sufficient space to allow electrolyte ion transportation and thus improve performance in supercapacitors.

The specific capacity of the SGF-3:1 electrode increases from the initial value to 104 F g^{-1} due to self-activation, then after 200 discharge cycles, there is a slow decrease in the specific capacity value (97% (102%) retention after 1000 cycles). The SCS-3:1 electrode exhibits a similar disposition. The specific capacity is slowly increased to 132 F g^{-1} for 100 cycles, followed by a decrease in the specific capacity value, also at 97% (101%) retention after 1000 cycles (Figure 6b). These results indicate that microporous, sucrose-based carbon electrodes used in supercapacitors have good stability and capacitance retention. The plot presented in Figure 6c shows the relationship between energy densities and power densities, calculated from the charge–discharge measurements. Materials obtained with the proposed method show an energy density of 4.7 Wh kg^{-1} at a power density of 2.8 kW kg^{-1} for SGF-3:1 and an energy density of 6.2 Wh kg^{-1} at a power density of 2.8 kW kg^{-1} for SCS-3:1. At the same time, cellulose materials show an energy density of 13 Wh kg^{-1} at a power density of 27 kW kg^{-1}. In another example of activated carbon nanotubes exhibiting

an energy density of 1.0 Wh kg^{-1} at a power density of 14.4 kW kg^{-1} [64], the obtained foams show similar electrochemical properties.

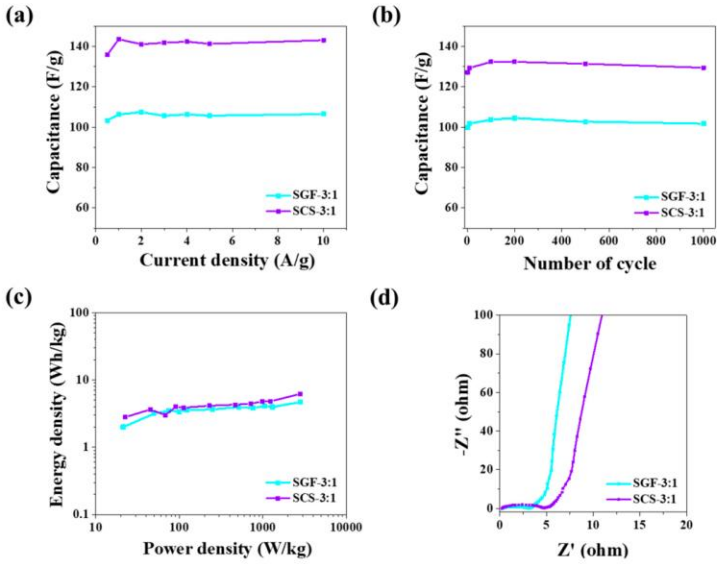

Figure 6. Electrochemical performance tests of the SCS-3:1 and SGF-3:1 samples: (**a**) specific capacitance as a function of current density; (**b**) specific capacitance as a function of cycle number; (**c**) specific capacitance as a function of power density; (**d**) Nyquist plot.

Figure 6d shows the electrochemical impedance spectra of electrodes SCS-3:1 and SGF-3:1, in a frequency range of 10^{-1} to 10^{5} Hz. Nyquist plots of the samples showed typical features of porous electrodes with an irregular semicircle at high frequencies, a relatively short 45° Warburg region at high-medium frequencies, and a slash at low frequencies. At low frequencies, the SMC-800 electrode exhibits an almost vertical line, owing to the high specific surface area and pore size distribution of SCS-3:1, coupled with the electrolyte easily penetrating into its pores [65]. These results indicate that the SCS-3:1 electrode has an almost ideal capacitance at low frequencies and good frequency response performance in accordance with the capacity calculated from the galvanostatic charge–discharge curves [6,66].

4. Conclusions

The obtained results fully meet the expectations arising from the previously presented research motivation. The present synthesis procedure has the advantage of being a single-step approach and only involving the use of simple organic precursors (sucrose and chitosan as carbon and nitrogen sources), plus graphene and H_3PO_4 during carbonization. The samples exhibit a correlation between the amount of sucrose used and their textural properties, especially surface area and pore volume. When the ratio of graphene to sucrose is 3:1, the BET is higher. The SGF-R and SCS-R samples show a microporous structure with small mesopores below 4 nm. The sucrose-based carbon SCS-3:1 is a combination of sucrose and chitosan (carbon and nitrogen source) with the highest specific surface area of 1313 m^2 g^{-1}. Cyclic voltammetry (CV), electrochemical impedance spectroscopy (EIS), and galvanostatic charge–discharge cycle tests have been applied to investigate the capacitive performance of the SGF-R and SCS-R electrodes, in 6 M KOH, at room

temperature. Electrochemical test results demonstrate that when the ratio of graphene and sucrose is equal to 3:1, the composite cathode for supercapacitors has a more stable performance than other samples. The SGF-R and SCS-R electrodes in 6 M KOH show specific capacitance in excess of 143 F g^{-1} at room temperature.

Author Contributions: Conceptualization, J.P.L.; methodology, J.P.L., P.K., A.I., and M.S.; formal analysis, M.S., A.I., and P.K.; investigation, M.S., P.K., and A.I.; data curation, M.S. and A.I.; writing—original draft preparation, A.I., M.S., and P.K.; writing—review and editing, A.I., M.S., and J.P.L.; visualization, M.S. and A.I.; supervision, J.P.L. and A.I.; project administration, M.S.; funding acquisition, M.S. All authors have read and agreed to the published version of the manuscript.

Funding: This research was funded by the National Science Centre, grant number 2019/35/N/ST5/02691.

Institutional Review Board Statement: Not applicable.

Informed Consent Statement: Not applicable.

Data Availability Statement: The data presented in this study are available on request from the corresponding author.

Acknowledgments: The authors would like to thank Daniell Cariazzo and Gelines Moreno-Fernández for valuable advice as well as the opportunity to implement a research internship at the CIC energiGUNE research institute, the PROM project—International scholarship exchange of doctoral students and academic staff as well as the "Excellence Initiative—Mobility for PhD students" under the program "Excellence Initiative—Research Learning".

Conflicts of Interest: The authors declare no conflict of interest.

References

1. Cano-Casanova, L.; Amorós-Pérez, A.; Ouzzine, M.; Román-Martínez, M.C.; Lillo-Rodenas, M.A. Enhancement of the TiO_2 photoactivity for propene oxidation by carbon incorporation using saccharose in hydrothermal synthesis. *J. Environ. Chem. Eng.* **2020**, *9*, 104941. [CrossRef]
2. Matos, J.; Laine, J. A carbon macro-network from the controlled pyrolysis of saccharose. *J. Mater. Sci. Lett.* **1998**, *17*, 649–651. [CrossRef]
3. Kubota, K.; Shimadzu, S.; Yabuuchi, N.; Tominaka, S.; Shiraishi, S.; Abreu-Sepulveda, M.; Manivannan, A.; Gotoh, K.; Fukunishi, M.; Dahbi, M. Structural Analysis of Sucrose-Derived Hard Carbon and Correlation with the Electrochemical Properties for Lithium, Sodium, and Potassium Insertion. *Chem. Mater.* **2020**, *32*, 2961–2977. [CrossRef]
4. Bernard, S.; Beyssac, O.; Benzerara, K.; Findling, N.; Tzvetkov, G.; Brown, G.E. XANES, Raman and XRD study of anthracene-based cokes and saccharose-based chars submitted to high-temperature pyrolysis. *Carbon* **2010**, *48*, 2506–2516. [CrossRef]
5. Myronyuk, I.F.; Mandzyuk, V.I.; Sachko, V.M.; Gun'ko, V.M. Structural features of carbons produced using glucose, lactose, and saccharose. *Nanoscale Res. Lett.* **2016**, *11*, 1–9. [CrossRef] [PubMed]
6. Wei, L.; Yushin, G. Electrical double layer capacitors with sucrose derived carbon electrodes in ionic liquid electrolytes. *J. Power Source* **2011**, *196*, 4072–4079. [CrossRef]
7. Bai, J.; Lu, B.; Bo, X.; Guo, L. Electrochemical property and electroanalytical application of large mesoporous carbons. *Electrochem. Commun.* **2010**, *12*, 1563–1567. [CrossRef]
8. Gao, Z.; Zhu, H.; Li, Y.; Fan, S.; Luo, H.; Xue, J.; Zhang, J. Preparation and electrochemical properties of sucrose-based porous carbon materials by combustion expansion-chemical activation method. *J. Appl. Electrochem.* **2020**, *50*, 549–558. [CrossRef]
9. Vazquez-Samperio, J.; Acevedo-Peña, P.; Guzmán-Vargas, A.; Reguera, E.; Cordoba-Tuta, E. Incorporation of heteroatoms into reticulated vitreous carbon foams derived from sucrose to improve its energy storage performance. *Int. J. Energy Res.* **2020**. [CrossRef]
10. Wei, L.; Yushin, G. Electrical double layer capacitors with activated sucrose-derived carbon electrodes. *Carbon* **2011**, *49*, 4830–4838. [CrossRef]
11. Krstić, S.; Kragović, M.; Dodevski, V.; Marinković, A.; Kaluđerović, B.; Žerjav, G.; Pintar, A.; Pagnacco, M.; Stojmenović, M. Influence of temperature and different hydroxides on properties of activated carbon prepared from saccharose. Characterization, thermal degradation kinetic and dyes removal from water solutions. *Sci. Sinter.* **2018**, *50*, 255–273. [CrossRef]
12. Vahdati-Khajeh, S.; Zirak, M.; Tejrag, R.Z.; Fathi, A.; Lamei, K.; Eftekhari-Sis, B. Biocompatible magnetic N-rich activated carbon from egg white biomass and sucrose: Preparation, characterization and investigation of dye adsorption capacity from aqueous solution. *Surf. Interfaces* **2019**, *15*, 157–165. [CrossRef]
13. Woźnica, N.; Hawełek, Ł.; Duber, S.; Fischer, H.; Honkimäki, V.; Pawlyta, M.; Bulou, A.; Burian, A. The atomic scale structure of saccharose-based carbons. *Philos. Mag.* **2017**, *97*, 1675–1697. [CrossRef]

14. Armandi, M.; Bonelli, B.; Geobaldo, F.; Garrone, E. Nanoporous carbon materials obtained by sucrose carbonization in the presence of KOH. *Microporous Mesoporous Mater.* **2010**, *132*, 414–420. [CrossRef]
15. Lang, X.; Wang, X.; Li, Y.; Cai, K.; Li, L.; Zhang, Q. Electrochemical performances of KOH activated carbon coated vanadium oxide with sucrose as carbon source for sulfur immobilizers of lithium-sulfur batteries. *Sustain. Energy Technol. Assess.* **2021**, *43*, 100947.
16. Zhao, H.; Lu, X.; Wang, Y.; Sun, B.; Wu, X.; Lu, H. Effects of additives on sucrose-derived activated carbon microspheres synthesized by hydrothermal carbonization. *J. Mater. Sci.* **2017**, *52*, 10787–10799. [CrossRef]
17. Wang, Q.; Li, H.; Chen, L.; Huang, X. Monodispersed hard carbon spherules with uniform nanopores. *Carbon* **2001**, *39*, 2211–2214. [CrossRef]
18. Kim, J.-K.; Cheruvally, G.; Ahn, J.-H. Electrochemical properties of $LiFePO_4$/C synthesized by mechanical activation using sucrose as carbon source. *J. Solid State Electrochem.* **2008**, *12*, 799–805. [CrossRef]
19. Wang, K.; Cai, R.; Yuan, T.; Yu, X.; Ran, R.; Shao, Z. Process investigation, electrochemical characterization and optimization of $LiFePO_4$/C composite from mechanical activation using sucrose as carbon source. *Electrochim. Acta* **2009**, *54*, 2861–2868. [CrossRef]
20. Scherdel, C.; Reichenauer, G. Microstructure and morphology of porous carbons derived from sucrose. *Carbon* **2009**, *47*, 1102–1111. [CrossRef]
21. Li, L.; Song, H.; Chen, X. Ordered mesoporous carbons from the carbonization of sulfuric-acid-treated silica/triblock copolymer/sucrose composites. *Microporous Mesoporous Mater.* **2006**, *94*, 9–14. [CrossRef]
22. Ting, C.-C.; Wu, H.-Y.; Vetrivel, S.; Saikia, D.; Pan, Y.-C.; Fey, G.T.K.; Kao, H.-M. A one-pot route to synthesize highly ordered mesoporous carbons and silicas through organic–inorganic self-assembly of triblock copolymer, sucrose and silica. *Microporous Mesoporous Mater.* **2010**, *128*, 1–11. [CrossRef]
23. Hwang, J.Y.; Li, M.; El-Kady, M.F.; Kaner, R.B. Next-Generation Activated Carbon Supercapacitors: A Simple Step in Electrode Processing Leads to Remarkable Gains in Energy Density. *Adv. Funct. Mater.* **2017**, *27*, 1605745. [CrossRef]
24. Chiu, Y.-H.; Lin, L.-Y. Effect of activating agents for producing activated carbon using a facile one-step synthesis with waste coffee grounds for symmetric supercapacitors. *J. Taiwan Inst. Chem. Eng.* **2019**, *101*, 177–185. [CrossRef]
25. Yang, C.; Lan, J.-L.; Liu, W.-X.; Liu, Y.; Yu, Y.-H.; Yang, X.-P. High-performance Li-ion capacitor based on an activated carbon cathode and well-dispersed ultrafine TiO_2 nanoparticles embedded in mesoporous carbon nanofibers anode. *ACS Appl. Mater. interfaces* **2017**, *9*, 18710–18719. [CrossRef]
26. Feng, J.; Chernova, N.A.; Omenya, F.; Tong, L.; Rastogi, A.C.; Whittingham, M.S. Effect of electrode charge balance on the energy storage performance of hybrid supercapacitor cells based on $LiFePO_4$ as Li-ion battery electrode and activated carbon. *J. Solid State Electrochem.* **2018**, *22*, 1063–1078. [CrossRef]
27. Okuda, R.; Nakano, K.; Suematsu, K.; Watanabe, K.; Ilnicka, A.; Łukaszewicz, J.P.; Shimanoe, K. Chemical Activation of Nitrogen-doped Carbon Derived from Chitosan with $ZnCl_2$ to Produce a High-performance Gas Diffusion-type Oxygen Electrode. *Electrochemistry* **2020**, *89*, 36–42. [CrossRef]
28. Ilnicka, A.; Kamedulski, P.; Skorupska, M.; Lukaszewicz, J.P. Metal-free nitrogen-rich carbon foam derived from amino acids for the oxygen reduction reaction. *J. Mater. Sci.* **2019**, *54*, 14859–14871. [CrossRef]
29. Ilnicka, A.; Lukaszewicz, J.P.; Shimanoe, K.; Yuasa, M. Urea treatment of nitrogen-doped carbon leads to enhanced performance for the oxygen reduction reaction. *J. Mater. Res.* **2018**, *33*, 1612. [CrossRef]
30. Huang, X.; Xie, Z.; He, X.; Sun, H.; Tong, C.; Xie, D. Electric double layer capacitors using activated carbon prepared from pyrolytic treatment of sugar as their electrodes. *Synth. Met.* **2003**, *135*, 235–236. [CrossRef]
31. Guo, P.; Gu, Y.; Lei, Z.; Cui, Y.; Zhao, X. Preparation of sucrose-based microporous carbons and their application as electrode materials for supercapacitors. *Microporous Mesoporous Mater.* **2012**, *156*, 176–180. [CrossRef]
32. Subramanian, N.; Viswanathan, B. Nitrogen-and oxygen-containing activated carbons from sucrose for electrochemical supercapacitor applications. *RSC Adv.* **2015**, *5*, 63000–63011. [CrossRef]
33. Kumar, R.; Soam, A.; Dusane, R.O.; Bhargava, P. Sucrose derived carbon coated silicon nanowires for supercapacitor application. *J. Mater. Sci. Mater. Electron.* **2018**, *29*, 1947–1954. [CrossRef]
34. Simon, P.; Gogotsi, Y. Materials for electrochemical capacitors. *Nanosci. Technol. Collect. Rev. Nat. J.* **2010**, 320–329. [CrossRef]
35. Luo, H.; Yang, Y.; Mu, B.; Chen, Y.; Zhang, J.; Zhao, X. Facile synthesis of microporous carbon for supercapacitors with a $LiNO_3$ electrolyte. *Carbon* **2016**, *100*, 214–222. [CrossRef]
36. Thommes, M.; Kaneko, K.; Neimark, A.V.; Olivier, J.P.; Rodriguez-Reinoso, F.; Rouquerol, J.; Sing, K.S. Physisorption of gases, with special reference to the evaluation of surface area and pore size distribution (IUPAC Technical Report). *Pure Appl. Chem.* **2015**, *87*, 1051–1069. [CrossRef]
37. Chmiola, J.; Yushin, G.; Gogotsi, Y.; Portet, C.; Simon, P.; Taberna, P.-L. Anomalous increase in carbon capacitance at pore sizes less than 1 nanometer. *Science* **2006**, *313*, 1760–1763. [CrossRef]
38. Huber, G.W.; Chheda, J.N.; Barrett, C.J.; Dumesic, J.A. Production of liquid alkanes by aqueous-phase processing of biomass-derived carbohydrates. *Science* **2005**, *308*, 1446–1450. [CrossRef]
39. Lee, Y.S.; Kim, Y.H.; Hong, J.S.; Suh, J.K.; Cho, G.J. The adsorption properties of surface modified activated carbon fibers for hydrogen storages. *Catal. Today* **2007**, *120*, 420–425. [CrossRef]

40. Paredes, J.; Martinez-Alonso, A.; Yamazaki, T.; Matsuoka, K.; Tascon, J.; Kyotani, T. Structural investigation of zeolite-templated, ordered microporous carbon by scanning tunneling microscopy and Raman spectroscopy. *Langmuir* **2005**, *21*, 8817–8823. [CrossRef]
41. Si, W.; Zhou, J.; Zhang, S.; Li, S.; Xing, W.; Zhuo, S. Tunable N-doped or dual N, S-doped activated hydrothermal carbons derived from human hair and glucose for supercapacitor applications. *Electrochim. Acta* **2013**, *107*, 397–405. [CrossRef]
42. Hao, P.; Zhao, Z.; Tian, J.; Li, H.; Sang, Y.; Yu, G.; Cai, H.; Liu, H.; Wong, C.; Umar, A. Hierarchical porous carbon aerogel derived from bagasse for high performance supercapacitor electrode. *Nanoscale* **2014**, *6*, 12120–12129. [CrossRef] [PubMed]
43. Ferrari, A.; Robertson, J. Resonant Raman spectroscopy of disordered, amorphous, and diamondlike carbon. *Phys. Rev. B* **2001**, *64*, 075414. [CrossRef]
44. Ferrari, A.C.; Robertson, J. Interpretation of Raman spectra of disordered and amorphous carbon. *Phys. Rev. B* **2000**, *61*, 14095. [CrossRef]
45. Kulkarni, S.B.; Patil, U.M.; Shackery, I.; Sohn, J.S.; Lee, S.; Park, B.; Jun, S. High-performance supercapacitor electrode based on a polyaniline nanofibers/3D graphene framework as an efficient charge transporter. *J. Mater. Chem. A* **2014**, *2*, 4989–4998. [CrossRef]
46. Tan, Y.; Xu, C.; Chen, G.; Fang, X.; Zheng, N.; Xie, Q. Facile synthesis of manganese-oxide-containing mesoporous nitrogen-doped carbon for efficient oxygen reduction. *Adv. Funct. Mater.* **2012**, *22*, 4584–4591. [CrossRef]
47. Liu, X.; Zhou, Y.; Zhou, W.; Li, L.; Huang, S.; Chen, S. Biomass-derived nitrogen self-doped porous carbon as effective metal-free catalysts for oxygen reduction reaction. *Nanoscale* **2015**, *7*, 6136–6142. [CrossRef] [PubMed]
48. Vázquez-Samperio, J.; Sánchez-Padilla, N.; Acevedo-Peña, P.; Cano, A.; Nava, N.; Morales-Acosta, D.; Oliver-Tolentino, M. Ni Prussian blue analogue/mesoporous carbon composite as electrode material for aqueous K-ion energy storage: Effect of carbon-framework interaction on its electrochemical behavior. *ChemistrySelect* **2018**, *3*, 11441–11450. [CrossRef]
49. Fan, X.; Zhang, L.; Zhang, G.; Shu, Z.; Shi, J. Chitosan derived nitrogen-doped microporous carbons for high performance CO_2 capture. *Carbon* **2013**, *61*, 423–430. [CrossRef]
50. Hulicova-Jurcakova, D.; Seredych, M.; Lu, G.Q.; Bandosz, T.J. Combined effect of nitrogen-and oxygen-containing functional groups of microporous activated carbon on its electrochemical performance in supercapacitors. *Adv. Funct. Mater.* **2009**, *19*, 438–447. [CrossRef]
51. Liu, H.; Song, H.; Chen, X.; Zhang, S.; Zhou, J.; Ma, Z. Effects of nitrogen-and oxygen-containing functional groups of activated carbon nanotubes on the electrochemical performance in supercapacitors. *J. Power Source* **2015**, *285*, 303–309. [CrossRef]
52. Seredych, M.; Hulicova-Jurcakova, D.; Lu, G.Q.; Bandosz, T.J. Surface functional groups of carbons and the effects of their chemical character, density and accessibility to ions on electrochemical performance. *Carbon* **2008**, *46*, 1475–1488. [CrossRef]
53. Chen, P.; Wang, L.-K.; Wang, G.; Gao, M.-R.; Ge, J.; Yuan, W.-J.; Shen, Y.-H.; Xie, A.-J.; Yu, S.-H. Nitrogen-doped nanoporous carbon nanosheets derived from plant biomass: An efficient catalyst for oxygen reduction reaction. *Energy Environ. Sci.* **2014**, *7*, 4095–4103. [CrossRef]
54. Wang, C.; Hu, F.; Yang, H.; Zhang, Y.; Lu, H.; Wang, Q. 1.82 wt.% Pt/N, P co-doped carbon overwhelms 20 wt.% Pt/C as a high-efficiency electrocatalyst for hydrogen evolution reaction. *Nano Res.* **2017**, *10*, 238–246. [CrossRef]
55. Fang, B.; Binder, L. A modified activated carbon aerogel for high-energy storage in electric double layer capacitors. *J. Power Source* **2006**, *163*, 616–622. [CrossRef]
56. Wu, D.; Chen, X.; Lu, S.; Liang, Y.; Xu, F.; Fu, R. Study on synergistic effect of ordered mesoporous carbon and carbon aerogel during electrochemical charge–discharge process. *Microporous Mesoporous Mater.* **2010**, *131*, 261–264. [CrossRef]
57. Yuan, D.; Chen, J.; Zeng, J.; Tan, S. Preparation of monodisperse carbon nanospheres for electrochemical capacitors. *Electrochem. Commun.* **2008**, *10*, 1067–1070. [CrossRef]
58. Hu, C.-C.; Wang, C.-C. Effects of electrolytes and electrochemical pretreatments on the capacitive characteristics of activated carbon fabrics for supercapacitors. *J. Power Source* **2004**, *125*, 299–308. [CrossRef]
59. An, K.H.; Jeon, K.K.; Heo, J.K.; Lim, S.C.; Bae, D.J.; Lee, Y.H. High-capacitance supercapacitor using a nanocomposite electrode of single-walled carbon nanotube and polypyrrole. *J. Electrochem. Soc.* **2002**, *149*, A1058. [CrossRef]
60. Pal, B.; Yang, S.; Ramesh, S.; Thangadurai, V.; Jose, R. Electrolyte selection for supercapacitive devices: A critical review. *Nanoscale Adv.* **2019**, *1*, 3807–3835. [CrossRef]
61. Zhao, Z.; Hao, S.; Hao, P.; Sang, Y.; Manivannan, A.; Wu, N.; Liu, H. Lignosulphonate-cellulose derived porous activated carbon for supercapacitor electrode. *J. Mater. Chem. A* **2015**, *3*, 15049–15056. [CrossRef]
62. Deng, Y.; Xie, Y.; Zou, K.; Ji, X. Review on recent advances in nitrogen-doped carbons: Preparations and applications in supercapacitors. *J. Mater. Chem. A* **2016**, *4*, 1144–1173. [CrossRef]
63. Chen, X.; Zhang, J.; Zhang, B.; Dong, S.; Guo, X.; Mu, X.; Fei, B. A novel hierarchical porous nitrogen-doped carbon derived from bamboo shoot for high performance supercapacitor. *Sci. Rep.* **2017**, *7*, 1–11. [CrossRef] [PubMed]
64. Shi, K.; Ren, M.; Zhitomirsky, I. Activated carbon-coated carbon nanotubes for energy storage in supercapacitors and capacitive water purification. *ACS Sustain. Chem. Eng.* **2014**, *2*, 1289–1298. [CrossRef]
65. Song, H.-K.; Hwang, H.-Y.; Lee, K.-H.; Dao, L.H. The effect of pore size distribution on the frequency dispersion of porous electrodes. *Electrochim. Acta* **2000**, *45*, 2241–2257. [CrossRef]
66. Macdonald, D.D. Reflections on the history of electrochemical impedance spectroscopy. *Electrochim. Acta* **2006**, *51*, 1376–1388. [CrossRef]

6. Literatura

[1] Y. Shao, M.F. El-Kady, J. Sun, Y. Li, Q. Zhang, M. Zhu, H. Wang, B. Dunn, R.B. Kaner, Design and mechanisms of asymmetric supercapacitors, Chemical Reviews, 118 (2018) 9233-9280.

[2] J.K. Nørskov, J. Rossmeisl, A. Logadottir, L. Lindqvist, J.R. Kitchin, T. Bligaard, H. Jonsson, Origin of the overpotential for oxygen reduction at a fuel-cell cathode, The Journal of Physical Chemistry B, 108 (2004) 17886-17892.

[3] P. Kamedulski, M. Skorupska, P. Binkowski, W. Arendarska, A. Ilnicka, J.P. Lukaszewicz, High surface area micro-mesoporous graphene for electrochemical applications, Scientific Reports, 11 (2021) 22054.

[4] G.-L. Chai, Z. Hou, D.-J. Shu, T. Ikeda, K. Terakura, Active sites and mechanisms for oxygen reduction reaction on nitrogen-doped carbon alloy catalysts: Stone–Wales defect and curvature effect, Journal of the American Chemical Society, 136 (2014) 13629-13640.

[5] K. Liu, S. Kattel, V. Mao, G. Wang, Electrochemical and computational study of oxygen reduction reaction on nonprecious transition metal/nitrogen doped carbon nanofibers in acid medium, The Journal of Physical Chemistry C, 120 (2016) 1586-1596.

[6] S.K. Singh, K. Takeyasu, J. Nakamura, Active sites and mechanism of oxygen reduction reaction electrocatalysis on nitrogen-doped carbon materials, Advanced Materials, 31 (2019) 1804297.

[7] L. Zhang, Z. Xia, Mechanisms of oxygen reduction reaction on nitrogen-doped graphene for fuel cells, The Journal of Physical Chemistry C, 115 (2011) 11170-11176.

[8] H. Kim, K. Min, S.E. Shim, D. Lim, S.-H. Baeck, Ni-doped Mn_2O_3 microspheres as highly efficient electrocatalyst for oxygen reduction reaction and Zn-air battery, International Journal of Hydrogen Energy, 47 (2022) 2378-2388.

[9] Y. Wang, T. Hu, Y. Chen, H. Yuan, Y. Qiao, Crystal facet-dependent activity of α-Mn_2O_3 for oxygen reduction and oxygen evolution reactions, International Journal of Hydrogen Energy, 45 (2020) 22744-22751.

[10] B. Chen, H.-J. Zhang, W. Zhao, T. Yuan, L. Sun, Y. Xue, Coal-Derived N-Doped Porous Carbon Accompanied with Fe_2O_3 for Oxygen Reduction Reaction, Journal of The Electrochemical Society, 169 (2022) 124511.

[11] S. Arya Gopal, A. Edathiparambil Poulose, C. Sudakar, A. Muthukrishnan, Kinetic insights into the mechanism of oxygen reduction reaction on Fe_2O_3/C composites, ACS Applied Materials & Interfaces, 13 (2021) 44195-44206.

[12] T. Odedairo, X. Yan, J. Ma, Y. Jiao, X. Yao, A. Du, Z. Zhu, Nanosheets Co_3O_4 interleaved with graphene for highly efficient oxygen reduction, ACS Applied Materials & Interfaces, 7 (2015) 21373-21380.
[13] L. Qin, R. Ding, H. Wang, J. Wu, C. Wang, C. Zhang, Y. Xu, L. Wang, B. Lv, Facile synthesis of porous nitrogen-doped holey graphene as an efficient metal-free catalyst for the oxygen reduction reaction, Nano Research, 10 (2017) 305-319.
[14] X. Zhang, X. Zhang, S. Zhao, Y.Q. Wang, X. Lin, Z.Q. Tian, P.K. Shen, Precursor modulated active sites of nitrogen doped graphene-based carbon catalysts via one-step pyrolysis method for the enhanced oxygen reduction reaction, Electrochimica Acta, 370 (2021) 137712.
[15] X. Lu, D. Wang, L. Ge, L. Xiao, H. Zhang, L. Liu, J. Zhang, M. An, P. Yang, Enriched graphitic N in nitrogen-doped graphene as a superior metal-free electrocatalyst for the oxygen reduction reaction, New Journal of Chemistry, 42 (2018) 19665-19670.
[16] K. Qu, Y. Zheng, S. Dai, S.Z. Qiao, Graphene oxide-polydopamine derived N, S-codoped carbon nanosheets as superior bifunctional electrocatalysts for oxygen reduction and evolution, Nano Energy, 19 (2016) 373-381.
[17] S. Ratso, I. Kruusenberg, M. Vikkisk, U. Joost, E. Shulga, I. Kink, T. Kallio, K. Tammeveski, Highly active nitrogen-doped few-layer graphene/carbon nanotube composite electrocatalyst for oxygen reduction reaction in alkaline media, Carbon, 73 (2014) 361-370.
[18] X. Hu, Y. Wu, H. Li, Z. Zhang, Adsorption and activation of O_2 on nitrogen-doped carbon nanotubes, The Journal of Physical Chemistry C, 114 (2010) 9603-9607.
[19] Y. Wang, W. Song, M. Li, Z. Wu, Oxygen reduction reaction mechanisms on heteroatom-doped single-walled carbon nanotube catalysts: Insights from a theoretical study, Journal of The Electrochemical Society, 166 (2019) F670.
[20] Y.J. Sa, C. Park, H.Y. Jeong, S.H. Park, Z. Lee, K.T. Kim, G.G. Park, S.H. Joo, Carbon nanotubes/heteroatom-doped carbon core–sheath nanostructures as highly active, metal-free oxygen reduction electrocatalysts for alkaline fuel cells, Angewandte Chemie, 126 (2014) 4186-4190.
[21] H. An, R. Zhang, Z. Li, L. Zhou, M. Shao, M. Wei, Highly efficient metal-free electrocatalysts toward oxygen reduction derived from carbon nanotubes@ polypyrrole core–shell hybrids, Journal of Materials Chemistry A, 4 (2016) 18008-18014.

[22] H. Zhang, Y. Niu, W. Hu, Nitrogen/sulfur-doping of graphene with cysteine as a heteroatom source for oxygen reduction electrocatalysis, Journal of Colloid and Interface Science, 505 (2017) 32-37.
[23] K. Cong, M. Radtke, S. Stumpf, B. Schröter, D.G. McMillan, M. Rettenmayr, A. Ignaszak, Electrochemical stability of the polymer-derived nitrogen-doped carbon: an elusive goal?, Materials for Renewable and Sustainable Energy, 4 (2015) 1-11.
[24] L. Lai, J.R. Potts, D. Zhan, L. Wang, C.K. Poh, C. Tang, H. Gong, Z. Shen, J. Lin, R.S. Ruoff, Exploration of the active center structure of nitrogen-doped graphene-based catalysts for oxygen reduction reaction, Energy & Environmental Science, 5 (2012) 7936-7942.
[25] K. Wan, Z.-P. Yu, Z.-X. Liang, Polyaniline-derived ordered mesoporous carbon as an efficient electrocatalyst for oxygen reduction reaction, Catalysts, 5 (2015) 1034-1045.
[26] J. Quílez-Bermejo, E. Morallón, D. Cazorla-Amorós, Oxygen-reduction catalysis of N-doped carbons prepared via heat treatment of polyaniline at over 1100^{o}C, Chemical Communications, 54 (2018) 4441-4444.
[27] H. Teng, J. Song, G. Xu, F. Gao, X. Luo, Nitrogen-doped graphene and conducting polymer PEDOT hybrids for flexible supercapacitor and electrochemical sensor, Electrochimica Acta, 355 (2020) 136772.
[28] S.K. Singh, X. Crispin, I.V. Zozoulenko, Oxygen reduction reaction in conducting polymer PEDOT: Density functional theory study, The Journal of Physical Chemistry C, 121 (2017) 12270-12277.
[29] Y. Zheng, Y. Jiao, L. Ge, M. Jaroniec, S.Z. Qiao, Two-step boron and nitrogen doping in graphene for enhanced synergistic catalysis, Angewandte Chemie International Edition, 52 (2013) 3110-3116.
[30] C. Han, Z. Chen, The mechanism study of oxygen reduction reaction (ORR) on non-equivalent P, N co-doped graphene, Applied Surface Science, 511 (2020) 145382.
[31] H. Lin, L. Chu, X. Wang, Z. Yao, F. Liu, Y. Ai, X. Zhuang, S. Han, Boron, nitrogen, and phosphorous ternary doped graphene aerogel with hierarchically porous structures as highly efficient electrocatalysts for oxygen reduction reaction, New Journal of Chemistry, 40 (2016) 6022-6029.
[32] Z.-S. Wu, S. Yang, Y. Sun, K. Parvez, X. Feng, K. Müllen, 3D nitrogen-doped graphene aerogel-supported Fe_3O_4 nanoparticles as efficient electrocatalysts for the oxygen reduction reaction, Journal of the American Chemical Society, 134 (2012) 9082-9085.

[33] B. Pal, S. Yang, S. Ramesh, V. Thangadurai, R. Jose, Electrolyte selection for supercapacitive devices: a critical review, Nanoscale Advances, 1 (2019) 3807-3835.
[34] S. Liu, L. Wei, H. Wang, Review on reliability of supercapacitors in energy storage applications, Applied Energy, 278 (2020) 115436.
[35] J. Libich, J. Máca, J. Vondrák, O. Čech, M. Sedlaříková, Supercapacitors: Properties and applications, Journal of Energy Storage, 17 (2018) 224-227.
[36] Z. Zhai, L. Zhang, T. Du, B. Ren, Y. Xu, S. Wang, J. Miao, Z. Liu, A review of carbon materials for supercapacitors, Materials & Design, (2022) 111017.
[37] H. Si, B. Wang, H. Chen, Y. Li, X. Zhang, X. Liang, L. Sun, S. Yang, D. Hou, Activated carbon prepared from rose branch using H_3PO_4-hydrothermal carbonization and activation and its apllication for supercapacitors, International Journal of Electrochemical Science, 14 (2019) 7899-7910.
[38] Q. Lu, S. Zhou, Y. Zhang, M. Chen, B. Li, H. Wei, D. Zhang, J. Zhang, Q. Liu, Nanoporous carbon derived from green material by an ordered activation method and its high capacitance for energy storage, Nanomaterials, 10 (2020) 1058.
[39] E. Gul, S.A. Shah, S.N.A. Shah, Chloride Salt-activated Carbon for Supercapacitors, Biomass-Based Supercapacitors: Design, Fabrication and Sustainability, (2023) 179-200.
[40] H. Benaddi, T. Bandosz, J. Jagiello, J. Schwarz, J. Rouzaud, D. Legras, F. Béguin, Surface functionality and porosity of activated carbons obtained from chemical activation of wood, Carbon, 38 (2000) 669-674.
[41] T. Zhu, Y. Lu, S. Zheng, Y. Chen, H. Guo, Influence of nitric acid acitivation on structure and capacitive performances of ordered mesoporous carbon, Electrochimica Acta, 152 (2015) 456-463.
[42] Z. Yang, R. Gleisner, D. H. Mann, J. Xu, J. Jiang, J. Zhu, Lignin based activated carbon using H_3PO_4 activation, Polymers, 12 (2020) 2829.
[43] J. Xu, L. Chen, H. Qu, Y. Jiao, J. Xie, G. Xing, Preparation and characterization of activated carbon from reedy grass leaves by chemical activation with H_3PO_4, Applied Surface Science, 320 (2014) 674-680.
[44] H. Marsh, D.S. Yan, T.M. O'Grady, A. Wennerberg, Formation of active carbons from cokes using potassium hydroxide, Carbon, 22 (1984) 603-611.
[45] J. Wang, S. Kaskel, KOH activation of carbon-based materials for energy storage, Journal of Materials Chemistry, 22 (2012) 23710-23725.
[46] Y.-X. Yang, K.-K. Ge, S. ur Rehman, H. Bi, Nanocarbon-based electrode materials applied for supercapacitors, Rare Metals, 41 (2022) 3957-3975.

[47] S. Ghosh, S. Barg, S.M. Jeong, K. Ostrikov, Heteroatom-doped and oxygen-functionalized nanocarbons for high-performance supercapacitors, Advanced Energy Materials, 10 (2020) 2001239.
[48] C. An, Y. Zhang, H. Guo, Y. Wang, Metal oxide-based supercapacitors: progress and prospectives, Nanoscale Advances, 1 (2019) 4644-4658.
[49] Z. Wang, M. Zhu, Z. Pei, Q. Xue, H. Li, Y. Huang, C. Zhi, Polymers for supercapacitors: Boosting the development of the flexible and wearable energy storage, Materials Science and Engineering: R: Reports, 139 (2020) 100520.
[50] K.-B. Wang, Q. Xun, Q. Zhang, Recent progress in metal-organic frameworks as active materials for supercapacitors, EnergyChem, 2 (2020) 100025.
[51] K. Li, J. Li, Q. Zhu, B. Xu, Three-dimensional MXenes for supercapacitors: a review, Small Methods, 6 (2022) 2101537.
[52] Y. Zhou, W. Guo, T. Li, A review on transition metal nitrides as electrode materials for supercapacitors, Ceramics International, 45 (2019) 21062-21076.
[53] T. Bhat, P. Patil, R. Rakhi, Recent trends in electrolytes for supercapacitors, Journal of Energy Storage, 50 (2022) 104222.
[54] Z. Fu, Z. Li, P. Si, F. Tao, A hierarchical energy management strategy for fuel cell/battery/supercapacitor hybrid electric vehicles, International journal of hydrogen energy, 44 (2019) 22146-22159.
[55] M.S. Asl, R. Hadi, L. Salehghadimi, A.G. Tabrizi, S. Farhoudian, A. Babapoor, M. Pahlevani, Flexible all-solid-state supercapacitors with high capacitance, long cycle life, and wide operational potential window: Recent progress and future perspectives, Journal of Energy Storage, 50 (2022) 104223.
[56] D. Majumdar, M. Mandal, S.K. Bhattacharya, Journey from supercapacitors to supercapatteries: recent advancements in electrochemical energy storage systems, Emergent Materials, 3 (2020) 347-367.
[57] G. Wang, L. Zhang, J. Zhang, A review of electrode materials for electrochemical supercapacitors, Chemical Society Reviews, 41 (2012) 797-828.
[58] S. Lu, W. Yang, M. Zhou, L. Qiu, B. Tao, Q. Zhao, X. Wang, L. Zhang, Q. Xie, Y. Ruan, Nitrogen-and oxygen-doped carbon with abundant micropores derived from biomass waste for all-solid-state flexible supercapacitors, Journal of Colloid and Interface Science, 610 (2022) 1088-1099.
[59] P. Haldar, Achieving wide potential window and high capacitance for supercapacitors using different metal oxides (viz.: ZrO_2, WO_3 and V_2O_5) and their

PANI/graphene composites with Na_2SO_4 electrolyte, Electrochimica Acta, 381 (2021) 138221.
[60] P. Dubey, V. Shrivastav, M. Singh, P.H. Maheshwari, S. Sundriyal, S.R. Dhakate, Electrolytic Study of Pineapple Peel Derived Porous Carbon for All-Solid-State Supercapacitors, ChemistrySelect, 6 (2021) 11736-11746.
[61] A. Eftekhari, Supercapacitors utilising ionic liquids, Energy Storage Materials, 9 (2017) 47-69.
[62] F. Al-Hazmi, G.H. Al-Harbi, G.W. Beall, A. Al-Ghamdi, A. Obaid, W.E. Mahmoud, One pot synthesis of graphene based on microwave assisted solvothermal technique, Synthetic Metals, 200 (2015) 54-57.
[63] R. Jakhar, J.E. Yap, R. Joshi, Microwave reduction of graphene oxide, Carbon, 170 (2020) 277-293.

7. Streszczenie

W niniejszej rozprawie doktorskiej przedstawiono wyniki badań przeprowadzonych w celu zaprojektowania i otrzymania nowych materiałów domieszkowanych heteroatomami azotu do zróżnicowanych zastosowań. Przeprowadzone badania skupiały się na poszukiwaniu alternatywnych katalizatorów dla reakcji redukcji tlenu oraz jako elektrody dla superkondensatorów. Prace obejmowały zoptymalizowanie metod syntezy materiałów węglowych poprzez wykorzystanie promieniowania mikrofalowego, templatów twardych ($CaCO_3$ i Na_2CO_3), a także poprzez zastosowanie kwasu ortofosforowego (V) w celu zwiększenia pola powierzchni właściwej i rozwoju porowatości materiałów węglowych. Otrzymane materiały zostały w pełni scharakteryzowane za pomocą technik fizyko-chemicznych takich jak analiza sorpcji azotu, spektrometria Ramana oraz metod mikroskopowych (HRTEM, SEM, AFM). Wzbogacenie struktury grafenowej było możliwe za sprawą naturalnych nośników azotu (żelatyny, chitozanu, zielonych alg), a także organicznego materiału chemicznego azodikarbonamidu (ADC). W celu określenia procentowej zawartości azotu oraz pozostałych pierwiastków zawartych w strukturze węglowej zastosowano analizę elementarną, dodatkowo w celu identyfikacji azotowych grup funkcyjnych wzbogacających strukturę grafenową wykorzystano rentgenowską spektroskopię fotoelektronów (XPS).

Wszystkie otrzymane materiały zostały poddane elektrochemicznej weryfikacji w celu ustalenia potencjalnego zastosowania. Otrzymane materiały węglowe domieszkowane azotem zostały przebadane w reakcji redukcji tlenu, a także wykorzystano jako elektrody w superkondensatorze. Badania elektrochemiczne dla reakcji redukcji tlenu obejmowały woltamperometrię cykliczną (CV) oraz liniową (LSV), a także testy stabilności materiałów węglowych w środowisku alkalicznym. Za pomocą metod elektrochemicznych określono mechanizm procesu redukcji tlenu. Ponadto określono wpływ obecności azotowych grup funkcyjnych na właściwości katalityczne w reakcji ORR. Testy elektrochemiczne elektrod w superkondensatorach obejmowały woltamperometrię cykliczną, cykle galwanostatycznego ładowania i rozładowania (GCD), a także spektroskopię impedancyjną (EIS) dla układu dwuelektrodowego. Dla otrzymanych materiałów węglowych określony został wpływ morfologii, pola powierzchni właściwej, a także obecności azotowych grup funkcyjnych na pojemność właściwą otrzymanych materiałów.

8. Abstract

This doctoral dissertation presents the research results conducted to design and obtain new materials doped with nitrogen heteroatoms for various applications. The research focused on searching for alternative catalysts for oxygen reduction reactions and as electrodes for supercapacitors. The works included optimization of the method of synthesis of carbon materials using microwave radiation, the use of hard templates ($CaCO_3$ and Na_2CO_3), as well as the use of orthophosphoric acid (V) to increase the specific surface area and develop the porosity of carbon materials. The obtained materials were fully characterized using physicochemical techniques using methods such as nitrogen sorption analysis, Raman spectroscopy, and microscopic methods (HRTEM, SEM, AFM). The enrichment of the graphene structure was possible thanks to natural nitrogen carriers (gelatine, chitosan, green algae) and organic chemical material azodicarbonamide (ADC). To determine the percentage content of nitrogen and other elements contained in the carbon structure, elemental analysis was used, and additionally, X-ray photoelectron spectroscopy (XPS) was used to identify nitrogen functional groups enriching the graphene structure.

Obtained materials were subjected to electrochemical verification in order to determine their potential application. The obtained carbon materials doped with nitrogen were tested in the oxygen reduction reaction and used as electrodes in a supercapacitor. Electrochemical studies for the oxygen reduction reaction included cyclic (CV) and linear (LSV) voltammetry, as well as tests of the stability of carbon materials in an alkaline environment. Using electrochemical methods, the mechanism of the oxygen reduction process was determined. In addition, the influence of the presence of nitrogen functional groups on the catalytic properties of the ORR reaction was determined. Electrochemical tests of supercapacitors electrodes included cyclic voltammetry, galvanostatic charge and discharge cycles (GCD) and impedance spectroscopy (EIS) for a two electrodes system. For the obtained carbon materials, the influence of morphology, specific surface area and the presence of nitrogen functional groups on the specific capacity of the obtained materials was determined.

9. Oświadczenia współautorów

Dr Piotr Kamedulski
Interdyscyplinarne Centrum Nowoczesnych Technologii
Uniwersytet Mikołaja Kopernika w Toruniu,
ul. Wileńska 4, 87-100 Toruń

Toruń, 31.07.2023 r.

Oświadczenie

W związku z ubieganiem się Pani mgr Małgorzaty Skorupskiej o stopień doktora w dziedzinie nauk ścisłych i przyrodniczych w dyscyplinie nauki chemiczne oświadczam, że w publikacji:

M. Skorupska, P. Kamedulski, J. P. Łukaszewicz, A. Ilnicka, The Improvement of Energy Storage Performance by Sucrose-Derived Carbon Foams via Incorporating Nitrogen Atoms, Nanomaterials, 2021, 11(3), 760; https://doi.org/10.3390/nano11030760

Mój wkład polegał na: pomocy w przygotowaniu metodologii prac badawczych, przeprowadzeniu części badań, wykonaniu analizy części wyników, udziale w przygotowaniu rysunków, udziale w przygotowaniu części manuskryptu.

Piotr Kamedulski

.....

Podpis

UNIWERSYTET MIKOŁAJA KOPERNIKA W TORUNIU
Wydział Chemii

UCZELNIA BADAWCZA
INICJATYWA DOSKONAŁOŚCI

Dr hab. Anna Ilnicka, prof. UMK
Wydział Chemii,
Uniwersytet Mikołaja Kopernika w Toruniu,
ul. Gagarina 7, 87-100 Toruń

Toruń, 01.09.2023 r.

Oświadczenie

W związku z ubieganiem się Pani mgr Małgorzaty Skorupskiej o stopień doktora w dziedzinie nauk ścisłych i przyrodniczych w dyscyplinie nauki chemiczne oświadczam, że w pracy:

1. M. Skorupska, A. Ilnicka, J.P. Łukaszewicz N-doped graphene foam obtained by microwave-assisted exfoliation of graphite, Scientific Reports, 2021, 11 (1), 1-11; https://doi.org/10.1038/s41598-021-81769-5

   Mój wkład polegał na: udziale w zaplanowaniu koncepcji pracy, udziale w zaplanowaniu części metodyki, udziale w przeprowadzeniu części badań, wykonaniu analizy części wyników, udziale w przygotowaniu rysunków, udziale w przygotowaniu części manuskryptu, sprawdzeniu i uzupełnieniu odpowiedzi na recenzje.

2. M. Skorupska, A. Ilnicka, P. Kamedulski, J. P. Łukaszewicz, The Improvement of Energy Storage Performance by Sucrose-Derived Carbon Foams via Incorporating Nitrogen Atoms, Nanomaterials, 2021, 11(3), 760; https://doi.org/10.3390/nano11030760

   Mój wkład polegał na: pomocy w zaplanowaniu części metodyki, przeprowadzeniu części badań, wykonaniu analizy części wyników, udziale w przygotowaniu rysunków, udziale w przygotowaniu części manuskryptu, sprawdzeniu i uzupełnieniu odpowiedzi na recenzje.

3. M. Skorupska, A. Ilnicka, J. P. Łukaszewicz, The effect of nitrogen species on the catalytic properties of N-doped graphene, Scientific Reports, 2021, 11(1), 1-11; https://doi.org/10.1038/s41598-021-03403-8

   Mój wkład polegał na: udziale w zaplanowaniu części metodyki, udziale w przygotowaniu części manuskryptu, sprawdzeniu i uzupełnieniu odpowiedzi na recenzje.

4. M. Skorupska, A. Ilnicka, J. P. Łukaszewicz, Successful Manufacturing Protocols of N-Rich Carbon Electrodes Ensuring High ORR Activity: A Review, Processes, 2022, 10(4), 643; https://doi.org/10.3390/pr10040643
   Mój wkład polegał na: współtworzeniu pomysłu na napisanie manuskryptu, udziale w zaplanowaniu koncepcji badań, udziale w przygotowaniu części manuskryptu, sprawdzeniu i uzupełnieniu odpowiedzi na recenzje.

5. M. Skorupska, A. Ilnicka, J. P. Łukaszewicz, Modified graphene foam as a high-performance catalyst for oxygen reduction reaction, RSC Advances, 2023, 13, 25437–25442, https://doi.org/10.1039/D3RA04203K
   Mój wkład polegał na: udziale w zaplanowaniu koncepcji badań, udziale w zaplanowaniu części metodyki, wykonaniu analizy części wyników, udziale w przygotowaniu rysunków, udziale w przygotowaniu części manuskryptu, sprawdzeniu i uzupełnieniu odpowiedzi na recenzje.

Anna Ilnicka
Podpis

UNIWERSYTET
MIKOŁAJA KOPERNIKA
W TORUNIU
Wydział Chemii

UCZELNIA
BADAWCZA
INICJATYWA DOSKONAŁOŚCI

Prof. dr hab. Jerzy P. Łukaszewicz
Wydział Chemii
Uniwersytet Mikołaja Kopernika w Toruniu
ul. Gagarina 7, 87-100 Toruń

Toruń, 01.09.2023r.

Oświadczenie

W związku z ubieganiem się Pani mgr Małgorzaty Skorupskiej o stopień doktora w dziedzinie nauk ścisłych i przyrodniczych w dyscyplinie nauki chemiczne oświadczam, że w pracy:

1. M. Skorupska, A. Ilnicka, J.P. Łukaszewicz N-doped graphene foam obtained by microwave-assisted exfoliation of graphite, Scientific Reports, 2021 11 (1), 1-11; https://doi.org/10.1038/s41598-021-81769-5
   Mój wkład polegał na: współtworzeniu pomysłu na przeprowadzenie badań, sprawdzeniu manuskryptu, sprawdzeniu i uzupełnieniu odpowiedzi na recenzje.

2. M. Skorupska, A. Ilnicka, P. Kamedulski, J. P. Łukaszewicz, The Improvement of Energy Storage Performance by Sucrose-Derived Carbon Foams via Incorporating Nitrogen Atoms, Nanomaterials, 2021, 11(3), 760; https://doi.org/10.3390/nano11030760
   Mój wkład polegał na: współtworzeniu pomysłu na przeprowadzenie badań, udziale w zaplanowaniu części metodyki, sprawdzeniu manuskryptu, sprawdzeniu i uzupełnieniu odpowiedzi na recenzje.

3. M. Skorupska, A. Ilnicka, J. P. Łukaszewicz, The effect of nitrogen species on the catalytic properties of N-doped graphene, Scientific Reports, (2021), 11(1), 1-11; https://doi.org/10.1038/s41598-021-03403-8
   Mój wkład polegał na: udziale w zaplanowaniu koncepcji badań, sprawdzeniu manuskryptu, sprawdzeniu i uzupełnieniu odpowiedzi na recenzje.

UNIWERSYTET MIKOŁAJA KOPERNIKA W TORUNIU Wydział Chemii
ul. Gagarina 7, 87-100 Toruń, Polska, tel. +48 56 611 43 02, e-mail: wydzial@chem.umk.pl
chem.umk.pl

4. M. Skorupska, A. Ilnicka, J. P. Łukaszewicz, Successful Manufacturing Protocols of N-Rich Carbon Electrodes Ensuring High ORR Activity: A Review, Processes, (2022), 10(4), 643; https://doi.org/10.3390/pr10040643
   Mój wkład polegał na: udziale w zaplanowaniu koncepcji manuskryptu, sprawdzeniu manuskryptu.

5. M. Skorupska, A. Ilnicka, J. P. Łukaszewicz, Modified graphene foam as a high-performance catalyst for oxygen reduction reaction, RSC Advances, 2023, 13, 25437–25442, https://doi.org/10.1039/D3RA04203K
   Mój wkład polegał na: udziale w nadzorowaniu badań, sprawdzeniu manuskryptu, sprawdzeniu i uzupełnieniu odpowiedzi na recenzje.

.....
Podpis

10. Dorobek naukowy

Publikacje naukowe z listy MEiN

1. P. Grabowska, M. Szkoda, M. Skorupska, J. P. Łukaszewicz, A. Ilnicka, *Synergistic Effects of Nitrogen-Doped Carbon and Praseodymium Oxide in Electrochemical Water Splitting*, Scientific Reports, 2023 (IF=4.6, MEiN=140), zaakceptowana przez edytora

2. M. Skorupska, A. Ilnicka, J. P. Łukaszewicz, *Modified graphene foam as a high-performance catalyst for oxygen reduction reaction,* RSC Advances, 2023, 13, 25437–25442; https://doi.org/10.1039/D3RA04203K (IF=4.036, MEiN=100)

3. M. Skorupska, K. Kowalska, M. Tyc, A. Ilnicka, M. Szkoda, J. P. Łukaszewicz, *Exfoliated graphite with spinel oxide as an effective hybrid electrocatalyst for water splitting*, RSC Advances, 2023, 13 (15), 10215-10220; https://doi.org/10.1039/d3ra00589e (IF=4.036 , MEiN=100)

4. A. Ilnicka, M. Skorupska, M. Szkoda, Z. Zarach, J. P. Łukaszewicz *N-doped carbon materials as electrodes for highly stable supercapacitors,* Materials Research Letters 2023, 11 (3), 213-221; https://doi.org/10.1080/21663831.2022.2139163 (IF=8.3, MEiN=140)

5. M. Szkoda, A. Ilnicka, M. Skorupska, M. Wysokowski, J. P. Łukaszewicz, *Modification of TiO_2 nanotubes by graphene-strontium and cobalt molybdate perovskite for efficient hydrogen evolution reaction in acidic medium,* Materials Research Letters, 2022, 12, 22577; https://doi.org/10.21203/rs.3.rs-2116956/v1 (IF=8.3, MEiN=140)

6. P. Kamedulski, M. Skorupska, I. Koter, M. Lewandowski, V. K. Abdelkader-Fernández, J. P. Łukaszewicz, *Obtaining N-Enriched Mesoporous Carbon-Based by Means of Gamma Radiation,* Nanomaterials, 2022, 12(18), 3156; https://doi.org/10.3390/nano12183156 (IF=5.3, MEiN=100)

7. M. Skorupska, A. Ilnicka, J. P. Łukaszewicz, *Successful Manufacturing Protocols of N-Rich Carbon Electrodes Ensuring High ORR Activity: A Review,* Processes, 2022, 10(4), 643; https://doi.org/10.3390/pr10040643 (IF=3.5, MEiN=70)

8. M. Skorupska, A. Ilnicka, J. P. Łukaszewicz, *The effect of nitrogen species on the catalytic properties of N-doped graphene,* Scientific Reports, 2021, 11(1), 1-11; https://doi.org/10.1038/s41598-021-03403-8 (IF=4.6, MEiN=140)

9. A. Ilnicka, M. Skorupska, M. Szkoda, Z. Zarach, P. Kamedulski, W. Zieliński, J. P. Łukaszewicz, *Combined effect of nitrogen-doped functional groups and porosity of porous carbons on electrochemical performance of supercapacitor*, Scientific Reports, 2021, 11 (1), 1-11; https://doi.org/10.1038/s41598-021-97932-x (IF=4.6, MEiN=140)

10. P. Kamedulski, M. Skorupska, P. Binkowski, W. Arendarska, A. Ilnicka, J. P. Łukaszewicz, *High surface area micro-mesoporous graphene for electrochemical applications,* Scientific Reports, 2021, 11 (1), 1-12; https://doi.org/10.1038/s41598-021-01154-0 (IF=4.6, MEiN=140)

11. A. Ilnicka, M. Skorupska, M. Tyc, K. Kowalska, P. Kamedulski, W. Zieliński, J. P. Łukaszewicz, *Green algae and gelatine derived nitrogen rich carbon as an outstanding competitor to Pt loaded carbon catalysts,* Scientific Reports, 2021, 11 (1), 1-13; https://doi.org/10.1038/s41598-021-86507-5 (IF=4.6, MEiN=140)

12. M. Skorupska, A. Ilnicka, P. Kamedulski, J. P. Łukaszewicz, *The Improvement of Energy Storage Performance by Sucrose-Derived Carbon Foams via Incorporating Nitrogen Atoms,* Nanomaterials, 2021, 11(3), 760; https://doi.org/10.3390/nano11030760 (IF=5.3, MEiN=100)

13. M. Skorupska, A. Ilnicka, J. P. Łukaszewicz *N-doped graphene foam obtained by microwave-assisted exfoliation of graphite,* Scientific Reports, 2021, 11 (1), 1-11; https://doi.org/10.1038/s41598-021-81769-5 (IF=4.6, MEiN=140)

14. W. Zieliński, P. Kamedulski, A. Smolarkiewicz-Wyczachowski, M. Skorupska, J. P. Łukaszewicz, A. Ilnicka, *Synthesis of Hybrid Carbon Materials Consisting of N-Doped Microporous Carbon and Amorphous Carbon Nanotubes,* Materials, 2020, 13 (13), 2997; https://doi.org/10.3390/ma13132997 (IF=3.4, MEiN=140)

15. A. Ilnicka, M. Skorupska, P. Romanowski, P. Kamedulski, J. P. Łukaszewicz, *Improving the Performance of Zn-Air Batteries with N-Doped Electroexfoliated Graphene,* Materials, 2020, 13(9), 2115; https://doi.org/10.3390/ma13092115 (IF=3.4, MEiN=140)

16. A. Ilnicka, P. Kamedulski, M. Skorupska, J. P. Łukaszewicz, *Metal-free nitrogen-rich carbon foam derived from amino acids for oxygen reduction reaction,* Journal of Materials Science, 2019, 54 (24), 14859-14871; https://doi.org/10.1007/s10853-019-03969-9 (IF=4.5, MEiN=100)

17. A. Ilnicka, M. Skorupska, P. Kamedulski, J. P. Łukaszewicz, *Electro-Exfoliation of Graphite to Graphene in an Aqueous Solution of Inorganic Salt and the Stabilization of Its Sponge Structure with Poly(Furfuryl Alcohol),* Nanomaterials, 2019, 9 (7), 971*;* https://doi.org/10.3390/nano9070971 (IF=5.3, MEiN=100)

18. P. Kamedulski, A. Ilnicka, J. P. Łukaszewicz, M. Skorupska, *Highly effective three-dimensional functionalization of graphite to graphene by wet chemical exfoliation methods,* Adsorption, 2019, 25, 631-638; https://doi.org/10.1007/s10450-019-00067-9 (IF=3.3 , MEiN=70)

<u>Czynny udział w konferencjach</u>

1. A. Ilnicka, M. Szkoda, D. Roda, P. Grabowska, **M. Skorupska**, J. P. Łukaszewicz, Wodór paliwem przyszłości – wyzwania i perspektywy dla rozwoju wydajnych elektrokatalizatorów, 65. Zjazd Naukowy Polskiego Towarzystwa Chemicznego, Toruń, 18-22.09.2023, komunikat ustny.
2. A. Ilnicka, **M. Skorupska,** M. Szkoda, P. Grabowska, L. Kubinska, J. P. Łukaszewicz, Highly stable and bifunctional catalysts based on graphene for production of green hydrogen, 33rd International Conference on Diamond and Carbon Materials, Majorka (Hiszpania), 10-14.09.2023, komunikat ustny.

3. P. Grabowska, **M. Skorupska**, A. Ilnicka, Badanie wpływu heteroatomów oraz struktury grafenowej na wydajność elektrokatalityczną tlenku typu perowskit domieszkowanego prazeodymem w reakcji elektrolizy wody, XVI Kopernikańskie Seminarium Doktoranckie, Toruń, 29-30.06.2023, komunikat ustny.
4. L. Kubińska, **M. Skorupska**, M. Szkoda, J. P. Łukaszewicz, A. Ilnicka, Hybrydowe materiały węglowe zawierające tlenki niklu i kobaltu jako bifunkcyjne materiały elektrodowe, NanoBioMateriały – od teorii do aplikacji, Toruń, Toruń, 14-16.06.2023, komunikat ustny.
5. P. Grabowska, **M. Skorupska**, M. Szkoda, J. P. Łukaszewicz, A. Ilnicka, Tlenki typu perowskit domieszkowane prazeodymem jako efektywnie działające elektrokatalizatory procesu otrzymywania zielonego wodoru, NanoBioMateriały - od teorii do aplikacji, Toruń, Toruń, 14-16.06.2023, prezentacja posterowa.
6. A. Ilnicka, P. Grabowska, **M. Skorupska**, M. Szkoda, J. P. Łukaszewicz, Hybrid electrode materials containing carbon and perovskite-like oxides as effective and highly stable catalysts for water splitting, E-MRS European Materials Research Society, Strasburg (Francja), 29.05-2.06.2023, komunikat ustny.
7. M. Szkoda, D. Roda, A. Ilnicka, **M. Skorupska**, J. P. Łukaszewicz, Molybdenum sulfide modified with nickel nanoparticles as an effective catalyst for hydrogen evolution reaction, E-MRS European Materials Research Society, Strasburg (Francja), 29.05-2.06.2023, prezentacja posterowa.
8. P. Grabowska, **M. Skorupska**, S. Kurtuluş, A. Ilnicka, Badanie wpływu katalizatorów węglowych zawierających heteroatomy azotu i boru na aktywność elektrochemiczną reakcji HER i OER, XVII Ogólnokrajowa Konferencja Młodzi Naukowcy w Polsce Badania i Rozwój, Lublin, 22.05.2023, prezentacja posterowa.
9. **M. Skorupska**, A. Ilnicka, J. P. Łukaszewicz „Nitrogen-doped graphene foams as efective catalysts for oxygen reduction reaction”, Solar2Chem Winter School “Materials and Methods for Solar Chemical Production” Universitat Politècnica de València (UPV), Hiszpania, 22-24.02.2023, prezentacja posterowa.
10. P. Kamedulski, R. Szczęsny, A. Ścigała, **M. Skorupska**, N. Szubarga, P. Gauden, “Eksperymentalne oraz teoretyczne badania nanostrukturalnych kompozytowych warstw światłoczułych Alq3/materiał węglowy”, XIII konferencja naukowo-techniczna: Materiały węglowe i kompozyty polimerowe: nauka - przemysł', Ustroń-Jaszowiec, 23-26.11.2021, prezentacja posterowa.

11. J. P. Łukaszewicz, A. Ilnicka, P. Kamedulski, **M. Skorupska**, „Building 3D Porous Graphene Electrode Platforms via Exfoliation of Commercial Graphene and Graphite Powders", Materials Research Meeting, Yokohama (Japonia), 13-16.12.2021, komunikat ustny.

12. M. Skorupska, A. Ilnicka, M. Tyc, K. Kowalska, M. Szkoda, J. P. Łukaszewicz, „Graphene-based catalysts for water splitting technology", The World Conference on Carbon „Carbon for a Cleaner Future", Londyn, 03-08-07.2022, komunikat ustny.

13. M. Skorupska, M. Szkoda, A. Ilnicka, J. P. Łukaszewicz, „Modification of TiO_2 nanotubes by strontium and cobalt molybdate perovskite for efficient hydrogen evolution reaction in acid and alkaline media", The World Conference on Carbon „Carbon for a Cleaner Future", Londyn, 03-08-07.2022, prezentacja posterowa.

14. M. Skorupska, A. Ilnicka, J. P. Łukaszewicz, Synteza bez platynowych materiałów 3D grafenowych do reakcji redukcji tlenu, XV Kopernikańskie Seminarium Doktoranckie, Toruń, 20-22.06.2022, komunikat ustny.

15. A. Ilnicka, **M. Skorupska**, M. Szkoda, M. Tyc, K. Kowalska, J. P. Łukaszewicz, „Elektrokatalizatory na bazie grafenu dla technologii rozszczepiania wody efektywnej metody produkcji zielonego wodoru", XV Międzynarodowe Targi Wynalazków i Innowacji, INTARG® 2022, Katowice, 11-12.05.2022, prezentacja wynalazku/posteru.

16. M. Skorupska, A. Ilnicka, J. P. Łukaszewicz, „Piany grafenowe domieszkowane heteroatomami do zastosowań elektrodowych w bateriach metal-powietrze", XV Międzynarodowe Targi Wynalazków i Innowacji - INTARG® 2022, Katowice, 11-12.05.2022, prezentacja wynalazku/posteru.

17. P. Kamedulski, R. Szczęsny, A. Ścigała, **M. Skorupska**, N. Szubarga, P. Gauden, "Eksperymentalne oraz teoretyczne badania nanostrukturalnych kompozytowych warstw światłoczułych Alq3/materiał węglowy", XIII konferencja naukowo-techniczna: Materiały węglowe i kompozyty polimerowe: nauka - przemysł, Ustroń-Jaszowiec, 23-26.11.2021, prezentacja posterowa.

18. J. P. Łukaszewicz, A. Ilnicka, P. Kamedulski, **M. Skorupska**, „Building 3D Porous Graphene Electrode Platforms via Exfoliation of Commercial Graphene and Graphite Powders", Materials Research Meeting, Yokohama (Japonia), 13-16.12.2021, komunikat ustny.

19. A. Ilnicka, **M. Skorupska**, M. Szkoda, Z. Zarach, P. Kamedulski, W. Zieliński, J. P. Łukaszewicz, "Hybrid carbon materials based on activated carbon and graphene as electrodes for highly stable supercapacitors", The Next Generation Group of the Carbon Society of Japan, konferencja on-line, 30.11.2021, komunikat ustny.
20. A. Ilnicka, **M. Skorupska**, M. Szkoda, P. Kamedulski, W. Zieliński, J. P. Łukaszewicz, „Hybrid nanostructured nitrogen-doped carbon as electrode for supercapacitors", 31st International Conference on Diamond and Carbon Materials, konferencja on-line, 6-9.09.2021, komunikat ustny.
21. **M. Skorupska**, A. Ilnicka, J. P. Łukaszewicz, „Pt-free catalyst of graphene and carbon foam for oxygen reduction reaction", 31st International Conference on Diamond and Carbon Materials, konferencja on-line, 6-9.09.2021, komunikat ustny.
22. A. Ilnicka, P. Kamedulski, W. Zieliński, **M. Skorupska**, J. P. Łukaszewicz, Graphene-based hybrid carbon materials for electrochemical application" Webinar on Graphene Technology" iGRAPHENE 2021, 24-25.03.2021, komunikat ustny.
23. **M. Skorupska**, A. Ilnicka, J. P. Łukaszewicz, Synthesis Of Carbon-Graphene Foams for Electrochemical Device, "Webinar on Graphene Technology" iGRAPHENE 2021, 24-25.03.2021, komunikat ustny.
24. A. Ilnicka, **M. Skorupska**, P. Kamedulski, W. Zieliński, J. P. Łukaszewicz, Hybrid materials containing nitrogen-doped carbon and graphene, Webinar on Graphene Technology" iGRAPHENE 2020, konferencja on-line, 19-20.10.2020, komunikat ustny.
25. **M. Skorupska**, A. Ilnicka, J. P. Łukaszewicz, Synthesis of N-doped Graphene foams by microwave exfoliation method, "Webinar on Graphene Technology" iGRAPHENE 2020, 19-20.10.2020, komunikat ustny.
26. **M. Skorupska**, A. Ilnicka, J. P. Łukaszewicz, Synthesis of graphene foams using the templating method, XII Interdyscyplinarna Konferencja Naukowa TYGIEL 2020 - „Interdyscyplinarność kluczem do rozwoju", on-line, 24-27.09.2020, komunikat ustny.
27. **M. Skorupska**, A. Ilnicka, J. P. Łukaszewicz, Synteza pian grafenowych z wykorzystaniem metody mikrofalowego rozwarstwienia, e-Kopernikańskie Seminarium Doktoranckie, on-line, 07.09.2020, komunikat ustny.
28. P. Kamedulski, **M. Skorupska**, P. Binkowski, P. Lewicki, J. P. Łukaszewicz, Innovative graphene-based materials and their electrochemical applications,

Graduate Student Symposium on Advantageous Electrochemistry, on-line, 10–11.09.2020, komunikat ustny.

29. A. Ilnicka, W. Zieliński, **M. Skorupska**, A. Smolarkiewicz-Wyczachowski, P. Kamedulski, J. P. Łukaszewicz, Synthesis of porous hybrid carbon materials consist of activated carbon and carbon nanotube, 2nd Global Conference on Carbon Nanotubes and Graphene Technologies, Lizbona, 3-14.02.2020, prezentacja posterowa.

30. **M. Skorupska**, A. Ilnicka, W. Zieliński, J. P. Łukaszewicz, Carbon tubes – Activated carbons hybrid materials obtained from chitosan and their structural properties, XXV Conference of Polish Chitin Society „New aspects on chemistry and application of chitin and its derivatives", Toruń, 25-27.09.2019, komunikat ustny.

31. A. Ilnicka, W. Zieliński, A. Smolarkiewicz-Wyczachowski, **M. Skorupska**, R. Golembiewski, J. P. Łukaszewicz, Conversion of polymers to carbon tubes on a carbon substrate obtained from chitin, Toruń, 25-27.09.2019, prezentacja posterowa.

32. **M. Skorupska**, A. Ilnicka, P. Kamedulski, J. P. Łukaszewicz, Application of electrochemical exfoliated graphene doped of nitrogen as a catalyst for oxygen reduction reaction, Scientific Workshops Polish Carbon Society, Poznań, 27.09.2019, komunikat ustny.

33. A. Ilnicka, **M. Skorupska**, P. Kamedulski, J. P. Łukaszewicz, Electrochemically exfoliated nitrogen and phosphorus doped graphene for use in oxygen reduction reaction, Nano(&)BioMaterialy – from theory to application, Toruń, 6-7.06.2019, prezentacja posterowa

34. P. Kamedulski, J. P. Łukaszewicza,, **M. Skorupska**, Obtaining a photosensitive carbon layer, Nano(&)BioMaterialy – from theory to application, Toruń, 6-7.06.2019, prezentacja posterowa.

35. P. Kamedulski, A. Ilnicka, J. P. Łukaszewicz, **M. Skorupska**, Three-dimensional functionalization of graphene - achievements to date, Scientific Workshops Polish Carbon Society, Ustroń, 2-5.04.2019, prezentacja posterowa.

36. A. Ilnicka, **M. Skorupska**, P. Kamedulski, J. P. Łukaszewicz, Otrzymywanie grafenu za pomocą elektrochemicznej eksfoliacji., I Scientific Workshops Polish Carbon Society, Ustroń, 2-5.04.2019, prezentacja posterowa.

37. J. P. Łukaszewicz, A. Ilnicka, P. Kamedulski, **M. Skorupska**, Electroexfoliation Versus Wet Chemistry Exfoliations as a Preliminary Stage for 3D Functionalization

of Graphene Flakes, Collaborative Conference on Materials Research (CCMR), Seoul, 3-7.06.2019, komunikat ustny.

38. P. Kamedulski, A. Ilnicka, J. P. Łukaszewicz, **M. Skorupska**, Trójwymiarowa funkcjonalizacja grafenu: dotychczasowe osiągnięcia, Scientific Workshops Polish Carbon Society, Wrocław, 21.09.2018, komunikat ustny.

39. J. P. Łukaszewicz, A. Ilnicka, P. Kamedulski, **M. Skorupska**, Towards new synthesis of Graphene - CNTs hybrid materials, 22nd International Conference on Graphene, Carbon Nanotubes and Nanostructures, Berlin, 17-18.09.2018, komunikat ustny.

40. P. Kamedulski, A. Ilnicka, J. P. Łukaszewicz, **M. Skorupska**, Three Dimensional Functionalization of Graphene Obtained from Commercial Graphite by Wet Chemistry Exfoliation, Tenth International Symposium - Effects of Surface Heterogeneity in Adsorption, Catalysis and related Phenomena, ISSHAC-10, Lublin, 27-31.08.2018, komunikat ustny.

41. A. Ilnicka, **M. Skorupska**, P. Kamedulski, J. P. Łukaszewicz, Synthesis of graphene by electrochemical exfoliation of graphite foil in electrolyte solutions, NanoBioMateriały–theory and practice, Toruń, 6-8.06.2018, prezentacja posterowa.

<u>Odbyte staże zagraniczne</u>

1. Odbycie stażu naukowego w ramach konkursu "Inicjatywa Doskonałości - Mobilność dla Doktorantów" w programie "Inicjatywa Doskonałości - Uczelnia Badawcza. Edycja I"
   • Termin realizacji stażu: 12.10.2020- 08.11.2020
   • Temat badawczy: Synteza materiałów grafenowych do zastosowań jako materiał elektrodowy w superkondensatorach
   • Miejsce realizacji stażu: Center for Cooperative Research on ALternative Energies (CIC energiGUNE) w Vitoria – Gasteiz, Hiszpania
   • Opiekun stażu: dr Daniel Carriazo

2. Tytuł projektu: Projekt PROM - Międzynarodowa wymiana stypendialna doktorantów i kadry akademickiej
   • Termin realizacji stażu: 09.11.2020- 06.12.2020

• Temat badawczy: Synteza materiałów grafenowych do zastosowań jako materiał elektrodowy w superkondensatorach

• Miejsce realizacji stażu: Center for Cooperative Research on ALternative Energies (CIC energiGUNE) w Vitoria – Gasteiz, Hiszpania

• Opiekun stażu: dr Daniel Carriazo

3. Odbycie stażu naukowego w ramach konkursu "Inicjatywa Doskonałości - Mobilność dla Doktorantów", edycja II w programie "Inicjatywa Doskonałości - Uczelnia Badawcza”

   • Termin realizacji stażu: 01.02.2023- 31.03.2023

   • Temat badawczy: Synteza materiałów węglowych do zastosowań jako materiały do elektrolizy wody

   • Miejsce realizacji stażu: Politechnika w Walencji, Instytut Technologii Chemicznej (ITQ) w Valencia, Hiszpania

   • Opiekun stażu: prof. Hermenegildo García

4. Odbycie stażu naukowego w ramach konkursu "Inicjatywa Doskonałości - Mobilność dla Doktorantów", edycja III w programie "Inicjatywa Doskonałości - Uczelnia Badawcza"

   • Termin realizacji stażu: 01.04.2020- 30.04.2023

   • Temat badawczy: Synteza materiałów węglowych do zastosowań jako materiały do elektrolizy wody

   • Miejsce realizacji stażu: Politechnika w Walencji, Instytut Technologii Chemicznej (ITQ) w Valencia, Hiszpania

   • Opiekun stażu: prof. Hermenegildo García

5. Staż naukowy w ramach konkursu im. Bekkera finansowanego przez NAWA, na realizację projektu

   • Termin realizacji stażu: 01.08.2023- 01.02.2024

   • Temat badawczy: Synteza i charakterystyka nowych nanocząstek dwu- i multimetalicznych w procesie restrukturyzacji galwanicznej do elektrokatalitycznej konwersji energii

   • Miejsce realizacji stażu: Wydział Chemii, Uniwersytet w Oslo, Norwegia

   • Opiekun stażu: dr Athanasios Chatzitakis

Granty uzyskane i kierowane przez doktoranta

1. Grant PRELUDIUM-18, finansowany przez Narodowego Centrum Nauki. Temat projektu badawczego: *Badania nad syntezą pian grafenowych o zróżnicowanym zastosowaniu,* nr DEC-2019/35/N/ST5/02691
2. Grant Młodych, przyznany przez Dziekana Wydziału Chemii UMK w Toruniu. Temat projektu: *Synteza pian grafenowych do zastosowań elektrodowych*, nr 2092/2019
3. Grant Młodych, przyznany przez Dziekana Wydziału Chemii UMK w Toruniu. Temat projektu: *Synteza pian grafenowych z wykorzystaniem metody templatowania*, nr 492/2020
4. Grant Młodych, przyznany przez Dziekana Wydziału Chemii UMK w Toruniu. Temat projektu: *Modyfikacja pian grafenowych domieszkowanych heteroatomami*, nr PDB/granty wydziałowe
5. Grant Młodych, przyznany przez Dziekana Wydziału Chemii UMK w Toruniu. Temat projektu: *Synteza i modyfikacje pian grafenowo-węglowych z wykorzystaniem metody miękkiego templatowania do zastosowań ORR, OER bądź HER*, nr WCh/podstawowa działalność badawcza (4001.00000001)

Granty promotorów z udziałem doktoranta

1. Grant Norweski. Tytuł: Katalizatory na bazie grafenu wolne od Pt dla technologii rozszczepienia wody jako zielona metoda produkcji wodoru, nr grantu NOR/SGS/IL-HYDROGEN/0202/2020-00, źródło finansowania: Narodowe Centrum Badań i Rozwoju (NCBR). Kierownik projektu: dr hab. Anna Ilnicka, prof. UMK. Rola pełniona w projekcie – wykonawca grantu.

Udział Doktoranta w grancie, umowa o dzieło:

Temat: *Opracowanie, synteza i charakterystyka grafenu i jego hybryd zawierających domieszki heteroatomów i tlenki metali (WP1),* nr umowy 27/2022

2. Grant LIDER-IX. Tytuł: Hybrydowe materiały nanorurki węglowe–grafen i nanorurki węglowe–węgiel aktywny: synteza i zastosowanie w elektrochemicznych akumulatorach energii, nr grantu LIDER/32/0116/L-9/17/NCBR/2018, źródło finansowania: Narodowe Centrum Badań i Rozwoju (NCBR). Kierownik projektu: dr hab. Anna Ilnicka, prof. UMK. Rola pełniona w projekcie – wykonawca grantu. Udział Doktoranta w grancie, umowa o dzieło:

a) Temat: *Synteza i charakterystyka materiałów węglowych nanorurki węglowe – węgiel aktywny (CNT-AC)*, nr umowy 46/2019
b) Temat: *Synteza i charakterystyka materiałów węglowych nanorurki węglowe – grafen (CNT-GR)*, nr umowy 43/2020
c) Temat: *Opracowanie, budowa i testowanie prototypowych magazynów energii z wykorzystaniem materiałów elektrodowych typu CNT-AC i CNT-GR*, nr umowy 5/2021

3. Grant OPUS-12. Tytuł: Trójwymiarowa funkcjonalizacja grafenu metodami fizycznymi i chemicznymi, nr grantu 2016/23/B/ST5/00658, źródło finansowania: Narodowe Centrum Nauki (NCN). Kierownik projektu: Prof. dr hab. Jerzy P. Łukaszewicz. Rola pełniona w projekcie – wykonawca grantu.

Udział Doktoranta w grancie, umowa o dzieło:
a) Temat: *Wykonanie eksperymentów anodowej i katodowej elektro-eksfoljacji grafitu w środowisku NaCl, KCl, NaOH, Na_2SO_4, $(NH4)_2SO_4$ (III etap)*, nr umowy 54/2019

b) Temat: *Wykonanie eksperymentów anodowej i katodowej elektro-eksfoljacji grafitu w środowisku NaCl, KCl, NaOH, Na_2SO_4, $(NH4)_2SO_4$ (IV etap)*, nr umowy 20/2020

Zgłoszenia patentowe

1. P. Grabowska, A. Ilnicka, M. Skorupska, M. Szkoda, J.P. Łukaszewicz, *Sposób otrzymywania materiału elektrodowego do zastosowania w reakcjach HER/OER*, numer zgłoszenia patentowego P.444241 z dnia 29.03.2023, Urząd Patentowy Rzeczpospolitej Polskiej.

Nagrody i osiągnięcia doktoranta

1. I nagroda za najlepszą prezentację ustną na XXV Konferenjcji PTChit, „New aspects in chemistry and the use of chitin and its derivatives", Toruń (25-27.09.2019).
2. Nagroda zespołowa I stopnia JM Rektora Uniwersytetu Mikołaja Kopernika w Toruniu za osiągnięcia zespołowe w 2019 roku; skład zespołu: prof. dr hab. Jerzy P. Łukaszewicz, dr Anna Ilnicka, mgr Piotr Kamedulski, **mgr Małgorzata Skorupska**, dr hab. Piotr A. Gauden, prof. UMK (data rozdania: 24.06.2020, Toruń).
3. Nagroda JM Rektora Uniwersytetu Mikołaja Kopernika w Toruniu za wysoko punktowaną publikację naukową, w roku 2020:

1) W. Zieliński, P. Kamedulski, A. Smolarkiewicz-Wyczachowski, **M. Skorupska**, J. P. Łukaszewicz, A. Ilnicka, Synthesis of Hybrid Carbon Materials Consisting of N-Doped Microporous Carbon and Amorphous Carbon Nanotubes, Materials, 2020, 13(13), 2997.
2) A. Ilnicka, **M. Skorupska**, P. Romanowski, P Kamedulski, J. P. Łukaszewicz, Improving the Performance of Zn-Air Batteries with N-Doped Electroexfoliated Graphene, Materials, 2020 13 (9), 2115.

4. Nagroda JM Rektora Uniwersytetu Mikołaja Kopernika w Toruniu za wysoko punktowaną publikację naukową, w roku 2021 :
1) A. Ilnicka, **M. Skorupska**, M. Tyc, K. Kowalska, P. Kamedulski, W. Zieliński, J. P. Łukaszewicz, Green algae and gelatine derived nitrogen rich carbon as an outstanding competitor to Pt loaded carbon catalysts, Scientific Reports, 2021, 11(1), 1-13.
2) **M. Skorupska**, A. Ilnicka, J. P. Łukaszewicz, N-doped graphene foam obtained by microwave-assisted exfoliation of graphite, Scientific Reports, 2021, 11, 2044.

5. Nagroda zespołowa III stopnia JM Rektora Uniwersytetu Mikołaja Kopernika w Toruniu za osiągnięcia zespołowe w 2020 roku; skład zespołu: prof. dr hab. Jerzy P. Łukaszewicz, dr Anna Ilnicka, mgr Piotr Kamedulski, mgr Wojciech Zieliński mgr **Małgorzata Skorupska**, lic Aleksander Smolarkiewicz-Wyczachowski, lic Paweł Nowak, lic Piotr Romanowski, dr Stanisław Truszkowski, dr Aly Hesham (data rozdania: 25.06.2021, Toruń).

6. Nagroda JM Rektora Uniwersytetu Mikołaja Kopernika w Toruniu za wysoko punktowaną publikację naukową, w roku 2022:
1) **M. Skorupska**, A. Ilnicka, J. P. Łukaszewicz, *The effect of nitrogen species on the catalytic properties of N-doped graphene*, Scientific Reports, 2021, 11(1), 1-11;
2) P. Kamedulski, **M. Skorupska**, P. Binkowski, W. Arendarska, A. Ilnicka, J. P. Łukaszewicz, High surface area micro-mesoporous graphene for electrochemical applications , Scientific Reports, 2021, 11 (1), 1-12.

7. Srebrny medal za wynalazek pt. Piany grafenowe domieszkowane heteroatomami do zastosowań elektrodowych w bateriach metal-powietrze, autorstwa **mgr Małgorzata Skorupska**, dr Anna Ilnicka, prof. dr hab. Jerzy P. Łukaszewicz. Prace nad zaprezentowanym rozwiązaniem zostały przeprowadzone w ramach projektu badawczego nr 2019/35/N/ST5/02691 finansowanego przez Narodowe Centrum

Nauki, XV Międzynarodowe Targi Wynalazków i Innowacji, INTARG® 2022, Katowice, 11-12.05.2022.

8. Złoty medal oraz nagrodę specjalną przyznaną przez Research Institute of Creative Education (Wietnam) za wynalazek pt. Elektrokatalizatory na bazie grafenu dla technologii rozszczepiania wody - efektywnej metody produkcji zielonego wodoru, autorstwa dr Anna Ilnicka, **mgr Małgorzata Skorupska**, dr inż. Mariusz Szkoda, lic. Magdalena Tyc, lic. Kinga Kowalska, prof. dr hab. Jerzy P. Łukaszewicz. Prace nad zaprezentowanym rozwiązaniem zostały przeprowadzone w ramach projektu badawczego nr NOR/SGS/IL-HYDROGEN/0202/2020-00 finansowanego przez Narodowe Centrum Badań i Rozwoju, XV Międzynarodowe Targi Wynalazków i Innowacji, INTARG® 2022, Katowice, 11-12.05.2022.

Udział w kursach

1. Udział w kursie pt: „Good Laboratory Practise Specialist Course", certyfikat nr 21/GLP/TO/05/2017, Toruń (27.05.2017)
2. Udział w kursie pt: „Communication within a team", certyfikat nr 180/06/2021, Live on-line (26.03.2021).
3. Odbycie kursów Interaktywnych Nature Masterclasses na temat pisania i publikowania tekstów naukowych: Part 1: *„Writing a research paper"*, Part 2: „*Publishing a research paper",* Part 3: „*Writing and publishing a review paper"*, a także „*Focus on Peer Review"* (05.2021).
4. Udział w szkoleniu pt: „Jak dobrze mówić? Sztuka komunikacji.", On-line (02.03.2022)
5. Udział w XVII Ogólnopolskim Webinarze, pt. „Wystąpienia publiczne - tego można się nauczyć!", On-line (02.03.2022).

Udział w organizacji konferencji naukowych, olimpiad i warsztatów

1. Organizator konferencji NanoBioMateriały - od teorii do aplikacji, Toruń, 14-16.06.2023
2. Członek Polskiego Towarzystwa Chemicznego od 2022.
3. Członek Polskiego Towarzystwa Węglowego od 2021.
4. Organizator I etapu 68 Olimpiady Chemicznej, organizowany przez Komitet Okręgowy Olimpiady chemicznej w Toruniu, Toruń, 20.11.2021.